

THE AXON GUIDE

A Guide to Electrophysiology & Biophysics Laboratory Techniques

**Molecular Devices (now part of MDS Analytical Technologies)
The Axon Guide
A Guide to Electrophysiology & Biophysics Laboratory Techniques**

Copyright

Third Edition © Copyright 2008, MDS Analytical Technologies. All rights reserved. No part of this publication may be reproduced, transmitted, transcribed, stored in a retrieval system, or translated into any language or computer language, in any form or by any means, electronic, mechanical, magnetic, optical, chemical, manual, or otherwise, without the prior written permission of MDS Analytical Technologies, 1311 Orleans Drive, Sunnyvale, California, 94089, United States of America.

Trademarks

CYBERAMP, DIGIDATA, GENECLAMP and PCLAMP are registered trademarks and AXOPATCH, AXOCLAMP and MULTICLAMP are trademarks of MDS Analytical Technologies.

These trademarks are not to be used in any type of promotion or advertising without written permission from MDS Analytical Technologies.

All other trademarks or registered trademarks are the property of their respective owners.

Disclaimer

MDS Analytical Technologies reserves the right to change its products and services at any time to incorporate technological developments. This publication is subject to change without notice. Although this manual has been prepared with every precaution to ensure accuracy, MDS Analytical Technologies assumes no liability for any errors or omissions, nor for any damages resulting from the application or use of this information.

Questions?

Phone: +1-800-635-5577

+1-408-747-1700

Fax: +1-408-747-3603

Web: www.moleculardevices.com/support

For additional offices, please see the contact information on the back cover of this publication.

Contents

List of Figuresix
List of Tablesxiii
Preface	xv
Introduction	xvii
Editorialxix
Contributorsxxi
1. Bioelectricity	
Electrical Potentials	1
Electrical Currents	1
Resistors and Conductors	3
Ohm's Law	5
The Voltage Divider	7
Perfect and Real Electrical Instruments	7
Ions in Solutions and Electrodes	9
Capacitors and their Electrical Fields	11
Currents Through Capacitors	12
Current Clamp and Voltage Clamp	14
Glass Microelectrodes and Tight Seals	16
Further Reading	17
2. The Laboratory Setup	
The <i>In Vitro</i> Extracellular Recording Setup	19
The Single-Channel Patch Clamping Setup	19
Vibration Isolation Methods	20
Electrical Isolation Methods	21
Radiative Electrical Pickup	21
Magnetically-Induced Pickup	22
Ground-Loop Noise	22
Equipment Placement	23
List of Equipment	24
Further Reading	26

3. Instrumentation for Measuring Bioelectric Signals from Cells

Extracellular Recording	27
Single-Cell Recording	28
Multiple-Cell Recording	28
Intracellular Recording Current Clamp	29
Voltage Follower	29
Bridge Balance	30
Junction Potentials.	32
Track	32
Current Monitor	33
Headstage Current Gain	35
Capacitance Compensation	35
Leakage Current.	39
Headstages for Ion-Sensitive Microelectrodes.	39
Bath Error Potentials	40
Cell Penetration: Mechanical Vibration, Buzz and Clear	45
Command Generation	45
Intracellular Recording—Voltage Clamp	46
The Ideal Voltage Clamp	47
Real Voltage Clamps	47
Large Cells—Two-Electrode Voltage Clamp	48
Small Cells—Discontinuous Single-Electrode Voltage Clamp	52
Discontinuous Current Clamp (DCC)	57
Continuous Single-Electrode Voltage Clamp (Whole-cell Patch Clamp)	58
Series-Resistance Compensation.	59
Pipette-Capacitance Compensation	64
Whole-Cell Capacitance Compensation	66
Rupturing the Patch.	68
Which One Should You Use: dSEVC or cSEVC?	69
Space Clamp Considerations	69
Single-Channel Patch Clamp	70
The Importance of a Good Seal	71
Resistor Feedback Technology	71
Capacitor Feedback Technology	74
Special Considerations for Bilayer Experiments	77
How Fast is “Fast”?	78
Measurement of Changes in Membrane Capacitance.	78
Seal and Pipette Resistance Measurement	79
Micropipette Holders	79
Current Conventions and Voltage Conventions	80

Definitions	80
Whole-Cell Voltage and Current Clamp	81
Patch Clamp	82
Summary	83
References	84
Patch Clamp	84
Two-Electrode Voltage Clamp	84
Single-Electrode Voltage Clamp	84
Space-Clamp Considerations	84
Other	84

4. Microelectrodes and Micropipettes

Electrodes, Microelectrodes, Pipettes, Micropipettes and Pipette Solutions	85
Fabrication of Patch Pipettes	87
Pipette Properties for Single-Channel vs. Whole-Cell Recording	89
Types of Glasses and their Properties	89
Thermal Properties of Glasses	91
Noise Properties of Glasses	92
Leachable Components	94
Further Reading	94

5. Advanced Methods in Electrophysiology

Recording from <i>Xenopus</i> Oocytes	97
What is a <i>Xenopus</i> Oocyte?	98
Two-Electrode Voltage Clamping of Oocytes	99
Patch Clamping <i>Xenopus</i> Oocytes	101
Further Reading	102
Patch-Clamp Recording in Brain Slices	102
The Cleaning Technique	103
The Blind Technique	106
Advantages and Disadvantages of the Two Methods of Patch Clamping Brain Slices	108
Further Reading	109
Macropatch and Loose-Patch Recording	109
Gigaseal-Macropatch Voltage Clamp	110
Loose-Patch Voltage Clamp	111
The Giant Excised Membrane Patch Method	117
Pre-Treatment of Muscle Cells	118
Pipette Fabrication	118

Seal Formation	120
Further Reading	120
Recording from Perforated Patches and Perforated Vesicles	121
Properties of Amphotericin B and Nystatin	121
Stock Solutions and Pipette Filling	121
Properties of Antibiotic Partitioning	122
The Advantages of the Perforated-Patch Technique	123
The Limitations of the Perforated-Patch Technique	123
Suggested Ways to Minimize the Access Resistance	124
Other Uses for Perforated Patches	125
Further Reading	128
Enhanced Planar Bilayer Techniques for Single-Channel Recording	129
Solving the Problems of High Resolution and Voltage Steps	130
Assembling a Bilayer Setup for High-Resolution Recordings	136
Further Reading	141

6. Signal Conditioning and Signal conditioners

Why Should Signals Be Filtered?	143
Fundamentals of Filtering	144
-3 dB Frequency	144
Type: High-pass, Low-pass, Band-pass or Band-reject (notch)	144
Order	144
Implementation: Active, Passive or Digital	144
Filter Function	144
Filter Terminology	145
- 3 dB Frequency	145
Attenuation	146
Pass Band	146
Stop Band	146
Phase Shift	146
Overshoot	146
Octave	146
Decade	146
Decibels (dB)	147
Order	148
10-90% Rise Time	149
Filtering for Time-Domain Analysis	149
Filtering for Frequency-Domain Analysis	151
Sampling Rate	152
Filtering Patch-Clamp Data	153

Digital Filters	153
Preparing Signals for A/D Conversion	155
Where to Amplify	155
Pre-Filter vs. Post-Filter Gain	156
Offset Control	157
AC Coupling and Autozeroing	158
Time Constant	160
Saturation	160
Overload Detection	160
Averaging	161
Line-Frequency Pick-Up (Hum)	161
Peak-to-Peak and rms Noise Measurements	161
Blanking	163
Audio Monitor—Friend or Foe?	163
Electrode Test	164
Common-Mode Rejection Ratio	164
References	165
Further Reading	165

7. Transducers

Temperature Transducers for Physiological Temperature Measurement	167
Thermistors	167
IC Temperature Transducers that Produce an Output Current Proportional to Absolute Temperature	168
IC Temperature Transducers that Produce an Output Voltage Proportional to Absolute Temperature	169
Temperature Transducers for Extended Temperature Ranges	169
Thermocouples	169
Resistance Temperature Detectors	170
Electrode Resistance and Cabling Affect Noise and Bandwidth	171
High Electrode Impedance Can Produce Signal Attenuation	171
Unmatched Electrode Impedances Increase Background Noise and Crosstalk	172
High Electrode Impedance Contributes to the Thermal Noise of the System	173
Cable Capacitance Filters Out the High-Frequency Component of the Signal.	174
EMG, EEG, EKG and Neural Recording	174
EMG	174
EKG	175
EEG.	175
Nerve Cuffs	175

Metal Microelectrodes	175
Bridge Design for Pressure and Force Measurements	176
Pressure Measurements	176
Force Measurements	177
Acceleration Measurements	177
Length Measurements	177
Implantable Length Gauges	177
Linear Potentiometers	178
Linear Variable Differential Transformers (LVDT)	178
Self-Heating Measurements	178
Isolation Measurements	178
Insulation Techniques	178
Further Reading	179

8. Laboratory Computer Issues and Considerations

Select the Software First	181
How Much Computer Do You Need?	181
The Machine Spectrum: Capability vs. Price	181
Memory	181
Hard Drive	182
Graphics Card	182
Peripherals and Options	182
Data Backup	182
Recommended Computer Configurations	183
Glossary	183

9. Acquisition Hardware

Fundamentals of Data Conversion	189
Quantization Error	190
Choosing the Sampling Rate	191
Converter Buzzwords	192
Gain Accuracy	192
Linearity Error	192
Differential Nonlinearity	192
Least Significant Bit (LSB)	193
Monotonicity	193
Deglitched DAC Outputs	193
Timers	194
Digital I/O	194

Optical Isolation	194
Operating Under Multi-Tasking Operating Systems	195
Software Support.	195

10. Data Analysis

Choosing Appropriate Acquisition Parameters.	197
Gain and Offset	197
Sampling Rate	197
Filtering	199
Filtering at Analysis Time	199
Integrals and Derivatives	200
Single-Channel Analysis	200
Goals and Methods	200
Sampling at Acquisition Time	201
Filtering at Acquisition Time	201
Analysis-Time Filtering	201
Generating the Events List	202
Setting the Threshold for a Transition	202
Baseline Definition	202
Missed Events	202
False Events	202
Multiple Channels	203
Analyzing the Events List	203
Histograms.	203
Histogram Abscissa Scaling	203
Histogram Ordinate Scaling.	203
Errors Resulting from Histogramming Events Data.	205
Amplitude Histogram	206
Fitting to Histograms.	206
Fitting	207
Reasons for Fitting.	207
Statistical Aspects of Fitting	208
Methods of Optimization	211
References	212

11. Noise in Electrophysiological Measurements

Thermal Noise	216
Shot Noise.	218
Dielectric Noise.	219
Excess Noise	220

Amplifier Noise	221
Electrode Noise	223
Electrode Noise in Single-Channel Patch Voltage Clamping	223
Seal Noise	232
Noise in Whole-Cell Voltage Clamping	234
External Noise Sources	236
Digitization Noise	237
Aliasing	238
Filtering	240
Summary of Patch-Clamp Noise	244
Headstage	244
Holder	244
Electrode	245
Seal	245
Limits of Patch-Clamp Noise Performance	246
Further Reading	246

A. Appendix: Guide to Interpreting Specifications

General	247
Thermal Noise	247
RMS Versus Peak-to-Peak Noise	248
Bandwidth—Time Constant—Rise Time	248
Filters	248
Microelectrode Amplifiers	249
Voltage-Clamp Noise	249
10–90% Rise Time (t_{10-90})	249
1% Settling Time (t_1)	249
Input Capacitance	249
Input Leakage Current	250
Patch-Clamp Amplifiers	250
Bandwidth	250
Noise	250
Index	253

List of Figures

Figure 1.1: Conservation of current. Current is conserved at a branch point..	2
Figure 1.2: A typical electrical circuit.	2
Figure 1.3: Summation of conductance.	3
Figure 1.4: Equivalent circuit for a single-membrane channel..	4
Figure 1.5: Ohm's law..	5
Figure 1.6: IR drop..	6
Figure 1.7: A voltage divider..	7
Figure 1.8: Representative voltmeter with infinite resistance..	8
Figure 1.9: The silver/silver chloride electrode.	10
Figure 1.10: The platinum electrode..	11
Figure 1.11: Capacitance. A charge Q is stored in a capacitor of value C held at a potential ΔV	12
Figure 1.12: Capacitors in parallel add their values..	12
Figure 1.13: Membrane behavior compared with an electrical current.	13
Figure 1.14: RC parallel circuit response..	14
Figure 1.15: Typical voltage-clamp experiment..	15
Figure 1.16: Intracellular electrode measurement.	16
Figure 1.17: Good and bad seals..	17
Figure 3.1: An ideal micropipette buffer amplifier.	29
Figure 3.2: A high-quality current source.	30
Figure 3.3: The "Bridge Balance" technique.	31
Figure 3.4: Illustration of bridge balancing while micropipette is extracellular.	32
Figure 3.5: Series current measurement.	33
Figure 3.6: Virtual-ground current measurement.	34
Figure 3.7: Bootstrapped power supplies.	37
Figure 3.8: Capacitance neutralization circuit..	38
Figure 3.9: Two-electrode virtual-ground circuit..	43
Figure 3.10: The ideal voltage clamp.	47
Figure 3.11: Conventional two-electrode voltage clamp.	48
Figure 3.12: Block diagram and timing waveforms..	52
Figure 3.13: Biphasic voltage response of a high-resistance micropipette..	55
Figure 3.14: Voltage and temporal errors caused by the presence of R_a	59
Figure 3.15: Series resistance correction.	60

Figure 3.16: Prediction implemented empirically by the computer.	62
Figure 3.17: Implementation of prediction based on the knowledge of cell parameters.	63
Figure 3.18: Pipette capacitance compensation circuit.	65
Figure 3.19: Whole-cell capacitance compensation circuit.	67
Figure 3.20: Using the injection capacitor to charge the membrane capacitance.	68
Figure 3.21: Resistive headstage.	72
Figure 3.22: Capacitive feedback headstage.	74
Figure 3.23: Signal handling during resets in the capacitor-feedback headstage.	76
Figure 3.24: Typical current noise in bilayer experiments.	78
Figure 4.1: Noise properties of glasses.	93
Figure 5.1: Stage V or VI oocytes as found in an ovarian lobe.	98
Figure 5.2: The Cleaning technique.	105
Figure 5.3: The Blind technique.	107
Figure 5.4: Combining whole-cell voltage clamping with loose-patch current recording.	112
Figure 5.5: Pipette fabrication for giant excised patch method.	119
Figure 5.6: Forming a cell-attached perforated patch and a perforated vesicle.	127
Figure 5.7: Aperture formation in a plastic cup (not drawn to scale).	137
Figure 5.8: Voltage-step activation of a K-channel from squid giant axon axoplasm.	140
Figure 6.1: Frequency response of 4th-order Bessel and Butterworth filters.	145
Figure 6.2: Illustration of filter terminology.	147
Figure 6.3: Difference between a 4th- and 8th-order transfer function.	149
Figure 6.4: Step response comparison between bessel and butterworth filters.	150
Figure 6.5: Use of a notch filter: inappropriately and appropriately.	151
Figure 6.6: Distortion of signal caused by high amplification prior to filtering.	157
Figure 6.7: Distortion of signal caused by AC-coupling at high frequencies.	158
Figure 6.8: Comparison of autozeroing to AC-coupling.	159
Figure 7.1: Electrode resistance and cabling can degrade a signal.	171
Figure 7.2: High electrode resistance can attenuate a signal and increase crosstalk.	172
Figure 7.3: Wheatstone Bridge circuit with amplifier.	176
Figure 9.1: Analog-to-digital conversion.	190
Figure 10.1: Histogram scaling.	204
Figure 10.2: Sampling error.	205
Figure 10.3: The likelihood function.	208

Figure 10.4: Confidence limits.	211
Figure 11.1: Noise equivalent circuits of a resistor.	216
Figure 11.2: Operational amplifier noise model.	221
Figure 11.3: Noise model of a simplified current-to-voltage converter.	221
Figure 11.4: Noise in whole-cell voltage clamping.	235
Figure 11.5: Folding of the frequency axis.	239
Figure 11.6: Squared transfer function of a Gaussian filter.	243



List of Tables

Table 3.1: Correction vs. Prediction.	64
Table 4.1: Electrical And Thermal Properties of Different Glasses.	89
Table 4.2: Chemical Compositions of Different Glasses.	91
Table 5.1: Brain Slice Techniques.	108
Table 7.1: Common Thermocouple Materials.	170
Table 9.1: Example Temperature Data.	189
Table 11.1: Thermal Noise of Resistors.	218
Table 11.2: Shot Noise.	219
Table A.1: Noise of a 10 MW Resistor in Microvolts rms.	247
Table A.2: rms Current in Picoamps.	250



Preface

MDS Analytical Technologies is pleased to present you with the third edition of The Axon Guide, a laboratory guide to electrophysiology and biophysics. The purpose of this guide is to serve as an information and data resource for electrophysiologists. It covers a broad scope of topics ranging from the biological basis of bioelectricity and a description of the basic experimental setup to a discussion of mechanisms of noise and data analysis.

The Axon Guide third edition is a tool benefitting both the novice and the expert electrophysiologist. Newcomers to electrophysiology will gain an appreciation of the intricacies of electrophysiological measurements and the requirements for setting up a complete recording and analysis system. For experienced electrophysiologists, we include in-depth discussions of selected topics, such as advanced methods in electrophysiology and noise.

This edition is the first major revision of the Axon Guide since the original edition was published in 1993. While the fundamentals of electrophysiology have not changed in that time, changes in instrumentation and computer technology made a number of the original chapters interesting historical documents rather than helpful guides. This third edition is up-to-date with current developments in technology and instrumentation.

This guide was the product of a collaborative effort of many researchers in the field of electrophysiology and of MDS Analytical Technologies' staff. We are deeply grateful to these individuals for sharing their knowledge and devoting significant time and effort to this endeavor.

David Yamane
Director, Electrophysiology Marketing
MDS Analytical Technologies

November 2007



Introduction

Axon Instruments, Inc., was founded in 1983 to design and manufacture instrumentation and software for electrophysiology and biophysics. Its products were distinguished by the company's innovative design capability, high-quality products, and expert technical support. Today, the Axon Instruments products are part of MDS Analytical Technologies' portfolio of life science and drug discovery products. The Axon brand of microelectrode amplifiers, digitizers, and data acquisition and analysis software provides researchers with ready-to-use, technologically advanced products which allows them more time to pursue their primary research goals.

Furthermore, to ensure continued success with our products, we have staffed our Technical Support group with experienced Ph.D. electrophysiologists.

In addition to the Axon product suite, MDS Analytical Technologies has developed three automated electrophysiology platforms. Together with the Axon Cellular Neuroscience products, MDS Analytical Technologies spans the entire drug discovery process from screening to safety assessment.

In recognition of the continuing excitement in ion channel research, as evidenced by the influx of molecular biologists, biochemists, and pharmacologists into this field, MDS Analytical Technologies is proud to support the pursuit of electrophysiological and biophysical research with this laboratory techniques workbook.

ACKNOWLEDGMENT TO MDS ANALYTICAL TECHNOLOGIES CONSULTANTS AND CUSTOMERS

MDS Analytical Technologies employs a talented team of engineers and scientists dedicated to designing instruments and software incorporating the most advanced technology and the highest quality. Nevertheless, it would not be possible for us to enhance our products without close collaborations with members of the scientific community. These collaborations take many forms.

Some scientists assist MDS Analytical Technologies on a regular basis, sharing their insights on current needs and future directions of scientific research. Others assist us by virtue of a direct collaboration in the design of certain products. Many scientists help us by reviewing our instrument designs and the development versions of various software products. We are grateful to these scientists for their assistance. We also receive a significant number of excellent suggestions from the customers we meet at scientific conferences. To all of you who have visited us at our booths and shared your thoughts, we extend our sincere thanks. Another source of feedback for us is the information that we

receive from the conveners of the many excellent summer courses and workshops that we support with equipment loans. Our gratitude is extended to them for the written assessments they often send us outlining the strengths and weaknesses of Axon Cellular Neuroscience products from MDS Analytical Technologies.

Editorial

Editor

Rivka Sherman-Gold, Ph.D.

Editorial Committee

Michael J. Delay, Ph.D.

Alan S. Finkel, Ph.D.

Henry A. Lester, Ph.D.¹

W. Geoffrey Powell, MBA

Rivka Sherman-Gold, Ph.D.

Layout and Editorial Assistance

Jay Kurtz

Artwork

Elizabeth Brzeski

Editor – 3rd Edition

Warburton H. Maertz

Editorial Committee – 3rd Edition

Scott V. Adams, Ph.D.

S. Clare Chung, Ph.D.

Toni Figl, Ph.D.

Warburton H. Maertz

Damian J. Verdnik, Ph.D.

1.Lester is at the California Institute of Technology, Pasadena, CA. The other editorial staff are from MDS Analytical Technologies.

Layout and Editorial Assistance – 3rd Edition

Simone Andrews

Eveline Pajares

Peter Valenzuela

Damian J. Verdnik, Ph.D.

Alfred Walter, Ph.D.

Acknowledgements

The valuable inputs and insightful comments of Dr. Bertil Hille, Dr. Joe Immel and Dr. Stephen Redman are much appreciated.

Contributors

The Axon Guide is the product of a collaborative effort of MDS Analytical Technologies and researchers from several institutions whose contributions to the Guide are gratefully acknowledged.

John M. Bekkers, Ph.D., Division of Neuroscience, John Curtin School of Medical Research, Australian National University, Canberra, A.C.T. Australia.

Richard J. Bookman, Ph.D., Department of Molecular & Cellular Pharmacology, Miller School of Medicine, University of Miami, Miami, Florida.

Michael J. Delay, Ph.D.

Alan S. Finkel, Ph.D.

Aaron Fox, Ph.D., Department of Neurobiology, Pharmacology and Physiology, University of Chicago, Chicago, Illinois.

David Gallegos.

Robert I. Griffiths, Ph.D., Monash Institute of Medical Research, Faculty of Medicine, Monash University, Clayton, Victoria, Australia.

Donald Hilgemann, Ph.D., Graduate School of Biomedical Sciences, Southwestern Medical School, Dallas, Texas.

Richard H. Kramer, Department of Molecular & Cell Biology, University of California Berkeley, Berkeley, California.

Henry A. Lester, Ph.D., Division of Biology, California Institute of Technology, Pasadena, California.

Richard A. Levis, Ph.D., Department of Molecular Biophysics & Physiology, Rush-Presbyterian-St. Luke's Medical College, Chicago, Illinois.

Edwin S. Levitan, Ph.D., Department of Pharmacology, School of Medicine, University of Pittsburgh, Pittsburgh, Pennsylvania.

M. Craig McKay, Ph.D., Department of Molecular Endocrinology, GlaxoSmithKline, Inc., Research Triangle Park, North Carolina.

David J. Perkel, Department of Biology, University of Washington, Seattle, Washington.

Stuart H. Thompson, Hopkins Marine Station, Stanford University, Pacific Grove, California.

James L. Rae, Ph.D., Department of Physiology and Biomedical Engineering, Mayo Clinic, Rochester, Minnesota.

Michael M. White, Ph.D., Department of Pharmacology & Physiology, Drexel University College of Medicine, Philadelphia, Pennsylvania.

William F. Wonderlin, Ph.D., Department of Biochemistry & Molecular Pharmacology, West Virginia University, Morgantown, West Virginia.

1. Bioelectricity

Chapter 1 introduces the basic concepts used in making electrical measurements from cells and the techniques used to make these measurements.

1.1. ELECTRICAL POTENTIALS

A cell derives its electrical properties mostly from the electrical properties of its membrane. A membrane, in turn, acquires its properties from its lipids and proteins, such as ion channels and transporters. An electrical potential difference exists between the interior and exterior of cells. A charged object (ion) gains or loses energy as it moves between places of different electrical potential, just as an object with mass moves “up” or “down” between points of different gravitational potential. Electrical potential differences are usually denoted as V or ΔV and measured in volts; therefore, potential is also termed voltage. The potential difference across a cell relates the potential of the cell’s interior to that of the external solution, which, according to the commonly accepted convention, is zero.

The potential difference across a lipid cellular membrane (“transmembrane potential”) is generated by the “pump” proteins that harness chemical energy to move ions across the cell membrane. This separation of charge creates the transmembrane potential. Because the lipid membrane is a good insulator, the transmembrane potential is maintained in the absence of open pores or channels that can conduct ions.

Typical transmembrane potentials amount to less than 0.1 V, usually 30 to 90 mV in most animal cells, but can be as much as 200 mV in plant cells. Because the salt-rich solutions of the cytoplasm and extracellular milieu are fairly good conductors, there are usually very small differences at steady state (rarely more than a few millivolts) between any two points within a cell’s cytoplasm or within the extracellular solution. Electrophysiological equipment enables researchers to measure potential (voltage) differences in biological systems.

1.2. ELECTRICAL CURRENTS

Electrophysiological equipment can also measure current, which is the flow of electrical charge passing a point per unit of time. Current (I) is measured in amperes (A). Usually, currents measured by electrophysiological equipment range from picoamperes to microamperes. For instance, typically, 10^4 Na^+ ions cross the membrane each millisecond that a single Na^+ channel is open. This current equals 1.6 pA (1.6×10^{-19} C/ion $\times 10^4$ ions/ms $\times 10^3$ ms/s; recall that 1 A is equal to 1 coulomb (C)/s).

Two handy rules about currents often help to understand electrophysiological phenomena: 1) current is conserved at a branch point (Figure 1.1); and 2) current always flows in a complete circuit (Figure 1.2). In electrophysiological measurements, currents can flow through capacitors, resistors, ion channels, amplifiers, electrodes and other entities, but they always flow in complete circuits.

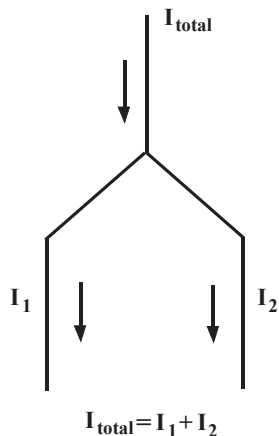


Figure 1.1: Conservation of current. Current is conserved at a branch point.

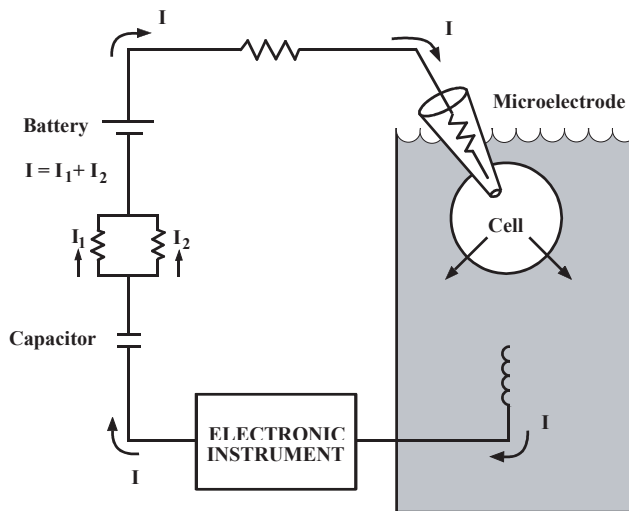


Figure 1.2: A typical electrical circuit.

Example of an electrical circuit with various parts. Current always flows in a complete circuit.

1.3. RESISTORS AND CONDUCTORS

Currents flow through resistors or conductors. The two terms actually complement one another—the former emphasizes the barriers to current flow, while the latter emphasizes the pathways for flow. In quantitative terms, resistance R (units: ohms (Ω)) is the inverse of conductance G (units: siemens (S)); thus, infinite resistance is zero conductance. In electrophysiology, it is convenient to discuss currents in terms of conductance because side-by-side (“parallel”) conductances simply sum (Figure 1.3). The most important application of the parallel conductances involves ion channels. When several ion channels in a membrane are open simultaneously, the total conductance is simply the sum of the conductances of the individual open channels.

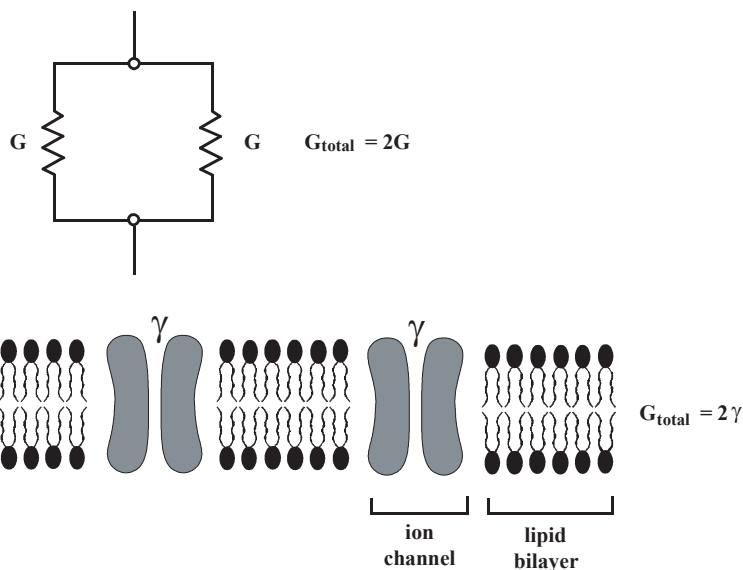


Figure 1.3: Summation of conductance.

Conductances in parallel summate together, whether they are resistors or channels.

A more accurate representation of an ion channel is a conductor in series with two additional circuit elements (Figure 1.4):

- 1 A switch that represents the gate of the channel, which would be in its conducting position when the gate is open, and

- 2 A battery that represents the reversal potential of the ionic current for that channel. The reversal potential is defined operationally as the voltage at which the current changes its direction. For a perfectly selective channel (*i.e.*, a channel through which only a single type of ion can pass), the reversal potential equals the Nernst potential for the permeant ion. The Nernst potential for ion A, E_A , can be calculated by the Nernst equation:

$$E_A = (RT/z_A F) \ln\{[A]_o/[A]_i\} = 2.303(RT/z_A F) \log_{10}\{[A]_o/[A]_i\} \quad (\text{units: volts}) \quad (1)$$

where R is the gas constant ($8.314 \text{ V C K}^{-1} \text{ mol}^{-1}$), T is the absolute temperature ($T = 273^\circ + ^\circ\text{C}$), z_A is the charge of ion A, F is Faraday's constant ($9.648 \times 10^4 \text{ C mol}^{-1}$), and $[A]_o$ and $[A]_i$ are the concentrations of ion A outside the cell and inside the cell, respectively. At 20°C ("room temperature"), $2.303(RT/z_A F) \log_{10}\{[A]_o/[A]_i\} = 58 \text{ mV} \log_{10}\{[A]_o/[A]_i\}$ for a univalent ion.

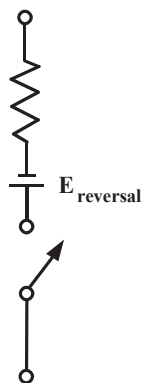


Figure 1.4: Equivalent circuit for a single-membrane channel.

A more realistic equivalent circuit for a single-membrane channel.

For instance, at room temperature, a Na^+ channel facing intracellular Na^+ concentration that is ten-fold lower than the extracellular concentration of this ion would be represented by a battery of +58 mV. A K^+ channel, for which the concentration gradient is usually reversed, would be represented by a battery of -58 mV.

Reversal potentials are not easily predicted for channels that are permeable to more than one ion. Nonspecific cation channels, such as nicotinic acetylcholine receptors, usually have reversal potentials near zero millivolts. Furthermore, many open channels have a nonlinear relation between current and voltage. Consequently, representing channels as resistors is only an approximation. Considerable biophysical research has been devoted to understanding the current-voltage relations of ion channels and how they are affected by the properties and concentrations of permeant ions.

The transmembrane potential is defined as the potential at the inner side of the membrane relative to the potential at the outer side of the membrane. The resting membrane potential (E_{rp}) describes a steady-state condition with no net flow of electrical current across the membrane. The resting membrane potential is determined by the intracellular and extracellular concentrations of ions to which the membrane is permeable and on their permeabilities. If one ionic conductance is dominant, the resting potential is near the Nernst potential for that ion. Since a typical cell membrane at rest has a much higher permeability to potassium (P_K) than to sodium, calcium or chloride (P_{Na} , P_{Ca} and P_{Cl} , respectively), the resting membrane potential is very close to E_K , the potassium reversal potential.

1.4. OHM'S LAW

For electrophysiology, perhaps the most important law of electricity is Ohm's law. The potential difference between two points linked by a current path with a conductance G and a current I (Figure 1.5) is:

$$\Delta V = IR = I/G \text{ (units: volts)} \quad (2)$$

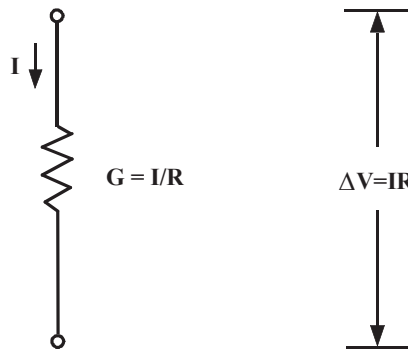


Figure 1.5: Ohm's law.

This concept applies to any electrophysiological measurement, as illustrated by the two following examples:

- 1 In an extracellular recording experiment: the current I that flows between parts of a cell through the external resistance R produces a potential difference ΔV , which is usually less than 1 mV (Figure 1.6). As the impulse propagates, I changes and, therefore, ΔV changes as well.

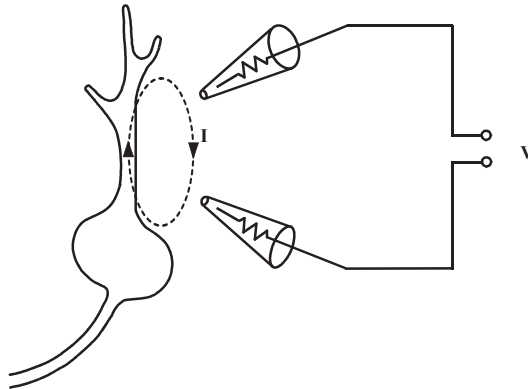


Figure 1.6: IR drop.

In extracellular recording, current I that flows between points of a cell is measured as the potential difference ("IR drop") across the resistance R of the fluid between the two electrodes.

- 2 In a voltage-clamp experiment: when N channels, each of conductance γ , are open, the total conductance is $N\gamma$. The electrochemical driving force ΔV (membrane potential minus reversal potential) produces a current $N\gamma\Delta V$. As channels open and close, N changes and so does the voltage-clamp current I . Hence, the voltage-clamp current is simply proportional to the number of open channels at any given time. Each channel can be considered as a γ conductance increment.

1.5. THE VOLTAGE DIVIDER

Figure 1.7 describes a simple circuit called a voltage divider in which two resistors are connected in series:

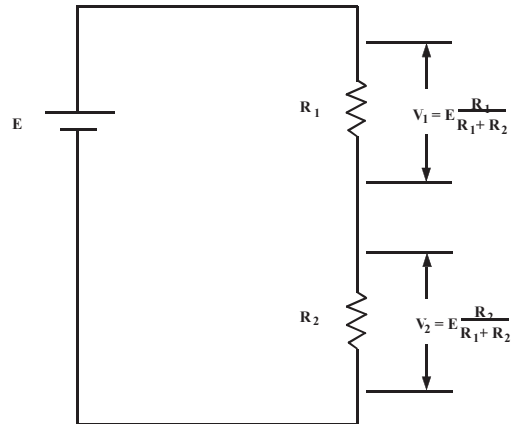


Figure 1.7: A voltage divider.

The total potential difference provided by the battery is E ; a portion of this voltage appears across each resistor:

$$\Delta V_1 = E \frac{R_1}{R_1 + R_2} \quad ; \quad \Delta V_2 = E \frac{R_2}{R_1 + R_2} \quad (2a)$$

When two resistors are connected in series, the same current passes through each of them. Therefore the circuit is described by:

$$\Delta V_1 + \Delta V_2 = E \quad (2b)$$

where E is the value of the battery, which equals the total potential difference across both resistors. As a result, the potential difference is divided in proportion to the two resistance values.

1.6. PERFECT AND REAL ELECTRICAL INSTRUMENTS

Electrophysiological measurements should satisfy two requirements: 1) They should accurately measure the parameter of interest, and 2) they should produce no perturbation of the parameter. The first requirement can be discussed in terms of a voltage divider. The second point will be discussed after addressing electrodes.

The best way to measure an electrical potential difference is to use a voltmeter with infinite resistance. To illustrate this point, consider the arrangement of Figure 1.8 A, which can be reduced to the equivalent circuit of Figure 1.8 B.

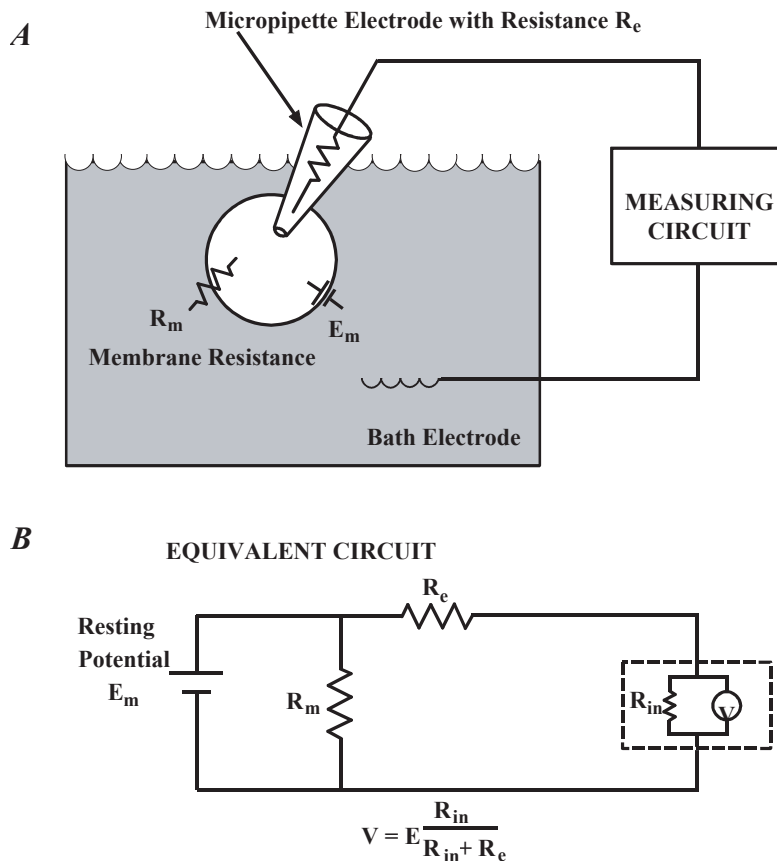


Figure 1.8: Representative voltmeter with infinite resistance.

Instruments used to measure potentials must have a very high input resistance R_{in} .

Before making the measurement, the cell has a resting potential of E_{rp} , which is to be measured with an intracellular electrode of resistance R_e . To understand the effect of the measuring circuit on the measured parameter, we will pretend that our instrument is a “perfect” voltmeter (*i.e.*, with an infinite resistance) in parallel with a finite resistance R_{in} , which represents the resistance of a real voltmeter or the measuring circuit. The combination R_e and R_{in} forms a voltage divider, so that only a fraction of E_{rp} appears at the input of the “perfect” voltmeter; this fraction equals $E_{rp}R_{in}/(R_{in} + R_e)$. The larger R_{in} , the closer

V is to E_{rp} . Clearly the problem gets more serious as the electrode resistance R_e increases, but the best solution is to make R_{in} as large as possible.

On the other hand, the best way to measure current is to open the path and insert an ammeter. If the ammeter has zero resistance, it will not perturb the circuit since there is no IR-drop across it.

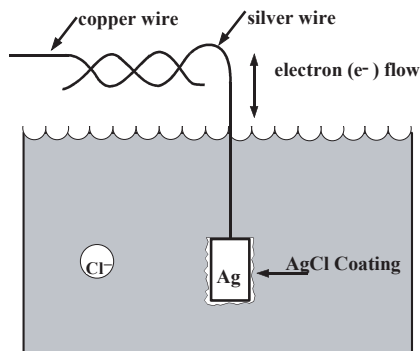
1.6.1. IONS IN SOLUTIONS AND ELECTRODES

Ohm's law—the linear relation between potential difference and current flow applies to aqueous ionic solutions, such as blood, cytoplasm and sea water. Complications are introduced by two factors:

- 1 The current is carried by at least two types of ions (one anion and one cation) and often by many more. For each ion, current flow in the bulk solution is proportional to the potential difference. For a first approximation, the conductance of the whole solution is simply the sum of the conductances contributed by each ionic species. When the current flows through ion channels, it is carried selectively by only a subset of the ions in the solution.
- 2 At the electrodes, current must be transformed smoothly from a flow of electrons in the copper wire to a flow of ions in solution. Many sources of errors (artifacts) are possible. Several types of electrodes are used in electrophysiological measurements; the most common is a silver/silver chloride (Ag/AgCl) interface, which is a silver wire coated with silver chloride (Figure 1.9). If electrons flow from the copper wire through the silver wire to the electrode AgCl pellet, they convert the AgCl to Ag atoms and the Cl^- ions become hydrated and enter the solution. If electrons flow in the reverse direction, Ag atoms in the silver wire that is coated with AgCl give up their electrons (one electron per atom) and combine with Cl^- ions that are in the solution to make insoluble AgCl. This is, therefore, a reversible electrode, *i.e.*, current can flow in both directions. There are several points to remember about Ag/AgCl electrodes:
 - a The Ag/AgCl electrode performs well only in solutions containing chloride ions.
 - b Because current must flow in a complete circuit, two electrodes are needed. If the two electrodes face different Cl^- concentrations (for instance, 3 M KCl inside a micropipette¹ and 120 mM NaCl in a bathing solution surrounding the cell), there will be a difference in the half-cell potentials (the potential difference between the solution and the electrode) at the two electrodes, resulting in a large steady potential difference in the two wires attached to the electrodes. This steady potential difference, termed liquid junction potential, can be subtracted electronically and poses few problems as long as the electrode is used within its reversible limits.
 - c If the AgCl is exhausted by the current flow, bare silver could come in contact with the solution. Silver ions leaking from the wire can poison many proteins. Also, the

1. A micropipette is a pulled capillary glass into which the Ag/AgCl electrode is inserted (see Chapter 4).

half-cell potentials now become dominated by unpredictable, poorly reversible surface reactions due to other ions in the solution and trace impurities in the silver, causing electrode polarization. However, used properly, Ag/AgCl electrodes possess the advantages of little polarization and predictable junction potential.



Electrode reaction:



This reaction can also be presented by:

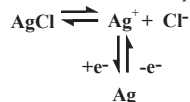


Figure 1.9: The silver/silver chloride electrode.

The silver/silver chloride electrode is reversible but exhaustible.

Another type of electrode, made of platinum (Pt) (Figure 1.10), is irreversible but not exhaustible. At its surface, Pt catalyzes the electrolysis of water. The gaseous H_2 or O_2 produced, depending on the direction of current flow, leaves the surface of the electrode. If both electrodes are Pt electrodes, the hydroxyl ions and protons are produced in equal numbers; however, local pH changes can still occur.

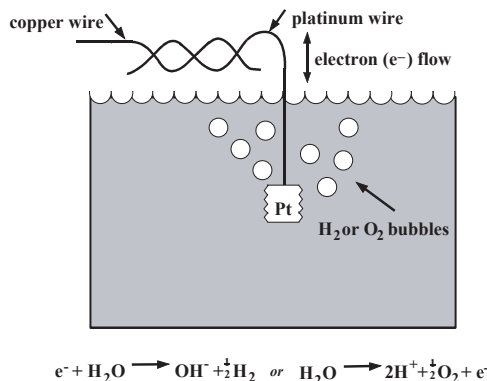


Figure 1.10: The platinum electrode.

A platinum electrode is irreversible but inexhaustible.

1.7. CAPACITORS AND THEIR ELECTRICAL FIELDS

The electrical field is a property of each point in space and is defined as proportional to the force experienced by a charge placed at that point. The greater the potential difference between two points fixed in space, the greater the field at each point between them. Formally, the electrical field is a vector defined as the negative of the spatial derivative of the potential.

The concept of the electrical field is important for understanding membrane function. Biological membranes are typically less than 10 nm thick. Consequently, a transmembrane resting potential of about 100 mV produces a very sizable electrical field in the membrane of about 10^5 V/cm. This is close to the value at which most insulators break down irreversibly because their atoms become ionized. Of course, typical electrophysiological equipment cannot measure these fields directly. However, changes in these fields are presumably sensed by the gating domains of voltage-sensitive ion channels, which determine the opening and closing of channels, and so the electrical fields underlie the electrical excitability of membranes.

Another consequence of the membrane's thinness is that it makes an excellent capacitor. Capacitance (C ; measured in farads, F) is the ability to store charge Q when a voltage ΔV occurs across the two "ends," so that:

$$Q = C\Delta V \quad (4)$$

The formal symbol for a capacitor is two parallel lines (Figure 1.12). This symbol arose because the most effective capacitors are parallel conducting plates of large area separated by a thin sheet of insulator (Figure 1.11) an excellent approximation of the lipid bilayer.

The capacitance C is proportional to the area and inversely proportional to the distance separating the two conducting sheets.

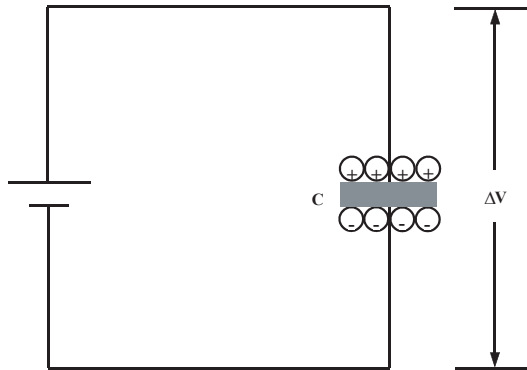


Figure 1.11: Capacitance. A charge Q is stored in a capacitor of value C held at a potential ΔV .

When multiple capacitors are connected in parallel, this is electronically equivalent to a single large capacitor; that is, the total capacitance is the sum of their individual capacitance values (Figure 1.12). Thus, membrane capacitance increases with cell size. Membrane capacitance is usually expressed as value per unit area; nearly all lipid bilayer membranes of cells have a capacitance of $1 \mu\text{F}/\text{cm}^2$ ($0.01 \text{ pF}/\mu\text{m}^2$).

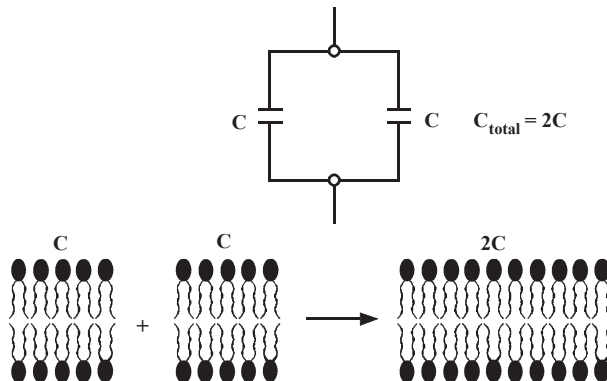


Figure 1.12: Capacitors in parallel add their values.

1.8. CURRENTS THROUGH CAPACITORS

Equation 4 shows that charge is stored in a capacitor only when there is a change in the voltage across the capacitor. Therefore, the current flowing through capacitance C is proportional to the voltage change with time:

$$I = C \frac{\Delta V}{\Delta t} \quad (5)$$

Until now, we have been discussing circuits whose properties do not change with time. As long as the voltage across a membrane remains constant, one can ignore the effect of the membrane capacitance on the currents flowing across the membrane through ion channels. While the voltage changes, there are transient capacitive currents in addition to the steady-state currents through conductive channels. These capacitive currents constitute one of the two major influences on the time-dependent electrical properties of cells (the other is the kinetics of channel gating). On Axon Cellular Neuroscience voltage- or patch-clamp amplifiers, several controls are devoted to handle these capacitive currents. Therefore it is worth obtaining some intuitive “feel” for their behavior.

The stored charge on the membrane capacitance accompanies the resting potential, and any change in the voltage across the membrane is accompanied by a change in this stored charge. Indeed, if a current is applied to the membrane, either by channels elsewhere in the cell or by current from the electrode, this current first satisfies the requirement for charging the membrane capacitance, then it changes the membrane voltage. Formally, this can be shown by representing the membrane as a resistor of value R in parallel with capacitance C (Figure 1.13).

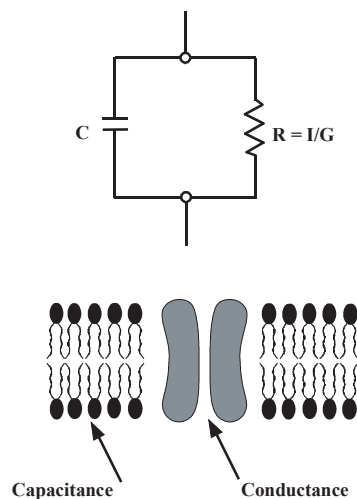


Figure 1.13: Membrane behavior compared with an electrical current.

A membrane behaves electrically like a capacitance in parallel with a resistance.

Now, if we apply a pulse of current to the circuit, the current first charges up the capacitance, then changes the voltage (Figure 1.14).

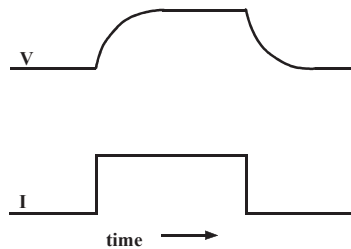


Figure 1.14: RC parallel circuit response.

Response of an RC parallel circuit to a step of current.

The voltage $V(t)$ approaches steady state along an exponential time course:

$$V(t) = V_{inf}(1 - e^{-t/\tau})$$

The steady-state value V_{inf} (also called the infinite-time or equilibrium value) does not depend on the capacitance; it is simply determined by the current I and the membrane resistance R :

$$V_{inf} = IR \quad (6)$$

This is just Ohm's law, of course; but when the membrane capacitance is in the circuit, the voltage is not reached immediately. Instead, it is approached with the time constant τ , given by:

$$\tau = RC \quad (7)$$

Thus, the charging time constant increases when either the membrane capacitance or the resistance increases. Consequently, large cells, such as *Xenopus* oocytes that are frequently used for expression of genes encoding ion-channel proteins, and cells with extensive membrane invaginations, such as the T-system in skeletal muscle, have a long charging phase.

1.9. CURRENT CLAMP AND VOLTAGE CLAMP

In a current-clamp experiment, one applies a known constant or time-varying current and measures the change in membrane potential caused by the applied current. This type of experiment mimics the current produced by a synaptic input.

In a voltage clamp experiment one controls the membrane voltage and measures the transmembrane current required to maintain that voltage. Despite the fact that voltage clamp

does not mimic a process found in nature, there are three reasons to do such an experiment:

- 1 Clamping the voltage eliminates the capacitive current, except for a brief time following a step to a new voltage (Figure 1.15). The brevity of the capacitive current depends on many factors that are discussed in following chapters.
- 2 Except for the brief charging time, the currents that flow are proportional only to the membrane conductance, *i.e.*, to the number of open channels.
- 3 If channel gating is determined by the transmembrane voltage alone (and is insensitive to other parameters such as the current and the history of the voltage), voltage clamp offers control over the key variable that determines the opening and closing of ion channels.

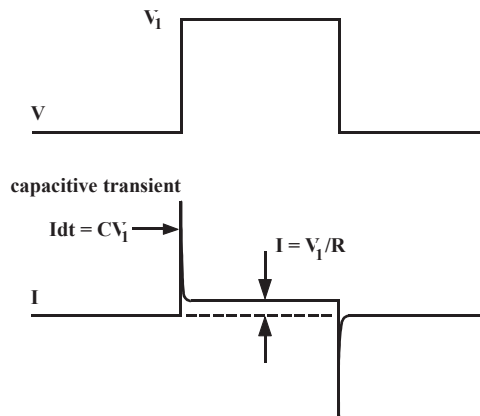


Figure 1.15: Typical voltage-clamp experiment.

A voltage-clamp experiment on the circuit of Figure 1.13.

The patch clamp is a special voltage clamp that allows one to resolve currents flowing through single ion channels. It also simplified the measurement of currents flowing through the whole-cell membrane, particularly in small cells that cannot be easily penetrated with electrodes. The characteristics of a patch clamp are dictated by two facts:

- 1 The currents measured are very small, on the order of picoamperes in single-channel recording and usually up to several nanoamperes in whole-cell recording. Due to the small currents, particularly in single-channel recording, the electrode polarizations and nonlinearities are negligible and the Ag/AgCl electrode can record voltage accurately even while passing current.
- 2 The electronic ammeter must be carefully designed to avoid adding appreciable noise to the currents it measures.

1.10. GLASS MICROELECTRODES AND TIGHT SEALS

Successful electrophysiological measurements depend on two technologies: the design of electronic instrumentation and the properties and fabrication of glass micropipettes. Glass pipettes are used both for intracellular recording and for patch recording; quartz pipettes have been used for ultra low-noise single-channel recording (for a detailed discussion of electrode glasses see Chapter 4). Successful patch recording requires a tight seal between the pipette and the membrane. Although there is not yet a satisfactory molecular description of this seal, we can describe its electrical characteristics.

Requirement 2) above (see Section 1.6., “*Perfect and Real Electrical Instruments*”) states that the quality of the measurement depends on minimizing perturbation of the cells. For the case of voltage recording, this point can be presented with the voltage divider circuit (Figure 1.16).

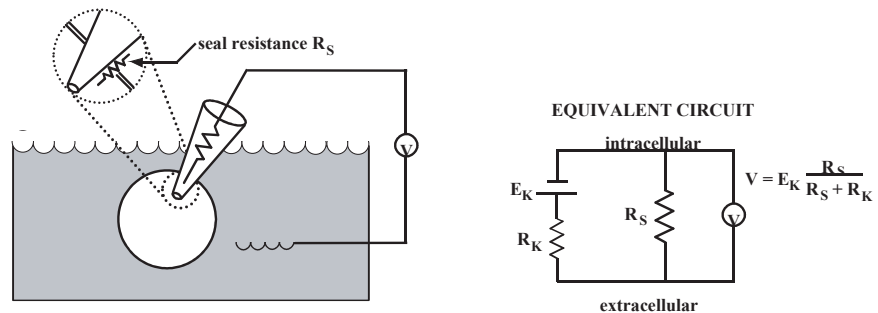


Figure 1.16: Intracellular electrode measurement.

This intracellular electrode is measuring the resting potential of a cell whose membrane contains only open K^+ channels. As the seal resistance R_S increases, the measurement approaches the value of E_K .

For the case of patch recording, currents through the seal do not distort the measured voltage or current, but they do add to the current noise. Current noise can be analyzed either in terms of the Johnson noise of a conductor, which is the thermal noise that increases with the conductance (see Chapter 7 and Chapter 11), or in terms of simple statistics. The latter goes as follows: If a current of N ions/ms passes through an open channel, then the current will fluctuate from one millisecond to the next with a standard deviation of \sqrt{N} . These fluctuations produce noise on the single-channel recorded traces. If an additional current is flowing in parallel through the seal (Figure 1.17), it causes an increase in the standard deviations. For instance, if the current through the seal is ten-fold larger than through the channel, then the statistical fluctuations in current flow produced by the seal are $\sqrt{10}$ (316%) larger than they would be for a “perfect” seal.

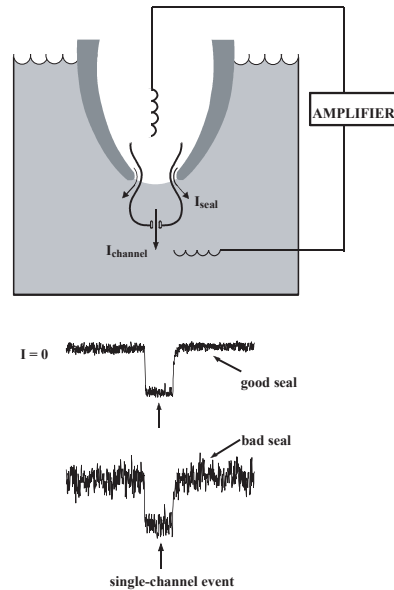


Figure 1.17: Good and bad seals.

In a patch recording, currents through the seal also flow through the measuring circuit, increasing the noise on the measured current.

1.11. FURTHER READING

Brown, K. T., Flaming, D. G. *Advanced Micropipette Techniques for Cell Physiology*. John Wiley & Sons, New York, NY, 1986.

Hille, B., *Ionic Channels in Excitable Membranes*. Second edition. Sinauer Associates, Sunderland, MA, 1991.

Horowitz, P., Hill, W. *The Art of Electronics*. Second edition. Cambridge University Press, Cambridge, UK, 1989.

Miller, C., *Ion Channel Reconstitution*. C. Miller, Ed., Plenum Press, New York, NY, 1986.

Sakmann, B., Neher, E. Eds., *Single-Channel Recording*. Plenum Press, New York, NY, 1983.

Smith, T. G., Lecar, H., Redman, S. J., Gage, P. W., Eds. *Voltage and Patch Clamping with Microelectrodes*. American Physiological Society, Bethesda, MD, 1985.

Standen, N. B., Gray, P. T. A., Whitaker, M. J., Eds. *Microelectrode Techniques: The Plymouth Workshop Handbook*. The Company of Biologists Limited, Cambridge, England, 1987.

2. The Laboratory Setup

Each laboratory setup is different, reflecting the requirements of the experiment or the foibles of the experimenter. Chapter 2 describes components and considerations that are common to all setups dedicated to measure electrical activity in cells.

An electrophysiological setup has four main requirements:

- 1 Environment: the means of keeping the preparation healthy;
- 2 Optics: a means of visualizing the preparation;
- 3 Mechanics: a means of stably positioning the microelectrode; and
- 4 Electronics: a means of amplifying and recording the signal.

This Guide focuses mainly on the electronics of the electrophysiological laboratory setup.

To illustrate the practical implications of these requirements, two kinds of “typical” setups are briefly described, one for *in vitro* extracellular recording, the other for single-channel patch clamping.

2.1. THE *IN VITRO* EXTRACELLULAR RECORDING SETUP

This setup is mainly used for recording field potentials in brain slices. The general objective is to hold a relatively coarse electrode in the extracellular space of the tissue while mimicking as closely as possible the environment the tissue experiences *in vivo*. Thus, a rather complex chamber that warms, oxygenates and perfuses the tissue is required. On the other hand, the optical and mechanical requirements are fairly simple. A low-power dissecting microscope with at least 15 cm working distance (to allow near-vertical placement of manipulators) is usually adequate to see laminae or gross morphological features. Since neither hand vibration during positioning nor exact placement of electrodes is critical, the micromanipulators can be of the coarse mechanical type. However, the micromanipulators should not drift or vibrate appreciably during recording. Finally, the electronic requirements are limited to low-noise voltage amplification. One is interested in measuring voltage excursions in the 10 μ V to 10 mV range; thus, a low-noise voltage amplifier with a gain of at least 1,000 is required.

2.2. THE SINGLE-CHANNEL PATCH CLAMPING SETUP

The standard patch clamping setup is in many ways the converse of that for extracellular recording. Usually very little environmental control is necessary: experiments are often

done in an unperfused culture dish at room temperature. On the other hand, the optical and mechanical requirements are dictated by the need to accurately place a patch electrode on a particular 10 or 20 μm cell. The microscope should magnify up to 300 or 400 fold and be equipped with some kind of contrast enhancement (Nomarski, Phase or Hoffman). Nomarski (or Differential Interference Contrast) is best for critical placement of the electrode because it gives a very crisp image with a narrow depth of field. Phase contrast is acceptable for less critical applications and provides better contrast for fine processes. Hoffman presently ranks as a less expensive, slightly degraded version of Nomarski. Regardless of the contrast method selected, an inverted microscope is preferable for two reasons: 1) it usually allows easier top access for the electrode since the objective lens is underneath the chamber, and 2) it usually provides a larger, more solid platform upon which to bolt the micromanipulator. If a top-focusing microscope is the only option, one should ensure that the focus mechanism moves the objective, not the stage.

The micromanipulator should permit fine, smooth movement down to a couple of microns per second, at most. The vibration and stability requirements of the micromanipulator depend upon whether one wishes to record from a cell-attached or a cell-free (inside-out or outside-out) patch. In the latter case, the micromanipulator needs to be stable only as long as it takes to form a seal and pull away from the cell. This usually takes less than a minute.

Finally, the electronic requirements for single-channel recording are more complex than for extracellular recording. However, excellent patch clamp amplifiers, such as those of the Axopatch™ amplifier series from MDS Analytical Technologies, are commercially available.

A recent extension of patch clamping, the patched slice technique, requires a setup that borrows features from both *in vitro* extracellular and conventional patch clamping configurations. For example, this technique may require a chamber that continuously perfuses and oxygenates the slice. In most other respects, the setup is similar to the conventional patch clamping setup, except that the optical requirements depend upon whether one is using the thick-slice or thin-slice approach (see Further Reading at the end of this). Whereas a simple dissecting microscope suffices for the thick-slice method, the thin-slice approach requires a microscope that provides 300- to 400-fold magnification, preferably top-focusing with contrast enhancement.

2.3. VIBRATION ISOLATION METHODS

By careful design, it should be possible to avoid resorting to the traditional electrophysiologist's refuge from vibration: the basement room at midnight. The important principle here is that prevention is better than cure; better to spend money on stable, well-designed micromanipulators than on a complicated air table that tries to compensate for a micromanipulator's inadequacies. A good micromanipulator is solidly constructed and compact, so that the moment arm from the tip of the electrode, through the body of the manipulator, to the cell in the chamber, is as short as possible. Ideally, the micromanipula-

tor should be attached close to the chamber; preferably bolted directly to the microscope stage. The headstage of the recording amplifier should, in turn, be bolted directly to the manipulator (not suspended on a rod), and the electrode should be short.

For most fine work, such as patch clamping, it is preferable to use remote-controlled micromanipulators to eliminate hand vibration (although a fine mechanical manipulator, coupled with a steady hand, may sometimes be adequate). Currently, there are three main types of remote-controlled micromanipulators available: motorized, hydraulic/pneumatic and piezoelectric. Motorized manipulators tend to be solid and compact and have excellent long-term stability. However, they are often slow and clumsy to move into position, and may exhibit backlash when changing direction. Hydraulic drives are fast, convenient and generally backlash-free, but some models may exhibit slow drift when used in certain configurations. Piezoelectric manipulators have properties similar to motorized drives, except for their stepwise advancement.

Anti-vibration tables usually comprise a heavy slab on pneumatic supports. Tables of varying cost and complexity are commercially available. However, a homemade table, consisting of a slab resting on partially-inflated inner tubes, may be adequate, especially if high-quality micromanipulators are used.

2.4. ELECTRICAL ISOLATION METHODS

Extraneous electrical interference (not intrinsic instrument noise) falls into three main categories: radiative electrical pickup, magnetically-induced pickup and ground-loop noise.

2.4.1. RADIATIVE ELECTRICAL PICKUP

Examples of radiative electrical pickup include line frequency noise from lights and power sockets (hum), and high frequency noise from computers. This type of noise is usually reduced by placing conductive shields around the chamber and electrode and by using shielded BNC cables. The shields are connected to the signal ground of the microelectrode amplifier. Traditionally, a Faraday cage is used to shield the microscope and chamber. Alternatively, the following options can usually reduce the noise: 1) find the source of noise, using an open circuit oscilloscope probe, and shield it; 2) use local shielding around the electrode and parts of the microscope; 3) physically move the offending source (*e.g.*, a computer monitor) away from the setup; or 4) replace the offending source (*e.g.*, a monochrome monitor is quieter than a color monitor). Note that shielding may bring its own penalties, such as introducing other kinds of noise or degrading one's bandwidth (see Chapter 11). Do not assume that commercial specifications are accurate. For example, a DC power supply for the microscope lamp might have considerable AC ripple, and the "shielded" lead connecting the microelectrode preamplifier to the main amplifier might need additional shielding. Solution-filled perfusion tubing entering the bath may act as an antenna and pick up radiated noise. If this happens, shielding of the tubing may be required. Alternatively, a drip-feed reservoir, such as is used in intravenous perfusion sets, may be inserted in series with the tubing to break the electrical continuity of the perfusion

fluid. Never directly ground the solution other than at the ground wire in the chamber, which is the reference ground for the amplifier and which may not be the same as the signal ground used for shielding purposes. Further suggestions are given in Section 6.6., “*Line-Frequency Pick-Up (Hum)*”.

2.4.2. MAGNETICALLY-INDUCED PICKUP

Magnetically-induced pickup arises whenever a changing magnetic flux passes through a loop of wire, thereby inducing a current in the wire. It most often originates in the vicinity of electromagnets in power supplies, and is usually identified by its non-sinusoidal shape with a frequency that is a higher harmonic of the line frequency. This type of interference is easily reduced by moving power supplies away from sensitive circuitry. If this is not possible, try twisting the signal wires together to reduce the area of the loop cut by the flux, or try shielding the magnetic source with “mu-metal.”

2.4.3. GROUND-LOOP NOISE

Ground-loop noise arises when shielding is grounded at more than one place. Magnetic fields may induce currents in this loop. Moreover, if the different grounds are at slightly different potentials, a current may flow through the shielding and introduce noise. In principle, ground loops are easy to eliminate: simply connect all the shields and then ground them at one place only. For instance, ground all the connected shields at the signal ground of the microelectrode amplifier. This signal ground is, in turn, connected at only one place to the power ground that is provided by the wall socket. In practice, however, one is usually frustrated by one’s ignorance of the grounding circuitry inside electronic apparatuses. For example, the shielding on a BNC cable will generally be connected to the signal ground of each piece of equipment to which it is attached. Furthermore, each signal ground may be connected to a separate power ground (but not on Axon Cellular Neuroscience amplifiers). The loop might be broken by lifting off the BNC shielding and/or disconnecting some power grounds (although this creates hazards of electrocution!). One could also try different power sockets, because the mains earth line may have a lower resistance to some sockets than others. The grounds of computers are notorious for noise. Thus, a large reduction in ground-loop noise might be accomplished by using optical isolation (see Chapter 9) or by providing the computer with a special power line with its own ground.

The logical approach to reducing noise in the setup is to start with all equipment switched off and disconnected; only an oscilloscope should be connected to the microelectrode amplifier. First, measure the noise when the headstage is wrapped in grounded metal foil; microelectrode headstages should be grounded through a low resistance (for instance, 1 M Ω), whereas patch-clamp headstages should be left open circuit. This provides a reference value for the minimum attainable radiative noise. Next, connect additional pieces of electronic apparatuses while watching for the appearance of ground loops. Last, install an electrode and add shielding to minimize radiative pickup. Finally, it should be admitted that one always begins noise reduction in a mood of optimistic rationalism, but invariably descends into frustrating empiricism.

2.5. EQUIPMENT PLACEMENT

While the placement of equipment is directed by personal preferences, a brief tour of electrophysiologists' common preferences may be instructive. Electrophysiologists tend to prefer working alone in the corners of small rooms. This is partly because their work often involves bursts of intense, intricate activity when distracting social interactions are inadmissible. Furthermore, small rooms are often physically quieter since vibrations and air currents are reduced. Having decided upon a room, it is usually sensible to first set up the microscope and its intimate attachments, such as the chamber, the manipulators and the temperature control system (if installed). The rationale here is that one's first priority is to keep the cells happy in their quiescent state, and one's second priority is to ensure that the act of recording from them is not consistently fatal. The former is assisted by a good environment, the latter by good optics and mechanics. Working outward from the microscope, it is clearly prudent to keep such things as perfusion stopcocks and micromanipulator controllers off the vibration isolation table. Ideally, these should be placed on small shelves that extend over the table where they can be accessed without causing damaging vibrations and are conveniently at hand while looking through the microscope.

Choice and placement of electronics is again a matter of personal preference. There are minimalists who make do with just an amplifier and a computer, and who look forward to the day when even those two will coalesce. Others insist on a loaded instrument rack. An oscilloscope is important, because the computer is often insufficiently flexible. Furthermore, an oscilloscope often reveals unexpected subtleties in the signal that were not apparent on the computer screen because the sample interval happened not to have been set exactly right. The oscilloscope should be at eye level. Directly above or below should be the microelectrode amplifier so that adjustments are easily made and monitored. Last, the computer should be placed as far as possible—but still within a long arm's reach—from the microscope. This is necessary both to reduce the radiative noise from the monitor and to ensure that one's elbows will not bump the microscope when hurriedly typing at the keyboard while recording from the best cell all week.

A final, general piece of advice is perhaps the most difficult to heed: resist the temptation to mess eternally with getting the setup just right. As soon as it is halfway possible, do an experiment. Not only will this provide personal satisfaction, it may also highlight specific problems with the setup that need to be corrected or, better, indicate that an anticipated problem is not so pressing after all.

2. The Laboratory Setup

2.5.1. LIST OF EQUIPMENT

Traditional Patch-Clamp Setup

Item	Suggested Manufacturers
Vibration isolation table	Newport Micro-g (Technical Manufacturing Corp.)
Microscope, inverted	Carl Zeiss Leica Microsystems Nikon Olympus
Micromanipulators hydraulic motorized piezoelectric	Narishige International USA Newport EXFO (Burleigh) Sutter Instrument
Patch-clamp amplifiers	MDS Analytical Technologies. (Axon Cellular Neuroscience)
Oscilloscopes	Tektronix
Pipette fabrication	
glass	Garner Glass Friedrich & Dimmock Sutter Instrument
pullers	Sutter Instrument
microforges	Narishige International USA homemade - based on: Carl Zeiss metallurgical microscope Olympus CH microscope
coaters	Narishige International USA
hydrophobic coating	Dow Corning Sylgard 184 Q-dope
Microelectrode holders	MDS Analytical Technologies (Axon Cellular Neuroscience) E. W. Wright
Chamber, temperature control	Narashige International USA
Computers	see Chapter 9

Patch-Slice Setup

Item	Suggested Manufacturers
Microscope, low power	Carl Zeiss
Vibratome (other requirements as for a traditional patch-clamp setup)	Vibratome

Extra/Intracellular Microelectrode Setup

Item	Suggested Manufacturers
Vibration isolation table	Newport Micro-g (Technical Manufacturing Corp.)
Microscope	Carl Zeiss Leica Microsystems Nikon Olympus
Micromanipulators mechanical	Narishige International USA Stoelting Sutter Instrument
hydraulic	Narishige International USA
piezoelectric	EXFO (Burleigh) Sutter Instrument
Microelectrode amplifiers	MDS Analytical Technologies (Axon Cellular Neuroscience)
Oscilloscopes	Tektronix
Electrode fabrication glass	Garner Glass Friedrich & Dimmock Sutter Instrument
pullers	David Kopf Sutter Instrument GlasswoRx
Microelectrode holders	MDS Analytical Technologies (Axon Cellular Neuroscience) E. W. Wright
Chamber, temperature control	Narishige International USA
Computers	See Chapter 9
Optical Recording Setup	
Photomultipliers	Hamamatsu

Imaging systems

MDS Analytical Technologies

2.6. FURTHER READING

Conventional intra- and extracellular recording from brain slices

Dingledine, R. Ed. *Brain Slices*. Plenum Press, New York, NY, 1983.

Geddes, L. A. *Electrodes and the Measurement of Bioelectric Events*. Wiley Interscience, 1972.

Purves, R. D. *Microelectrode Methods for Intracellular Recording and Ionophoresis*. Academic Press, San Diego, CA, 1986.

Smith, T. G., Jr., Lecar, H., Redman, S. J., Gage, P. W. Ed. *Voltage and Patch Clamping with Microelectrodes*. American Physiological Society, Bethesda, MD, 1985.

Standen, N. B., Gray, P. T. A., Whitaker, M. J. Ed. *Microelectrode Techniques*. The Company of Biologists Limited, Cambridge, UK, 1987.

General patch-clamp recording

Hamill, O. P., Marty, A., Neher, E., Sakmann, B., Sigworth, F. J. Improved patch-clamp techniques for high-resolution current from cells and cell-free membrane patches. *Pflügers Arch.* 391: 85–100, 1981.

Sakmann, B. and Neher, E. Ed. *Single-Channel Recording*. Plenum Press, New York, NY, 1983.

Smith, T. G., Jr. et al., op. cit.

Standen, N. B. et al., op. cit.

Patch-slice recording

Edwards, F. A., Konnerth, A., Sakmann, B., Takahashi, T. A thin slice preparation for patch clamp recordings from neurons of the mammalian central nervous system. *Pflügers Arch.* 414: 600–612, 1989.

Blanton, M. G., Lo Turco, J. J., Kriegstein, A. Whole cell recording from neurons in slices of reptilian and mammalian cerebral cortex. *J. Neurosci. Meth.* 30: 203–210, 1989.

Vibration isolation methods

Newport Catalog. Newport Corporation, 2006.

Electrical isolation methods

Horowitz, P., Hill, W. *The Art of Electronics*. Cambridge, 1988.

Morrison, R. *Grounding and Shielding Techniques in Instrumentation*. John Wiley & Sons, New York, NY, 1967.

3. Instrumentation for Measuring Bioelectric Signals from Cells¹

There are several recording techniques that are used to measure bioelectric signals. These techniques range from simple voltage amplification (extracellular recording) to sophisticated closed-loop control using negative feedback (voltage clamping). The biggest challenges facing designers of recording instruments are to minimize the noise and to maximize the speed of response. These tasks are made difficult by the high electrode resistances and the presence of stray capacitances². Today, most electrophysiological equipment sport a bevy of complex controls to compensate electrode and preparation capacitance and resistance, to eliminate offsets, to inject control currents and to modify the circuit characteristics in order to produce low-noise, fast and accurate recordings.

3.1. EXTRACELLULAR RECORDING

The most straight-forward electrophysiological recording situation is extracellular recording. In this mode, field potentials outside cells are amplified by an AC-coupled amplifier to levels that are suitable for recording on a chart recorder or computer. The extracellular signals are very small, arising from the flow of ionic current through extracellular fluid (see Chapter 1, “*Bioelectricity*”). Since this saline fluid has low resistivity, and the currents are small, the signals recorded in the vicinity of the recording electrode are themselves very small, typically on the order of 10–500 μV .

The most important design criterion for extracellular amplifiers is low instrumentation noise. Noise of less than 10 μV peak-to-peak ($\mu\text{V}_{\text{p-p}}$) is desirable in the 10 kHz bandwidth. At the same time, the input bias current³ of the amplifier should be low ($< 1 \text{ nA}$)

-
1. In this chapter “Pipette” has been used for patch-clamp electrodes. “Micropipette” has been used for intracellular electrodes, except where it is unconventional, such as single-electrode voltage clamp. “Electrode” has been used for bath electrodes. “Microelectrode” has been used for extracellular electrodes.
 2. Some level of capacitance exists between all conductive elements in a circuit. Where this capacitance is unintended in the circuit design, it is referred to as stray capacitance. A typical example is the capacitance between the micropipette and its connecting wire to the headstage enclosure and other proximal metal objects, such as the microscope objective. Stray capacitances are often of the order of a few picofarads, but much larger or smaller values are possible. When the stray capacitances couple into high impedance points of the circuit, such as the micropipette input, they can severely affect the circuit operation.
 3. In the ideal operational amplifier (op amp), no current flows into the inputs. Similarly, in the ideal transistor, no current flows into the gate. In practice, however, amplifying devices always have an input current. This current is commonly known as the input bias current.

so that electrodes do not polarize. Ideally, the amplifier will have built-in high-pass and low-pass filters so that the experimenter can focus on the useful signal bandwidth.

3.1.1. SINGLE-CELL RECORDING

In single-cell extracellular recording, a fine-tipped microelectrode is advanced into the preparation until a dominant extracellular signal is detected. This will generally be due to the activity of one cell. The microelectrode may be made of metal, *e.g.*, glass-insulated platinum, or it may be a saline-filled glass micropipette.

While not specifically targeted at extracellular recording, the Axoclamp™ 900A and the MultiClamp™ 700B amplifiers are particularly suitable for single-cell extracellular recording if the extracellular electrode is a microelectrode of several megohms or more. The input leakage current of these amplifiers is very low and headstages are designed to directly accommodate the micropipette holder. If necessary, capacitance compensation can be used to speed up the response. The x100 AC-coupled output signal of the MultiClamp 700B amplifier, in particular, is useful for measuring small extracellular signals, because up to 2000x further amplification can be applied to the signal with the built-in output gain. Thus the total amplification is 200,000x, allowing for easier measurement of extracellular potentials of less than 1 mV.

The Axon CyberAmp® 380 programmable signal conditioner amplifier has special ultra low-noise probes suitable for extracellular recording. These probes do not have the special features of the Axoclamp 900A and the MultiClamp 700B amplifiers, but for low-resistance electrodes, from tens of ohms up to a few hundred kilohms, these ultra low-noise probes have superior noise characteristics. The AI 402 x50 probe for the CyberAmp 380 amplifier contributes less noise than the thermal noise of a 250 Ω resistor. Electrodes can be connected directly to the CyberAmp 380 amplifier without using a separate low-noise probe. In this case, the additional noise due to the amplifier will still be very low—less than the thermal noise of a 5 k Ω resistor. If electrodes are directly connected to the main instrument, there is always a risk of picking up line-frequency noise or noise from other equipment. Using a probe located very close to the electrode greatly reduces the probability that it will pick up extraneous noise.

3.1.2. MULTIPLE-CELL RECORDING

In multiple-cell extracellular recording, the goal is to record from many neurons simultaneously to study their concerted activity. Several microelectrodes are inserted into one region of the preparation. Each electrode in the array must have its own amplifier and filters. If tens or hundreds of microelectrodes are used, special fabrication techniques are required to produce integrated pre-amplifiers. If recording is required from up to 16 sites, two CyberAmp 380 amplifiers can be alternately used with one 16-channel A/D system such as the Digidata® 1440A digitizer.

3.2. INTRACELLULAR RECORDING CURRENT CLAMP

3.2.1. VOLTAGE FOLLOWER

The traditional method for recording the cell interior potential is the current-clamp technique, also commonly known as “Bridge” recording, and occasionally as “voltage-follower” recording. The essence of the technique is the connection of a micropipette to a unity gain buffer amplifier that has an input resistance many orders of magnitude greater than that of the micropipette and the input resistance of the cell (Figure 3.1). The output of the buffer amplifier follows the voltage at the tip of the electrode. The ideal buffer amplifier draws no input bias current, therefore the current through the micropipette is “clamped” at zero.

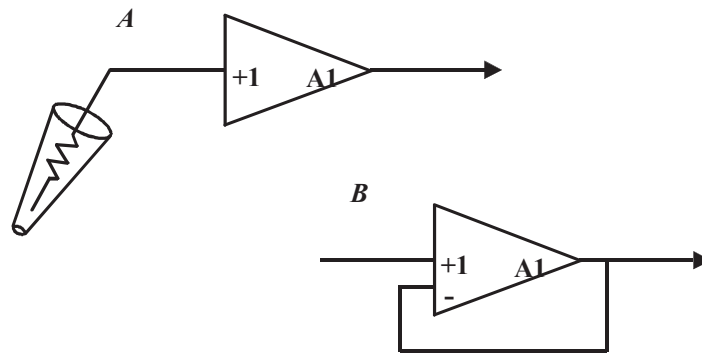


Figure 3.1: An ideal micropipette buffer amplifier.

In A the buffer (A1) is represented in block-diagram form as a unity-gain amplifier.

Note: The symbol +1 indicates a non-inverting input of gain x1. B shows how A1 is built from an operational amplifier with unity feedback.

If a high-quality current injection circuit (current source) is connected to the input node, all of the injected current flows down the micropipette and into the cell (see Figure 3.2). The current source can be used to inject a pulse of current to stimulate the cell, a DC current to depolarize or hyperpolarize the cell, or any variable waveform that the user introduces into the control input of the current source.

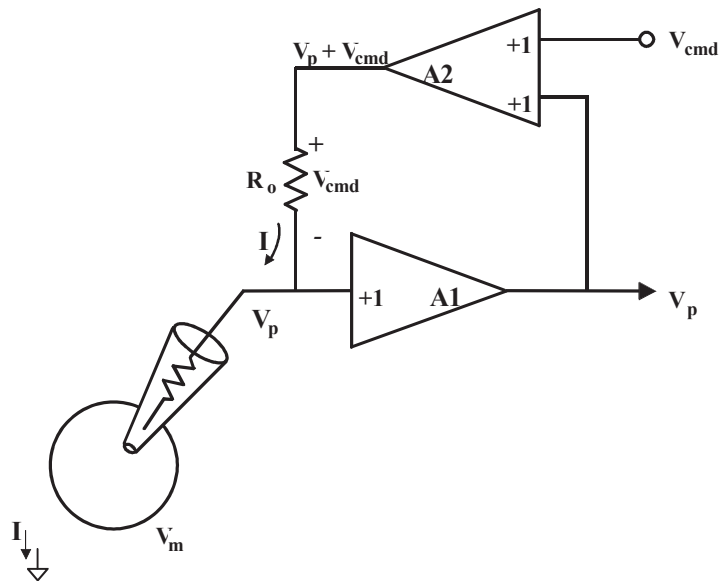


Figure 3.2: A high-quality current source.

A high-quality current source can be made by adding a second amplifier to the buffer amplifier circuit. The inputs to A2 are a command voltage, V_{cmd} , and the pipette voltage (V_p) buffered by A1. The voltage across the output resistor, R_o , is equal to V_{cmd} regardless of V_p . Thus the current through R_o is given exactly by $I = V_{cmd}/R_o$. If stray capacitances are ignored, all of this current flows through the pipette into the cell, then out through the cell membrane into the bath grounding electrode.

3.2.2. BRIDGE BALANCE

Can the intracellular potential be measured if the current injected down the micropipette is a variable waveform? Without special compensation circuitry, the answer is no. The variable current waveform causes a corresponding voltage drop across the micropipette. It is too difficult to distinguish the intracellular potential from the changing voltage drop across the micropipette. However, special compensation circuitry can be used to eliminate the micropipette voltage drop from the recording. The essence of the technique is to generate a signal that is proportional to the product of the micropipette current and the micropipette resistance. This signal is then subtracted from the buffer amplifier output (Figure 3.3). This subtraction technique is commonly known as “Bridge Balance” because in the early days of micropipette recording, a resistive circuit known as a “Wheatstone Bridge” was used to achieve the subtraction. In all modern micropipette amplifiers, operational amplifier circuits are used to generate the subtraction, but the name has persisted.

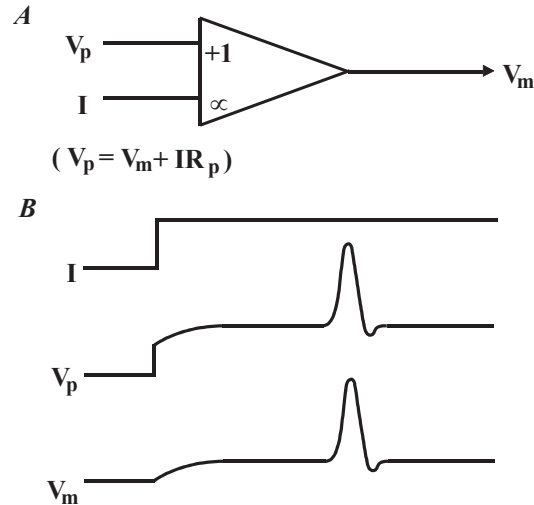


Figure 3.3: The “Bridge Balance” technique.

This technique is used to separate the membrane potential (V_m) from the total potential (V_p) recorded by the micropipette. The technique is schematically represented in A. A differential amplifier is used to subtract a scaled fraction of the current (I) from V_p . The scaling factor is the micropipette resistance (R_p). The traces in B illustrate the operation of the bridge circuit. When the current is stepped to a new value, there is a rapid voltage step on V_p due to the ohmic voltage drop across the micropipette. Since the micropipette is intracellular, changes in V_m are included in V_p . Thus the V_p trace shows an exponential rise to a new potential followed by some membrane potential activity. The bridge amplifier removes the instantaneous voltage step, leaving the V_m trace shown.

There are several ways to set the bridge balance. A commonly used technique is to apply brief repetitive pulses of current to the micropipette while it is immersed in the preparation bath. The Bridge Balance control is advanced until the steady-state pulse response is eliminated (Figure 3.4). At this point, the circuit is balanced and the micropipette resistance can be read from the calibrated readout of the Bridge Balance control. The same technique can even be used after the micropipette has penetrated the cell. Details of how to achieve this are described in the Axoclamp 900A and MultiClamp 700B manuals.

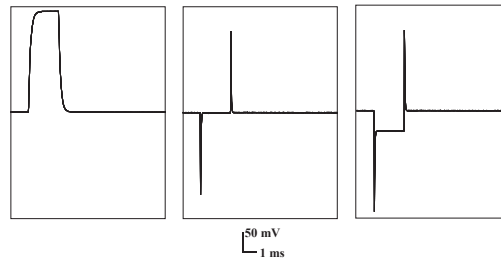


Figure 3.4: Illustration of bridge balancing while micropipette is extracellular.

All traces show the V_m output from the bridge-balance circuit. A 5 nA, 2 ms pulse is applied to a 50 M Ω electrode. No bridge balance is used in the left trace, revealing the full voltage drop across the micropipette. In the middle trace, optimum bridge balance is used and the voltage drop across the micropipette is eliminated from the record. The transients at the onset and finish of the step result from the finite bandwidth of the headstage amplifier. In the right trace, the bridge-balance control is advanced too far; the voltage drop across the micropipette is overcompensated and a reverse-polarity step appears.

It is important that the micropipette resistance be constant. Clearly, if the micropipette resistance varies as the current flows there will be no unique setting of the Bridge Balance control and the measurement will include an artifact due to the variable voltage drop across the micropipette.

3.2.3. JUNCTION POTENTIALS

A second extraneous contributor to the measured voltage at the output of the micropipette buffer amplifier is the sum of the junction potentials. Junction potentials occur wherever dissimilar conductors are in contact. The largest junction potentials occur at the liquid-metal junction formed where the wire from the amplifier input contacts the electrolyte in the micropipette and at the liquid-liquid junction formed at the tip of the micropipette. The sum of all of the junction potentials can be eliminated by introducing a single DC potential of the opposite polarity. In micropipette experiments, the junction potentials can often sum to a few hundred millivolts. The ± 500 mV range of the offset controls provided by all Axon Cellular Neuroscience microelectrode amplifiers is more than sufficient to compensate for even the worst-case junction potentials.

3.2.4. TRACK

A special form of automatic offset compensation is available in many patch clamp amplifiers, including the Axopatch™-1 and the Axopatch 200 amplifier series. In Axopatch amplifiers this technique is called “Track.” In some instruments of other manufacturers it is called “Search.” The Track circuit is used only during seal formation. During seal formation the tip comes in and out of contact with the membrane and rapid shifts in the tip potential of the headstage sometimes occur. These potential shifts lead to equivalent rapid shifts in the current record, which may exceed the dynamic range of the headstage. Since

the headstage itself saturates, AC coupling at the oscilloscope or any other form of external DC offset removal will not be useful. Instead, the Track circuit dynamically adjusts the offset potential of the micropipette itself, so that the current is forced to be zero on average. It is important that the Track circuit be switched off before recording of ionic currents commences since the Track circuit introduces the same type of distortion produced by AC coupling.

3.2.5. CURRENT MONITOR

Current-clamp circuits include a monitor output proportional to the current waveform. In some current-clamp amplifiers, the monitor output is merely a scaled version of the control voltage driving the current-clamp circuit. As long as the micropipette resistance is moderate and the current-clamp circuit output does not exceed its linear operating range, this technique is accurate. However, if the micropipette resistance is very high and the current-clamp circuitry saturates, the actual current through the micropipette will be less than the expected current. This simple monitor output will not indicate the failure to pass the expected current. A better technique is to actually measure the current by monitoring the voltage drop across a resistor in series with the micropipette (Figure 3.5). This is a superior technique used in all of Axon's micropipette current-clamp amplifiers, including the Axoclamp 900A and MultiClamp 700A and 700B.

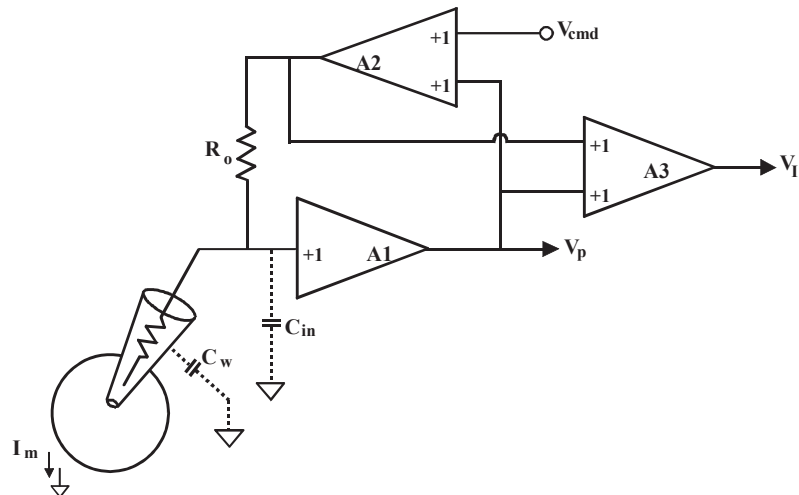


Figure 3.5: Series current measurement.

The circuit in Figure 3.2 is extended by the addition of a differential amplifier (A3) to measure the voltage drop across the current setting resistor, R_o . This voltage drop is proportional to the total current (I) flowing through R_o . For high-frequency currents (*e.g.*, the transient current during a step change in the command potential), the current through R_o is not quite identical to the membrane current (I_m). There is an additional

current that flows through the capacitance (C_w) of the wall of the micropipette and another current that flows into the input capacitance (C_{in}) of the amplifier. Nevertheless, if precautions are taken to minimize C_w (e.g., shallow bath immersion, Sylgard or mineral oil coating) and C_{in} (e.g., bootstrapped buffer amplifier, capacitance neutralization), the error current in these stray capacitances can be minimized and the output signal, V_1 , is a good representation of the membrane current.

Another way to measure the true micropipette current is to use a separate circuit called a “virtual ground” (Figure 3.6). Instead of connecting the bath ground electrode directly to ground, it is connected to the virtual ground formed at the negative input of an inverting operational amplifier. The negative input in this configuration is called a “virtual” ground because the operational amplifier endeavors to keep the negative input equal to the ground potential at the positive input. To achieve this goal, the operational amplifier output must continuously pass a current through the feedback resistor (into the node at the negative input) that is equal and opposite to the bath ground current. Thus the voltage at the output of the operational amplifier is directly proportional to the bath current.

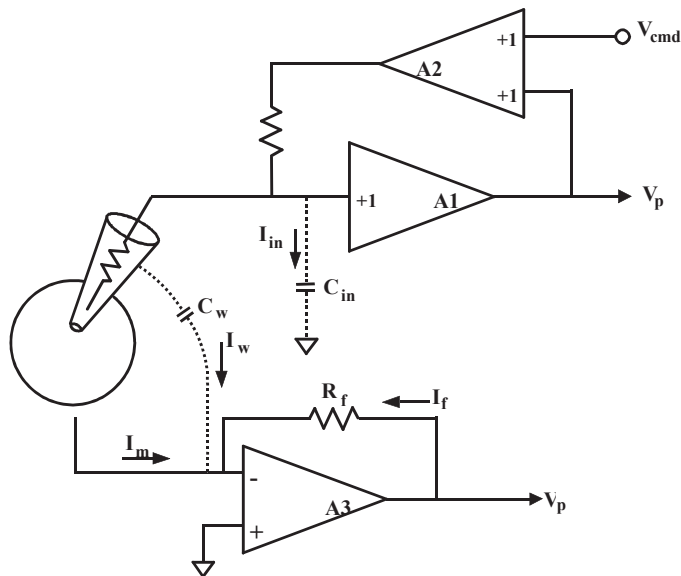


Figure 3.6: Virtual-ground current measurement.

The bath grounding electrode is connected to the negative input of operational amplifier A3. The output (V_1) continually adjusts to pass current through the feedback resistor (R_f) equal and opposite to the total current flowing into the junction at the negative input of A3. The potential at the negative input is “virtually” equal to ground at all times. Most of the current measured by A3 is the membrane current, I_m . However, during rapid potential changes, transient current flows through the capacitance (C_w) of the wall of the micropi-

ette and the input capacitance (C_{in}) of the amplifier. The current (I_w) through C_w flows into the bath and is recorded by the virtual-ground circuit. The current (I_{in}) through C_{in} flows into the system ground and is not recorded by the virtual-ground circuit.

Since the series current-measurement technique is much more convenient, it is routinely used in preference to the virtual-ground current-measurement technique. The virtual-ground technique is inconvenient for several reasons:

- 1 The input lead to the virtual ground is very sensitive and easily picks up line-frequency and other interference.
- 2 It is extremely difficult to use two microelectrode amplifiers in the same preparation bath if one or both of them uses a virtual-ground current-measurement circuit. If one amplifier uses a virtual ground, the individual micropipette currents will be difficult to identify because the virtual-ground current monitor measures the summed current from all sources. If two amplifiers use a virtual ground, large DC-error currents will flow between the virtual-ground circuits because of the small differences in offset voltages between the two circuits. This is equivalent to the problem that would exist if two voltage sources were connected in parallel.
- 3 The virtual-ground probe is just one more box of electronics that has to be mounted in the crowded space around the preparation bath.

Nevertheless, the virtual ground technique is still used in some circumstances, most commonly with high-voltage two-electrode voltage-clamp amplifiers, because of the technical difficulty of making a series current-measurement circuit operate at high voltages.

The Bath Error Potentials section below describes an important variation on the virtual-ground design to eliminate the voltage error due to current flow through the grounding electrode.

3.2.6. HEADSTAGE CURRENT GAIN

The HS-9A and HS-2A headstages used with the Axoclamp 900A and Axoclamp 2B amplifiers all have unity voltage gain but come in a variety of current-passing capabilities. The current-passing range and resolution are determined by the size of a single resistor in the headstage. This resistor (R_o) has two functions. In addition to determining the size and resolution of the current that can be passed, it also determines the sensitivity with which current is measured. In the standard HS-9A headstage, R_o is 10 M Ω ; this is arbitrarily assigned a current-passing gain of $H = 1$. To pass more current, a headstage with a smaller value of R_o is required. The headstage with $R_o = 1$ M Ω can pass ten times as much current as the standard headstage; it is assigned a current-passing gain of $H = 10$. The headstage designed for ion-sensitive micropipettes can only pass very tiny currents. The value of R_o in this headstage is 100 G Ω ; the current-passing gain is $H = 0.0001$.

3.2.7. CAPACITANCE COMPENSATION

The high-frequency performance of the micropipette amplifier is compromised by the presence of capacitance at the amplifier input. This capacitance comes from several

sources: the capacitance across the glass wall (transmural capacitance) of the immersed part of the micropipette; the stray capacitance from the rest of the micropipette to nearby grounded surfaces; the stray capacitance from the micropipette holder; and the capacitance to ground at the input of the buffer operational amplifier.

The input capacitance and the micropipette form a simple low-pass filter. That is, high-frequency signals at the tip of the micropipette are shunted to ground by the input capacitance. There are several ways to improve the bandwidth of the recording system.

The best is to minimize the physical magnitude of the various elements contributing to the input capacitance. The transmural capacitance of the immersed part of the micropipette can be quite large. Typically, it is 1 pF or more per millimeter of immersion depth. An effective way to reduce this capacitance is to thicken the wall of the micropipette. This can be done by coating the micropipette with Sylgard or an equivalent material (see Chapter 4). Other materials have been used, and in extreme cases, researchers have used a wide micropipette to form a jacket over the narrower recording micropipette.

The other obvious way to reduce the transmural capacitance is to reduce the fluid level so that the immersion depth is minimal. This is not always as effective as might be expected, because surface tension causes the bath solution to creep up the surface of the micropipette. This generates significant capacitance between the inside of the micropipette and the film of solution on the outside. Forming this film can be prevented by making the surface of the micropipette hydrophobic by dipping the filled micropipette into mineral oil (or silane) immediately before using it. Note that it is essential to fill the micropipette first with the aqueous electrolyte pipette solution so that the aqueous solution prevents the mineral oil from entering the tip. Finally, one should try not to place the holder or the microelectrode too close to grounded surfaces (such as the microscope objective).

Once the physical magnitude of the stray capacitance has been minimized, electrical techniques can be used to reduce the effective magnitude. There are three such techniques:

- 1** Some researchers surround the micropipette with a metal shield that is connected to the unity-gain output of the buffer amplifier. The principle here is to make sure that the stray capacitance does not have a signal voltage across it. As long as there is no signal voltage across the capacitance, no high-frequency current is drawn and the bandwidth is increased. Unfortunately, this technique can significantly compromise the noise performance of the amplifier because random noise generated in the buffer amplifier is coupled back into its input via the shield capacitance. For this reason, MDS Analytical Technologies does not recommend the use of a driven shield.
- 2** Unity-gain feedback can be used to reduce the component of stray capacitance that exists between the amplifier input and its power supplies and case (Figure 3.7). In a technique known as “bootstrapping,” sophisticated circuitry is used to superimpose the unity-gain output of the buffer amplifier back onto its own power supplies and the headstage case. This eliminates the high-frequency current loss through the power supply capacitance and consequently increases the bandwidth. Since the power supply

capacitance is present whether or not the power supply is bootstrapped, there is no noise penalty due to implementing the technique. Bootstrapped power supplies are implemented in the Axoclamp 900A and MultiClamp 700B amplifiers and contribute to their excellent noise and bandwidth characteristics.

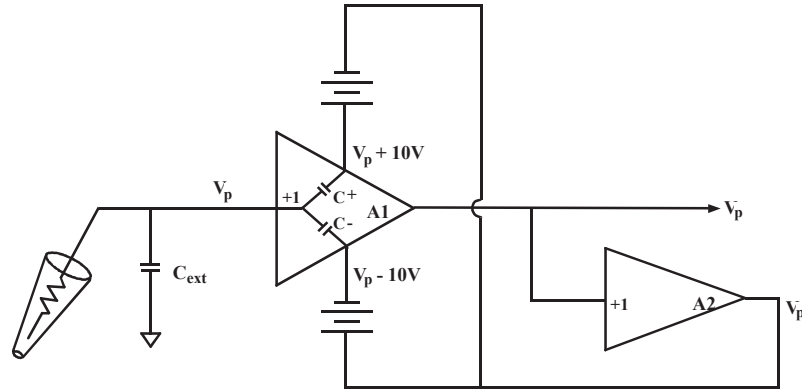


Figure 3.7: Bootstrapped power supplies.

Bootstrapped power supplies are used to increase the bandwidth by minimizing the high-frequency current loss through the power-supply capacitance. The power-supply capacitance is made up of C^+ and C^- from the positive input of A1 to the positive and negative power supplies, respectively. All of the stray capacitances other than C^+ and C^- are lumped together and called C_{ext} in this figure. The power supplies of A1 are batteries. The center point of the batteries is connected to a buffered version of V_p . If the batteries are 10 V, the power supplies for A1 are $(V_p + 10\text{ V})$ and $(V_p - 10\text{ V})$. The voltages across C^+ and C^- are constant at +10 V and -10 V, respectively. Hence, there are no transient currents in neither C^+ nor C^- , except at very high frequencies where these simple amplifier models are not appropriate. To ensure stability, the bandwidth of A2 must be half or less of the bandwidth of A1. In practical implementations such as the MultiClamp 700B and Axoclamp 900A microelectrode amplifiers, the batteries are simulated by electronics.

- 3 Finally, but not least, the technique known as “capacitance compensation” or “negative capacitance” can be used to reduce the effective value of whatever capacitance remains. An amplifier at the output of the unity-gain buffer drives a current-injection capacitor connected to the input (Figure 3.8). At the ideal setting of the amplifier gain, the current injected by the injection capacitor is exactly equal to the current that passes through the stray capacitance to ground. If the amplifier gain is increased past the ideal setting, the current injected back into the input will cause the input signal to overshoot. As the gain is increased past a certain setting, the circuit will oscillate with potentially disastrous consequences for the cell.

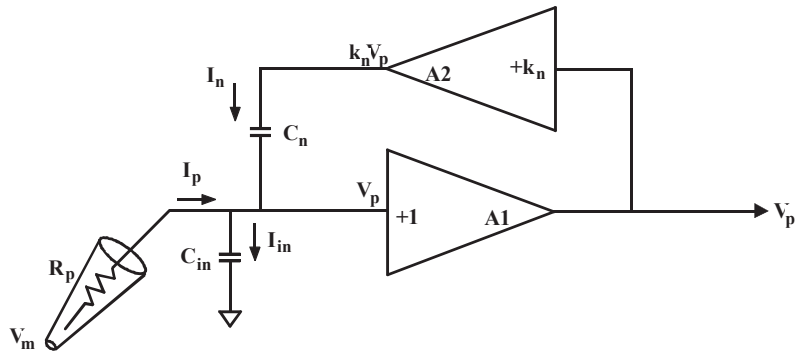


Figure 3.8: Capacitance neutralization circuit.

Amplifier A2 places a voltage proportional to the pipette potential (V_p) across the capacitance-neutralization capacitor (C_n). At a particular setting of the gain (k_n) of A2, the current (I_n) through C_n is exactly equal to the current (I_{in}) through the stray capacitance (C_{in}) at the input of A1. By conservation of current, the pipette current (I_p) is zero. In the ideal case, the effective capacitance loading the pipette resistance (R_p) is zero and the bandwidth is therefore very high. In practice, limitations due to the finite bandwidth of the amplifiers, the distributed nature of C_{in} and other second-order effects limit the recording bandwidth.

An important consideration in the design of a capacitance neutralization circuit is to avoid introducing much additional noise from the circuitry itself. Low-noise amplifiers must be used and the size of the injection capacitor must be small. Axon Cellular Neuroscience HS-2 series headstages were produced in two varieties. The low-noise “L” series headstages used a 3 pF injection capacitor. The medium-noise “M” series headstages used a 10 pF injection capacitor. Generally, the M series headstages were only used for the current-passing micropipette (ME2 on an Axoclamp 900A amplifier) in a two-micropipette voltage-clamp setup. Noise in this micropipette is less important than noise in the voltage recording micropipette (ME1), and it is sometimes useful to have a larger compensation range on the current-passing micropipette.

With the Axoclamp 900A amplifier, the HS-9A headstage series was introduced. These headstages have an increased capacitance neutralization range (-10 to 35.5 pF), independent of the gain of the headstage. These headstages can be used equally effectively as voltage-recording or current-passing electrodes with the Axoclamp 900A amplifier. The choice of HS-9A headstages for TEVC depends on the size of the typical current to be measured.

A problem often encountered in TEVC is saturation of the amplifier output, because of the limits imposed by the power supply ultimately supplying the current to the microelectrode. If the optimum gain of the capacitance neutralization amplifier is moderately high,

(*e.g.*, 2), the amplifier may saturate during large signals. In many experiments, large inputs would be unusual, and even if they occurred the speed penalty incurred would not be disastrous. However, in two-electrode voltage clamp experiments, large signal excursions are common and speed is crucial. To eliminate the saturation of the capacitance compensation circuit, the Axoclamp 900A amplifier uses ± 180 V amplifiers in the capacitance neutralization circuit in two-electrode voltage clamp mode.

If everything were ideal, the bandwidth of the recording system would approach the bandwidth of the buffer amplifier alone (typically a few megahertz). However, in practice the bandwidth is limited by the phase delays in the capacitance compensation pathway, and by the false assumption that the stray capacitance can be represented by a lumped capacitor at the input of the amplifier. The capacitance is distributed along the length of the micropipette. Nevertheless, the techniques described above can be used to substantially improve the bandwidth. It is not unusual to achieve bandwidths of 30 kHz with micropipettes that would have a bandwidth of just one or two kilohertz if the above techniques were not implemented.

3.2.8. LEAKAGE CURRENT

Ideally, a micropipette headstage should pass zero current into the micropipette when the current command is at zero. In practice, there is a leakage current created from two sources. The first is the inherent bias current of the operational amplifier's input. This is usually of the order of a few picoamps or less. The second is the current that flows through the current injection resistor (R_o in Figure 3.2) because of voltage offsets in the current-control circuitry. A trim potentiometer can be used to reduce this offset. In fact, an optimal setting can be found where a small offset is left across R_o so that the resistor current compensates the operational amplifier bias current and leaves a net zero current through the micropipette. However, the leakage current will quickly grow again to unacceptable levels if the offsets in the control circuitry change significantly with temperature or time. To avoid this problem, MDS Analytical Technologies uses extremely high-quality, low-drift operational amplifiers in its Axon Cellular Neuroscience micropipette amplifiers.

3.2.9. HEADSTAGES FOR ION-SENSITIVE MICROELECTRODES

The most demanding application in terms of low-leakage current requirements is the measurement of ion concentration using ion-sensitive microelectrodes (ISMs). In spite of the current popularity about ion-sensitive intracellular dyes, ISMs are still the best means available for determining extracellular and, in some cases, intracellular ion concentrations. These electrodes can be very difficult to fabricate because of the efforts required to place the highly hydrophobic ion-sensitive resin at the very tip of the electrode. Due to the hydrophobic nature of the liquid resin, ISMs are also very sensitive to current passing into the electrode. Even the tiniest amount of leakage current from the headstage can cause the resin to move. If the resin leaks out of the electrode it can contaminate the preparation and destroy cells in the vicinity of the electrode. If the resin moves up the barrel of the pipette, the response of the electrode is slowed dramatically or destroyed.

There are two ways to ensure low-leakage currents for these microelectrodes: First, use special operational amplifiers that have bias currents of just a few tens of femtoamps. Second, make the value of R_o very large (100 G Ω) so that the current induced by small offset voltages across R_o is small.

3.2.10. BATH ERROR POTENTIALS

In most experiments, the bathing solution is grounded by a solid grounding electrode (such as an Ag/AgCl pellet in the bath, or which can be connected to the bath via an agar/KCL bridge) and all measurements are made relative to ground, on the assumption that the bath is also at ground. This assumption may not be true in experiments in which the Cl⁻ concentration or temperature of the bathing solution is significantly changed, or where the membrane current is sufficiently large to cause a significant voltage drop across the resistance of the grounding electrode. The latter circumstance would normally occur only when voltage clamping very large cells such as frog oocytes, in which case the ionic current may be of the order of several microamps or even several tens of microamps.

Depending upon the grounding method, the resistance of the bath grounding electrode (R_b) could be as much as 10 k Ω , although with care it is not difficult to achieve R_b values less than 1 k Ω .

In a simple two-electrode voltage clamp (TEVC) setup, the voltage drop across R_b is indistinguishable from the membrane potential. That is, the potential (V_1) recorded by the voltage-recording micropipette is the sum of the transmembrane potential (V_m) and the bath potential (V_b). Problems arise if the product of the clamp current (I_2) and R_b is significant. For example, for $I_2 = 5 \mu\text{A}$ and $R_b = 2 \text{k}\Omega$, the error voltage is 10 mV. In some experiments, a worst-case error of this magnitude might be tolerable; but if the error were to be much greater, the position of the peak of I-V curves and other responses would be seriously affected.

To faithfully record V_m , either V_b must be made equal to or nearly equal to zero, or the value of V_b must be independently measured and subtracted from the potential recorded by ME1. There are several methods to choose from:

- 1 The best method is to minimize R_b in the first place.
- 2 Electronically predict and subtract the error voltage. This technique is known as “series-resistance compensation.”
- 3 Use an independent electrode to measure V_b and subtract this value from V_1 .
- 4 Set up an independent clamping circuit to clamp V_b , measured near the surface of the cell, to zero.
- 5 Set up an independent virtual-ground circuit to clamp V_b , measured near the surface of the cell, to zero, while simultaneously measuring the bath current.

Minimizing R_b

There are three main contributors to R_b :

- 1 The cell access resistance from the membrane surface to the bath.
- 2 The resistance of an agar bridge, if used.
- 3 The resistance of the grounding wire.

Cell Access Resistance

The access resistance to a sphere is given by:

$$R_a = \frac{\rho}{4\pi r} \quad (1)$$

where ρ is the resistivity (typically 80 Ωcm for Ringer's solution at 20 °C [Hille, 1984]) and r is the radius of the sphere in centimeters.

Modeling an oocyte as a 1 mm diameter sphere:

$$R_a = 127 \Omega$$

Resistance of an Agar Bridge

The resistance of a cylindrical agar bridge is given by (Hille, 1984):

$$R_{agar} = \frac{\rho \times \text{length}(cm)}{\text{area}(cm^2)} \quad (2)$$

where length refers to the length of the agar bridge and area is the cross-sectional area of the agar bridge.

For a 1 cm-long agar bridge with a 2 mm internal diameter (ID) filled with Ringer's solution:

$$R_{agar} = 2.6 \text{ k}\Omega$$

For an agar bridge 1 cm long x 1 mm ID, filled with Ringer's solution:

$$R_{agar} = 10.2 \text{ k}\Omega$$

The resistivity of 3 M KCl is approximately 20 times lower than for Ringer's solution. Thus, for an agar bridge filled with 3 M KCl, having the same length as above:

$$R_{agar} = 130 \Omega \text{ if the ID is 2mm}$$

$$R_{agar} = 510 \Omega \text{ if the ID is 1mm}$$

Resistance of Grounding Wire

When immersed in 0.9% saline, the impedance of a 1 mm diameter Ag/AgCl pellet is in the range of 300–600 Ω , depending on how much of the surface is in contact with the saline.⁴

Conclusion

The access resistance to the cell is quite small and beyond the control of the experimenter. The other major contributors to R_b are the resistance of the agar bridge and the resistance of the grounding electrode.

To minimize R_b , it would be best to eliminate the agar bridge and ground the preparation directly with an Ag/AgCl pellet. The pellet should be as large as practical, and the area of contact between the pellet and the solution should be maximized.

However, if the bathing solution is changed during the experiment, the DC offset of the Ag/AgCl pellet will change with the chloride activity. Thus, in this case it is essential to either use an agar bridge to prevent the DC offset of the bath from changing, or to use a bath-potential recording headstage with a 3 M KCl electrode to follow and remove the shift. Another advantage of an agar bridge is that it prevents metal ions from the grounding electrode from entering the bathing solution.

If an agar bridge is used, it is best to fill it with 3 M KCl instead of Ringer's solution in order to minimize R_b . When the agar bridge is filled with 3 M KCl, the sum of all components of R_b will be approximately 1–2 k Ω . If leakage of KCl from the agar bridge is a problem, it may be necessary to fill the agar bridge with Ringer's solution. In this case, R_b will be several kilohms or more.

Series-Resistance Compensation

This sophisticated technique is used to minimize the effects of the electrode resistance in a whole-cell voltage clamp. It is described later in this chapter and is of paramount importance when there is no alternative available. However, series-resistance compensation is never completely effective. The other methods discussed in this section are more reliable and easier to apply when it comes to eliminating the voltage error across R_b .

4. Measurements made at Axon Instruments, Inc. using a 700 Hz signal source.

Measure and Subtract V_b

Another technique used to eliminate the effects of the IR voltage drop across the bath resistance is to actively measure the bath potential outside the cell.

In this method, the bath is grounded by any preferred method. The bath potential is allowed to shift because of solution changes, temperature changes or current flow. The changing values of the bath potential (V_b) are continuously monitored by a 3 M KCl-filled electrode placed near the cell. The measured value of V_b is subtracted from the potentials measured by the intracellular microelectrodes. For microelectrodes being used for voltage recording, this subtraction yields the true transmembrane potential (V_m). The signal provided to all subsequent circuits in the amplifier is V_m .

This method operates well. The minor inconveniences are the more complex electronics, the noise of the bath electrode that is added to the noise of the intracellular recording micropipette, and some (minor) potential for instability in a two-electrode voltage clamp if the bandwidth of the bath potential headstage is greater than the bandwidth of the intracellular recording micropipette.

Clamp V_b Using a Bath Clamp

Another means to eliminate the effect of the voltage drop across R_b is to actively control the bath potential measured near the outside surface of the cell. This is achieved using a two-electrode virtual-ground circuit (Figure 3.9). One electrode (SENSE) is a voltage-sensing electrode. This electrode is placed in the preparation bath near the cell surface. It is connected to the virtual-ground circuit by an agar bridge or other means, of resistance R_{b2} . Since there is no current flow through this electrode, there is no voltage drop across R_{b2} . The other electrode (I_{BATH}) is placed in the preparation bath. This electrode carries the ionic current. The feedback action of the operational amplifier ensures that the potential at the SENSE electrode is equal to the potential at the negative amplifier input (ignoring the offset voltage at the inputs to the operational amplifier).

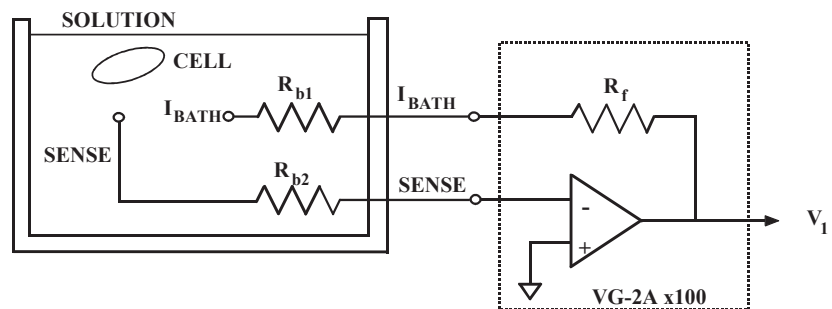


Figure 3.9: Two-electrode virtual-ground circuit.

In this implementation, separate electrodes are used to pass the bath current and control the bath potential (unlike Figure 3.6 above). The basic operation is the same as for the vir-

tual-ground circuit described earlier, except that instead of connecting the feedback resistor directly to the negative input of the operational amplifier, it is connected indirectly via the bath solution. The bath potential near the surface of the cell is recorded by the SENSE electrode (resistance R_{b2}) and forced by the feedback action of the operational amplifier to be near ground. The bath current required to achieve this is passed by the operational amplifier through the feedback resistor (R_f) and through the bath current electrode (I_{BATH} ; resistance R_{b1}).

Clamp V_b Using a Virtual-Ground Current Monitor

This technique is identical to the bath clamp described above, except that in this case instead of being ignored, the output of the circuit is used to monitor the current flowing from the micropipettes into the bath. The output (V_I) of this circuit is proportional to the bath current.

$$V_I = (R_{b1} + R_f)I_{BATH} \quad (3)$$

There are several problems with this technique. First, if the output is used to record the bath current, it is usual to ignore the R_{b1} term (because its value is unknown) and to assume that

$$V_I = R_f I_{BATH} \quad (4)$$

Thus, there is a small error equal to $R_{b1}/(R_{b1} + R_f)$. Second, if there are fluid-filled tubes connected to the bath, and if some of these run outside of the Faraday cage, they will act as antennas and conduct a lot of hum current into the bath that will be recorded by the virtual-ground circuit. Third, if it is desired to use more than one amplifier with the same preparation, it is essential that no more than one of them uses a virtual-ground circuit to clamp the bath potential. This is not a serious problem, since it is easy to make one virtual-ground serve the needs of both amplifiers. The problem is serious, however, if one of the amplifiers introduces command signals via the virtual-ground bath clamp. This is a practice employed by some manufacturers because in some circumstances it is easier to design the electronics for this mode of operation. However, if command potentials are introduced via the bath electrode, it is extremely difficult to perform experiments using two amplifiers, *e.g.*, whole-cell patch clamp of two fused cells.

When used with consideration for the measurement error, and if hum pick up is avoided, a virtual-ground circuit to measure I_{BATH} offers excellent performance.

Summary

As a first priority, we recommend that the value of R_b be minimized by the techniques described above. If it is still considered to be important to compensate for the IR voltage drop, a virtual-ground headstage (such as the VG-9A series) can be used to clamp the bath

potential, or a unity-gain voltage follower headstage (such as the HS-9A and HS-2A series) can be used to record and subtract the bath potential.

3.2.11. CELL PENETRATION: MECHANICAL VIBRATION, BUZZ AND CLEAR

Often when a micropipette is pressed against a cell, the membrane dimples but the micropipette fails to penetrate. A variety of methods are used to overcome this problem. The oldest and frequently effective trick is to tap the micromanipulator gently. Since this “method” is difficult to calibrate and reproduce, two electronic alternatives are widely used. One is to drive a brief, high-frequency oscillatory current through the micropipette. This is often done by briefly increasing the capacitance compensation such that the compensation circuit oscillates. On the Axoclamp amplifiers, a dedicated feature called “Buzz” is provided for this purpose. On the Axoclamp 900A amplifier, this feature has a duration control setting; on the Axoclamp 2B amplifier, buzz duration can also be controlled via its remote buzz accessory unit. The duration used should be long enough for penetration, but short enough to prevent damage to the cell. The mechanism of penetration is unknown, but it may involve attraction between the charge at the tip of the micropipette and bound charges on the inside of the membrane.

The second electronic alternative is to drive a large positive or negative current step into the cell.

In the Axoclamp 900A amplifier, both the duration and height of the current pulse are adjustable. Again, the mechanism of penetration is not known. One cannot even predict *a priori* whether a positive or a negative pulse will be more effective.

None of the three methods described here can be described as “best.” For a particular cell type, the researcher must experiment to find the method that works best with those cells.

3.2.12. COMMAND GENERATION

In general, current and voltage commands arise from a variety of sources; internal oscillators in the instrument, internal DC current or voltage controls, external input from a computer, *etc.* These commands are usually summed in the instrument so that, for example, an externally generated step command can be superimposed on the internally generated holding potential.

An important consideration when using externally generated commands is the attenuation provided by the instrument’s command input. Manufacturers attenuate the external command so that the effects of noise and offset in the external signal generator are minimized. Noise is particularly common on the analog output of most computer interfaces. To illustrate the problem, imagine a micropipette amplifier used for current injection into cells that has a current passing capacity of ± 100 nA maximum. Compare the situation for two different values of the command input attenuation. In the first case, the amplifier passes 1 nA for each millivolt from the computer. If there is a 2 mV of wide-band digital noise on the output of the D/A converter, this will generate 2 nA of noise in the recording a substantial fraction of the usable range. Further, if the D/A converter had a 3 mV offset,

then instead of a command of zero generating 0 nA, it would generate 3 nA. In the second case, the amplifier passes 1 nA for each 100 mV from the computer. This time, the 2 nA of noise from the D/A converter only generates 20 pA of noise in the recording, and the 3 mV offset error only generates a 30 pA current error. The full ± 100 nA range of the amplifier can still be controlled, since most D/A converters produce up to ± 10 V.

All of the Axon Cellular Neuroscience current-clamp and voltage-clamp instruments from MDS Analytical Technologies use the maximum possible attenuation so that the ± 10.24 V output from the D/A converter corresponds to the normal maximum operating limits of the instrument.

Another important consideration when using externally generated commands is the presence or absence of polarity inversion. To minimize the risk of making mistakes during an experiment, it is best that the instrument does not invert the command signal. Thus the user should always know that a positive command from the computer will generate a positive current or voltage in the instrument.

3.3. INTRACELLULAR RECORDING—VOLTAGE CLAMP

In the voltage-clamp technique, the membrane potential is held constant (*i.e.*, “clamped”) while the current flowing through the membrane is measured. Usually, the investigator has no inherent interest in the membrane current, but is interested in the membrane conductance, since conductance is directly proportional to the ion-channel activity. Current is measured because the investigator has no direct way of measuring conductance. By holding the membrane potential constant (or at the very least, constant after a rapid step), the investigator ensures that the current is linearly proportional to the conductance being studied.

Micropipette voltage-clamp techniques for whole-cell current measurement traditionally assign the role of potential measurement and current passing to two different intracellular micropipettes. This is done using the conventional two-electrode voltage-clamp technique, or it is simulated by time-division multiplexing (time-sharing) using the discontinuous single-electrode voltage-clamp technique. Separation of the micropipette roles by either of these methods avoids the introduction of errors in the measurement due to unknown and unstable voltage drops across the series resistance of the current-passing micropipette.

The so-called “whole-cell patch” voltage clamp is a technique wherein only one micropipette is used full-time for both voltage recording and current passing. A method known as series-resistance compensation (see Section 3.3.7., “*Series-Resistance Compensation*”) attempts to eliminate the aberrations arising when one micropipette is made to perform the work of two. For series-resistance compensation to work, the micropipette resistance must be reasonably low compared to the impedance of the cell. Since the resistance of intracellular micropipettes generally is too high, researchers use very blunt micropipettes that can be tightly sealed to a patch of membrane. The patch of membrane is subse-

quently ruptured so that the micropipette provides a low-resistance access to the whole cell, hence the term “whole-cell patch” clamp.

3.3.1. THE IDEAL VOLTAGE CLAMP

The ideal voltage clamp simply consists of a battery, a switch, a wire, the cell and an ammeter (Figure 3.10). Since the wire has zero resistance when the switch is closed, the membrane potential steps instantly to the battery voltage. This generates an impulse of current that charges the membrane capacitance, followed by a steady-state current to sustain the voltage across the membrane resistance.

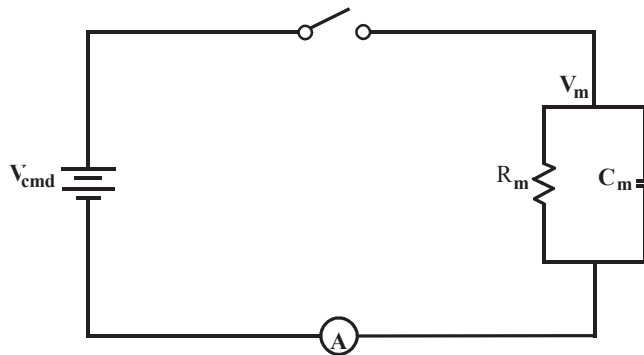


Figure 3.10: The ideal voltage clamp.

The ideal voltage clamp simply consists of a battery, a switch, a wire, the cell and an ammeter. When the switch closes, the membrane potential steps instantly to the battery voltage. (For simplicity, it is assumed that $V_m = 0$ before the step.) There is an impulse of current injecting a charge $Q = C_m V_{cmd}$; the steady-state current is V_{cmd}/R_m .

In this experiment, the voltage is the independent variable. Its value is controlled and equal to the battery value. The current is the dependent variable; its value is measured by an ammeter. For this reason, the voltage-clamp circuit is sometimes called a “current follower.”

3.3.2. REAL VOLTAGE CLAMPS

There are many reasons for real voltage clamps to be inferior to the ideal voltage clamp. These include finite resistance of the current-passing micropipette, limited bandwidth of the voltage-recording micropipette, capacitive coupling between the two micropipettes, limited bandwidth of the clamp amplifier, and non-ideal phase shifts in the membrane. These phenomena and the minimization of their impact are discussed in the following sections.

3.3.3. LARGE CELLS—TWO-ELECTRODE VOLTAGE CLAMP

The theory of two-electrode voltage clamping is discussed in detail by Finkel and Gage (1985). Without attempting to duplicate that discussion, some of the most important conclusions will be presented here.

A conventional two-electrode voltage clamp is shown in Figure 3.11. This figure has been simplified by ignoring several frequency-dependent components: the input capacitance at the input of micropipette ME1, the coupling capacitance between the micropipettes, and the special phase lead and lag circuitry that is often introduced deliberately into the electronics. Furthermore, series resistance in the membrane and the bathing solution has been ignored. In the figure, the sole frequency-dependent component is the membrane capacitance.

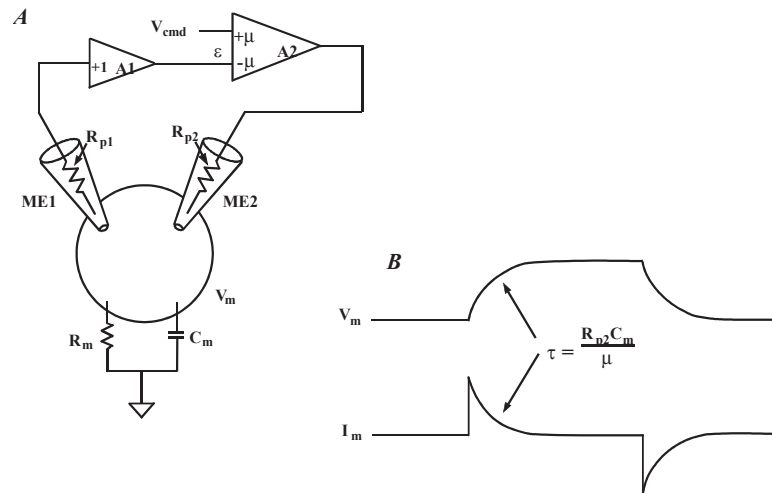


Figure 3.11: Conventional two-electrode voltage clamp.

- A. The membrane potential (V_m) is recorded by a unity-gain buffer amplifier (A1) connected to the voltage-recording microelectrode (ME1). V_m is compared to the command potential (V_{cmd}) in a high-gain differential amplifier (A2; gain = μ). The output of A2 is proportional to the difference (ϵ) between V_m and V_{cmd} . The voltage at the output of A2 forces current to flow through the current-passing microelectrode (ME2) into the cell. The polarity of the gain in A2 is such that the current in ME2 reduces ϵ .
- B. Unlike the ideal case, there is a finite time required to charge the cell capacitance. The time constant for the current and potential transients is $\tau = R_{p2} C_m / \mu$, where R_{p2} is the resistance of ME2. If it was infinite, or if R_{p2} was zero, the response would approach the ideal case.

Error

The steady-state membrane potential (V_m) after a step change in the command voltage (V_{cmd}) is:

$$V_m = V_{cmd} \frac{\mu K}{\mu K + 1} \quad (5)$$

where μ is the gain of the clamp amplifier and K is the attenuation of the clamp amplifier caused by the cell membrane resistance (R_m) and the resistance (R_{p2}) of the output micropipette (ME2):

$$K = \frac{R_m}{R_m + R_{p2}} \quad (6)$$

As the product μK becomes very large, the difference between V_m and V_{cmd} becomes very small. Ideally, the error will be very low: just a fraction of one percent. The gain of the clamp μ is typically set by a front-panel gain control in the range of about 100 to 10,000. If K were unity, the error would vary from 1 percent down to 0.01 percent. However, if K is less than unity (as it always is), the error will be worse. If the output micropipette resistance is 90 M Ω and the membrane resistance is 10 M Ω , K is 0.1 and the error will be ten times worse than if K were unity. If the two resistances are equal, K will be 0.5. Thus, as a rule of thumb it is desirable to use an output micropipette whose resistance is as low as possible, ideally about the same size or smaller than the membrane resistance.

Step Response and Bandwidth

After a step command, the membrane potential relaxes exponentially towards its new value. For $\mu K \gg 1$, the time constant for the relaxation is:

$$\tau = \frac{R_{p2} C_m}{\mu} \quad (7)$$

Increasing the clamp gain decreases the time constant for the step response. For example, if $R_{p2} = 10$ M Ω , $C_m = 1000$ pF and $\mu = 100$, the time constant is 100 μ s.

Stated differently, increasing the clamp gain also increases the bandwidth with which V_m can follow changes in V_{cmd} . The -3 dB frequency of the bandwidth is:

$$f_{-3} = \frac{\mu}{2\pi R_{p2} C_m} \quad (8)$$

Stability

The voltage clamp circuit shown in Figure 3.12 is unconditionally stable. The membrane capacitance provides a 90° phase shift, which is required for stability in all negative feedback circuits. Unfortunately, other factors combine to make the circuit unstable at high clamp gains.

The coupling capacitance (C_x) between the micropipettes is extremely destabilizing. Values as small as 0.01 pF can lead to oscillation if μ has a magnitude of several hundred or more. There are several ways to minimize this coupling capacitance. The two best ways are by:

- 1 Introducing the two micropipettes into the preparation at a wide angle, preferably greater than 90°.
- 2 Placing a grounded metal shield between the two micropipettes. This shield should be large enough to block all line-of-sight pathways between the two micropipettes and their holders.

Another destabilizing factor is the non-ideal nature of the membrane. In Figure 3.11, the membrane is simply modeled as a parallel resistor and capacitor. In practice, a distributed model applies. The capacitance elements are themselves non-ideal; they should be modeled by an ideal capacitor with a series-resistance component. For real membranes, the phase shift at high frequencies is less than 90°. In the Axoclamp 900A amplifier, a phase-shift control is included to allow the user to empirically introduce a phase lag to the circuit to build the total high-frequency phase shift up to 90°.

The input capacitance of the voltage-recording micropipette (ME1) adds another frequency-dependent variable into the system that also tends to decrease the stability. The effect of this input capacitance is usually minimized by carefully adjusting the capacitance neutralization control to maximize the bandwidth of ME1.

Small instabilities in the voltage clamp usually show up as an overshoot in the current and voltage responses. Full instability shows up as a continuous oscillation that can destroy the cell. In some voltage clamps, special circuits are used to detect oscillations and take appropriate action to avoid damage to the cell. The Axoclamp 2 series and the GeneClamp[®] 500 amplifiers do not include an oscillation guard circuit. The Axoclamp 900A amplifier includes an oscillation detection feature that automatically reduces the voltage clamp gain, protecting the cells from harm.

Membrane Conductance Changes

It can be shown that the current response to a step change in the membrane conductance is identical to the membrane potential response to a step change in the command voltage. This is fortunate, because it means that if the voltage clamp is set up optimally by observing the response to a repetitive command step, it is also optimally set up for measuring conductance changes. In order for this equivalence to be maintained, it is essential that the experimenter not use tricks such as filtering the command voltage to eliminate an

overshoot in the response. This is a bad practice because it disguises the dynamic performance of the clamp circuit.

Noise

There are several sources of noise in a two-electrode voltage-clamp circuit, but the most important is the thermal and excess noise of the input micropipette, ME1. To the voltage-clamp circuit, this noise appears as an extra command signal. It is imposed across the membrane and leads to a noise current. Because of the membrane capacitance, this noise current increases directly with frequency in the bandwidths of interest. The magnitude of the noise is worst in cells with large C_m values.

Since the current noise increases with frequency, a single-pole filter is inadequate. An active two-pole filter is required at minimum; while a four-pole filter is preferred. The Axoclamp 900A amplifier includes a four-pole filter with a corner frequency up to 30 kHz on each output. The user can choose between a Bessel and a Butterworth filter.

Micropipette Selection

Ideally, both micropipettes should have very small resistances. The resistance of ME1 should be small to minimize the micropipette noise, and the resistance of ME2 should be small to maximize the product μK . However, low-resistance micropipettes are more blunt than high-resistance micropipettes and do more damage to the cell. In general, it is more important to use a low resistance micropipette for ME2. If its value is high, the amplifier's power supply will saturate at a lower current, causing a voltage-clamp error because the ME2 headstage cannot inject enough current to hold the membrane voltage "clamped." As a result, the recorded data will be of dubious merit. A relatively high-resistance micropipette for ME1 has its problems—increased noise and reduced bandwidth—but at least it does not introduce an error.

Input vs. Output Offset Removal

Certain offset-removal circuits act only on the output signal delivered to the oscilloscope or data acquisition system. Examples of these are the AC input of the oscilloscope itself, the DC-offset removal in the CyberAmp 380 amplifier, and the output offset controls in the Axoclamp 900A. Adjusting these controls does not affect the membrane currents injected through the micropipette.

On the other hand, some offset-removal circuits act on the input signal seen by the voltage-clamp circuit. For example, the micropipette-offset controls alter the potential that is clamped by the voltage-clamp circuit. Thus the actual membrane potential is affected when these controls are altered and, consequently, the membrane current is affected. Care should be taken not to alter the setting of an input-offset control once the experiment has begun.

3.3.4. SMALL CELLS—DISCONTINUOUS SINGLE-ELECTRODE VOLTAGE CLAMP

In discontinuous single-electrode voltage clamp (dSEVC) the tasks of voltage recording and current passing are allocated to the same micropipette. Time-sharing techniques are used to prevent interactions between the two tasks. The principles of operation are discussed in detail by Finkel and Redman (1985).

A block diagram and a timing diagram illustrating the technique are shown in Figure 3.12. A single micropipette (ME1) penetrates the cell and the voltage recorded (V_p) is buffered by a unity-gain headstage (A1). To begin the discussion, assume that V_p is exactly equal to the instantaneous membrane potential (V_m). A sample-and-hold circuit (SH1) samples V_m and holds the recorded value (V_{ms}) for the rest of the cycle. A sample-and-hold circuit (SH1) samples V_m and holds the recorded value (V_{ms}) for the rest of the cycle.

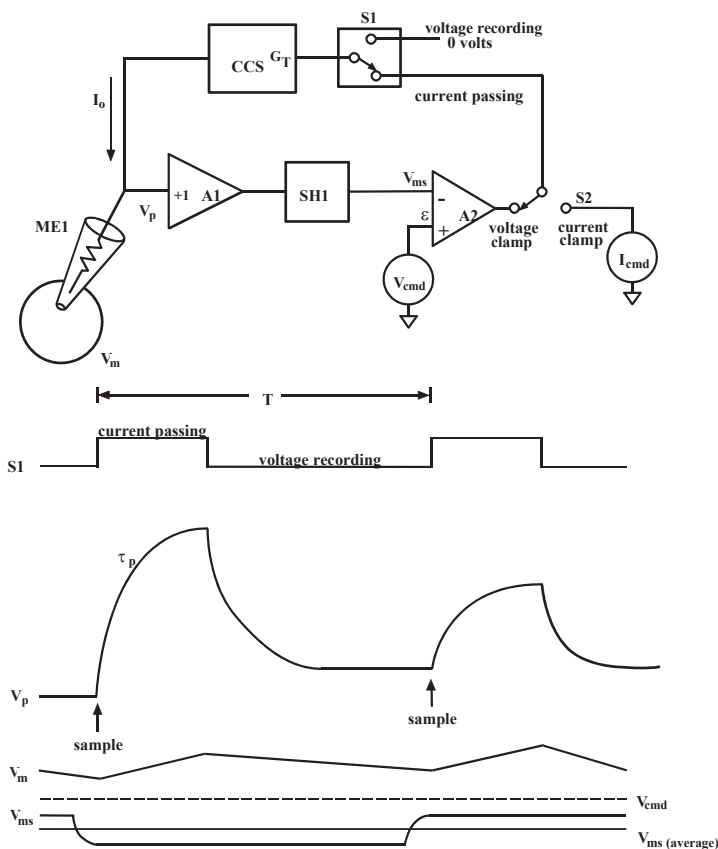


Figure 3.12: Block diagram and timing waveforms.

V_{ms} is compared with a command voltage (V_{cmd}) in a differential amplifier (A2). The output of this amplifier becomes the input of a controlled-current source (CCS) if the switch S1 is in the current-passing position.

The CCS injects a current into the micropipette that is directly proportional to the voltage at the input of the CCS irrespective of the resistance of the micropipette. The gain of this transconductance circuit is G_T .

The period of current injection is illustrated at the start of the timing waveform. S1 is shown in the current-passing position during which a square pulse of current is injected into the micropipette, causing a rise in V_p .

The rate of rise is limited by the parasitic effects of the capacitance through the wall of the glass micropipette to the solution and the capacitance at the input of the buffer amplifier. The final value of V_p mostly consists of the IR voltage drop across the micropipette due to the passage of current I_o through the micropipette resistance R_p . Only a tiny fraction of V_p consists of the membrane potential (V_m) recorded at the tip.

S1 then switches to the voltage-recording position. When the input of the CCS is 0 volts, its output current is zero and V_p passively decays. During the voltage-recording period V_p decays asymptotically towards V_m . Sufficient time must be allowed for V_p to reach within a millivolt or less of V_m . This requires a period of up to nine micropipette time constants (τ_p). At the end of the voltage-recording period, a new sample of V_m is taken and a new cycle begins.

The actual voltage used for recording purposes is V_{ms} . As illustrated in the bottom timing waveform, V_{ms} moves in small increments about the average value. The difference between $V_{ms,avg}$ and V_{cmd} is the steady-state error (ϵ) of the clamp that arises because the gain (G_T) of the CCS is finite. The error becomes progressively smaller as G_T is increased.

Minimum Sampling Rate and Maximum Gain

If the sampling rate (f_s) is too slow, the dSEVC will become unstable. This is because the resultant long current-passing period (T_i) allows the membrane potential to charge right through and past the desired potential before the clamp has had an opportunity to take a new sample of potential and adjust the current accordingly. The larger the cell membrane capacitance (C_m) the larger the value of T_i (and hence the slower the sampling rate) that can be used for a given average gain (G_T). The stability criterion is:

$$0 < \frac{G_T T_i}{C_m} < 2 \quad (9)$$

For optimum response (critical damping) we require:

$$\frac{G_T T_i}{C_m} = 1 \quad (10)$$

Thus for a given G_T , if C_m is small, T_i must be small (*i.e.*, f_s must be large).

For example, if $G_T = 1 \text{ nA/mV}$ and $C_m = 100 \text{ pF}$, then T_i must be $100 \text{ }\mu\text{s}$ for optimum response. If T_i is greater than $100 \text{ }\mu\text{s}$, the step response will overshoot and at $200 \text{ }\mu\text{s}$ the clamp will oscillate. (Note that in Axoclamp amplifiers, $T_i = 100 \text{ }\mu\text{s}$ corresponds to a sampling rate of 3 kHz because the duty cycle (discussed later) is 30% .)

If T_i in this example cannot be as short as $100 \text{ }\mu\text{s}$ because the micropipette response is too slow, then a lower value of G_T will have to be used to maintain optimum response.

Fastest Step Response

In a critically damped system, that is, where the gain has been turned up to achieve the fastest possible response with no overshoot, the clamp can settle to its final value in as little as one or two periods.

Error Number One—Clamping the Micropipette

If the micropipette voltage does not have sufficient time to decay to zero before a new sample of V_m is taken, the sample will include a micropipette artifact voltage. The clamp circuit will be incapable of distinguishing this micropipette artifact voltage from the membrane potential and thus it will voltage clamp the sum of the two potentials. This leads to inaccurate and bizarre data collection. For example, cells with known rectifiers will generate I-V curves that are almost linear.

This error is easily avoided by carefully observing the monitor output on the Axoclamp 900A amplifier. It is essential that the micropipette voltage trace on this output be given sufficient time to decay to zero before the sample is taken. The user can achieve this by adjusting the sampling frequency and by optimizing the micropipette capacitance compensation. With the Axoclamp 900A amplifier, the micropipette voltage monitor is transmitted to the computer through a USB 2.0 connection. When dSEVC is activated, a window displaying the micropipette voltage is automatically displayed. This facilitates the experimenter in observing the micropipette voltage and avoiding clamp errors.

Error Number Two—Steady-State Clamp Error

Even if the sampling is such that there is negligible voltage drop across the micropipette, there will still be a steady-state error due to the finite gain, G_T , of the clamp. To minimize the error, it is necessary to use as high a gain setting as possible, consistent with stable operation.

Ripple in the Membrane Potential

Due to the switching nature of the dSEVC circuit, the actual membrane potential changes during each cycle. The size of the ripple is proportional to the command voltage; for a clamp at the resting membrane potential, the ripple is zero. Typically, the ripple is no more than one or two percent of the command voltage. The actual error between V_m and V_{cmd} is worst at the end of each cycle, just when the sample is taken. Therefore, the presence of ripple means that the average value of V_m is closer to V_{cmd} than is suggested by the sampled voltages.

Aliased Noise and the Anti-Aliasing Filter

The dSEVC is a sampling system, and thus it suffers from the noise amplification property called “aliasing” (see Chapter 11). The only way to prevent aliasing is to sample two or more times more rapidly than the bandwidth of the signal. For example, if the micropipette has a 20 kHz bandwidth, the sample rate should be 40 kHz or more to prevent aliasing. Unfortunately, in the dSEVC there is a competing consideration: the sample period (T) should be at least ten times longer than the micropipette time constant. For a 20 kHz micropipette, the time constant is about 8 μ s; therefore the sampling period should not be less than 80 μ s, equivalent to a 12.5 kHz sampling rate.

The anti-alias filter is a special filter used in the Axoclamp 2-series amplifiers to reduce the bandwidth of the micropipette. Ordinarily, this is not desirable, because the sampling rate has to be reduced to suit. However, some micropipettes have a biphasic decay after a current pulse (Figure 3.13). There is an initial rapid decay as the micropipette capacitance is discharged, followed by a smaller, slower decay resulting from ion redistribution in the tip. For these micropipettes, the maximum sampling rate is severely restricted by the slow phase of the micropipette decay. However, the wide-bandwidth noise of the micropipette is related to the initial fast phase. For these micropipettes, it makes sense to slightly filter the micropipette response to try to remove some of the wideband noise as long as this can be achieved without increasing the ultimate settling time (which is limited by the slow decay). This filtering is provided by a variable single-pole filter called the Anti-Alias Filter. With the Axoclamp 900A amplifier, the anti-alias filter is applied along with the lag filter. This implementation leads to increased clamp stability and speed.

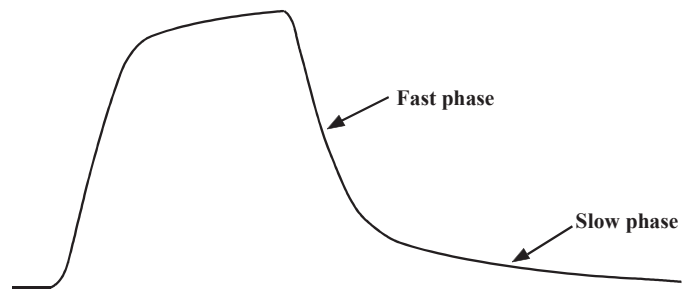


Figure 3.13: Biphasic voltage response of a high-resistance micropipette.

The voltage response of a high-resistance micropipette is often biphasic. The initial fast phase reflects the time constant formed by the micropipette resistance and the stray capacitance. This time constant sets the cutoff frequency for thermal noise. The slow phase is thought to be due to ion redistribution in the tip. The maximum sampling rate during dSEVC is limited by the time taken for the slow phase to settle.

Capacitance Neutralization Noise

Another source of noise in discontinuous single-electrode voltage clamps arises from the capacitance neutralization circuitry. A fundamental property of all capacitance neutralization circuits is that they introduce noise in excess of what is contributed by the thermal noise of the recording micropipette and the input noise of the buffer amplifier. The excess noise becomes progressively larger as the amount of capacitance neutralization is increased to reduce the micropipette time constant. In discontinuous systems the micropipette time constant must be reduced more than in continuous systems because of the need for the micropipette voltage to decay to V_m within the time allotted for passive recording. Compared to a continuous two-electrode voltage clamp, the dSEVC will always be a factor of three or more times noisier at similar gains.

Selecting the Duty Cycle

The duty cycle is the fraction of each period spent in current passing. As the duty cycle approaches unity, the clamp fails to operate properly because insufficient time is left for the micropipette artifact to decay, unless the sampling period is made unreasonably slow. On the other hand, if the duty cycle is made very small, the magnitude of the current pulse becomes very large (to maintain a given average current). Since there are conflicting requirements on the selection of the duty cycle, a compromise must be found. It has been shown that the best compromise is a duty cycle equal to 0.3. This is the value used in the Axoclamp amplifiers.

Useful Signal Bandwidth

As a general rule, the useful signal bandwidth is about one tenth of the switching rate. If the dSEVC is switching at 20 kHz, it is reasonable to expect to record membrane currents to within a bandwidth of 2 kHz.

Current and Voltage Measurement

Since the system is injecting current through the micropipette during every cycle, there is no place that a continuous record of the membrane current and voltage exists. Instead, sample-and-hold amplifiers must be used to store the values measured at the appropriate times.

For the V_m output, the appropriate time to measure the voltage is at the end of the period of passive decay, just before the next current pulse begins. This sampled value is held for the duration of the cycle.

For the I_m output, the current is sampled during the middle of the current pulse. The value is held until the next current pulse. Since the user is interested in the average current

entering the cell, the output of the sample and hold is multiplied by the duty cycle before being presented on the output.

Conditions For Good dSEVC

- 1** The micropipette resistance should be as small as possible.
- 2** The micropipette capacitance should be minimized.
- 3** The membrane time constant must be at least ten times the micropipette time constant.

Comparison with Two-Electrode Voltage Clamp

The TEVC is generally superior to the dSEVC. If the gains are adjusted for a similar steady-state error, the TEVC will generally have just one third of the noise of the dSEVC. If the gain of the TEVC is increased so that the noise of the two clamps is similar, the TEVC will generally settle three times faster.

It is clear that a dSEVC should not be used in preference to a TEVC. It should only be used in those cases where it is impractical to implement a TEVC, either because the cells are not individually discernible or because they are too small.

3.3.5. DISCONTINUOUS CURRENT CLAMP (DCC)

Discontinuous current clamp mode (DCC) uses the same circuitry and principles as the dSEVC mode. The main difference is that in dSEVC the amplitude of each current pulse depends on the difference between the membrane potential and the command potential, whereas in DCC the amplitude is determined by the experimenter. Thus, to inject a constant current into the cell, a DC command is presented and successive current pulses should be identical.

The main use of the discontinuous current clamp technique is to aid in the setup of the instrument before selecting dSEVC. DCC-mode recording has been used in some experiments in place of Bridge-mode recording to eliminate the possibility of a badly balanced Bridge introducing an error in the voltage measurement. However, in general, the advantage of DCC mode is small because in DCC mode the capacitance neutralization control plays a similar role to the Bridge Balance control in continuous current clamping. If the micropipette response is too slow, the transient after the current pulses will not have decayed to baseline before the next sample is taken, and a current-dependent error voltage will be measured. Thus, DCC mode just replaces one problem with another. At the same time, DCC mode has more noise and a lower signal-recording bandwidth, so its use as a substitute for Bridge mode should be undertaken with caution.

3.3.6. CONTINUOUS SINGLE-ELECTRODE VOLTAGE CLAMP (WHOLE-CELL PATCH CLAMP)

To implement a continuous single-electrode voltage clamp (cSEVC; also known as a whole-cell patch clamp), a blunt, low-resistance pipette is sealed by suction to the surface of the membrane. The patch of membrane enclosed within the tip of the pipette is ruptured by one of a variety of techniques. The electrolyte solution in the pipette then forms an electrical continuity with the interior of the cell. It is equivalent to an extremely low-resistance (*e.g.*, 1–10 M Ω) intracellular micropipette.

The voltage at the top of the pipette is controlled by a voltage-clamp circuit. It is important to realize that this is quite different from the situation in TEVC or dSEVC. In both of the latter cases, the voltage at the tip of the voltage-recording micropipette is controlled (remember, in dSEVC, time-division multiplexing effectively yields two micropipettes: the voltage-recording micropipette and the current-passing micropipette). In cSEVC, the same electrode is used simultaneously for voltage recording and for current passing. The voltage recorded at the top of the pipette is the sum of the membrane potential V_m , which the experimenter wishes to control, and the current-induced voltage drop across the pipette.

The current through the series resistance of the pipette and the residual resistance of the ruptured patch is often sufficiently large to introduce significant voltage errors. Techniques exist for compensating these errors. To get a feeling for the magnitude of the errors, assume that the maximum compensation is 90%, beyond which the system oscillates and destroys the cell. Further assume that the access resistance (R_a ; the sum of the pipette resistance and the residual resistance of the ruptured patch) is 5 M Ω . After compensation, the effective value of R_a ($R_{a,eff}$) would be just 0.5–1 M Ω . In this case, a 10 nA current would cause a 50 mV uncompensated voltage error, reduced to 5 mV by the compensation. Clearly, the cSEVC technique cannot be used to record large currents. Even for modest whole-cell currents, care must be taken to compensate for the series resistance and then correctly interpret the residual error. The dSEVC technique should be considered as an alternative to the cSEVC technique when the access resistance is too large.

The temporal resolution of the whole-cell patch clamp is also affected by $R_{a,eff}$. The time constant for resolving currents is the product of $R_{a,eff}$ (assuming that the membrane resistance is much greater) and the membrane capacitance ($\tau = R_{a,eff}C_m$). Thus the technique is also limited to small cells where this product is small enough for the desired time resolution to be achieved. Figure 3.14 illustrates the voltage and temporal errors caused by the presence of R_a .

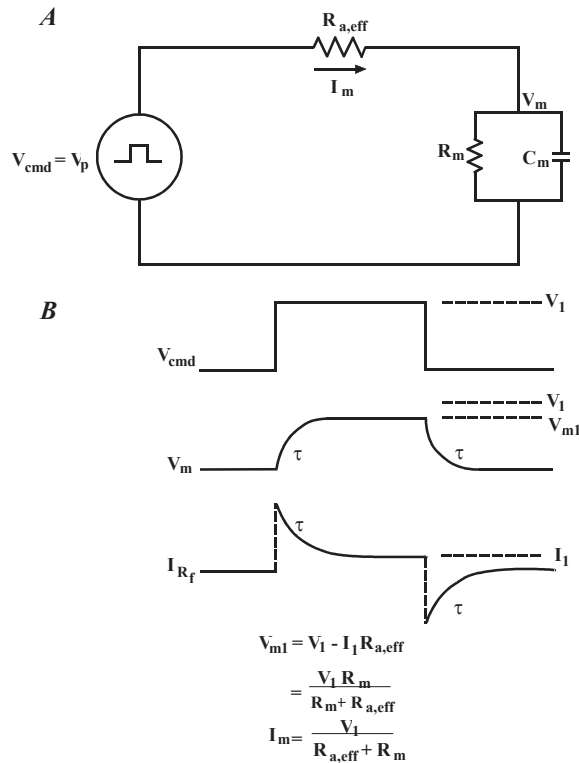


Figure 3.14: Voltage and temporal errors caused by the presence of R_a .

- A. The cSEVC circuit is simply illustrated as a voltage source (V_{cmd}) in series with the effective access resistance ($R_{a,\text{eff}}$) and the membrane (R_m , C_m). The cSEVC circuit ensures that the pipette potential (V_p) is equal to V_{cmd} .
- B. After V_{cmd} steps to V_1 , a steady-state current, I_m , flows in the circuit. The membrane potential is equal to $V_{\text{cmd}} - I_m R_{a,\text{eff}}$. After the step change in the command potential, I_m and V_m settle exponentially to their steady-state values with $\tau = [R_{a,\text{eff}} R_m / (R_{a,\text{eff}} + R_m)] C_m$, but since in general $R_m \gg R_{a,\text{eff}}$, a good approximation is $\tau \approx R_{a,\text{eff}} C_m$.

3.3.7. SERIES-RESISTANCE COMPENSATION

In the ideal experiment, the resistance of the patch micropipette in whole-cell experiments would be zero. In this case, the time resolution for measuring membrane currents and changing the membrane voltage would be limited only by the speed of the electronics (typically just a few microseconds).

Positive Feedback (“correction”)

Series-resistance compensation using positive feedback is an attempt to achieve this ideal electronically. This technique is also called “correction.” It is the same technique that has been widely used in conventional two-electrode voltage clamps. Basically, a signal propor-

tional to the measured current is used to increase the command potential. This increased command potential compensates in part for the potential drop across the micropipette (Figure 3.15). The amount of compensation achievable is limited by two considerations. First, as the compensation level (α) approaches 100%, the increase in the command potential hyperbolically approaches infinity. For example, at 90% compensation, the command potential is transiently increased by a factor of ten ($V_{cmd}/(1 - \alpha)$). Thus at large compensation levels the electronic circuits approach saturation. Second, the current feedback is positive; therefore, the stability of the circuit is degraded by the feedback and at 100% compensation the circuit becomes an oscillator. In practice, the oscillation point is much lower than 100% because of non-ideal phase shifts in the micropipette and the cell membrane.

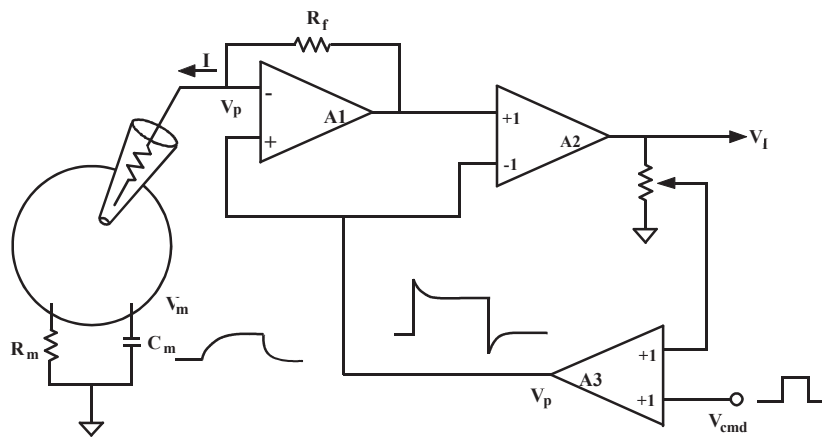


Figure 3.15: Series resistance correction.

In this figure, a single pipette is used to voltage-clamp the cell. Operational amplifier A1 is configured as a current-to-voltage converter. Differential amplifier A2 subtracts the pipette potential (V_p) to generate the current output (V_I). A fraction (α) of V_I is summed with the command voltage (V_{cmd}) used to control V_p . This causes both a transient and a steady-state increase in V_p compared with V_{cmd} . As a result, the membrane charges faster, the voltage drop across the electrode resistance is compensated and the bandwidth is increased.

The first problem, saturation of the electronics, could in principle be reduced by using high-voltage (*e.g.*, ± 120 V) operational amplifiers. However, this approach has not been pursued because these types of operational amplifiers have more noise and worse drift than good conventional operational amplifiers. The second problem, stability, has been partially reduced by adding a variable low-pass filter in the current-feedback loop (*e.g.*, the “lag” control of the Axopatch-1D and the Axopatch 200 series amplifiers, and “bandwidth” in the MultiClamp 700 series amplifiers). By empirically setting the low-pass filter

cutoff frequency, large percentage compensations can be used, but these only apply to the currents at bandwidths below that of the filter cutoff. Thus the DC, low- and mid-frequency series resistance errors can be substantially reduced while the high-frequency errors remain large.

Supercharging (“prediction”)

Another technique for speeding up the response to a command step is the “supercharging” technique, also known as “prediction.” In contrast to the “correction” method of series-resistance compensation, “prediction” is an open-loop method. That is, there is no feedback and there is little risk of oscillations.

Supercharging is accomplished by adding a brief “charging” pulse at the start and the end of the command voltage pulse. This means that initially the membrane is charging towards a larger final value than expected (Figure 3.16). In its crudest form, the charging-pulse amplitude or duration are adjusted empirically by the investigator so that the membrane potential does not overshoot. Since the membrane potential is not directly observable by the user, this is accomplished by adjusting the controls until the current transient is as brief as possible. Once the optimum setting for one step size has been found, the size of the supercharging pulse for all other step sizes can be calculated by the computer. Since the large, transient supercharging current has to be carried by the feedback resistor in the headstage, the amount of supercharging that can be used is limited by saturation of the current-to-voltage converter in the headstage.

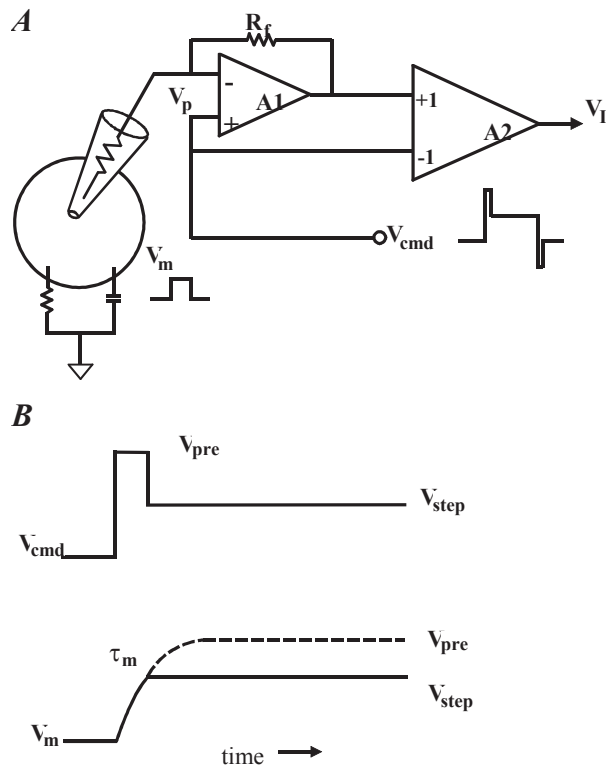


Figure 3.16: Prediction implemented empirically by the computer.

- A. A brief charging pulse is added to the start and the end of V_{cmd} . The size and duration of the charging pulse is empirically determined to give the fastest charging current. V_m charges rapidly to its final value. V_{cmd} and the supercharging pulses are not part of a positive feedback circuit.
- B. An expanded view of V_{cmd} and V_m . Initially, V_m increases towards the amplitude (V_{pre}) of the pre-pulse. However, the pre-pulse is terminated early, just when V_m reaches the desired command voltage, V_{step} .

The Axopatch 200 amplifier pioneered an alternative technique for generating the supercharging current. This technique takes advantage of having full knowledge of the R_a and C_m values. Fortunately, this information is generally available on modern whole-cell patch-clamp amplifiers as part of the technique used to unburden the feedback resistor (R_f) from the necessity of passing the charging current into the cell (*i.e.*, whole-cell capacitance compensation). Once these parameters are determined, it is possible to automatically boost changes in the command voltage to supercharge the cell (Figure 3.17). This technique has the significant advantage that no empirical determination of the charging-pulse amplitude or time is needed and that it works with any command-voltage shape without requiring a computer to calculate the supercharging pulse.

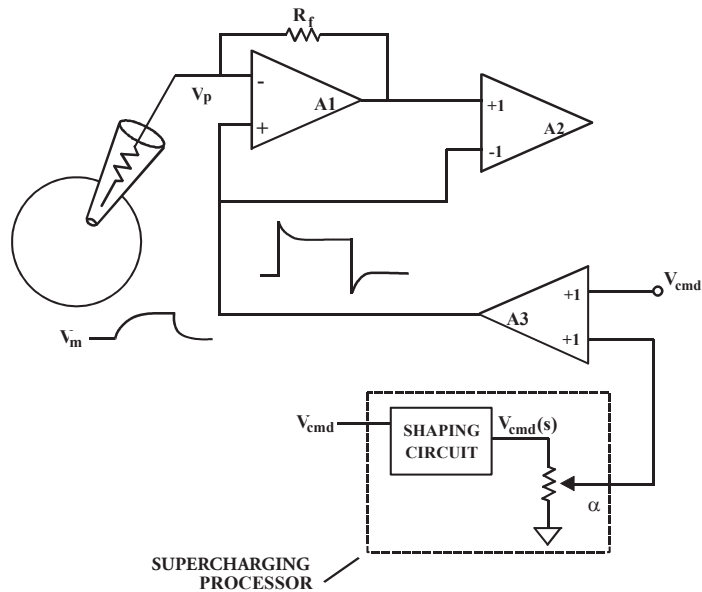


Figure 3.17: Implementation of prediction based on the knowledge of cell parameters.

The supercharging pulse added to V_{cmd} is a fraction (α) of a shaped version of V_{cmd} itself. The shaped version, $V_{cmd}(s)$, is generated in the whole-cell capacitance compensation circuit described later. Since the calculation of the supercharging pulse is determined by the parameters of the cell and V_{cmd} itself, the system works with all commands (step, triangle, sine, *etc.*) without the need for an empirical determination of the shape and amplitude for each command shape and size.

Supercharging is appropriate for a specific type of experiment, but it is inappropriate in others and its use should be carefully considered. The appropriate application is the measurement of ionic currents that activate during the time that the membrane potential is normally changing. If supercharging is applied, it might be possible to clamp the potential to its final value before the ionic current substantially activates.

There are two significant shortcomings that the investigator should be aware of when using the supercharging technique:

- 1 The technique does not correct for the voltage error that occurs when current flows through the series resistance of the pipette.
- 2 The dynamic response of the circuit is not improved. That is, there is no improvement in the speed with which changes in current (and hence, changes in conductance) can be resolved. Membrane current changes are still filtered by the time constant of the access resistance and the membrane capacitance. The investigator

should not be misled by the rapid settling of the response to a command step into thinking that this settling time represents the time resolution of the recording system.

Neither of these problems occurs with the correction method of series-resistance compensation. The relative merits of correction versus prediction are shown in Table 3.1.

Table 3.1: Correction vs. Prediction.

	Error correction	Fast response to V_{cmd} change	Fast response to R_m change	Stability
Correction	Yes	Yes	Yes	Not guaranteed
Prediction	No	Yes	No	Guaranteed

Usually, the type of series-resistance compensation provided in a patch clamp amplifier is a combination of correction and prediction. The Axopatch 200 and MultiClamp 700 amplifier series allow the prediction and correction components of the circuitry to be set independently so that the researcher can optimize the technique that is most appropriate for the experiment. Optimum performance is usually achieved by combining series-resistance “correction” with series-resistance “prediction.”

Limitations of Series-Resistance Compensation

Series-resistance compensation is an attempt to electronically reduce the effect of the pipette resistance. Because of practical limitations, it is never perfect. Even if 100% compensation could be used with stability, this would only apply to DC and medium-speed currents. Very fast currents cannot be fully corrected.

3.3.8. PIPETTE-CAPACITANCE COMPENSATION

When the command voltage is stepped, a large amount of current flows into the pipette capacitance during the transition from one potential to the next. In an intracellular micropipette amplifier, such as the Axoclamp 900A amplifier, this is reduced by setting the capacitance neutralization controls, as discussed in the earlier section titled Capacitance Compensation. In a patch-clamp amplifier, such as the Axopatch 200 and MultiClamp 700 amplifier series, a variation of the technique is used for the same purpose—to reduce or even eliminate the transient. This section discusses pipette capacitance compensation in a patch clamp.

Compensating the pipette capacitance in a patch clamp has three purposes. First, many researchers want to remove the transient from the records for “cosmetic” reasons. Second, during the transient the potential at the top of the pipette is changing slowly while the pipette capacitance charges. By rapidly charging the pipette capacitance through the compensation circuitry, the potential at the top of the pipette is stepped more rapidly, reducing the likelihood that rapid-onset ionic currents will be distorted. Third, uncompensated pipette capacitance has a detrimental effect on the stability of the series-resistance correction circuitry. The component of the current that flows into the pipette capacitance is not

in series with any resistance. Thus the series-resistance correction circuit exceeds 100% compensation for this component of the current as soon as the circuit is switched in.

In the Axopatch and MultiClamp amplifiers, two pairs of pipette capacitance compensation controls are available. With these controls, it is often possible to reduce the pipette transients to extremely low levels. The bulk of the transient is reduced by using the fast magnitude and time constant (τ) controls. The magnitude control compensates the net charge. The τ control adjusts the time constant of the charge compensation to match the time constant of the command pathway and to compensate for small non-idealities in the frequency response of the pipette and electronics.

The residual slow component seen in many pipettes is reduced by using the slow magnitude and τ controls. A simplified circuit of the fast and slow compensation circuitry is shown in Figure 3.18.

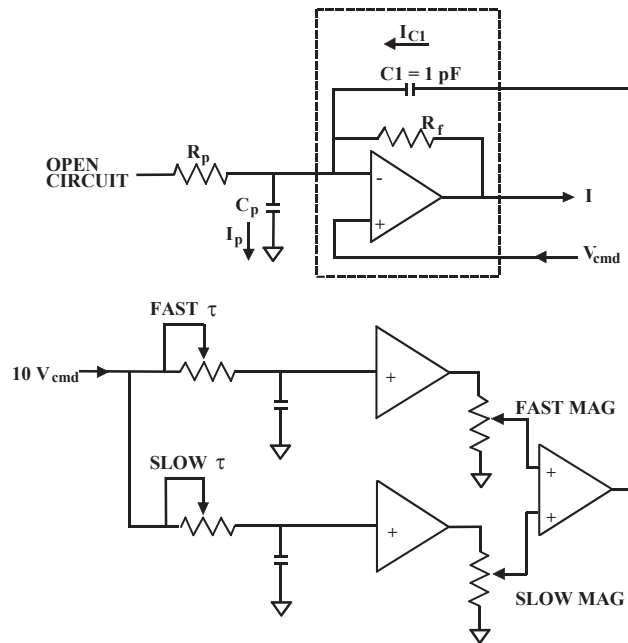


Figure 3.18: Pipette capacitance compensation circuit

When the command potential (V_p) changes, current I_p flows into C_p to charge it to the new potential. If no compensation is used, I_p is supplied by the feedback element (R_f), resulting in a large transient signal on the output (I).

By properly setting the fast and slow magnitude and τ controls, a current (I_{C1}) can be induced in capacitor $C1$ (connected to the headstage input) to exactly equal I_p . In this case no current needs to be supplied by R_f and there is no transient on the output.

3.3.9. WHOLE-CELL CAPACITANCE COMPENSATION

When the membrane potential is stepped, there is a significant current transient required to charge the membrane capacitance. This is true whether the cell is clamped using a two-electrode clamp or a single-electrode clamp. Since it is impossible to record meaningful currents during this transient (the membrane potential has not settled), this transient is ignored in most two-electrode voltage-clamp or discontinuous single-electrode voltage-clamp experiments. However, when whole-cell voltage clamping is performed using a patch-clamp amplifier, it is common to suppress this transient from the recording.

It is important to understand that the transient is not suppressed in the belief that somehow the data during this period is more meaningful in a patch-clamp amplifier than it is in a two-electrode voltage clamp. The transient is suppressed for technological reasons. In a patch-clamp amplifier the value of the feedback resistor for whole-cell clamping is typically 500 M Ω . In an instrument driven from ± 15 volt power supplies, the maximum current that can be passed through a 500 M Ω resistor is less than 30 nA. The transient current required to apply a 100 mV step to a cell that is clamped through a 1 M Ω resistor is typically 100 nA. If series-resistance compensation is used, much larger currents are required. Since the 500 M Ω resistor cannot pass the required current, the system would saturate and the time to effect a step would be prolonged significantly. In order to prevent saturation of the system, the transient current is injected through a capacitor. Since the current monitor output on patch clamps is only proportional to the current through the feedback resistor, the transient current is not seen, even though in reality it is still being passed through the pipette into the cell.

The settings of the whole-cell capacitance controls to eliminate the transient are unique to the cell being clamped. The values of the cell membrane capacitance and the access resistance can be directly read from the controls. Figure 3.19 is a simplified circuit illustrating how the whole-cell capacitance controls operate.

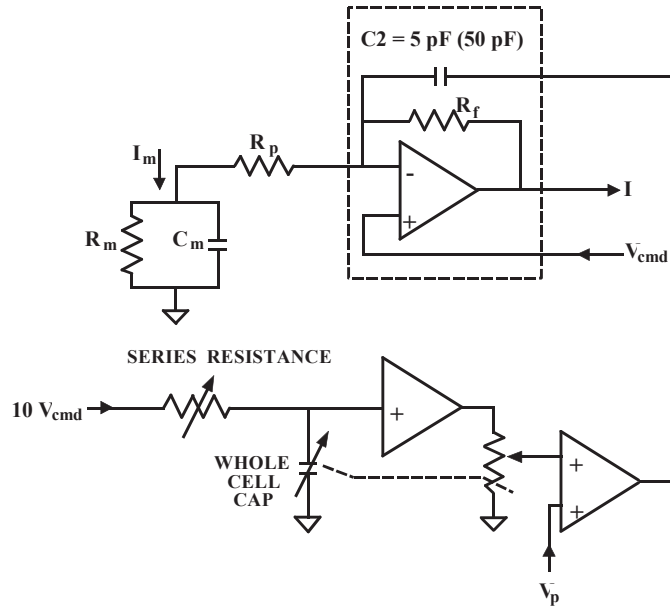


Figure 3.19: Whole-cell capacitance compensation circuit.

Assume that the fast and slow electrode compensation controls have already been set to compensate for C_p . By appropriately adjusting the series-resistance and whole-cell capacitance controls, the current injected through $C2$ will supply the transient membrane current (I_m). These adjustments do not alter the time constant for charging the membrane. Their function is to offload the burden of this task from the feedback resistor, R_f . In many cells, even a small command voltage of a few tens of millivolts can require such a large current to charge the membrane that it cannot be supplied by R_f . The headstage output saturates for a few hundred microseconds or a few milliseconds, thus extending the total time necessary to charge the membrane. This saturation problem is eliminated by the appropriate adjustment of the series-resistance and whole-cell capacitance controls. This adjustment is particularly important during series-resistance correction since series-resistance correction increases the current-passing demands on R_f . By moving the pathway for charging the membrane capacitance from R_f to $C2$, the series-resistance circuitry can operate without causing the headstage input to saturate. The effect of transferring the current-passing burden from R_f to $C2$ is illustrated in Figure 3.20.

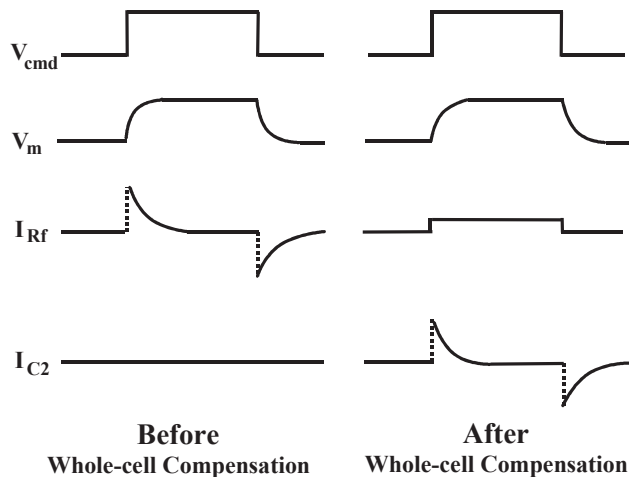


Figure 3.20: Using the injection capacitor to charge the membrane capacitance.

V_{cmd} is the patch-clamp voltage command; V_m is the voltage across the cell membrane; I_{Rf} is the current across the patch-clamp feedback resistor; I_{C2} is the current injected across the patch-clamp compensation capacitor.

The traces in this figure were recorded using an Axopatch 200 amplifier and a model cell. After perfect whole-cell compensation is applied, the current to charge the membrane capacitor is removed from the I_{Rf} trace and only the steady-state current remains. All of the transient current appears in the I_{C2} trace. (The I_{C2} trace in the figure was recorded using an oscilloscope probe connected to the internal circuitry). The I and V_m outputs on the Axopatch 200 amplifier show the I_{Rf} and V_{cmd} trace illustrated in Figure 3.20. It is easy to mistakenly think that the time course for charging the membrane is very fast, but this is clearly not the case. Use of an independent electrode in the cell would show that the cell charging rate is not affected by these adjustments.

Absolute Value

The absolute value of the membrane capacitance is displayed on the whole-cell capacitance dial after the whole-cell current transient has been eliminated. This value may be used to estimate the surface area of the cell assuming that the membrane capacitance per unit area is $1 \mu\text{F}/\text{cm}^2$.

3.3.10. RUPTURING THE PATCH

To go from the patch to the whole-cell mode, the usual method used to rupture the membrane under the pipette is to apply a pulse of gentle suction. This can be done by mouth or by syringe.

“Zap” is another alternative for going whole-cell. In this technique, a large, brief hyperpolarizing voltage pulse (about 1.5 V) is applied to the cell. This pulse initiates dielectric breakdown of the membrane patch and allows access to the interior of the cell. It is important to use the briefest pulse consistent with low-access resistance. If the pulse is too long, the seal might be lost. Both the Axopatch 200B and MultiClamp 700B amplifier allow the Zap pulse to be applied for 0.5 ms or less at the minimum.

With some cells it is difficult to go whole cell without losing the seal. An alternative is the perforated patch technique, which is discussed in Chapter 5.

3.3.11. WHICH ONE SHOULD YOU USE: dSEVC OR cSEVC?

Two methods can be used to implement a whole-cell patch voltage clamp. The first is the discontinuous single-electrode voltage clamp (dSEVC) method. The second is the continuous single-electrode voltage clamp (cSEVC) method. The cSEVC method is more commonly known as the “whole-cell patch clamp”; but formally, the term cSEVC is more descriptive of the method. Both methods have their pros and cons. The dSEVC is generally superior when the currents being clamped are modest or large in size (> 5 nA), leading to a concern that the error due to the uncompensated series resistance might be significant. In dSEVC mode, if the sampling rate is correctly chosen and the capacitance compensation correctly set, there is no error due to series resistance. For small currents, the dSEVC mode is less attractive because it is more difficult to set up and because it is noisier. Moreover, the error due to the uncompensated series resistance can generally be made negligible for small currents, making the cSEVC mode very attractive.

The cSEVC mode is available on patch-clamp amplifiers (Axopatch 200B and MultiClamp 700B) as the “whole-cell patch” mode. In a patch-clamp amplifier, the voltage-clamp circuit is a current-to-voltage converter located in the headstage (described in detail below; see Figure 3.21). The Axoclamp 900A amplifier offers the dSEVC mode, and the voltage-clamp circuit is located in the main unit. There are fewer ancillary controls in the Axoclamp 900A amplifiers pertaining to whole-cell patch clamp as compared to the Axopatch 200B and MultiClamp 700B amplifiers. For example, the Axoclamp 900A amplifier does not have a whole-cell capacitance compensation control.

3.3.12. SPACE CLAMP CONSIDERATIONS

There is one limitation to the performance of the voltage clamp that cannot be electrically compensated. This is the deviation of the cell from a sphere centered on the tip of the voltage-recording micropipette. The voltage clamp is maintained at the tip of the voltage-recording micropipette. If all portions of the cell membrane are separated from this tip by equal access resistance, then the membrane will be uniformly voltage clamped. However, many cells have processes such as axons, dendrites and filopodia attached to the cell body (where the micropipettes are usually located). The membranes of these processes are separated from the cell body by an axial access resistance whose value depends on the distance to each portion of the membrane and the cross section in that region of the cell. Thus there is a voltage drop across the access resistance that becomes substantial for distal components of the membrane. Even though the somatic membrane potential may be well

controlled, the axonal or dendritic membrane potential may be very poorly controlled. In these cases, the time course of synaptic currents, regenerative currents and measurements of reversal potentials may be grossly distorted.

As a general rule, the voltage clamp is considered to be acceptable if the length of the attached axon or dendrites is no more than 1/10 of the length constants. Even this short length will cause significant distortion of fast currents (see Figure 7 in Rall and Segev, 1985). Calculation of the length constant for a cell is complicated since it depends on the geometry of the particular cell under investigation. Some of the common ways to avoid the problems of poor space clamping are as follows:

- 1 Restrict investigations to spherical cells. Many cultured cells are convenient.
- 2 Ligate attached axons. For example, the axon of large molluscan neurons can be tied off with nylon thread.
- 3 Use short segments. For example, short segments (100 μm) of arteriolar syncytia can be separated from the arteriole by careful cutting with a razor blade.
- 4 Restrict the range of the clamp to a short segment of the cell. This is the essence of the “sucrose gap” technique sometimes used on axons.
- 5 Restrict the measurement to currents that are generated close to the micropipettes. For example, the end plate currents in muscle fibers can be well clamped, even though the bulk membrane current is very poorly clamped.
- 6 Restrict the measurement to the current flowing through a large patch of membrane instead of the whole cell. The “macro patch” technique is a special case of the single-channel patch-clamp technique described in Chapter 5, in which there are sufficient channels for an ensemble current to be recorded.
- 7 Apply the patch pipette not at the cell body, but out on the process. This technique has been successfully applied to dendrites, for example, where electrical access to the cell is achieved far from the cell body along a dendritic shaft. This should improve voltage clamp in nearby dendritic spines.

3.4. SINGLE-CHANNEL PATCH CLAMP⁵

The single-channel patch clamp is a special case of the voltage-clamp technique. This technique permits the direct measurement of the dynamic activity of individual membrane-bound channel proteins.

Like the whole-cell patch technique, a blunt pipette is sealed onto a patch of membrane. If single-channel recording is intended, the membrane at the tip of the pipette is preserved (*i.e.*, not ruptured). The current recorded is then simply the current that flows through the membrane at the tip of the pipette. Since this membrane area is very small, there is a

5. Parts of this section have been reprinted with permission from Finkel, A. S., Progress in Instrumentation Technology for Recording from Single Channels and Small Cells, in *Cellular and Molecular Neurobiology: A Practical Approach*, Oxford University Press, 1991.

good chance that just one or a few ion channels are located in the patched membrane. Individual ion-channel currents can thus be recorded. Previously, the only way to estimate kinetics or conductance of these channels was the technique of “noise” or “fluctuation” analysis. Noise analysis yields an estimate of the mean lifetimes of the channels and the mean amplitudes, but no information about actual opening and closing transitions nor about the shape of the conductance changes.

In single-channel recording, the current through the series resistance of the pipette is negligible, perhaps only a few picoamps flowing through a series resistance of just 10 M Ω . The resulting voltage error is just a few tens of microvolts and is always ignored.

3.4.1. THE IMPORTANCE OF A GOOD SEAL

When a heat-polished pipette is pressed against a cell membrane it may adhere tightly. The interior of the pipette is then isolated from the extracellular solution by the seal that is formed. If the resistance of this seal is infinite, no current can leak across it.

Current leakage through the seal resistance has a crucial bearing on the quality of the patch current recording. Firstly, depending on the size of the seal resistance, a fraction of the current passing through the membrane patch will leak out through the seal and will not be measured. The lower the seal resistance the larger the fraction of undetected current.

Secondly, thermal movement of the charges in the conducting pathways of the seal constitute the major source of noise in the recording unless the seal resistance is very high (several gigohms or more). A high seal resistance is a prerequisite of low-noise recordings.

High-resistance seals, often called “gigaseals,” require that very clean pipettes be used and that they only be used once. If this is the case, gigaseals will routinely form after the application of gentle suction. When good gigaseals are formed, the noise due to the leakage current is virtually eliminated and other sources of noise remain the dominant limitations in the resolution of the recording technique. These are the noise of the electronics, the pipette glass, the input capacitance and the feedback resistor. Commercial patch clamp amplifiers such as the Axopatch 200B amplifier have minimized the noise of the electronics and the feedback element in the headstage. Chapter 4 describes the attributes of desirable glasses and the ways to fabricate low-noise pipettes. It also discusses the use of Sylgard coatings to minimize pipette capacitance.

3.4.2. RESISTOR FEEDBACK TECHNOLOGY

Current-to-Voltage Converter

The basic concept behind the design of patch-clamp electronics is very simple (Figure 3.21). A sensitive current-to-voltage converter is fabricated using a high-megohm resistor (R_f) and an operational amplifier (A1). The pipette is connected to the negative input and the command voltage is connected to the positive input. Since the operational amplifier has extremely high gain, the potential at the negative input is forced to follow the potential at the positive input. All current flowing in the micropipette also flows

through R_f . This current is proportional to the voltage across R_f which is measured at the output of the differential amplifier (A2).

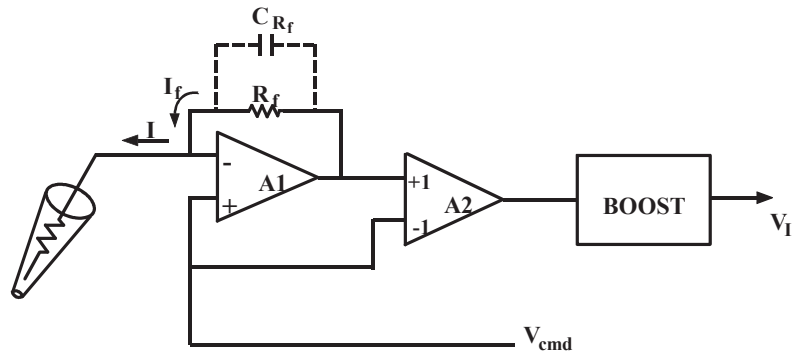


Figure 3.21: Resistive headstage.

Operational amplifier A1 is configured as a current-to-voltage converter. Differential amplifier A2 subtracts V_{cmd} from the output of A1 to generate a voltage that is purely proportional to the voltage across R_f and hence the feedback current, I_f . The boost circuit increases the high-frequency gain to compensate for the narrow bandwidth of the feedback resistor.

In principle, the patch clamp is equivalent to a conventional two-electrode voltage clamp in which the output circuit is connected back to the input pipette. In practice, the patch clamp is better behaved. The patch-clamp system is simpler since all of the gain is in a single operational amplifier stage. The stray capacitance across the feedback resistor guarantees stability. Furthermore, because the gain of this operational amplifier is so high, the difference between the command potential and the potential of the micropipette is negligible. Remember that the potential that is controlled is the potential at the top of the micropipette, not the potential at its tip.

Problems

The special demands of patch clamping lead to complicating factors in the design of a good headstage.

- 1 Integrated circuit operational amplifiers do not have the required combination of ultra-low noise and sub-picoamp bias currents. Thus the operational amplifier has to be made from a composite of low-noise FETs⁶, such as the U430 type, and conventional operational amplifiers. The voltage noise of the input FETs leads to noise current being injected into the input capacitance. If this input capacitance is

6. Field Effect Transistor.

large, this source of noise becomes dominant; it is proportional to the product of the input capacitance and the noise of the input FETs.

- 2 The minimum theoretically achievable current noise is lower for larger R_f values; therefore it is important to choose large R_f values. The largest value typically used is $50\text{ G}\Omega$, since it allows a reasonable maximum current of more than 200 pA to be measured. Unfortunately, for reasons that are not well understood, high-value resistors are several times noisier than predicted by thermal-noise theory. Since the noise of these resistors cannot be predicted, various brands of resistors must be tested until the best one is found.
- 3 The inherent bandwidth of a $50\text{ G}\Omega$ resistor is limited by the stray capacitance across the resistor (C_{Rf} in Figure 3.21). For example, a $50\text{ G}\Omega$ resistor with 0.1 pF stray capacitance has a 5 ms time constant, corresponding to a bandwidth of only 32 Hz . This poor time resolution is unacceptable for measuring ionic currents. Therefore, the high-frequency components of the headstage output signal must be boosted. This is typically achieved by an analog frequency compensation circuit. This circuit is made complicated by the fact that R_f cannot be considered as an ideal capacitor in parallel with an ideal resistor; thus a simple high-pass filter cannot be used. Complex circuits consisting of up to four poles and three zeros in the transfer function are commonly used. The placement of the poles and zeros must be carefully set for the particular resistor.
- 4 The current required to charge the input capacitance during a step voltage command can easily exceed the maximum current that can be passed by R_f from the typical 13 V swing of the operational amplifier. For example, to linearly charge 5 pF of input capacitance to 100 mV in $10\text{ }\mu\text{s}$ would require a charging current of 50 nA . This is well beyond the 260 pA that can be passed by a $50\text{ G}\Omega$ resistor driven from $\pm 13\text{ V}$. Thus, special circuits are typically added to inject the required charging current through a capacitor.
- 5 The best high-value resistors seem to be available only in a miniature “surface mount” form. This means that the headstage electronics have to be manufactured in a hybrid. This manufacturing technique has some advantages. First, the U430 input FETs and other FETs typically used to switch between different values of R_f can be used in an unpackaged form. This is to be preferred, since the sealing glasses used in packaged transistors typically have a leakage resistance that increases the noise. Second, it means that the sensitive input components can be maintained in a hermetically sealed environment that reduces the rate at which they age due to environmental contamination.

If the Probe Output is Slow, How Can Voltage Clamping be Fast?

In resistive-feedback headstages (but not capacitive-feedback headstages, discussed below) the current output of the current-to-voltage (I-V) converter in the probe is slow. The high-frequency boost occurs afterwards and cannot influence the events at the pipette. Thus, one might conclude that the voltage clamp of the pipette must also be slow.

In fact, despite the slow current output of the I-V converter, the voltage clamp of the pipette is rapid. The pipette is connected to the negative input (summing junction) of the op amp. The command potential is connected to the positive input of the op amp. The operation of the op amp in this configuration is to force the potential at the summing junction to rapidly follow the potential at the positive input. If the command potential is a step, the potential at the summing junction (and hence the pipette) is also a step. The current required to achieve this step is passed through the feedback resistor (R_f) and the associated stray feedback capacitance (C_{Rf}) of the I-V converter. The output of the I-V converter settles to the final value with time constant $R_f C_{Rf}$. This relatively slow settling occurs despite the fact that the step at the summing junction is fast.

In this discussion, we have carefully referred to the fact that it is the pipette that is rapidly voltage clamped. The membrane potential is voltage clamped to its final value much more slowly. To a reasonable approximation, the time constant for voltage clamping the membrane is $R_p C_m$, where R_p is the pipette resistance and C_m is the membrane capacitance.

3.4.3. CAPACITOR FEEDBACK TECHNOLOGY

Rationale

A newer technology in single-channel recording is the capacitor-feedback technique, also known as the integrating headstage technique. While this technique was talked about for many years, it was only first attempted and described in 1985 by Offner and Clark. Practical implementations did not become commercially available until 1989.

In this technique, the feedback resistor in the headstage is replaced by a capacitor (C_f in Figure 3.22). When a capacitor is used instead of a resistor, the headstage acts as an integrator. That is, for a constant input current, the output of the headstage is a ramp. The slope of the ramp is proportional to the current. To recover a voltage that is simply proportional to the input current, the integrator must be followed by a differentiator (A2).

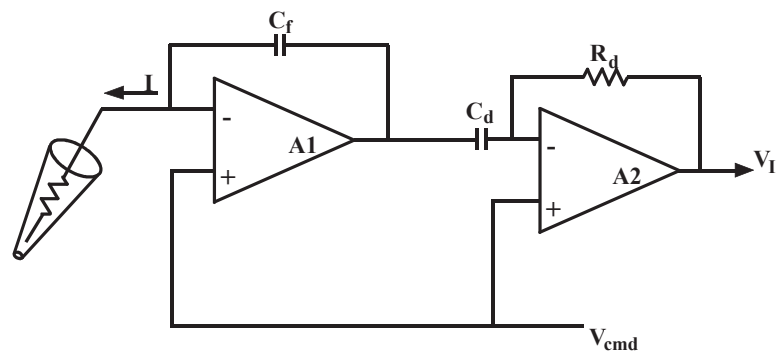


Figure 3.22: Capacitive feedback headstage.

The feedback element around operational amplifier A1 is capacitor (C_f). Thus the output of A1 is the integral of the pipette current. The actual current is recovered from the integral by differentiating it in the differentiator formed by C_d , R_d and A2.

Compared with resistor-feedback picoamp current-to-voltage converters (RIV), capacitor feedback current-to-voltage converters (CIV) exhibit less noise, increased dynamic range, wider bandwidth and improved linearity.

Noise, Dynamic Range, Linearity and Bandwidth

- 1 The noise of the CIV is lower for two reasons. First, the capacitors do not generate as much thermal noise as resistors do. (There is an equivalent resistor noise source due to the differentiator, but with careful design this can be made negligible.) Second, capacitors are commercially available that are free of the excess noise sources that plague high-gigohm resistors.

The noise benefit of the CIV is eliminated if C_f is large (10 pF or more). This is because from the noise point of view, C_f sums with the other sources of input capacitance. The voltage noise of the input FETs leads to a current injection into the total input capacitance. If this input capacitance is large, this source of noise becomes dominant.

The lower noise of the CIV can be realized only in situations where all other noise sources are minimized. That is, the experimenter should use a low-noise glass and pipette holder, Sylgard coating, and a high-resistance seal. By carefully removing other sources of noise, the reduced noise of the CIV can be realized in real patches, not just in theory.

- 2 The capacitor-feedback headstage has an equivalent transfer resistance (R_T) given by

$$R_T = R_d \frac{C_d}{C_f} \quad (10)$$

Because the noise is theoretically independent of the C_f value and the gain of the differentiator, R_T may be kept quite low, *e.g.*, 100 M Ω . At this gain, the maximum current that can be recorded is 500 times greater than for an RIV using a 50 G Ω feedback resistor. Thus the CIV potentially has vastly improved dynamic range.

- 3 In the section on Resistor Feedback Technology, it was pointed out that in order to achieve an acceptable bandwidth of, *e.g.*, 20 kHz for single-channel recording, a complex boost circuit has to be used to correct the frequency response. Even if the boost box has as many as four poles and three zeros, the frequency response of R_f is not perfectly corrected. The imperfections of the correction are most easily seen by observing the step response of the headstage. Frequently, there will be overshoots and ripples that can amount to as much as 2% of the response. However, because excellent capacitors are available, the step response is inherently square with a CIV.

- 4 The bandwidth of a CIV can be very wide. It is maximized by using a small value of C_f and a small value of R_d . For practical values ($C_f = 1$ pF and $R_d = 150$ k Ω), the bandwidth is of the order of 70 kHz or more. This is considerably better than the 20 kHz of a good RIV using a 50 G Ω feedback resistor.

Whether it is practical to use this increased bandwidth or not is another matter. The noise of both the RIV and the CIV headstages increases dramatically with frequency.

Problems

There are two major problems that make the capacitor feedback technology difficult to implement. The first problem is that after a sustained net DC input current the integrator voltage ramps towards one of the power-supply limits. When this happens, the integrator must be reset by discharging the capacitor. The frequency of the resets depends on the size of C_f and the average input current. For example, if C_f is 1 pF and the input current is 2 pA, the output of the integrator will ramp at 2 V/s. If the resetting circuitry is triggered when the integrator voltage exceeds 10 V, resets will occur every five seconds.

The reset itself lasts approximately 50 μ s. During the reset, sample-and-hold circuits are used to maintain the current output at its value immediately prior to the start of the reset. If it is acceptable to lose 0.1% of the data, resets as frequent as every 50 ms would be acceptable. In the above example, this corresponds to an input current of 200 pA. For single-channel recording, this is more than adequate.

Figure 3.23 shows the signal pathway for the capacitor-feedback headstage. The output current (I) of the capacitor-feedback headstage is normally connected through a switch to the output pre-filter amplifier, then to the low-pass filter, and finally to the post-filter amplifier. The signal also goes through a low-pass filter to a sample-and-hold amplifier. During reset, the switch shifts to the RESET position. Simultaneously, the sample-and-hold amplifier is switched to the hold mode so that the signal immediately before the reset transient occurs is presented to the output amplifiers.

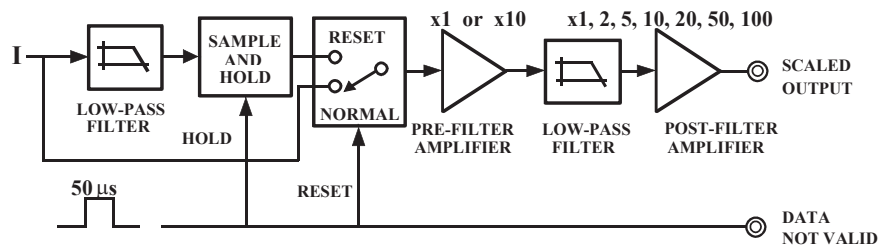


Figure 3.23: Signal handling during resets in the capacitor-feedback headstage.

A capacitor feedback is not practical for whole-cell recordings. Due to the large whole-cell currents the resets would be too frequent unless the value of C_f was increased. In practice, it is hardly worth it. It is simpler to switch to a modest-sized resistor (e.g., 500 M Ω) and

avoid the problem of resets altogether. Reverting to resistor-feedback methods for whole-cell recordings does not represent a setback in terms of noise because the 500 M Ω resistor is not the dominant source of noise.

During the measurement of voltage-activated single-channel currents, the resets can be made irrelevant. This is done by using a control pulse to force a reset immediately prior to the voltage step. This guarantees that C_f is in its discharged state at the beginning of the voltage step and is therefore unlikely to need resetting during the step.

The second problem is that during resets transients are injected into the headstage input by the reset circuitry. If left uncompensated, these would cause unwanted and possibly damaging current pulses to be injected down the micropipette into the patch. Special compensation circuitry needs to be included in the design to exactly balance out these injected currents.

There are other transient problems that occur during and after the reset. These include dielectric absorption in the differentiator and feedback capacitors, and other ill-defined transients that work their way into the system. Compensation circuitry must also be included to compensate for these transients.

Overall, the need to reset and to compensate for the many transients that occur during reset make the design of an integrating patch clamp challenging. However, in a well-designed system, the reset transients measured at the output will be less than 1 pA measured in a 1 kHz bandwidth.

3.4.4. SPECIAL CONSIDERATIONS FOR BILAYER EXPERIMENTS

The Advantage of Resets in Bilayer Experiments

While they are normally considered to be a nuisance, there is one application where resets are quite an advantage. This is in voltage-step experiments in bilayers. During a reset, a low resistance of about 10 k Ω is placed in parallel to the feedback capacitor. This resistor allows currents up to 1 mA to pass out of the headstage to rapidly charge the bilayer capacitance. Voltage steps as large as 100 mV are normally achieved with one or two resets separated by less than a millisecond.

Noise vs. Access Resistance

In bilayer experiments, the access resistance is quite low, usually ranging from a few kilohms to several tens of kilohms. The access resistance is in series with the membrane capacitance and produces voltage noise just as though the headstage had high intrinsic noise.

For bilayer recording done at a low bandwidth (<1 kHz), the $e_n C_{in}$ noise has not yet become the major contributor to the overall noise (where e_n is the voltage noise of the probe input FETs and C_{in} is the capacitance at the input of the headstage primarily due to the bilayer membrane capacitance). If the access resistance is large enough, it becomes the dominant noise contributor at low bandwidths.

Figure 3.24 shows the dependence of peak-to-peak noise on access resistance in a 1 kHz bandwidth for a given bilayer membrane capacitance. It can be seen that the lower the access resistance, the lower the noise. It is therefore important that the patch-clamp instrument be capable of operating without oscillation even when extremely small, or zero, access resistances are used. The CV-203BU headstage for the Axopatch 200B amplifier and the CV-7B/BL headstage for the MultiClamp 700B amplifier have been designed for complete stability even with extremely low access resistances.

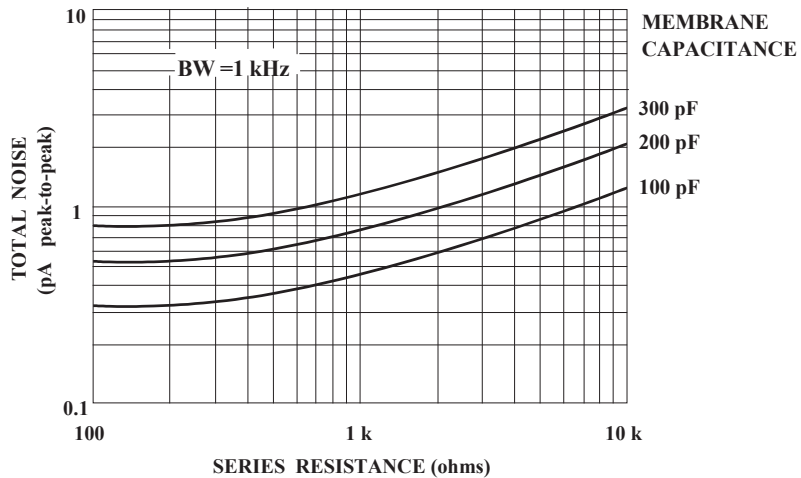


Figure 3.24: Typical current noise in bilayer experiments.

3.4.5. HOW FAST IS “FAST”?

The speed of the observed transitions of single-channel currents is the same as the response time of the electronics. Whenever recordings are made at wider bandwidths, the observed transition rates become shorter. It is not clear that we will ever be able to resolve the actual transition time using electrical measurements (perhaps optical techniques will emerge to do the job); but the discovery of new lower limits to the transition rate will be made possible by the low-noise wide-bandwidth patch clamps such as the Axopatch 200 series amplifiers.

3.4.6. MEASUREMENT OF CHANGES IN MEMBRANE CAPACITANCE

The measurement of minute changes in membrane capacitance, such as the changes that occur during exocytosis, was made practical by the whole-cell patch-clamp technique. Two methods can be used. The simplest and the most traditional way is to use a fitting technique to find the time constant of the current response to a voltage step. By assuming a simple cell model, the membrane capacitance can be easily deduced. This technique is relatively easy to apply, but it has a resolution no better than 100–200 fF, which is insuffi-

cient to resolve the 10–20 fF capacitance increases occurring during fusion of single granules with the membrane.

A much more sensitive technique involves the use of a lock-in amplifier (also known as a phase detector). In this technique, a sinusoidal command voltage is applied to the cell. The magnitude of this voltage must be small enough so that the cell's properties are essentially linear. One measures two outputs that are proportional to the sinusoidal current response at two orthogonal frequencies. It can be shown that the magnitudes of these two responses are a function of the access resistance, the membrane resistance and the cell capacitance. With a third measurement of the DC current, and assuming that the reversal potential of the DC currents is known, there is sufficient information to calculate the value of all three parameters. The resolution of this technique can be as good as 1 fF, with measurements being made up to one hundred times per second.

Joshi and Fernandez (1988) have described a similar technique where all of the phase-sensitive measurements and sinusoidal stimulations are performed by software. This has the great advantage of not requiring any special equipment other than the patch clamp.

3.4.7. SEAL AND PIPETTE RESISTANCE MEASUREMENT

The micropipette resistance is easily measured with micropipette amplifiers by passing a pulse of current through the micropipette. Generally, a convenient pulse size such as 0.1, 1 or 10 nA is used. If the pulse size is 1 nA, the micropipette potential without any Bridge Balance is 1 mV/M Ω of micropipette resistance. For example, if the pulse response is 55 mV, the micropipette resistance is 55 M Ω . Alternatively, the Bridge Balance control can be adjusted to null the pulse response and the micropipette resistance can be measured directly from the Bridge Balance dial.

In patch clamps, the measurement of the combined pipette and seal resistance is not quite as straight forward because the patch clamp is normally used in voltage-clamp mode rather than current-clamp mode. In this case, a voltage step is applied to the pipette. The combination of the pipette and seal resistance is calculated from the current response using the formula:

$$R = V/I$$

For example, if the test pulse is 1 mV and the current response is 67 pA, the resistance is 15 M Ω .

With the MultiClamp 700B and Axoclamp 900A amplifiers, the Commander software controlling the amplifier can apply a pulse and automatically calculate the electrode resistance, whether in current or voltage clamp mode.

3.4.8. MICROPIPETTE HOLDERS

High-quality micropipette holders are crucial to successful single-channel recording. Two characteristics of the holder are important. First, the holder must be mechanically stable. When working with a cell-attached patch, drift of the micropipette is unacceptable.

Clearly, a low-drift micromanipulator is required (as discussed in Chapter 2). But if the holder is loose in the headstage connector or if the pipette does not seat properly, drift will occur despite the high quality of the micromanipulator. One common, exasperating problem associated with loose holders is movement of the pipette when suction is applied, which either prevents seal formation or damages the cell. The HL-U holders from MDS Analytical Technologies fit all recent Axon Cellular Neuroscience headstages and have been designed to fit snugly into the headstage connector and to firmly grip the pipette to prevent drift. Second, the holder must not introduce noise. To assure this:

- 1 Select the right holder material. When a holder is connected to the headstage, even before a pipette is connected, the open-circuit noise goes up slightly. The reasons are not understood. Empirical tests have shown that when used with glass micropipettes, polycarbonate adds the least noise. The HL-U holders use polycarbonate for the pipette cap and the body of the holder. The portion that plugs into the headstage is made of Teflon. Teflon in this position does not add noise, and it facilitates smooth insertion and removal.
- 2 Use a small pin for the electrical connection. Large pins have more capacitance contributed by the surrounding grounded surfaces.
- 3 Do not use a shield. Surrounding the holder with a driven or grounded shield adds to the input capacitance and thus increases the noise.

3.5. CURRENT CONVENTIONS AND VOLTAGE CONVENTIONS

The terminology used in this discussion applies to all Axon Cellular Neuroscience amplifiers manufactured by MDS Analytical Technologies.

3.5.1. DEFINITIONS

Positive Current

The flow of positive ions out of the headstage into the microelectrode and out of the microelectrode tip into the preparation is termed positive current.

Inward Current

Current that flows across the membrane, from the outside surface to the inside surface, is termed inward current.

Outward Current

Current that flows across the membrane, from the inside surface to the outside surface, is termed outward current.

Positive Potential

The term positive potential means a positive voltage at the headstage input with respect to ground.

Transmembrane Potential

The transmembrane potential (V_m) is the potential at the inside of the cell minus the potential at the outside. This term is applied equally to the whole-cell membrane and to membrane patches.

Depolarizing / Hyperpolarizing

The resting V_m value of most cells is negative. If a positive current flows into the cell, V_m initially becomes less negative. For example, V_m might shift from an initial resting value of -70 mV to a new value of -20 mV. Since the absolute magnitude of V_m is smaller, the current is said to depolarize the cell (*i.e.*, it reduces the “polarizing” voltage across the membrane). This convention is adhered to even if the current is so large that the absolute magnitude of V_m becomes larger. For example, a current that causes V_m to shift from -70 mV to +90 mV is still said to depolarize the cell. Stated simply, depolarization is a positive shift in V_m . Conversely, hyperpolarization is a negative shift in V_m .

3.5.2. WHOLE-CELL VOLTAGE AND CURRENT CLAMP**Depolarizing / Hyperpolarizing Commands**

In whole-cell voltage clamping, whether it is performed by TEVC, dSEVC, cSEVC or whole-cell patch clamp, a positive shift in the command voltage causes a positive shift in V_m and is said to be depolarizing. A negative shift in the command voltage causes a negative shift in V_m and is said to be hyperpolarizing.

Transmembrane Potential vs. Command Potential

In whole-cell voltage clamping, the command potential controls the voltage at the tip of the intracellular voltage-recording microelectrode. The transmembrane potential is thus equal to the command potential.

Inward / Outward Current

In a cell generating an action potential, depolarization is caused by a flow of positive sodium or calcium ions into the cell. That is, depolarization in this case is caused by an inward current.

During intracellular current clamping, a depolarizing current is a positive current out of the micropipette tip into the interior of the cell. This current then passes through the membrane out of the cell into the bathing solution. Thus, in intracellular current clamping, a depolarizing (positive) current is an outward current.

An inward sodium current flows in some cells after a depolarizing voltage step. When the cell is voltage clamped, the sodium current is canceled by an equal and opposite current flowing into the headstage via the microelectrode. Thus it is a negative current. When two-electrode voltage clamping was first used in the early 1950's, the investigators chose to call the negative current that they measured a depolarizing current because it corresponded to the depolarizing sodium current. This choice, while based on sound logic, was unfortunate because it means that from the recording instrument's point of view, a nega-

tive current is hyperpolarizing in intracellular current-clamp experiments but depolarizing in voltage-clamp experiments.

To prevent confusion, Axon Cellular Neuroscience instruments always use current and voltage conventions based on the instrument's perspective. That is, the current is always unambiguously defined with respect to the direction of flow into or out of the headstage. Some instrument designers have put switches into the instruments to reverse the current and even the command voltage polarities so that the researcher can switch the polarities depending on the type of experiment. This approach has been rejected by MDS Analytical Technologies because of the real danger that if the researcher forgets to move the switch to the preferred position, the data recorded on the computer could be wrongly interpreted. MDS Analytical Technologies believes that the data should be recorded unambiguously.

3.5.3. PATCH CLAMP

By design, the patch-clamp command voltage is positive if it increases the potential inside the micropipette. Whether it is hyperpolarizing or depolarizing depends upon whether the patch is “cell attached,” “inside out” or “outside out.” The patch-clamp pipette current is positive if it flows from the headstage through the tip of the micropipette into the patch membrane.

Cell-Attached Patch

The membrane patch is attached to the cell. The pipette is connected to the outside surface of the membrane. A positive command voltage causes the transmembrane potential to become more negative, therefore it is hyperpolarizing. For example, if the intracellular potential is -70 mV with respect to 0 mV outside, the potential across the patch is also -70 mV. If the potential inside the pipette is then increased from 0 mV to $+20$ mV, the transmembrane potential of the patch hyperpolarizes from -70 mV to -90 mV.

From the examples it can be seen that the transmembrane patch potential is inversely proportional to the command potential, and shifted by the resting membrane potential (RMP) of the cell. A positive pipette current flows through the pipette across the patch membrane into the cell. Therefore a positive current is inward.

Inside-Out Patch

The membrane patch is detached from the cell. The surface that was originally the inside surface is exposed to the bath solution. Now the potential on the inside surface is 0 mV (bath potential). The pipette is still connected to the outside surface of the membrane. A positive command voltage causes the transmembrane potential to become more negative, therefore it is hyperpolarizing. For example, to approximate resting membrane conditions of $V_m = -70$ mV, the potential inside the pipette must be adjusted to $+70$ mV. If the potential inside the pipette is increased from $+70$ mV to $+90$ mV, the transmembrane potential of the patch hyperpolarizes from -70 mV to -90 mV.

From the example it can be seen that the transmembrane patch potential is inversely proportional to the command potential. A positive pipette current flows through the pipette across the patch membrane from the outside surface to the inside surface. Therefore a positive current is inward.

Outside-Out Patch

The membrane patch is detached from the cell in such a way that the surface that was originally the outside surface remains exposed to the bath solution. The potential on the outside surface is 0 mV (bath potential). The pipette interior is connected to what was originally the inside surface of the membrane. A positive command voltage causes the transmembrane potential to become less negative, therefore it is depolarizing. For example, to approximate resting membrane conditions, assuming that $V_m = -70$ mV, the potential inside the pipette must be adjusted to -70 mV. If the potential inside the pipette is then increased from -70 mV to -50 mV, the transmembrane potential of the patch depolarizes from -70 mV to -50 mV.

The membrane potential is directly proportional to the command potential. A positive pipette current flows through the pipette across the patch membrane from the inside surface to the outside surface. Therefore a positive current is outward.

3.5.4. SUMMARY

1 Positive current corresponds to:

Cell-attached patch	patch inward current
Inside-out patch	patch inward current
Outside-out patch	patch outward current
Whole-cell voltage clamp	outward membrane current
Whole-cell current clamp	outward membrane current

2 A positive shift in the command potential is:

Cell-attached patch	hyperpolarizing
Inside-out patch	hyperpolarizing
Outside-out patch	depolarizing
Whole-cell voltage clamp	depolarizing

3 The correspondence between the command potential (V_{cmd}) and the transmembrane potential (V_m) is:

Cell-attached patch	$V_m = RMP - V_{cmd}$
Inside-out patch	$V_m = -V_{cmd}$
Outside-out patch	$V_m = V_{cmd}$
Whole-cell voltage clamp	$V_m = V_{cmd}$

3.6. REFERENCES

3.6.1. PATCH CLAMP

Rae, J.L. and Levis, R.A. Patch voltage clamp of lens epithelial cells: theory and practice. *Molec. Physiol*, 6, 115–162, 1984.

Hamill, O. P., Marty, A., Neher, E., Sakmann, B., and Sigworth, F.J. Improved patch-clamp techniques for high-resolution current recording from cells and cell-free membrane patches. *Pflügers Archiv*, 391, 85–100, 1981.

Sakmann, B. and Neher, E., Eds. *Single-Channel Recording*. New York: Plenum Press, 1983.

Joshi, C. & Fernandez, J. M. Capacitance measurements: an analysis of the phase detector technique used to study exocytosis and endocytosis. *Biophys. J.* 53, 885–892, 1988.

Finkel, A. S., *Progress in instrumentation technology for recording from single channels and small cells*, in *Cellular and Molecular Neurobiology: A Practical Approach*. Oxford University Press, 1991.

3.6.2. TWO-ELECTRODE VOLTAGE CLAMP

Finkel, A.S. & Gage, P.W. Conventional voltage clamping with two intracellular microelectrodes, in *Voltage and Patch Clamping with Microelectrodes*. Ed. T. Smith Jr. et al., Baltimore: Williams & Wilkins, 1985.

3.6.3. SINGLE-ELECTRODE VOLTAGE CLAMP

Finkel, A.S. & Redman, S.J. Theory and operation of a single microelectrode voltage clamp. *J. Neurosci. Meths.* 11, 101–127, 1984.

3.6.4. SPACE-CLAMP CONSIDERATIONS

Rall, W. & Segev, I. Space-clamp problems when voltage clamping branched neurons with intracellular microelectrodes. in *Voltage and Patch Clamping with Microelectrodes*. Eds. T. Smith Jr. et al., Baltimore: Williams & Wilkins, 1985.

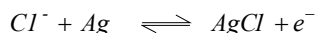
3.6.5. OTHER

Hille, B. *Ionic Channels of Excitable Membranes*. Sunderland, Massachusetts: Sinauer Associates. 1984.

4. Microelectrodes and Micropipettes

4.1. ELECTRODES, MICROELECTRODES, PIPETTES, MICROPIPETTES AND PIPETTE SOLUTIONS¹

Electrodes convert ionic current in solution into electron current in wires; they are made of materials that can participate in a reversible reaction with one of the ions in the solution. The most frequently used electrode material in electrophysiology is a silver (Ag) wire coated with a composite of Ag and silver-chloride (AgCl). For this electrode, chloride ions (Cl⁻) react with the Ag to produce AgCl plus an electron (e⁻), or an electron reacts with AgCl to produce Ag plus Cl⁻. Thus, the current carried by chloride ions in the solution is converted into electrons according to the following reversible reaction:



The electrical potential at one of these electrodes is equal to the standard electrochemical potential for Ag/AgCl plus $RT/F \ln(a\text{Cl}^-)$, where R is the gas constant (8.314 V C K⁻¹ mol⁻¹), T is the absolute temperature on the Kelvin scale, F is Faraday's constant (9.648 x 10⁴ C mol⁻¹), and aCl⁻ is the activity (*i.e.*, the effective concentration) of Cl⁻ in solution near the electrode solution interface. The potential difference between a pair of these electrodes should be zero if they are immersed in connected compartments with equal chloride concentrations. These concentrations must be kept constant during the course of an experiment or an offset voltage will occur. An offset may be encountered when a Ag/AgCl electrode is used as a bath electrode and the bath Cl⁻ concentration is changed. To prevent this type of voltage offset, many investigators connect their bath electrode through an agar bridge that maintains a constant Cl⁻ concentration in the immediate vicinity of the Ag/AgCl electrode.

Intracellular and patch microelectrodes contain a AgCl-coated Ag wire placed in a solution-filled glass micropipette. The electrolyte solution provides the fluid connection from the cell to the electrode. Thus, the glass “electrodes” one pulls are not electrodes at all but simple conduits of proper geometry to establish this fluid bridge. In recognition of this, microelectrodes are often referred to as “pipettes” or “micropipettes.”

1. Please see footnote 1 in Chapter 3.

The composition of the pipette solution depends on the type of measurement being made. Standard intracellular microelectrodes that are used to penetrate the cell membrane must be filled with a highly concentrated electrolyte solution, usually 2–4 M salt. The high electrolyte concentration reduces the electrode resistance. This minimizes the rectifying current flow, lowers voltage noise and provides a wider recording bandwidth. A solution this concentrated dominates the liquid junction potential formed between the pipette solution and the cell cytoplasm and results in a final junction potential that depends primarily on the relative mobilities of the anions and cations in the filling solution. This is important for the measurement of DC voltages because the cytoplasm anions are, predominantly, low mobility ions (mostly negative charges on large proteins), whereas the cations are small, high-mobility charges. The difference in the mobilities of the cellular anions and cations may result in a positive liquid junction potential. This positive liquid junction potential would lead to the measurement of an artificially depolarized membrane resting potential. The concentrated pipette solution is important because it negates the development of the liquid junction potential, thus preventing an erroneous measurement of the resting potential. However, there is a disadvantage in using the concentrated filling solution since it can enter the cell and produce a hyperosmotic load that would cause the cell to swell and alter its normal anion and cation content. While pipettes with very small tip diameters can minimize or prevent concentrated solution from entering the cell, they do so at the expense of noise, diminishing current passing ability, and limiting recording bandwidth. These limitations result from the high resistance of small-tip pipettes. In practice, the choice of the pipette tip size reflects a compromise between its ability to prevent the concentrated solution from entering the cell and the pipette's resistance.

Patch micropipettes are usually filled with a solution that is iso-osmotic to cell cytoplasm to allow current measurements in the absence of bulk water flow. Because of the much larger diameter of the patch pipette tip (1–2 μm) as compared to the tip diameter of an intracellular microelectrode (0.01–0.1 μm), the lower ionic-strength filling solution results in an electrode whose resistance is as low as a few megohms. The specific choice of the filling solution is dictated by the specific experiment to be done. Care must be taken to minimize junction-potential artifacts. When the pipette tip is immersed in the bath, a junction potential is generated. Its magnitude depends on the concentrations and mobilities of the ions in both the pipette solution and the bath (see discussions of the Henderson equation in electrochemistry textbooks). The junction potential is usually nulled while the pipette tip is immersed in the bath. When the seal forms, the junction potential disappears or changes its magnitude, and, consequently, the nulling voltage is no longer correct. The junction potential also changes upon going whole cell. These effects must be taken into account or offset errors will exist in either single-channel or whole-cell current recordings.

The filling solution in a patch pipette can be changed during the course of an experiment by inserting a fine tube into the back of the pipette through a special post in the electrode holder. Different solutions can be injected into the tube. Since the tube can be placed quite close to the pipette tip, the new solution can reach the vicinity of the pipette tip after a short diffusion delay. The procedure of draining excess solution from the pipette

depends on the specific setup. This technique cannot be applied to standard intracellular microelectrodes; due to their small tip size, the tube cannot be placed close enough to the tip to allow changing the tip solution within a reasonable time.

The pipette is mounted in a holder that contains a Ag/AgCl electrode and a proper connector to plug into the headstage of the amplifier. The holder must be constructed of a low-noise, inert material, which is often chosen empirically. Axon Cellular Neuroscience holders are constructed from polycarbonate, which yields low noise with several patch-clamp pipettes. HL-U headstages have an electrode well to accommodate pipettes with an outside diameter 1.0–1.7 mm. The HL-1-17 (for the non-U-type CV-type headstages) and HL-2-17 holders (for the HS-type and VG-type headstages) have an electrode well that can accommodate pipettes with an outside diameter of 1.5–1.7 mm. Pipettes of this size have an internal bore that allows insertion of a 1 mm diameter Ag/AgCl pellet electrode. The HL-1-12 (for the non-U-type CV-type headstages) and HL-2-12 (for the HS-type and VG-type headstages) holders have a pipette well that can accommodate pipette sizes of 1.0–1.2 mm diameter. This pipette size requires an electrode made of small-gauge Ag wire coated with AgCl. A simple yet effective coating procedure is to clean the silver wire down to bare metal using fine sand paper and immerse the cleaned wire in bleach (Clorox) for 20–30 minutes, until the wire is uniformly blackened by the Ag/AgCl coating. Coating of the silver wire must be repeated whenever the AgCl becomes scraped from the wire. Disruption of the coat can be minimized either by heat polishing the back of each pipette before insertion into the holder or by encapsulating the coated portion of the wire in a perforated Teflon sleeve.

The selection of the glass used for making the electrodes is more important for patch pipettes than for intracellular micropipettes. Most intracellular micropipettes are made from Corning #7740 Pyrex glass (Corning Inc., Corning, NY). However, when used for tiny current measurements as in patch recordings, this glass is too noisy. The best patch pipettes are made from glasses with low loss factors (see Table 4.1). These glasses generate lower noise, and often have lower capacitances and fewer time constants to compensate.

4.2. FABRICATION OF PATCH PIPETTES

Glass tubing selected for the fabrication of patch pipettes should have walls of substantial thickness (0.2–0.3 mm). A thick wall generates lower electrical noise and increases bluntness at the tip, thereby preventing penetration into the cell during seal formation. Most investigators use glass tubing with a 1.5–2.0 mm outside diameter and a 1.15–1.2 mm inside diameter.

If not pre-cleaned, the glass tubing should be cleaned prior to the preparation of the patch pipette. Sonicating the glass in 100% ethanol in an ultrasonic cleaner is an effective cleaning procedure. After cleaning, the glass should be placed in an oven at 200 °C for 10–30 minutes to achieve complete drying. This heat treatment is necessary for low-noise recording in environments with very high humidity.

Patch pipettes require much blunter tips than standard intracellular micropipettes and it is usually impossible to pull them adequately on single-stage electrode pullers. Many laboratories have modified standard vertical pipette pullers to operate as multiple-stage pipette pullers. Pulling pipettes, however, has become remarkably easier with the advent of microprocessor-driven microelectrode pullers like those available from the Sutter Instrument Company. With these pullers, it is possible to implement very complicated multistage pulls of glass pipettes and to store the parameters required for the desired operation in the instrument's memory.

For the lowest noise recordings, patch pipettes must be coated with a hydrophobic material to prevent the bathing solution from creeping up the wall of the pipette and, thus, limit a substantial noise source. A commonly used compound is Sylgard #184 from Dow Corning (Midland, MI). Coating the glass with Sylgard also improves the electrical properties of the glass. After preparing the Sylgard solution per the manufacturer's instructions, it can be stored in the freezer in small, well-capped centrifuge tubes for several weeks. When brought to room temperature for use in painting electrodes, this freezer-stored Sylgard will last for several hours before it begins to polymerize. Sylgard is painted on the pipette tip using a small utensil, such as a piece of capillary tubing pulled over flame to a reasonably fine tip. Sylgard painting can be done using the magnifications available with standard dissecting microscopes. The pipette is coated to within 100 μm or less from its tip. It is important that the Sylgard be directed away from the tip by gravity at all times during the painting procedure. Otherwise, it will flow into the tip and make firepolishing and/or sealing impossible. After painting, Sylgard can be cured by holding the tip for 5–10 seconds in the hot air stream coming from a standard heat gun of the type used in electronics fabrication.

To promote gigaohm seals and to reduce the possibility of tip penetration into the cell during seal formation, pipette tips should be firepolished. Firepolishing is accomplished by connecting to a micromanipulator a rod of inert material to which a short loop of platinum iridium wire has been fastened. The ends of this wire must be soldered to two other pieces of wire that can be connected to a voltage or current source to allow current passing through the platinum wire. The platinum loop is generally bent into a very fine hairpin so that it can be brought to within a few microns of the electrode tip under direct observation using a compound microscope. Magnifications of 600x–1500x are required for adequate visibility. The platinum wire is usually coated with a glass, such as Pyrex or Corning #7056, to prevent sputtering. After positioning the electrode tip near the glass-coated wire, current is passed through the wire to heat it. The amount of current required depends on the softening temperature of the glass from which the pipette is constructed. The hot platinum wire heats the electrode tip and causes sharp corners to round and rough surfaces to smooth. This polishing is best done under direct observation at a magnification of 600x–1500x.

4.3. PIPETTE PROPERTIES FOR SINGLE-CHANNEL VS. WHOLE-CELL RECORDING

Whereas some properties of pipettes used for single-channel and whole-cell recordings are similar, other properties are entirely different. Most importantly, reducing the noise of the pipette is much more crucial in single-channel recording than in whole-cell recording. The dominant noise source in whole-cell recording is the pipette resistance that is in series with the capacitance of the entire cell. Hence, the noise contribution of the pipette is not as important. However, in order to provide sufficient bandwidth for whole-cell current recording and to limit command voltage errors, the resistance of a pipette used in whole-cell recording should not exceed a few megohms. Limiting the pipette resistance is not required in single-channel recording; nor does a higher pipette resistance, up to several tens of megohms, result in a significant increase in the noise (see Chapter 11 for further discussion of pipette noise). In either single-channel or whole-cell recording, capacitance currents following voltage steps must be sufficiently small and simple in time course to allow the researcher to compensate them by simple circuitry in the patch-clamp amplifier. Additionally, whether used for single-channel or whole-cell recording, pipettes must be made of glasses that do not leach compounds from their walls since these compounds might alter the currents measured from a particular channel.

4.4. TYPES OF GLASSES AND THEIR PROPERTIES

Patch-clamp pipette glasses can be classified on the basis of the temperature at which they soften, on the basis of their electrical properties, or on the basis of their major chemical constituents. Many of these properties are itemized in specifications provided by the manufacturers. Therefore, it is often possible to choose glasses that should be effective for patch clamping just by considering their specifications. Table 4.1 lists the properties of a number of glasses that have been used for patch clamping. Glasses are listed in increasing order of loss factors.

Table 4.1: Electrical And Thermal Properties of Different Glasses.

Glass	Loss Factor	Log ₁₀ Volume Resistivity	Dielectric Constant	Softening Temp. °C	Description
7940	0.0038	11.8	3.8	1580	Quartz (fused silica)
1724	0.0066	13.8	6.6	926	Aluminosilicate
7070.	25	11.2	4.1	—	Low loss borosilicate
8161	0.50	12.0	8.3	604	High lead
Sylgard	0.581	13.0	2.9	—	#184 Coating compound
7059	0.584	13.1	5.8	844	Barium-borosilicate

4. Microelectrodes and Micropipettes

Glass	Loss Factor	Log ₁₀ Volume Resistivity	Dielectric Constant	Softening Temp. °C	Description
7760	0.79	9.4	4.5	780	Borosilicate
7040	1.00	9.6	4.8	700	Kovar seal borosilicate
KG-12	1.00	9.9	6.7	632	High lead
1723	1.00	13.5	6.3	910	Aluminosilicate
0010	1.07	8.9	6.7	625	High lead
EN-1	1.30	9.0	5.1	716	Kovar seal borosilicate
7720	1.30	8.8	4.7	755	Tungsten seal borosilicate
7056	1.50	10.2	5.7	720	Kovar seal borosilicate
3320	1.50	8.6	4.9	780	Tungsten seal borosilicate
7050	1.60	8.8	4.9	705	Series seal borosilicate
KG-33	2.20	7.9	4.6	827	Kimax borosilicate
7740	2.60	8.1	5.1	820	Pyrex borosilicate
1720	2.70	11.4	7.2	915	Aluminosilicate
N-51A	3.70	7.2	5.9	785	Borosilicate
R-6	5.10	6.6	7.3	700	Soda lime
0080	6.50	6.4	7.2	695	Soda lime

Note that the electrical properties and the thermal properties of the glasses are not necessarily related to each other. Note also that Sylgard has better electrical properties than most glasses shown in the table. It is, therefore, not surprising that heavy Sylgard coating of pipettes fabricated from many types of glasses improves their electrical properties.

Table 4.2 shows the chemical constituents of many of the same glasses listed in Table 4.1. This table may be useful in deciding which glasses are likely to contain leachable components that might affect channel currents.

Table 4.2: Chemical Compositions of Different Glasses.

Glass	Chemical Constituent													
	SiO ₂	B ₂ O ₃	Al ₂ O ₃	Fe ₂ O ₃	PbO	BaO	CaO	MgO	Na ₂ O	K ₂ O	Li ₂ O	As ₂ O ₃	Sb ₂ O ₃	SO ₃
1724	Not Available													
7070	70.7	24.6	1.9	___	___	0.2	0.8	0.8	___	___	0.56	___	___	___
8161	38.7	___	0.2	___	51.4	2.0	0.3	0.04	0.2	6.6	___	0.04	0.38	___
7059	50.3	13.9	10.4	___	___	25	___	___	0.08	___	___	___	___	___
7760	78.4	14.5	1.7	___	___	___	0.1	0.1	2.7	1.5	___	0.18	___	___
7040	66.1	23.8	2.9	___	___	___	0.1	0.1	4.1	2.7	___	0.1	___	___
KG-12	56.5	___	1.5	___	28.95	___	0.1	0.1	3.7	8.6	___	0.4	0.25	___
1723	57.0	4.0	16.0	___	___	6.0	10.0	7.0	___	___	___	___	___	___
0010	61.1	___	___	___	22.5	___	0.3	0.1	7.2	7.3	___	___	___	___
EN-1	65.0	18.0	7.6	___	0.01	2.7	0.1	0.1	2.3	3.2	0.6	___	___	___
7720	71.4	15.2	2.0	___	6.1	0.3	0.2	0.1	3.7	0.3	___	___	0.5	___
7056	69.0	17.3	3.9	___	___	___	0.12	___	0.91	7.5	0.68	0.48	___	___
3320	75.3	14.3	___	___	___	___	0.1	0.1	4.0	___	___	___	0.8	___
7050	67.6	23.0	3.2	___	___	0.1	0.1	0.1	5.1	0.2	___	___	___	___
KG-33	80.4	12.9	2.6	___	0.005	___	0.05	___	4.0	0.05	___	___	___	___
7740	80.4	13.0	2.1	___	___	___	0.1	0.1	4.1	___	___	___	___	___
1720	62.0	5.3	17.0	___	___	___	8.0	7.0	1.0	___	___	___	___	___
N51-A	72.3	9.9	7.3	___	0.02	___	0.9	0.05	6.5	0.7	___	0.02	___	___
R-6	67.7	1.5	2.8	___	___	2.0	5.7	3.9	15.6	0.6	___	___	___	0.2
0080	73.0	0.04	___	___	___	0.1	4.8	3.2	16.8	0.4	___	___	___	0.22

4.5. THERMAL PROPERTIES OF GLASSES

Glasses that soften at lower temperatures offer several advantages over glasses that soften at higher temperatures when fabricating patch-clamp pipettes. First, they do not impose a burden on the heating filaments of microelectrode pullers. Since low-filament current is required to pull these glasses, filaments rarely change their properties with extended use and do not require replacement even after one or two years of continued operation. Second, pipettes with extremely blunt tips can be more readily fabricated from these glasses than from glasses with high softening temperatures. Blunt tips provide the lowest access

resistance (R_a) for whole-cell recording. Furthermore, the blunt-tapered pipettes are less likely to penetrate into the cell when pressed against the cell membrane during seal formation. High-lead glasses pull at the lowest temperatures and are remarkably amenable to firepolishing. It is possible to pull pipettes at such a low temperature that their tips are broken and jagged, forming tip openings with diameters in excess of 50 μm , and yet the pipettes are easily firepolished into usable patch pipettes. Although the resulting tips are exceedingly blunt, these pipettes are effective in forming a tight seal with the cell even when the final pipette resistance is $< 0.5 \text{ M}\Omega$.

Blunt tips are very beneficial for perforated-patch recording because they are capable of drawing in large omega-shaped pieces of membrane when suction is applied. The large surface area of the omega-shaped membrane maximizes the number of parallel channels created by amphotericin B or nystatin, thus minimizing the final R_a that is achievable (see Chapter 5).

Most of the pipettes used for patch-clamp recording are fabricated from borosilicate glasses. These glasses soften at temperatures in the 700–850 $^{\circ}\text{C}$ range (see Table 4.1). Although those at the low end of the range are quite easily pulled and firepolished, they are clearly not as good as the high-lead glasses in this regard. Compared to high-lead glasses, the success of firepolishing borosilicate glasses depends more on the shape of the tip obtained after pulling. However, with the advent of multi-stage, computerized pipette pullers, one can routinely make both patch and whole-cell pipettes from almost any glass.

Aluminosilicate glasses are very hard glasses with high softening temperatures. They produce low-noise single-channel recordings. However, their low noise comes at a high price. Glasses in this class soften at temperatures above 900 $^{\circ}\text{C}$ and, therefore, pulling them wears out the coils and filaments of pipette pullers. Consequently, the coils change their properties with time and must be replaced or readjusted frequently. Moreover, pipettes fabricated from aluminosilicate glasses produce undesirably thin-walled tips after pulling. This, along with their high softening temperature, makes them much more difficult to firepolish than softer glasses.

4.6. NOISE PROPERTIES OF GLASSES

While there is no simple way to predict the noise that will be generated from a particular glass when it is used for single-channel patch clamping, it has been observed that the noise of a patch pipette is related to its loss factor. The loss factor is a parameter used by glass manufacturers to describe the dielectric properties of a glass. Figure 4.1 illustrates the dependence of the noise of a patch pipette on the loss factor of the glass. Patch pipettes fabricated from various glasses, coated with Sylgard to within 100 μm of the tip and filled with solution were sealed to Sylgard lining the bottom of a fluid-filled chamber. The rms noise was measured using an rms meter, with the pipette in air just above the bath and then again with the pipette sealed to Sylgard. The 10 kHz rms noise in this figure was calculated by subtracting the noise measured in air from the noise measured when the pipette was sealed to Sylgard.

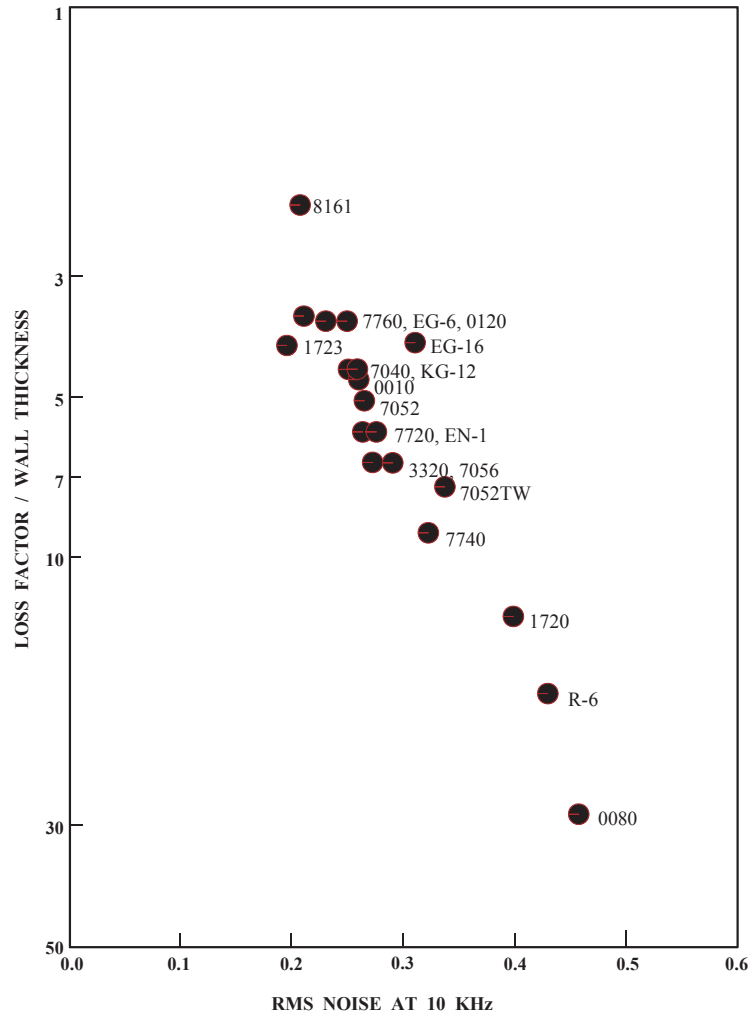


Figure 4.1: Noise properties of glasses.

The dependence of the rms noise of a patch pipette on the loss factor of the glass.

As seen in Figure 4.1, glasses with the lowest loss factor exhibit the lowest noise. Furthermore, noise decreases as the wall thickness increases (compare 7052 with 7052TW, thin walled). Even greater improvement in noise can be achieved using quartz (fused silica) pipettes. The noise of pipettes fabricated from Corning 7070 (low loss electrical) or Corning 1724 (aluminosilicate) glasses could also be improved if proper techniques of fabricating patch pipettes from these glasses would be developed. The noise values shown in Figure 4.1 are higher than would be obtained with the Axopatch™ 200B amplifier in sin-

gle-channel recording mode since its capacitive headstage produces lower noise than is produced by standard resistive headstages. It has been observed that as the noise of the headstage electronics decreases, the noise of other components, such as holder and glass, is reduced as well.

4.7. LEACHABLE COMPONENTS

Glasses are complicated substances made of many different compounds as shown in Table 4.2. While glasses have major constituents that lead to their classification as soda lime, aluminosilicate, borosilicate, *etc.*, they have many trace compounds whose location in the glass is unknown. Glasses may have components on their surfaces that can leach into an aqueous environment with which they are in contact. Leachable components could be particularly problematic in single-channel and whole-cell recording due to the close proximity of the channels to the glass. The literature contains reports of undesirable effects of the leaching of constituents from the glass on membrane currents.

4.8. FURTHER READING

Cota, G., Armstrong, C. M. Potassium channel “inactivation” induced by soft-glass patch pipettes. *Methods in Enzymology*. Plenum Press. New York and London, 1983.

Sakmann, B., Neher, E. Geometric parameters of pipettes and membrane patches. *Single-Channel Recording*. Sakmann, B., Neher, E., Eds. pp. 37–51. Plenum Press. New York and London, 1983.

Cota, G., Armstrong, C. M. Potassium channel “inactivation” induced by soft-glass patch pipettes. *Biophys. J.* 53, 107–109, 1988.

Corey, D. P., Stevens, C. F. Science and technology of patch-recording electrodes. *Single-Channel Recording*. Sakmann, B., Neher, E. Eds. pp. 53–68. Plenum Press, New York and London, 1983.

Hammill, O.P., Marty, A., Neher, E., Sakmann, B., Sigworth, F.J. Improved patch-clamp techniques for high resolution current-recording from cells and cell-free membrane patches. *Pflügers Arch.* 391, 85–100, 1981.

Rae, J. L., Levis, R. A. Patch-clamp recordings from the epithelium of the lens obtained using glasses selected for low noise and improved sealing properties. *Biophys. J.* 45, 144–146, 1984.

Rae, J. L., Levis, R. A. Patch voltage clamp of lens epithelial cells: theory and practice. *Molec. Physiol.* 6, 115–162, 1984.

Rae, J. L., Levis, R. A., Eisenberg, R. S. *Ion Channels*. Narahashi, T. Ed. pp. 283–327. Plenum Press, New York and London, 1988.

Ogden, D. C., Stanfield, P. R. *Microelectrode Techniques: The Plymouth Workshop Handbook*. Standen, N. B., Gray, P. T. A., Whitaker, M. J. Eds. pp. 63–81. The Company of Biologists Limited, Cambridge, 1987.

Furman, R. E., Tanaka, J. C. Patch electrode glass composition effects on ion channel currents. *Biophys J.* 53, 287–292, 1988.

Rojas, L., Zuazaga, C. Influence of the patch pipette glass on single acetylcholine channels recorded from *Xenopus* myocytes. *Neurosci. Lett.* 88: 39–44, 1988.

5. Advanced Methods in Electrophysiology

5.1. RECORDING FROM XENOPUS OOCYTES

The *Xenopus* oocyte expression system was introduced by Gurdon in 1971 as a means to study various aspects of the control of gene expression. Injection of exogenous DNA into the oocyte nucleus or mRNA into the cytoplasm led to the expression of functional proteins by the oocytes. Early studies dealt with the expression of proteins that are of little interest to electrophysiologists, such as globin, interferon and various viral proteins. Consequently, electrophysiologists and biophysicists paid scant attention to studies of protein expression in oocytes. However, beginning in 1982, Miledi and co-workers demonstrated that various types of ion channels and receptors could also be expressed in oocytes after injection of mRNAs that had been isolated from the appropriate tissue. For example, injection of Torpedo electric organ mRNA led to the expression of functional nicotinic acetylcholine receptors, while injection of rat brain mRNA resulted in the expression of a large number of different voltage- and ligand-gated ion channels, among them the voltage-gated Na⁺ channels, NMDA and non-NMDA subtypes of glutamate receptors, and GABA_A receptors.

Since these initial experiments, a number of workers have adopted this expression system to study various aspects of the structure and function of ion channels and receptors. Some of the more common types of studies that have employed expression of exogenous ion channels and receptors in oocytes include:

- 1 Analyzing the properties of mutated channels as a means to understand structure-function relationships in ion channels;
- 2 Studying the post-translational processing and the assembly of multisubunit channels and receptors;
- 3 Comparing the properties of channels from various tissues expressed in a common environment;
- 4 Examining the modulation of channel and receptor function by various second messenger systems;
- 5 Analyzing various aspects of receptor-effector coupling; and
- 6 Functional screening of cloned genes that encode channels and receptors (expression cloning).

Most of these experiments involve electrophysiological recording from oocytes. This describes the mechanics of recording from oocytes and points out some oocyte features of which one should be aware in order to obtain high-quality recordings.

5.1.1. WHAT IS A XENOPUS OOCYTE?

Xenopus oocytes are egg precursors that, upon proper hormonal stimulation, pass through the frog's oviduct and become eggs, which can then be fertilized to make more frogs. Oocytes are stored in the abdominal cavity and can be removed surgically for experimental purposes. They go through six developmental stages (termed stages I to VI). Most researchers use only the large stage V and VI oocytes, which can be used interchangeably in electrophysiological experiments. Oocytes are found in clumps called ovarian lobes, which are made up of oocytes, connective tissue, blood vessels and follicle cells. Figure 5.1 shows an individual stage V or VI oocyte as found in an ovarian lobe.

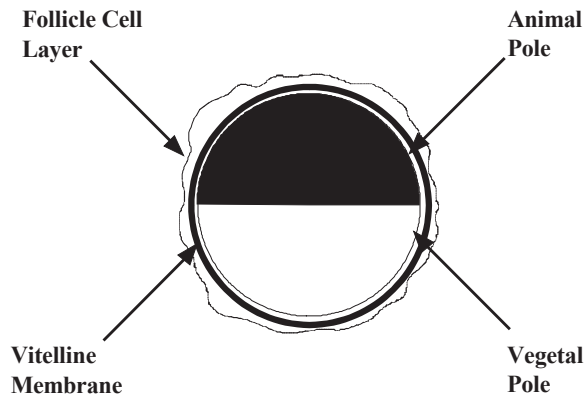


Figure 5.1: Stage V or VI oocytes as found in an ovarian lobe.

The oocyte is a large cell, with a diameter of approximately 1–1.2 mm. It is surrounded by the vitelline membrane, which is a glycoprotein matrix that gives the oocyte some structural rigidity and helps it maintain a spherical shape. The mesh formed by this matrix is rather large; consequently, small molecules and even small proteins such as α -bungarotoxin (molecular weight 8,000 dalton) can interact with proteins on the oocyte surface. Since devitellinized oocytes are extremely fragile, the vitelline membrane is usually removed only for single-channel recording, where the surface of the oocyte must be sufficiently clean to allow the formation of a gigohm seal. A layer of follicle cells surrounds the vitelline membrane. The individual cells in the follicle cell layer are electrically coupled to each other and to the oocyte through gap junctions, so that electrical events taking place in the follicle cells can be detected in the oocyte.

The follicle cell layer is a potential source for many problems. Therefore, most researchers remove it prior to mRNA injection or recording by one of two ways: 1) an extensive colla-

genase treatment to completely strip off the layer by immersing the oocyte for 1–3 hours in a calcium-free saline containing 2 mg/mL collagenase Type IA (Sigma Chemical Company, St. Louis, MO) until about half of the oocytes have been released from the ovarian lobe; or 2) a less extensive collagenase treatment followed by manual removal of the follicular layer with watchmaker's forceps. The latter is preferred, since oocytes that undergo the extensive collagenase treatment sometimes do not survive as long as those treated less extensively. Some of the problems introduced by the follicle cell layer are rather trivial. For instance, it is more difficult to impale a follicle-encased oocyte with an injection needle or a microelectrode. Other complications, however, can create major problems. The electrical coupling between the oocyte proper and the follicle cells means that one records from both. Numerous examples of oocyte “endogenous” receptors that turned out to be in the follicle cell layer were published. In fact, the *Xenopus* oocyte is a nearly ideal expression system for ion channels and receptors since it has very few types of endogenous channels and receptors, an advantage that is defeated if the follicle cells are left on the oocyte.

One of the striking features of a *Xenopus* oocyte is its two-toned color scheme: the animal pole hemisphere is dark colored, while the vegetal pole is light colored. This polarity is maintained inside the oocyte: the nucleus is found in the animal pole, and different populations of mRNAs exist in the hemispheres. In addition, a standing Cl^- current flows from one pole to the other, indicating that the distribution of channels in the oocyte membrane is not homogeneous. Published reports showed that ACh receptors expressed from exogenous mRNAs are also unevenly distributed; although receptors were expressed all over the oocyte, more receptors were expressed on the vegetal pole. It is not clear if there is any relation between the site of RNA injection and the location of the expressed channels on the oocyte membrane. This non-homogeneity is not important for whole-cell recording, but could be important for single-channel recording.

5.1.2. TWO-ELECTRODE VOLTAGE CLAMPING OF OOCYTES

Two factors need to be taken into consideration when voltage clamping oocytes. First, with an apparent surface area on the order of $10^6 \mu\text{m}^2$, there is an enormous amount of membrane that must be charged in order to clamp the cell. In fact, the situation is even worse than it may appear since there is considerable invagination of the surface membrane, thereby doubling or even tripling the surface area compared to an “ideal” spherical oocyte. Second, one can encounter currents up to 10 μA or larger after mRNA injection, potentially causing appreciable series resistance errors. In the case of currents from cloned K^+ and Na^+ channels, which activate rapidly and can give rise to very large currents, there may be an inadequate control of the voltage during the initial phases of channel activation.

The response time (τ) of a voltage clamp to a step voltage change is:

$$\tau = \frac{R_I C_m}{A} \quad (1)$$

where R_I is the resistance of the current-passing electrode, C_m is the membrane capacitance, and A is the gain of the command amplifier. Since not much can be done about C_m (*“Combining Whole-Cell Clamp with Focal Current Recording”* on page 111), the only two things one can do in order to achieve fast clamping of the cell is to use the lowest R_I and largest A possible. One “advantage” of the oocyte’s large size is that one can use low-resistance electrodes for both the voltage-recording and current-passing electrodes. (This can hardly be regarded as an advantage, since the large size of the oocyte is what caused the problem in the first place). Electrodes that have resistances of 0.5–2 M Ω when filled with 3 M KCl are used. The particular type of glass is unimportant; both regular and fiber-filled electrode glass have been used successfully. Since the electrodes have rather large tip openings, they usually do not clog very often; the same set of electrodes can be used repeatedly during the course of a day. The electrodes’ low resistance eliminates the need in a negative-capacitance circuit to correct for the frequency response of the voltage-recording electrode, thereby eliminating this potential source of clamp instability. To achieve the fastest response, the electrodes must be shielded in order to reduce capacitive coupling between them. Two rather simple ways of doing this are 1) Placing a grounded sheet of metal between the two electrodes (making sure that it doesn’t make contact with the bath), or 2) wrapping a wire around a piece of tubing that fits over the voltage electrode like a sleeve, and then grounding the wire. In the latter case, the shield should extend as close to the bath as possible.

The other parameter that one can control in order to maximize the speed of the voltage clamp is the command amplifier gain. As with other types of cell-electrode combinations, one must usually introduce a frequency response compensation network to ensure clamp stability at high gains. Therefore, the absolute gain of the clamp and the command voltage of the amplifier are less important than the maximum gain reached before the clamp becomes unstable. The LAG and (AC) GAIN controls of the Axoclamp™ 900A micro-electrode amplifier allow one to fine-tune the clamp. For oocytes, start with the LAG at about 0.2 ms and the GAIN set to its lowest position, and gradually increase it as much as possible until the clamp starts oscillating. The lower the LAG setting, the faster the clamp. Axoclamp 900-series amplifiers include an Oscillation Detection circuit that automatically reduces the voltage clamp gain when oscillation in the circuit is detected.

The goal is to achieve a fast voltage clamp. But, how fast is fast enough? The actual speed required depends on the type of signal being measured. For example, when studying a ligand-activated ion channel that is activated by bath application of an agonist, it makes no difference if the clamp settles in 2 ms or 20 ms, since the exchange time of the chamber is the limiting factor in the rate of activation. On the other hand, when studying voltage-gated channels, one wants the fastest clamp attainable. A well-tuned, two-microelectrode voltage clamp can clamp an oocyte fast enough to study the gating kinetics of most voltage-gated channels. However, it is probably impossible to clamp an oocyte fast enough to study the activation kinetics of fast-gating voltage-gated Na⁺ channels in which the rising phase of the current can be on the order of 1 ms or shorter. It is still possible to study slower processes, such as inactivation or pharmacological properties, even if the clamp is not fast enough to study the activation process. A faster clamp can be achieved

either by recording from smaller oocytes (stage II or III) whose capacitances are approximately one-fifth those of the larger stage V and VI oocytes, or applying the more common “macropatch” technique. Either of these two approaches provides a sufficiently fast clamp for studying the kinetics of Na⁺ channel activation.

Electrode penetration is most easily achieved simply by advancing the electrode into the oocyte until it dimples the membrane and then visibly pops into the cell. Due to the large size of the oocyte, a coarse, inexpensive manipulator provides adequate control of movement. Typical resting potentials in a physiological saline solution (100 mM NaCl, 2 mM KCl, 1.8 mM CaCl₂, 1 mM MgCl₂, 5 mM HEPES, pH 7.6) are approximately -40 mV or more negative. The voltage clamp is tuned by applying a small (2 mV) square wave at the resting potential and then gradually increasing the gain of the clamp. As the gain increases, the voltage trace “squares up” and the capacitive transient in the current trace gets faster and faster. Instability in the clamp will first appear as small oscillations in the traces; the oscillations will increase as the gain increases. If oscillations do appear, the TIME CONSTANT control should be adjusted until they disappear. This process should be continued until one reaches the highest gain possible without any apparent oscillations. In general, if the electrodes are shielded as described above, full gain can be achieved.

5.1.3. PATCH CLAMPING XENOPUS OOCYTES

While oocytes are obviously too large for the whole-cell mode of patch clamping, they are amenable to all three configurations of single-channel recording, *i.e.*, cell-attached, inside-out and outside-out. One of the major requirements for achieving the high-resistance seals necessary for single-channel recording is a clean membrane surface. With oocytes, one must remove the vitelline membrane prior to patch clamping by placing the oocyte in a hypertonic stripping solution (usually 200 mM K-aspartate, 20 mM KCl, 1 mM MgCl₂, 10 mM EGTA, 10 mM HEPES, pH 7.4) and allowing it to shrink. As the oocyte shrinks, the vitelline membrane detaches from the cell membrane and appears as a transparent sphere around the oocyte. One can then manually remove the vitelline membrane using fine watchmaker’s forceps. Since devitellinized oocytes will stick to glass or plastic (but not to agarose) after a few minutes of contact, the shrinking and vitelline membrane removal is usually carried out in small petri dishes with a layer of 2% agarose on the bottom. This allows one to prepare a number of oocytes at once. At this point, the oocytes are extremely fragile. In particular, stripped oocytes have a propensity for disintegrating when they are at an air-water interface; therefore, extreme care must be taken when transferring them to the recording chamber.

Once the vitelline membrane has been removed, gigohm seals can be obtained with high success rates. Oocytes, like most cells, contain stretch-activated channels that can interfere with recording “interesting” channels in the cell-attached mode. Therefore, most researchers prefer to use excised patches for single-channel work, where the incidence of stretch-activated channel currents is much lower. The actual mechanics of obtaining excised patches is the same as for any cell type, with the exception that some researchers prefer to rupture the membrane by applying positive pressure rather than suction, since suction can sometimes cause yolk platelets to clog the pipette tip.

5.2. FURTHER READING

- Barnard, E.A., Miledi, R., Sumikawa, K. Translation of exogenous messenger RNA coding for nicotinic acetylcholine receptors induces functional receptor in *Xenopus* oocytes. *Proc. R. Soc. Lond. B* 215:241–246, 1982.
- Gurdon, J.B., Lane, C.D., Woodland, H.R., Marbaix, G. Use of frog eggs and oocytes for the study of messenger RNA and its translation in living cells. *Nature*. 233:177–182, 1971.
- Krafte D., Lester, H.A. Expression of functional sodium channels in stage II–III *Xenopus* oocytes. *J. Neurosci. Meth.* 26:211–215, 1989.
- Methfessel, C., Witzemann, V., Takahashi, T., Mishina, M., Numa, S., Sakmann, B. Patch clamp measurements on *Xenopus laevis* oocytes: currents through endogenous channels and implanted acetylcholine receptor and sodium channels. *Pflügers Arch.* 407:577–588, 1986.
- Snutch, T.P. The use of *Xenopus* oocytes to probe synaptic communication. *Trend Neurosci.* 11:250–256, 1988.
- Stühmer, W., Methfessel, C., Sakmann, B., Noda, M. Y., Numa, S. Patch clamp characterization of sodium channels expressed from rat brain cDNA. *Eur. Biophys. J.* 14:131–138, 1987.
- Stühmer, W., and Parekh, A.B., *Electrophysiological Recordings from Xenopus Oocytes in Single-Channel Recording*, 2nd Ed., Sakmann, B., and Neher, E., eds., pp. 341–355, 1995.

5.3. PATCH-CLAMP RECORDING IN BRAIN SLICES

Although it is commonly accepted that patch-clamp techniques offer many technical advantages over conventional intracellular microelectrode recording configurations, one nagging limitation has been the belief that, in order to allow formation of gigaohm seals with patch electrodes, cells must be treated in some way that leaves their membrane “clean.” Such treatment might entail dissociation of tissue by enzymatic digestion or mechanical disruption, and might or might not be followed by growth in tissue culture. These techniques invariably result in significant damage to the cells or severe alteration of their environment, at least transiently, during the preparation of the cells for recording. Alternatively, tissue explants or slices can be maintained in “organotypic” culture, allowing many of the cell-cell interactions to be maintained and mitigating some of the problems described above. However, with any of these approaches, the possibility remains that significant alteration of cellular properties occurs prior to recording.

Therefore, it is of great interest to be able to apply patch-recording techniques to neurons in acute tissue slices. The marriage of these two approaches offers many of the advantages of both, with few of the limitations:

- 1 Cells in tissue slices are likely to be much closer to their original state than cells subjected to the above-mentioned treatments. No disruption of the normal cellular environment need take place until the preparation of slices and disruption is limited to the surface of the slice.
- 2 The increased signal-to-noise ratio and improved voltage-clamp quality, compared with conventional intracellular recording using sharp microelectrodes, provide substantial benefits for cellular electrophysiology. These benefits are particularly helpful when measuring small or rapid events.
- 3 The ability to control the intracellular environment is greatly enhanced by whole-cell recording, thus facilitating the study of interactions between intracellular biochemistry and electrophysiology.

It should be noted however, that not all problems are solved by applying whole-cell techniques. “Washout” of intracellular biochemical machinery may affect electrophysiological properties, and control of membrane potential in branched or elongated neurons is often inadequate.

Two strategies have been applied in obtaining patch-clamp recordings from tissue slices. One approach, the “cleaning” technique, involves removing overlying neuropil or cellular debris from a visually-identified cell using a relatively large pipette filled with the same solution used to superfuse the slice. Recording is then possible in a manner similar to standard patch recording. In the other approach, called the “blind” technique, the recording pipette is lowered into a tissue slice without high-magnification visual guidance; seal formation is monitored using electrical measurements.

5.3.1. THE CLEANING TECHNIQUE

Tissue preparation for this technique uses procedures slightly modified from those used for standard slices. The slices must be thin enough to allow good cellular visibility (100–300 μm , depending on the age of the animal), but thicker slices result in a greater number of undamaged cells. Generally, vibrating microtomes are preferable to tissue choppers because their use results in less dead or damaged tissue at the cut surface, and because they facilitate preparation of thin slices. Special care should be taken when preparing thin slices to ensure that the bathing medium remains ice cold in order to maintain the necessary firm tissue consistency. Following their preparation and prior to recording, slices are commonly incubated at 37 °C for about one hour. This procedure softens the tissue and facilitates subsequent cleaning of cells. Various methods may be used for storing slices, but care is needed to avoid damage to the cut surfaces resulting from procedures such as placing slices on filter paper. Slices may be stored at room temperature or warmed to 30–35 °C.

The only major piece of equipment required for this technique, in addition to a standard recording setup, is an upright microscope equipped with a water-immersion objective, most commonly 40x magnification. Use of an inverted microscope is not feasible since, even if very thin slices are used, visibility through the tissue to a recording pipette is signif-

icantly impaired. Hoffman or Nomarski differential-interference-contrast optics can be helpful, but are not necessary. Unless manipulators are mounted on the stage, it is extremely helpful to use a fixed-stage microscope, so that changing focus does not cause movement of the tissue with respect to cleaning or recording pipettes.

An objective with high numerical aperture is important. A commonly used apparatus is the Zeiss 40x water-immersion objective, which has a numerical aperture of 0.75. This objective offers a working distance of approximately 1.6 mm. The pipettes must, therefore, be placed at a very shallow angle (15° from the horizontal is common). One consideration in mounting micromanipulators is that the movement in true horizontal and vertical directions is preferable to a coordinate system with an axis oriented parallel to the pipette. An advantage of this arrangement is the ability to lower the recording pipette directly onto the target cell in a single motion.

The recording chamber must allow continuous superfusion of the slice; it must also permit immobilization of the tissue despite the fluid flow, and do so using a device that does not interfere with the objective or the pipettes. One solution to this problem is a net consisting of a U-shaped piece of flattened platinum wire with a parallel array of very fine nylon monofilaments, such as stocking fibers, glued across the arms of the U-shaped wire (Edwards et al., 1989; Sakmann et al., 1989). The net can be placed on the slice and is usually heavy enough to prevent movement. Although the filaments may cause some damage to the surface of the tissue, they may be placed sufficiently far apart to leave considerable working space (the precise distance depends on the cellular architecture in the slice). Another solution is to attach the slice to the bottom of the recording chamber using a plasma clot (Blanton et al., 1989).

The pipette used for cleaning should have a tip much larger in diameter than a recording pipette, usually in the range of 5–20 μm. The optimal tip size depends on several factors; in general, larger tips are preferable for larger cells and for deeper cleaning. However, the consistency of the tissue and cell density may also affect the choice of tip diameter. For example, with particularly “sticky” tissue, such as neocortex, small cleaning pipettes may tend to become clogged with membranous debris. For a given preparation, it is best to arrive empirically at an appropriate size. Additionally, since debris tends to accumulate on the jagged edges of broken pipettes, it is usually best to pull unbroken pipettes to the appropriate size. To minimize any damage that the process might inflict on the cell, the cleaning pipette should be filled with the same solution used for the bathing medium. Note that some researchers, instead of using a separate cleaning electrode, perform the cleaning with the same recording electrode for the sake of expediency.

The first step in establishing a recording is to locate a healthy cell; it is usually possible to distinguish cells in good condition by their appearance of solidity or opacity. In such neurons, it is often possible to follow dendritic processes for some distance. Some healthy cells may be observed whose somata are on the surface of the slice and which display a “clean” membrane suitable for immediate patching with no further cleaning. Such neurons often have dendrites that can be seen projecting into the depths of the slice. It seems that cells

that have lost most of their dendrites due to the slicing procedure are often “sick,” as characterized by a granular and/or transparent appearance of the soma.

Once a healthy cell has been located, the next step is to remove the overlying neuropil. Mouth control of the pressure applied to the back of the pipette permits rapid, highly precise application of pressure and suction. It is often best to begin by applying positive pressure gently with the pipette placed just at the surface of the slice and directly above the targeted cell. Blowing accomplishes two goals. First, it provides information about the consistency of the tissue, which may be rather variable from slice to slice and which differs dramatically from one brain region to another. Second, application of positive pressure begins the process of disrupting the tissue overlying the desired cell. When tissue has been visibly disrupted, slight suction helps remove the loosened debris (Figure 5.2). Repeated application of this blowing and sucking cycle, with appropriate movement of the pipette to remove specific chunks of tissue, eventually results in a clean cell.

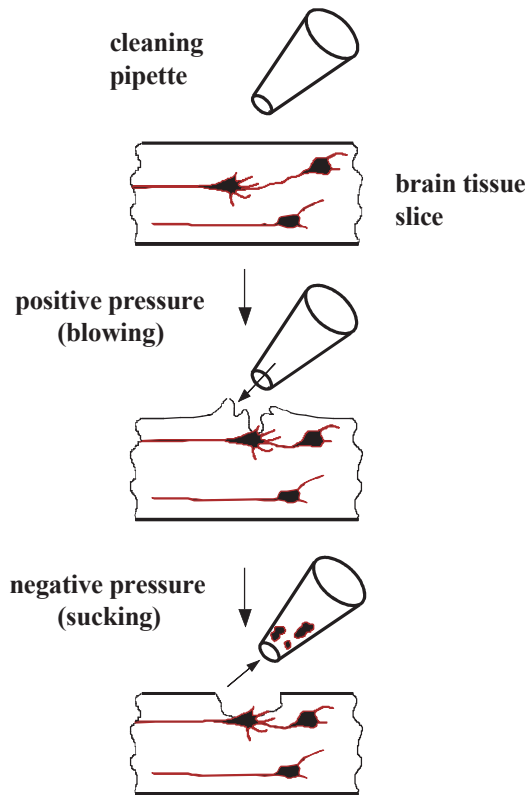


Figure 5.2: The Cleaning technique.

Use of a cleaning pipette to remove tissue overlying a cell in tissue slices. Reproduced with permission according to Edwards et al., (1989).

At first, this procedure may take a long time. It is almost inevitable that an inexperienced experimenter, who has not yet developed a feel for the tissue, will kill cells by applying pressure or suction that is too vigorous. With practice, however, one can clean even deep cells quite rapidly. Careful and repeated adjustment of the focus aids greatly in determining the degree of cleaning required at each stage. Depending on the particular type of tissue, a few tricks to facilitate and accelerate the process of producing clean cells may be applied. For example, in regions of densely packed somata, such as the CA1 pyramidal cell layer of the hippocampus, it is possible to remove tissue at the slice surface over a relatively large length of the cell layer by applying continuous suction and moving the pipette along the layer as if using a vacuum cleaner to remove dead tissue. Inspection of the underlying neurons often reveals at least one clean pyramidal cell.

After completing the cleaning procedure, patch-clamp recordings of cleaned cells in slices are carried out following essentially the same procedures that would be applied to cells in culture. All four major patch-recording configurations—cell-attached, inside-out, outside-out and whole-cell—are possible, as well as the nystatin-perforated patch technique (see Section 5.8., “*Recording from Perforated Patches and Perforated Vesicles*”).

5.3.2. THE BLIND TECHNIQUE

Apart from a microelectrode holder with the appropriate diameter for patch pipettes, and with a side port for pressure application, no special equipment is necessary to adapt a standard slice setup equipped for intracellular recording to one suitable for blind-patch recording. A dissecting microscope is sufficient. The recording pipette should have a resistance in the bath of approximately 3–5 M Ω ; the optimal resistance depends on the size and type of cell being recorded.

The procedure for establishing gigohm seals is very simple (Figure 5.3). It is possible to use either the current-clamp or voltage-clamp recording mode. A small repetitive current or voltage pulse is applied to the electrode at relatively high frequency (*e.g.*, 10 Hz) and the voltage or current response is monitored with an oscilloscope. Continuous, slight pressure is applied to the back of the pipette, for example, by blowing gently into the tubing connected to the pipette and closing a stopcock to retain the pressure. The pipette is then slowly lowered into the tissue in the region where the desired cells are found. It is advanced slowly—1–5 steps per second, each step of 1–2 μm —into the tissue until a sudden increase in resistance is detected at the pipette tip, indicating contact with a cell. Often a further advance of 1–2 μm causes a further increase in the resistance. Release of the positive pressure should result in another approximate doubling of the resistance if the electrode is indeed contacting a cell. Although gigohm seals sometimes form spontaneously at this stage, the next step is to apply light suction to cause the seal to form. This may occur rapidly, in less than one second, or slowly, up to several seconds, requiring constant, gentle suction. The patch is then ruptured by additional suction creating electrical continuity between the pipette and cell interior.

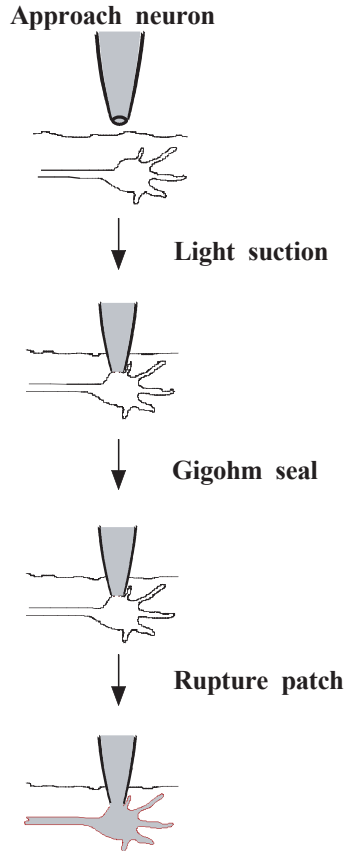


Figure 5.3: The Blind technique.

Obtaining a recording using the blind technique by advancing the patch pipette through a tissue slice. According to the method of Blanton et al., (1989).

Although this technique can be applied successfully, achieving a good recording on nearly every attempt, it is almost inevitable that at some point one will encounter some difficulty either in generating seals or establishing whole-cell recordings. Through experience, it is possible to identify the problem-causing aspects of the procedure. Often, changing the pipette size helps. A general rule is to use smaller tips to improve sealing, and larger ones to facilitate the transition to the whole-cell mode. One should be prepared to use a number of pipettes, since the probability of obtaining a recording on the second attempt to apply suction to the same pipette is very small. Another critical variable, which applies to all patch-clamp recording, is the intracellular solution whose osmolarity should be verified routinely, particularly when difficulties are encountered.

5.3.3. ADVANTAGES AND DISADVANTAGES OF THE TWO METHODS OF PATCH CLAMPING BRAIN SLICES

It is impossible to give a complete discussion of the relative merits of the cleaning and blind techniques here. However, some of the important considerations are outlined in the following table.

Table 5.1: Brain Slice Techniques.

Cleaning Technique	Blind Technique
<ul style="list-style-type: none">• Need upright microscope and water-immersion objective.• Vibrating microtome almost essential.• Maximum slice thickness limited by visibility.• Once a cell is located, additional time is invested in cleaning.• Cell is visually identified.• Can see neighboring cells and apply local stimuli.• All four standard patch-clamp configurations possible, plus the perforated patch technique.• Recording quality similar to standard patch clamp techniques.	<ul style="list-style-type: none">• Need no special equipment beyond that for intracellular recording in slices.• Vibrating microtome strongly recommended, essential for some tissues.• Maximum slice thickness limited by viability.• Less preparation time for each penetration, but no certainty of cell health.• Need post-hoc identification of cell type unless electrophysiological identification is possible or a homogeneous cell population is used.• Visually-guided local stimulation is not possible.• All four standard patch-clamp configurations possible, plus the perforated patch technique.• High or unstable access resistance is often a problem with whole-cell mode (possibly due to debris in the pipette tip).

5.4. FURTHER READING

Blanton, M.G., Loturco, J.J., Kriegstein, A.R., Whole cell recording from neurons in slices of reptilian and mammalian cerebral cortex. *J. Neurosci. Methods.* 30:203–210, 1989.

Coleman, P.A., Miller, R.F., Measurements of passive membrane parameters with whole-cell recording from neurons in the intact amphibian retina. *J. Neurophysiol.* 61:218–230, 1989.

Edwards, F.A., Konnerth, A., Sakmann, B., Takahashi, T., A thin slice preparation for patch clamp recordings from neurones of the mammalian central nervous system. *Pflügers Arch.* 414:600–612, 1989.

Gähwiler, B.H., Organotypic cultures of neural tissue. *Trends Neurosci.* 11:484–489, 1988.

Hestrin, S., Nicoll, R.A., Perkel, D.J., Sah, P., Analysis of excitatory synaptic action in the rat hippocampus using whole cell recording from thin slices. *J. Physiol.*, 422, 203–225, 1990.

Rall, W., Segev, I., Space clamp problems when voltage clamping branched neurons with intracellular microelectrodes. T.G.J. Smith, H. Lecar, S.J. Redman, P.W. Gage (Eds.), *Voltage and Patch Clamping With Microelectrodes.* Bethesda: American Physiological Society, pp. 191–215, 1985.

Sakmann, B., Edwards, F., Konnerth, A., Takahashi, T., Patch clamp techniques used for studying synaptic transmission in slices of mammalian brain. *Q J Exp Physiol* 74: 1107–18, 1989.

Sakmann, B., and Stuart, G., Patch-pipette Recordings from the Soma, Dendrites, and Axon of Neurons in Brain Slices in *Single-Channel Recording*, 2nd Ed., Sakmann, B., and Neher, E., eds. pp. 199–211, 1995.

5.5. MACROPATCH AND LOOSE-PATCH RECORDING

Measuring the local density of a specific type of ion channel in different regions of a cell provides valuable information. This kind of information is helpful for understanding the specialized functions of axons, cell bodies and dendrites in neurons, as well as for studying mechanisms of sensory transduction, the spatial distribution of ion channels near the muscle end-plate, and localized changes in channel density or channel properties resulting from single-transduction events. To efficiently address these areas of research, one needs a method that is intermediate in scale between single-channel patch clamp and whole-cell voltage clamp. Macropatch recording methods fulfill this need.

Two approaches are used to record ionic currents from patches of membrane containing tens to hundreds of ion channels. The first applies standard gigohm-seal (gigaseal) patch-clamp methods employing large-diameter patch pipettes (5–10 μm tip diameter) and is

used to sample currents from much larger areas than are commonly used in single-channel recording (which is done with 0.5–2 μm tip diameter pipettes). The second method of macropatch recording has been termed loose-patch recording. This method, which enables one to gather data that could not be obtained with the gigaseal method, differs from single-channel recording in three ways:

- 1 The tip of the loose-patch pipette is usually much larger than the conventional single-channel patch pipette;
- 2 The loose-patch pipette does not form a gigaseal with the membrane, whereas gigohm seals are required for single-channel recording; and
- 3 The loose-patch pipette can be reused and repositioned to map the spatial distribution of channel subtypes on individual cells (Thompson and Coombs, 1988).

5.5.1. GIGASEAL-MACROPATCH VOLTAGE CLAMP

Macroscopic patch currents can be recorded using standard patch-clamp instrumentation and a large patch pipette having a resistance of a few hundred kilohms. A gigaseal is formed using suction. This method can be applied to cell-attached and excised patches. Data analysis uses the same methods that are applied in whole-cell clamp experiments. Consequently, data concerning the kinetic behavior and local amplitude of ionic currents can be rapidly acquired. This method has been used to record macroscopic currents in *Xenopus* oocytes (Hoshi et al., 1990), which are particularly amenable to this method of recording because channel expression can be controlled, to a certain degree, by the experimental conditions.

There are a few problems associated with this method that have to be considered in the experimental design. The patch-clamp amplifier must be able to fully compensate for the greater capacitance of larger patches. When voltage pulses are applied to macropatches in the cell-attached configuration, current flowing in the patch will change the cell voltage; this change can be significant. For example, with a macropatch current of 100 pA and a cell input resistance of 100 M Ω , the cell voltage will change by 10 mV. Dynamic current-dependent errors of this type are difficult to correct and are most severe in small cells. In some preparations it may be impossible to use cell-attached macropatches to obtain accurate I/V curves, especially for rapidly changing currents. One can eliminate this source of error by studying excised patches.

Milton & Caldwell (1990) identified a more subtle error associated with macropatch recording. They observed that the suction used to form the seal between the patch pipette and the membrane can cause a change in ion channel density in the patch. With large patch pipettes, a noticeable membrane bleb may form in the orifice of the pipette during suction. This membrane bleb can be visualized under a microscope. It appears that the ion-channel density decreases during bleb formation, possibly because of a flow of lipid into the bleb causing membrane rearrangement and changes in channel distribution. Therefore, the gigaseal-macropatch method may be unsuitable for mapping ion-channel

densities because the procedure modifies the channel density before the measurement is made.

5.5.2. LOOSE-PATCH VOLTAGE CLAMP

In loose-patch recording it is not necessary to form a tight seal between the patch pipette and the plasma membrane; therefore, strong suction is not needed. This has at least two advantages:

- 1 The pipette can be repositioned to sample currents from a number of patches on the same cell; and
- 2 The loose-patch method can be used to measure local currents in voltage-clamped preparations where establishing gigaseals is impossible due to the presence of adherent connective tissue, basement membrane or glial cells. Note that loose-patch recording is done only in the cell-attached configuration.

The low seal resistance between the pipette and the membrane presents the principal technical difficulty one must overcome in applying loose-patch methods. Low seal resistance creates two types of problems. First, the current flowing through the seal resistance and capacitance introduces noise in the current record, thus limiting the resolution (see Chapter 3, “*The Importance of a Good Seal*”). A more significant problem arises from the fact that membrane current flowing through the seal resistance is lost.

The following discussion will focus on the errors introduced by low seal resistance and the procedures used to limit errors to acceptable levels. Three designs are available to combat the problems associated with low seal resistance in loose-patch recording. The choice of the most appropriate method depends on the nature of the preparation. The original literature should be consulted for further details.

Combining Whole-Cell Clamp with Focal Current Recording

The first method to be introduced combines whole-cell voltage clamping with loose-patch current recording. This is the preferred method for many applications. The cell is voltage clamped by a microelectrode or a whole-cell patch pipette using standard microelectrode voltage-clamp or patch-clamp instrumentation, while current is recorded from a restricted area of membrane with a loose-patch pipette using patch-clamp instrumentation. Voltage-clamp pulses are applied via the whole-cell clamp while the loose-patch pipette is maintained at the bath potential to ensure that no current flows across the seal resistance. This method has been used to record local currents in large molluscan neurons (Neher and Lux, 1969; Johnson and Thompson, 1989; Thompson and Coombs 1989; Premack et al., 1990) and in muscle cells (Almers et al., 1983). The method is particularly well suited for measuring the kinetics and current/voltage relationships of macroscopic currents expressed in *Xenopus* oocytes where a whole-cell voltage clamp is severely limited by the large capacitance of the cell and high intracellular series resistance. The electrode arrangement is shown in Figure 5.4.

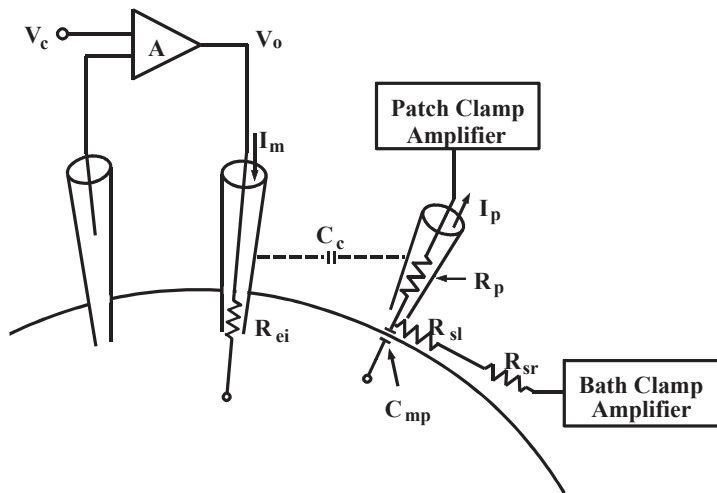


Figure 5.4: Combining whole-cell voltage clamping with loose-patch current recording.

Schematic diagram of a cell with voltage clamp electrodes and the large patch pipette in place. The symbols used in the figure are as follows: A , voltage clamp open loop gain; C_c , coupling capacitance between voltage clamp current electrode and patch electrode; C_{mp} , capacitance of membrane patch; I_c , current error; I_m , membrane current supplied by voltage clamp; I_p , patch membrane current supplied by patch clamp amplifier; R_{ci} , resistance of voltage clamp current electrode; R_p , axial resistance of patch electrode; R_{sl} , resistance of seal between patch pipette and cell membrane; R_{sr} , series resistance between the outside of the patch electrode and the bath clamp amplifier; V_c , voltage clamp command voltage; V_o , voltage clamp output voltage. Reproduced with permission according to Johnson and Thompson (1989).

A reusable loose-patch pipette (5–20 μm in diameter; axial resistance (R_p) of 100–500 $\text{k}\Omega$) is used in cell-attached configuration. The resistance of the seal is monitored by applying test voltage steps via the patch amplifier and measuring the amplitude of the resulting current steps. After contacting the cell, gentle suction is applied until the sum of the seal resistance (R_{sl}) and the axial resistance of the pipette (R_p) increases by at least 10 fold; increases greater than 100-fold are common. The suction is released to avoid pulling a “finger” of membrane and cytoplasm into the pipette since this would increase the series resistance and lead to errors in voltage control and current measurement. Since the lumen of the loose-patch pipette is held at the bath potential and R_p is low compared to R_{sl} , there is no need to compensate for the finite value of R_{sl} .

This method allows one to simultaneously measure whole-cell and patch currents as well as whole-cell and patch capacitances. The areas of the cell and of the patch can be estimated by measuring the whole-cell and patch capacitances. A convenient way to do this is to apply a triangle-wave voltage command to the whole-cell voltage clamp and record the

resulting whole-cell and patch current waveforms. The patch capacitance (c) is calculated from the change in the time derivative of the voltage (dV/dt) at a vertex of the triangle wave and the corresponding jump in patch current (I), using the following equation (Neher, 1971; Palti, 1971):

$$c = \frac{I}{dV/dt} \quad (2)$$

Because the voltage of the patch pipette is equal to the bath voltage and only the voltage across the membrane patch covered by the pipette is changing, the capacitance of the patch pipette itself is rejected. The capacitance of the whole cell is measured in a similar fashion. However, the interpretation is complicated by current contributed from poorly clamped regions (see Johnson and Thompson (1989) for further discussion).

There are several issues to consider when applying this combined voltage-clamp method. The most important requirement is that the patch current must be measured from a well-clamped region of membrane, *i.e.*, from a region that is “space clamped” by the whole-cell voltage clamp amplifier. In order to accurately measure current-voltage relationships and limit the capacitive current flowing across the patch during voltage steps, the loose-patch pipette should be positioned close to the point where the whole-cell voltage is controlled. Cell geometry and electrode positioning should be considered when designing the physical layout of the experiment. These considerations limit the kinds of preparations that can be studied with the method. It is reasonable to use the loose-patch pipette to record local current densities at different points on a well-clamped spherical cell body. However, it would be inappropriate to record patch currents from a thin dendrite when the voltage clamp is applied to the soma.

The most significant error results from current flowing in the seal resistance between the loose-patch pipette and the bath. This error current (I_e), which is not measured by the patch-clamp amplifier, is given by:

$$I_e = \frac{I_p R_p}{R_p + R_{sl}} \quad (3)$$

where R_p is the resistance of the loose-patch pipette and R_{sl} is the seal resistance. If $(R_p + R_{sl})$ is ten times larger than R_p the error in the measured current is 10%. To minimize the error, one can reduce R_p by using a patch pipette with a blunt taper and increase R_{sl} by using suction to improve the seal with the membrane. Enzyme treatment with dispase, pronase or trypsin can be used to clean the cell surface and improve the seal resistance.

Two kinds of errors caused by series resistance should be considered:

- 1 The voltage drop that results from macroscopic patch currents flowing through the axial resistance of the patch pipette (R_p) will produce an insignificant error in most cases. For example, if the value of R_p is 300 k Ω and the maximal patch current is 500 pA, the resulting voltage error is 0.15 mV.
- 2 A more troublesome error occurs when the bath voltage outside the patch pipette changes due to large whole-cell currents flowing in the series resistance (R_{sr}) between the cell membrane and the bath ground or virtual ground.

The error current is given by:

$$I_e = \frac{I_m R_{sr}}{R_{sl}} \quad (4)$$

where R_{sr} is the sum of the series resistances of the bath, the agar bridges and the liquid-silver chloride junction at the bath electrode; it typically has a value of several kilohms.

Bath series resistance creates an insidious problem when membrane currents are large. However, the error can be reduced by measuring the bath voltage with a separate electrode and using it as the reference voltage at the patch-clamp amplifier. Good practice dictates that the bath voltage be used to correct the membrane voltage signal applied to the whole-cell clamp amplifier as well. Instability can result, however, if the bath voltage is measured with a greater bandwidth than the membrane voltage. To remedy this, one can limit the frequency response of the bath voltage follower, but this degrades performance and causes other errors. A better solution is to eliminate the need to subtract the bath voltage at the other circuits by voltage clamping the bath to ground potential. This can be accomplished using an independent voltage-clamp amplifier operating at a high gain and bandwidth. Two separate agar bridges and silver-chloride electrodes can be used to measure the bath voltage and pass current to the bath. Because of the low resistance of these electrodes, a simple voltage-clamp circuit employing a single operational amplifier is adequate for clamping the bath to ground potential. This arrangement ensures that the bath voltage does not change during clamp steps. The output of the circuit provides the record of whole-cell current.

Other problems can be overcome by a careful design of the experimental layout. Since this method uses several voltage-clamp amplifiers working simultaneously, it is necessary to limit capacitive coupling between electrodes. This can be achieved by inserting a grounded shield between the whole-cell current electrode and the macropatch pipette, and by lowering the volume of saline to the minimum required for covering the cell. To reduce high frequency noise in the patch recording, the submerged tip of the pipette should be coated with Sylgard (Dow Corning, Midland, MI) and only the tip should be filled with saline. Johnson and Thompson (1989) provide a thorough analysis of the problems and the approaches used to reduce errors to acceptable levels.

Voltage Pulses Applied to the Loose-Patch Pipette

Ionic currents can also be studied by applying voltage pulses directly to the loose-patch pipette, thus eliminating the need for an independent whole-cell clamp. Errors resulting from the finite seal resistance and the axial resistance of the pipette are more severe in this case and require more elaborate compensation. The advantage of this method is that membrane currents can be recorded locally without the need to establish an overall space clamp. This loose-patch method has been very successful in studies of acetylcholine (ACh) receptor and Na⁺-channel distribution near muscle end-plates (Almers et al., 1983a,b).

Although extra effort is required with this method, it may be the best approach for some preparations. It is important to remember that current flowing across a macropatch can cause a significant change in cell voltage. In its simplest form, this method uses a large diameter patch pipette in a cell-attached configuration and a conventional patch-clamp amplifier (Almers et al., 1983a,b; Stühmer et al., 1983). In this configuration, the axial resistance of the pipette (R_p) and the seal resistance (R_{sl}) act as a voltage divider. When a voltage command pulse is applied to the pipette (V_p), it will be attenuated at the pipette tip. The voltage at the pipette tip (V_t) is given by (Stühmer et al., 1983):

$$V_t = V_p \frac{R_{sl}}{R_p + R_{sl}} \quad (5)$$

When R_{sl} is large, as is the case in gigaseal recordings, the error is insignificant. In loose-patch applications, however, R_p and R_{sl} are approximately equal and a large fraction of the current delivered to the pipette will flow through the seal resistance. It is necessary to correct the amplitude of command-voltage steps by a factor equal to $R_{sl}/(R_p + R_{sl})$. To do so, R_p is measured before the pipette contacts the cell and $R_p + R_{sl}$ is monitored continually throughout the experiment. Almers et al., (1983a,b) used a computer to calculate a correction factor $A = R_{sl}/(R_p + R_{sl})$ before each voltage step. The correction factor was used to scale command-voltage steps applied by the computer by $1/A$ to ensure that the intended voltage appeared at the pipette tip. Recorded currents were divided by A to correct for current (often termed leakage current) flowing through the seal resistance. This digital approach to seal resistance compensation is technically sound. To implement it, the user has to develop a software program for continuously updating the parameters needed for scaling the amplitude of the command pulses and correct for leakage current; an extra effort that is well justified in some applications.

Seal resistance compensation can also be achieved with an analog circuit. Stühmer et al., (1983) pioneered a method that uses an active voltage divider and potentiometers to compensate for measured values of R_p and R_{sl} . Their circuit allows one to null R_p and limit the series resistance errors to acceptable values. When correctly adjusted, their design ensures that the input impedance of the patch pipette is near zero so that there is minimal loss of membrane current across the seal. A disadvantage of this method is that it requires

the user to build a specialized patch-clamp headstage and other circuitry following the example provided by Stühmer et al., (1983).

With both digital and analog seal-resistance compensation, accuracy depends on one's ability to measure R_p and $(R_{sl} + R_p)$ and on the assumption that these resistances remain constant during voltage steps that activate conductances in the patch. The error increases as the amplitude of the voltage step and the conductance of the membrane patch increase. It is not certain that R_p and R_{sl} are independent of the current amplitude. In practice, one often observes an unexpected flattening of the current-voltage relationship for inward or outward current activation when the voltage step or the patch current become large. Because most of the uncertainty in current measurement depends on R_{sl} , one should use suction and/or enzyme treatment to maximize the seal. It also helps to limit the diameter of the patch pipette to about 20 μm or less. R_p is minimized by using pipettes with a blunt taper.

Loose-Patch Clamp with Concentric Patch Pipettes

Almers et al., (1984) introduced a modification of the loose-patch method that employs a two-chambered concentric patch electrode. The electrode is fashioned from two glass capillaries, one inside the other, with the inner capillary held in place by support rods during the pull. The concentric electrode is pushed against the cell surface where it separates a central membrane patch from an annular surround. The voltage-clamp amplifier is designed to clamp both the center patch and the surround to the command potential. Membrane current is measured in the central barrel of the electrode while the outer annulus acts as a guard. Since the inner and outer barrels are at the same potential during the command steps, current loss from the central membrane region to ground is minimized and R_{sl} takes a value that is effectively infinite. This approach is historically related to vaseline-gap and sucrose-gap voltage-clamp methods. It has been used successfully to voltage clamp mammalian skeletal muscle. However, the implementation is somewhat difficult since it requires the construction of an elaborate concentric electrode and some specialized instrumentation. It may still be the best approach in some cases and the original literature should be consulted for further details.

References

- Almers, W., Stanfield, P.R., Stühmer, W., Lateral distribution of sodium and potassium channels in frog skeletal muscle: measurements with a patch-clamp technique. *J.Physiol.* 336, 261–284, 1983a.
- Almers, W., Stanfield, P.R., Stühmer, W., Slow changes in currents through sodium channels in frog muscle membrane. *J. Physiol.* 339, 253–271, 1983b.
- Almers, W., Roberts, W.M., Ruff, R.L., Voltage clamp of rat and human skeletal muscle: measurements with an improved loose-patch technique. *J.Physiol.* 347, 751–768, 1984.
- Hoshi, T., Zagotta, W.N., Aldrich R.W., Biophysical and molecular mechanisms of Shaker potassium channel inactivation. *Science* 250, 533–538, 1990.

Johnson, J.W, Thompson, S., Measurement of non-uniform current density and current kinetics in *Aplysia* neurons using a large patch method. *Biophys. J.* 55, 299–308, 1989.

Milton, R.L., Caldwell, J.H., Na current in membrane blebs: Implications for channel mobility and patch clamp recording. *J. Neurosci.* 10, 885–893, 1990.

Neher, E., Two fast transient current components during voltage clamp on snail neurons. *J.Gen.Physiol.* 58, 36–53, 1971.

Neher, E., Lux, H.D., Properties of somatic membrane patches of snail neurons under voltage clamp. *Pflügers Arch.* 322, 35–38, 1971.

Palti, Y., Varying potential control voltage clamp on axons. in *Biophysics and Physiology of Excitable Membranes*. W.F. Adelman, Jr., Ed. Von Nostrand Reinhold Co. pp. 194–205, 1971.

Premack, B.A., Thompson, S., Coombs-Hahn, J., Clustered distribution and variability in kinetics of transient K channels in molluscan neuron cell bodies. *J. Neurosci.* 9, 4089–4099, 1990.

Stühmer, W., Roberts, W.M., Almers, W., The loose patch clamp. in *Single-Channel Recording*. Sakmann, B., Neher, E., Eds. pp. 123–132, 1983.

Thompson, S. and Coombs, J., Spatial distribution of Ca currents in molluscan neuron cell bodies and regional differences in the strength of inactivation. *J. Neurosci.* 8, 1929–1939, 1988.

5.6. THE GIANT EXCISED MEMBRANE PATCH METHOD

Many physiologically important ion pumps, exchangers and co-transporters are electrogenic. The giant excised membrane patch method has been developed to improve electrophysiological studies of such mechanisms. Although whole-cell recording techniques are often employed in transport studies, a method offering free access to the cytoplasmic membrane surface and faster voltage clamping was strongly desirable. While the excised membrane patch method was an attractive alternative, the conventional patch clamp techniques were not useful. First, the single turnover rates of transporters (1–10,000 per second) are far too small to expect resolution of the current generated by a single transporter. Second, the magnitudes of “macroscopic” currents expected in excised patches are difficult to measure because they are much smaller than the patch leak currents.

The giant excised membrane patch technique enables one to achieve 1–10 gigohm seals routinely, using pipette tips with inner diameters of 12–40 μm . The giant membrane patch produced by this method has 2–15 pF membrane capacitance, representing a 100-fold increase of membrane area over the area of conventional, single-channel patch membrane. Pipette diameters of > 50% of the cell diameter can be employed when recording from small, spherical cells.

The giant patch method has proven to be advantageous for fast macroscopic current recording whenever free access to a large surface area of the cytoplasmic membrane is desired. To date, the giant patch method has been applied successfully to cardiac, skeletal and tracheal myocytes, pancreas acinus cells, a Jurkat human T-cell line, Sf9 cells and *Xenopus* oocytes. The method should be useful for a wide range of studies of electrogenic mechanisms involving native proteins and proteins expressed from cloned genes. Promising applications include studies of macroscopic current modulation by intracellular compound (*e.g.*, enzymes or ions acting from the cytoplasmic side of the membrane), studies of charge movement generated during channel gating, and studies of partial reactions of transporters.

5.6.1. PRE-TREATMENT OF MUSCLE CELLS

Cell-surface invaginations of muscle cells limit the ability to form large-diameter seals. To promote sealing, cells can be pretreated to induce separation of the surface membrane from the underlying cell structure or produce large-scale surface membrane “blebbing.” In some cases both separation and blebbing occur. To accomplish this, digested pieces of tissue are placed in a “storage solution” consisting of 60–150 mM KCl, 10 mM EGTA, 1–5 mM MgCl₂, 20 mM dextrose, 15 mM HEPES, pH 7, for 1–12 hours. This treatment is similar to the treatment previously used to induce blebbing in skeletal muscle (Standen et al., 1984). Disruption of volume regulation and the Donnan equilibrium is clearly important for the blebbing process. Large-scale (20–50 μm) membrane bleb formation or apparent lifting of sarcolemma away from myofilaments are routinely obtained after 2 h treatment. The treatment has been found effective in inducing blebbing in many different cell types. However, blebbing is not necessarily conducive to large-diameter seal formation in all cell types, and other methods may be required. For instance, giant patches have not been obtained on the blebbed membrane of oocytes, although they are routinely obtained on hypertonically shrunken oocytes after mechanical removal of the vitelline layer.

5.6.2. PIPETTE FABRICATION

Large-diameter (1.5–1.8 mm), thin-walled glass pipettes are used to fabricate pipettes with large-diameter tips and relatively steep descents at their tips. The type of glass is unimportant. A conventional double-pull technique using standard patch-pipette pullers can be employed. For work with myocytes, light fire polishing with barely visible effects on the tip favors the spontaneous formation of inside-out patches upon membrane excision, rather than vesicles that must be disrupted mechanically. Pipette A in Figure 5.5 shows a typical pipette tip with a 17 μm inner diameter.

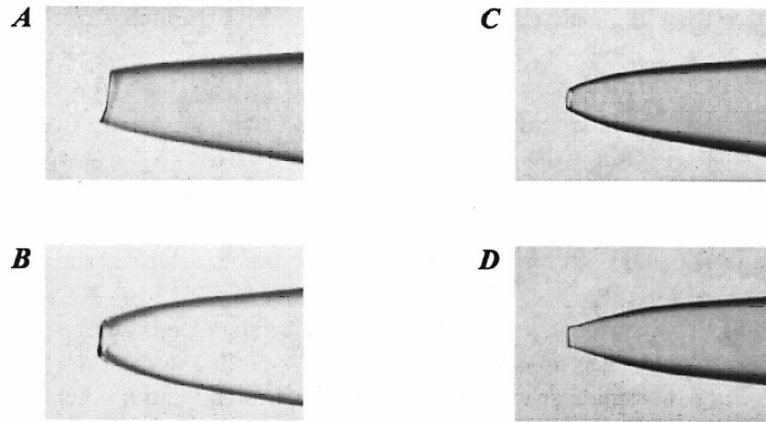


Figure 5.5: Pipette fabrication for giant excised patch method.

- A. Oocyte electrode before fire polish.
- B. Oocyte electrode after fire polish.
- C. Myocyte electrode after cutting and fire polish.
- D. Myocyte electrode after fire polish (no cutting).

Alternatively, pipettes can be pulled to smaller diameters and then scratched gently on the edge of a soft glass bead to the desired diameter, leaving a rough edge (pipette B in Figure 5.5, 17 μm diameter). When such electrodes are employed without fire polishing, the membrane usually remains localized at the pipette opening during sealing, and vesicles are obtained in most cases upon membrane excision. For very large cells, particularly for oocytes, a different procedure is employed. Pipettes are first scratched to a 30–50 μm diameter (pipette C in Figure 5.5) and then melted to a diameter of 18–35 μm (pipette D Figure 5.5) close to a glass bead placed on a microforge. The resulting bullet-shaped pipette tips are advantageous for fast voltage clamping, and the oocyte membrane remains localized to the rim of the pipettes. We have had good success preparing electrodes by melting the tip into a bead of soft glass, followed by cooling and “cutting” by a small pull.

A number of hydrocarbon mixtures consisting of oils, waxes and Parafilm (American National Can Co.) allow large-diameter, high-resistance seal formation. Viscous oils can be used by simply dipping the dry pipette tip into the oil of choice followed by washing with the desired filling solution. The most consistent success has been obtained with acetyltocopherol (Sigma Chemical Co.). Silicone oils, phospholipids and plasticizers are usually not useful, and seals formed with oils alone are generally unstable. Seal stability can be improved with a highly viscous mixture of Parafilm, acetyltocopherol (or light mineral oil) and heavy mineral oil. The standard mixture is prepared by mixing approximately three parts by weight of finely shredded Parafilm with each of the two oils and vigorously stirring over heat for 30–60 minutes. When a thin mixture is prepared, pipette tips can simply be dipped. With a thick mixture, a peanut-sized amount of the mixture is

smear with a plastic rod on a clean surface, and a thin film of the mixture is drawn into air by lifting the rod. The pipette tip is then passed quickly through the film, and the procedure is repeated once more. In order to reduce the pipette capacitance, a thick mixture is applied as close as possible to the tip. The pipette is then backfilled and a brief, strong, positive-pressure pulse is applied with a syringe to clear the tip. The pipette tip usually appears clean and is visually indistinguishable from that of an untreated electrode.

5.6.3. SEAL FORMATION

Seals are formed in the usual manner by applying gentle negative pressure at the cell surface. Maintenance of positive pressure up to the time of sealing is essential both to keep the electrode tip clean and to prevent contamination of the pipette tip with bath solution constituents. When working with myocytes, membrane vesicles rather than inside-out patches are often obtained upon membrane excision, as indicated by the absence of the characteristic currents. Although membrane position in the pipette tip can usually be visualized, membrane patches cannot be visually distinguished from vesicles. The method of choice to disrupt vesicles is to touch the tip of the pipette against an air bubble or a bead of hydrocarbon placed on the wall of the patch chamber. Success rate is about 50%.

To date, the best success with oocytes has been obtained by shrinking oocytes with 200 mM K-aspartate rather than sucrose. Patches from oocytes are excised by gently moving the pipette tip from side to side in gradually increasing distances. Dark, granular cytoplasmic material is often excised with the oocyte patches, and vesicles are obtained only rarely. The cytoplasmic material can be washed away by rapid pulses of solution directed at the patch.

5.7. FURTHER READING

Collins, A., Somlyo, A. V., Hilgemann, D. W., The giant cardiac membrane patch method: Simulation of outward Na/Ca exchange current by MgATP. *J. Physiol.* 454, 27–57, 1992.

Hilgemann, D. W., Giant excised cardiac sarcolemmal membrane patches: sodium and sodium-calcium exchange currents. *Pflügers Archiv.* 415, 247–249, 1989.

Hilgemann, D. W., *The Giant Membrane Patch in Single-Channel Recording*, 2nd Ed., Sakmann, B., Neher, E., eds. pp. 307–326, 1995.

Hilgemann, D. W., Regulation and deregulation of cardiac Na-Ca exchange in giant excised sarcolemmal membrane patches. *Nature* 344, 242–245, 1990.

Standen, N. B., Stanfield, P. R., Ward, T. A., Wilson, S. W. A new preparation for recording single-channel currents from skeletal muscle. *Proceedings of the Royal Society of London (Biology)* B221, 455–464, 1984.

5.8. RECORDING FROM PERFORATED PATCHES AND PERFORATED VESICLES

The study of ion channel function and modulation by neurotransmitters and hormones advanced dramatically with the advent of patch clamping in the mid-1970's. Approximately a decade later, a variation of the single-channel patch-clamp recording method was introduced and termed the perforated-patch recording method. Perforated-patch recording techniques allow the measurement of whole-cell currents, single-channel currents and transmembrane voltages much less invasively than do standard patch-clamp or microelectrode approaches.

5.8.1. PROPERTIES OF AMPHOTERICIN B AND NYSTATIN

Perforated-patch recording, as presently implemented, uses either nystatin or amphotericin B to gain electrical access to the cell's interior. These polyene antibiotics form channels in cholesterol- or ergosterol-containing membranes. The channels formed by both perforating compounds are permeable to monovalent cations and Cl^- but exclude multivalent ions such as Ca^{2+} or Mg^{2+} . The monovalent cations are nine times more permeant than Cl^- through the channels formed by either perforating compound. When measured in molar salt concentrations, the single-channel conductance of amphotericin channels is twice that of nystatin channels.

5.8.2. STOCK SOLUTIONS AND PIPETTE FILLING

Because of their limited water solubility, amphotericin and nystatin stock solutions of 30 mg/mL are prepared in DMSO. These stock solutions lose activity upon prolonged storage and freezing. Therefore, it is best to prepare them freshly before use and use within 1 hour. A convenient approach is to weigh 6 mg of the antibiotic powder into each of 40–50 microcentrifuge tubes and store them indefinitely in the freezer without loss of activity. At the time of use, the powder is solubilized by pipetting 100 μL fresh DMSO into the tube. Solubilization is enhanced by sonication or vortex mixing (but this is apparently not required). Stock solution can be added directly to the desired pipette filling solution to a final concentration of 120–350 $\mu\text{g}/\text{mL}$. Since 120 $\mu\text{g}/\text{mL}$ appears to be a saturating concentration, it is not clear if higher concentrations offer any advantage. Vortex mixing for a few seconds or sonication for a minute is recommended for maximum solubilization of the antibiotic in the pipette filling solution. When the antibiotic is in excess, some of it settles out of solution and adheres quite well to the wall of a plastic tube or syringe. Therefore, the saturated solution can be used without adding much particulate matter to the pipette interior. The filling solution can be filtered after adding the antibiotics, but care must be taken since some filters might inactivate these compounds. With either antibiotic, the final solution is yellow in color and slightly turbid. After filtration with either a 0.22 or 0.45 micron filter, the final solution is perfectly clear. With nystatin, it is possible to make up larger volumes of the stock solution and adjust the pH to neutrality before use. Under these conditions, no precipitate forms when the final filling solution is made. This approach has not been used with amphotericin B because of its higher cost. The perforating activity of either compound begins to decrease about 3 hours after preparing the stock solution. Since whole-cell recording experiments can easily last for 1–3

hours employing the perforated-patch approach, it is advisable to use stock and antibiotic-containing filling solutions within one hour of preparation.

Both amphotericin and nystatin seem to interfere with seal formation. Although it is possible to seal some cells when either compound is present in the pipette filling solution, the success rate is lower than when an antibiotic-free filling solution is used with the same cells. Therefore, it is best to fill the tip of the pipette with an antibiotic-free solution and then to backfill with the antibiotic-containing solution. The tip-filling process can be accomplished by simply dipping the tip into the desired solution. With borosilicate glasses, 1–5 seconds of tip immersion suffices, whereas with the more hydrophobic lead-containing glasses, 30–60 seconds may be required. With high-lead glasses, gentle suction for a second or so may be beneficial. With any glass, it is important that the antibiotic-free solution not exceed 500 μm distance from the tip; otherwise, the time required for the diffusion of the antibiotic from the backfilling solution to the tip will be excessive. For example, if the pipette is filled up to 1.0 mm from the tip with an antibiotic-free solution, more than an hour will be required for the antibiotic to reach a tip-concentration comparable to that in the backfilling solution. Ideally, the tip should be filled to a distance that allows the antibiotic to reach the tip within a few seconds following a gigohm seal formation. Since the time required for seal formation depends on the cells and the setup, tip filling distances should be optimized by each investigator. Consistently optimal tip filling is routinely possible by first overfilling the tip and then forcing the excess solution out by applying positive pressure to the back of the pipette while observing it under a dissecting microscope.

5.8.3. PROPERTIES OF ANTIBIOTIC PARTITIONING

Following seal formation, the antibiotic slowly diffuses to the tip where it contacts the membrane and begins to partition and form channels. While most of the time delay can be attributed to diffusion, some investigators reported that incorporating a mild detergent like Pluronic F-127 into the filling solution decreases the perforation time. Since it is unlikely that this detergent could affect the diffusion time of the antibiotics, it seems that, at least in some cells, the membrane partitioning (channel formation) time of the antibiotics is appreciable and that mild detergents decrease this time.

In a real experiment, one can observe the partitioning by applying a voltage pulse to the pipette at frequent intervals. As perforation occurs, the size of the capacity transient increases and the time constant of the transient decreases. The time constant to charge the cell capacitance is approximately $R_a C_m$, where R_a is the access resistance and C_m is the cell capacitance. When R_a is large, a brief voltage pulse will not charge the capacitance fully before the pulse turns off. Therefore, as partitioning continues and R_a decreases, the capacity transient gets larger since an increasing fraction of the cell capacity gets charged during the brief pulse. The decaying phase of the transient gets shorter as R_a decreases. In most cells, a properly filled pipette will produce minimized R_a by 20–30 minutes after seal formation. R_a of less than 20 $\text{M}\Omega$ is often achieved in about 5 minutes. Some investigators begin recording at this time. However, R_a continues to fall and finally becomes stable after 20–30 minutes. Once R_a stabilizes, it remains stable for 2.5–3 hours before begin-

ning to increase (presumably due to loss of activity of the antibiotic). The remarkable stability of R_a is one of the main virtues of the technique. For example, using amphotericin, one investigator reported R_a of 3.4 M Ω that did not change by more than 100 k Ω for three hours.

5.8.4. THE ADVANTAGES OF THE PERFORATED-PATCH TECHNIQUE

The perforated-patch technique has several advantages over conventional whole-cell patch-clamp approaches:

- 1 The channels formed by either amphotericin or nystatin are impermeable to molecules as large as or larger than glucose. Therefore, whole-cell recordings can be done without dialyzing important substances from the cell's cytoplasm. Currents run down significantly slower; physiologically relevant second-messenger cascades and mechanisms important to cell signaling and channel regulation remain operative.
- 2 Intracellular multivalent ions are not affected by the pipette-filling solution since the channels formed by the antibiotics are not permeated by these ions. Therefore, intracellular Ca^{2+} , for example, can be measured by optical techniques simultaneously with recording whole-cell currents.
- 3 With carefully fabricated pipettes and the use of appropriate composition of the filling solution, the perforation technique is less damaging to cells than are intracellular microelectrodes or standard whole-cell patch clamping. It is not uncommon to be able to record from a single cell for 3 hours. In some instances, freshly dissociated cells plate out on the bottom of the recording chamber while their whole-cell currents are being measured. The ability to plate out is indicative of the cells' viability.
- 4 Unlike the frequently experienced loss of seal when suction or voltage pulses are applied to disrupt the membrane patch (to "go whole cell"), seals are rarely lost with the perforating-patch approach.
- 5 The R_a achieved with the perforated-patch technique is as low or lower than that obtained by standard approaches. Moreover, once achieved, the low R_a of the perforated patch is usually considerably more stable than that produced with standard techniques.
- 6 In many cells, whole-cell capacitance is easier to compensate when using perforated patches. It appears that the equivalent circuit of the perforated patch is often better approximated by a single RC than is the access resistance and capacitance in a standard whole-cell recording.

5.8.5. THE LIMITATIONS OF THE PERFORATED-PATCH TECHNIQUE

The perforated-patch technique has some disadvantages when compared to the conventional whole-cell patch-clamp approaches:

- 1 The perforated-patch approach does not allow one to dialyze the cell's cytoplasm and replace its content with compounds other than the small ions included in the filling

solution, as is possible with conventional methods. Therefore, the effects of such compounds on intercellular mechanisms cannot be studied.

- 2 The pipette-filling solution and the cell cytoplasm exist in Donnan Equilibrium. Thus, the pipette must contain an impermeant anion and a Cl^- concentration that match the cell interior. Failure to do so results in a Cl^- flux either into or out of the cell (depending on the direction of the mismatch). A charge balancing cation and water will follow, resulting in changes in cell volume. Due to the low Cl^- permeability of the antibiotic channels as compared to their cation permeability, it may take approximately 30 minutes to reach this equilibrium. It is not yet clear if there is a way to alleviate this problem since it is difficult to find an impermeant anion that matches the effective valence of the intracellular impermeant anions. Recently, it has been reported that including 20–25 mM Cl^- and 125–130 mM methanesulfonate in the pipette solution appears to keep cell volume reasonably stable.

On the other hand, this disadvantage can be exploited for studies of volume-activated currents by purposefully mismatching the pipette and cytoplasmic Cl^- concentrations causing swelling and shrinking of cells. To date, this approach has not been employed.

In addition to the influx and efflux of ions described above, the cells that are voltage-clamped by the perforated-patch technique are very susceptible to volume changes caused by external perturbations. In a standard whole-cell recording configuration, cell volume is kept reasonably constant by the large volume of the pipette-filling solution and the high hydraulic conductivity of the pipette tip. In contrast, when applying the perforated-patch method, the access to a cell is provided by a million or so tiny parallel channels. While these channels can provide electrical access comparable to that obtained by a standard patch pipette, their composite hydraulic conductivity is significantly lower than that of a single orifice with the same total electrical resistance.

- 3 The perforation process requires considerably longer time for achieving access into the cell interior, as determined by the low R_a , than do suction or voltage pulses. When rapid measurements from a large number of cells is important, standard whole-cell patch-clamp approaches would be more productive.
- 4 While the relative Na^+ , K^+ and Cl^- permeabilities of nystatin and amphotericin channels are known, the permeation by other anions and cations, particularly multivalent ions that are generally considered impermeant, needs further study.

5.8.6. SUGGESTED WAYS TO MINIMIZE THE ACCESS RESISTANCE

Clearly, the access resistance (R_a) cannot be lower than the resistance of the pipette itself. The resistance of the patch of membrane to be perforated is in series with the electrode tip and, therefore, the total resistance is the sum of the two. The final patch resistance depends upon the total number of antibiotic channels formed (partitioning) and the single-channel conductance of each channel. The total number of channels equals the number of channels formed in a unit surface area times the patch area. These simple

considerations suggest the following ways to minimize R_a :

- 1 The largest pipette tips compatible with seal formation should be used to minimize the pipette resistance.
- 2 Pipette geometry should maximize the size of the omega-shaped membrane patch that is drawn into the tip during seal formation. This maximizes the surface area available for channel insertion.
- 3 The perforating compound that produces the highest total conductance should be used. It may not be simple to predict the conductance-producing ability of a compound since it requires both the partitioning (number of channels formed) and single-channel conductance to be maximal. To date, amphotericin B has produced the lowest R_a . This can be anticipated since the single-channel conductance of amphotericin channels is twice that of nystatin, at least in measurements made in salts at molar concentration. However, the relative conductance of the two types of channels in lower salt concentrations (*e.g.*, 150 mM) is unknown. In addition, there are no relevant studies of the relative partitioning of the two compounds when presented to the membrane in saturating concentrations. To date, the lowest patch resistance obtained by perforating with amphotericin is about 2 M Ω . The lowest resistance pipette that is capable of forming gigohm seals is approximately 0.5 M Ω . Thus, at present, an R_a value of approximately 2.5 M Ω appears to be the lowest one can achieve. Lower R_a values will require either perforating compounds with higher single-channel conductance or finding ways to enhance the partitioning of the existing antibiotics. It is unlikely that larger pipettes than those presently used would be successful in forming seals.

5.8.7. OTHER USES FOR PERFORATED PATCHES

Cellular Voltage Measurements

In addition to whole-cell recording using patch-clamp amplifiers like the Axopatch™ amplifier in the voltage-clamp or current-clamp mode, the perforated-patch method is useful for making cellular voltage measurements, such as for resting and action potentials. These can be done either with patch clamp amplifiers operating in current-clamp mode or with standard microelectrode amplifiers like the Axoclamp 900A or MultiClamp™ 200B amplifiers. In any cellular voltage measurement, two main factors affect the accuracy of the measurement:

- 1 The extent to which the cell's voltage is altered by current flow through the shunt resistance along the electrode's outer surface at either the penetration or seal sites; and
- 2 The extent to which the pipette-filling solution alters the electrolyte concentrations in the cell cytoplasm. High shunt resistances and minimal alteration of the cell content are desirable.

Patch electrodes, with their tens to hundreds of gigohm seal resistances, clearly have much higher shunt resistances than do intracellular microelectrodes. On the other hand, patch electrodes sealed to cells cause rapid changes in the concentrations of the cellular electro-

lytes if the pipette-filling solution contains different electrolyte concentrations than the cytoplasm. Intracellular microelectrodes, which are usually filled with molar concentrations of potassium salts, also alter cellular electrolytes but not as rapidly as do patch electrodes. Therefore, the perforated-patch technique provides both the advantage of the higher shunt resistance than intracellular microelectrodes without the significant change in cytoplasmic content caused by conventional patch electrodes.

Single-Channel Recording in Outside-Out Vesicles

The outside-out patch configuration has been particularly useful because it allows direct application of agents to the extracellular side of the membrane while maintaining complete voltage control during single channel recording. These patches have been required for studying ligand-gated ion channels such as the nicotinic acetylcholine, GABA_A, glycine and glutamate receptors. Likewise, transmitters that regulate channels through non-diffusible second messengers must be examined with outside-out patches. For example, activation of atrial potassium channels is not seen with cell-attached patches when muscarinic agonists are applied to the bath, but is seen with direct application of transmitter to an outside-out patch.

Unfortunately, conventional outside-out patches have a drawback. The formation of these cell-free patches requires replacement of cytoplasm with artificial pipette solutions. In many cases, this “washout” is accompanied by a loss of ion channel activity and/or modulation. For example, in GH3 pituitary tumor cells, the neuropeptide thyrotropin releasing hormone (TRH) triggers mobilization of intracellular calcium that in turn regulates calcium and potassium channel activity. With outside-out patches, TRH fails to regulate potassium channels. Furthermore, calcium channel activity runs down within 15 minutes. These problems had prevented direct detection of transmitter-induced inhibition of single calcium channels until the development of a new patch clamp configuration, termed the perforated vesicle, that results in the formation of outside-out patches that retain cytoplasmic factors and organelles.

Developments in single-channel recording combine the outside-out patch recording method with the perforated-patch technique. In this application, a perforating antibiotic is used to produce an outside-out patch, termed perforated vesicle, that retains the cytoplasmic content of the cell forming the equivalent to tiny single-channel cells. Thus, the perforated vesicle is an extension of the nystatin-perforated patch technique.

Similar to the protocol described above, nystatin stock solution (25 mg/mL) is prepared by dissolving 2 mg nystatin in 80 μ L DMSO. Since this pore-forming agent is susceptible to oxidation, the stock solution can be frozen and used within two days. Simple pipette solutions can be used (*e.g.*, 150 mM KCl, 5 mM MgCl₂, 10 mM KHepes, pH 7.1) because nucleotides, proteins and calcium buffers cannot permeate through nystatin perforations. Four (4) μ L of nystatin stock solution is pipetted into a glass tube and then 1 mL of filtered pipette solution is added. After covering the tube and vortexing, the slightly cloudy solution is vigorously sonicated for 30 seconds in a cylindrical bath sonica-

tor to completely dissolve the nystatin, giving a final concentration of 100 $\mu\text{g}/\text{mL}$. This aqueous solution can be used for only 3 hours.

Conventional patch pipettes are fabricated. When filled with pipette solution, their resistance is 2–4 $\text{M}\Omega$. Smaller pipettes minimize the surface area of the perforated patch and, thus, give larger series resistances (R_s). On the other hand, larger pipette tips were found to form fragile patches that could spontaneously break forming the conventional whole-cell configuration. Pipettes are coated with Sylgard to reduce their capacitance. This not only lowers noise for single-channel recording, but also permits accurate series resistance measurements.

Pipettes are momentarily dipped in nystatin-free pipette solution and then backfilled with nystatin-containing solution. A cell-attached seal is then formed. After compensating, electrode capacitance (e.g., 3 pF), R_s is monitored by examining the unfiltered current response to a 10 mV voltage step from -70 mV (holding potential). The height of the capacitance transient is equal to the voltage step divided by R_s . Series resistance is monitored for 5–20 minutes to ensure that it decreases smoothly to a value less than 50 $\text{M}\Omega$. Cells that show an abrupt decrease in R_s should be discarded.

The patch-clamp amplifier is switched from voltage-clamp (V-clamp) mode to current-clamp (I-clamp) mode with zero resting current and the pipette is withdrawn from the cell to form a perforated vesicle (Figure 5.6). Switching to I-clamp ensures that no large changes in current could pass through the patch and disrupt the resealing of the membrane that forms the vesicle. The patch-clamp amplifier is then switched to V-clamp mode to record single-channel activity.

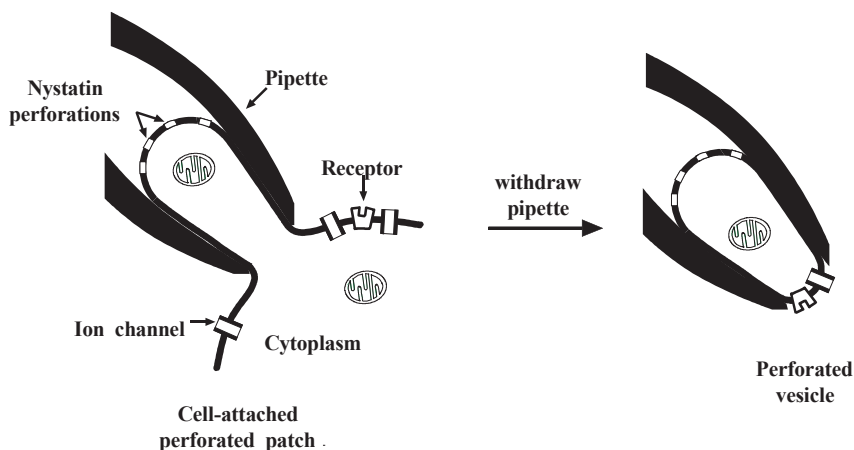


Figure 5.6: Forming a cell-attached perforated patch and a perforated vesicle.

The formation of a perforated vesicle can be verified by many methods. In some cases, vesicles can be seen with 400x magnification. The presence of cytoplasm can be con-

firmed by preloading the cells with a fluorescent dye. For example, cells may be treated with 40 μM carboxyfluorescein diacetate, a membrane-permeant nonfluorescent compound. After crossing the membrane, this agent is hydrolyzed to yield water-soluble carboxyfluorescein. The presence of organelles can also be verified with specific dyes. Rhodamine 123 specifically partitions into functioning mitochondria and produces a characteristic punctate staining that can be detected in GH3 cells and perforated vesicles. Channel activity can also verify the presence of nystatin perforations. With normal vesicles, channel currents appear attenuated and rounded. Furthermore, channels in the inner face of the vesicle are not accessible to bath-applied hydrophilic inhibitors and have opposite voltage dependence to channels in the vesicle surface that is in contact with the bath. In contrast, perforated-vesicle channel activity can be recorded only from the portion of the vesicle in contact with the bath. Through the use of fluorescent dyes and channel recordings, the perforated vesicle can be differentiated from normal excised vesicles and outside-out patches.

The nystatin-perforated vesicle method allows the study of channel activity and modulation that is lost with conventional outside-out patches. Initial studies indicate that cyclic AMP-dependent protein kinase, phosphodiesterase, phosphatase, G-proteins, phospholipase C and intracellular calcium stores can modulate ion channels in perforated vesicles excised from GH3 cells. Two channel types that quickly “wash out” of conventional patches from these cells, L-type calcium channels and voltage-gated potassium channels, survive for extended periods with perforated vesicles. Perforated vesicles were excised successfully from a variety of cell lines and primary cultured pituitary cells. Thus, it appears likely that this patch clamp configuration will aid the study of ion channel modulation in many systems.

5.9. FURTHER READING

Falke, L.C., Gillis, K.D., Pressel, D.M., Mislér, S., Perforated patch recording allows long-term monitoring of metabolite-induced electrical activity and voltage-dependent Ca^{2+} currents in pancreatic islet B-cells. *FEBS Lett.*, 251: 167–172, 1989.

Finkelstein, A., *Water movement through lipid bilayers, pores, and plasma membranes: theory and reality*, Vol. 4, Wiley-Interscience, New York, p. 127, 1987.

Holz, R., Finkelstein, A., The water and nonelectrolyte permeability induced in thin lipid membranes by the polyene antibiotics nystatin and amphotericin B. *J. Gen. Physiol.*, 56: 125–145, 1970.

Horn, R., Diffusion of nystatin in plasma membrane is inhibited by a glass-membrane seal. *Biophys. J.*, 60: 329–333, 1991.

Horn, R., Marty, A., Muscarinic activation of ionic currents measured by a new whole-cell recording method. *J. Gen. Physiol.*, 92: 145–159, 1988.

Korn, S.J., Bolden, A., Horn, R., Control of action potential duration and calcium influx by the calcium-dependent chloride current in AtT-20 pituitary cells. *J. Physiol. (Lond)*, 439: 423–437, 1991.

Korn, S.J., Horn, R., Influence of sodium-calcium exchange on calcium current rundown and the duration of calcium-dependent chloride currents in pituitary cells, studied with whole cell and perforated patch recording. *J. Gen. Physiol.*, 94: 789–812, 1989.

Korn, S.J., Marty, A., Connor, J.A., Horn, R., Perforated patch recording. *Methods in Neuroscience* 4: 264–373, 1991.

Kurachi, Y., Asano, Y., Takikawa, R., Sugimoto, T., Cardiac Ca current does not run down and is very sensitive to isoprenaline in the nystatin-method of whole cell recording. *Archiv. Pharm.*, 340: 219–222, 1990.

Levitan, E.S., Kramer, R.H., Neuropeptide modulation of single calcium and potassium channels detected with a new patch clamp configuration. *Nature*, 348: 545–547, 1990.

Lindau, M., Fernandez, J.M., IgE-mediated degranulation of mast cells does not require opening of ion channels. *Nature*, 319: 150–153, 1986.

Lucero, M.T., Pappone, P.A., Membrane responses to norepinephrine in cultured brown fat cells. *J. Gen. Physiol.*, 95: 523–544, 1990.

Rae, J., Cooper, K., Gates, G., Watsky, M., Low access resistance perforated patch recordings using amphotericin B. *J. Neurosci. Methods.*, 37: 15–26, 1991.

5.10. ENHANCED PLANAR BILAYER TECHNIQUES FOR SINGLE-CHANNEL RECORDING

The planar bilayer recording technique, in which ion channels are incorporated into an artificial, planar lipid bilayer either by fusion of vesicles containing the channels with the bilayer or by direct insertion of water-soluble channels, provides a unique approach for studying single ion channels, enabling experimental designs that are impractical or impossible using standard patch-clamp methods. For example, the effects of membrane composition on channel function can be rigorously studied, changes in solution composition on either side of the membrane can be made easily, and channels can be incorporated from membranes that are normally inaccessible to patch-clamp methods (*e.g.*, cytoplasmic vesicles, sarcoplasmic reticulum) (Wonderlin et al., 1990; Wonderlin et al., 1991). The utility of the planar bilayer method for studying single ion channels, however, is often limited by a low recording bandwidth, primarily due to the high background current noise, and poor resolution of voltage step activation of ion channel activity due to the large, slow capacitive current transient associated with a voltage step applied to a bilayer. These limitations may be especially problematic in investigations of small-conductance, rapidly gating channels, the kinetics of channel-blocking drugs, or voltage-gated ion channels that must be activated by voltage steps because of steady-state inactivation. The purpose of this brief

tutorial is to describe a combination of equipment and methods that partially overcome these limitations and improve the quality of planar bilayer recordings. With this approach, it is reasonable to attempt to record single-channel activity with low background noise (< 0.35 pA rms at 5 kHz) and rapid resolution (<< 1 ms) of currents after a voltage step. Several general considerations regarding the equipment and techniques necessary for making high-resolution recordings will be presented first, followed by a more detailed description of the implementation of the approach. For more detailed discussion of the equipment and methods, see Wonderlin et al., 1990.

5.10.1. SOLVING THE PROBLEMS OF HIGH RESOLUTION AND VOLTAGE STEPS

Minimizing the Background Current Noise

Bilayer recording systems are prone to high background current noise which can easily obscure single-channel gating and often may require low-pass filtering of the current record to a bandwidth of a few hundred hertz or less. This heavy filtering may obscure rapid gating fluctuations, and it badly distorts the current response to a voltage step. Unlike gigohm-seal (gigaseal) patch-clamp recording, thermal noise currents in either the large value (*e.g.*, 50 GΩ) feedback resistor of a resistive headstage amplifier or in the seal resistance are generally insignificant for bilayer recordings. Rather, the majority of the background noise in a planar bilayer recording system results from “voltage clamping” across the bilayer capacitance (C_b) voltage noise present in the following sources:

- 1 The FET input of the patch amplifier,
- 2 The voltage command circuitry, and
- 3 The access resistance R_a , *i.e.*, the resistance of the solutions and electrodes in series with the bilayer.

The spectral density of the current noise $S_{i(f)}^2$ produced by voltage clamping a noise voltage in either the FET input or the voltage command across the bilayer capacitance is given by Ohm’s law:

$$S_{i(f)}^2 = \frac{e_n^2}{X_c^2} \tag{6}$$

where e_n is the rms noise voltage ($V/\sqrt{\text{Hz}}$) and X_c is the capacitive reactance of the bilayer. The capacitive reactance is $1/(2\pi C_b f)$, where f is the frequency and C_b is the bilayer capacitance. Therefore:

$$S_{i(f)}^2 = e_n^2 (2\pi C_b f)^2 \tag{7}$$

The spectral density of the current noise produced by voltage clamping the thermal voltage noise in the access resistance R_a across the bilayer capacitance is:

$$S_{i(f)}^2 = 4kT \operatorname{Re}\{Y(f)\} \quad (8)$$

where $\operatorname{Re}\{Y(f)\}$ is the real part of the admittance of R_a in series with C_b , and is given by

$$\operatorname{Re}\{Y(f)\} = \frac{\alpha^2}{R_a(1 + \alpha^2)} \quad (9)$$

with $\alpha = 2\pi f R_a C_b$. For a constant bandwidth, at the lower limit of R_a (small α), $\operatorname{Re}\{Y(f)\} = R_a(2\pi C_b f)^2$, and equations (7) and (8) have a similar form. At the upper limit of R_a (large α), $\operatorname{Re}\{Y(f)\} = 1/R_a$. The transition from a linear to a reciprocal dependence on R_a produces maxima in plots of this noise component against R_a (see Figure 2A of Wonderlin et al., 1990).

Strategies for Minimizing the Background Current Noise

Reduce the Bilayer Capacitance. The single most effective approach to reducing the background current noise is to reduce the bilayer diameter and hence its capacitance. This assumes that the access resistance is not increased (see Wonderlin et al., 1990 and “*Choosing a Recording Configuration*” on page 137) for a discussion of open chamber versus pipette/bilayer configurations). There is, however, a practical limit to the extent of reduction as the bilayer diameter must be large enough both to allow easy visualization and physical manipulation and to ensure an acceptable rate of channel incorporation. Bilayer diameters in the 40–60 μm range (having 10–25 pF C_b at 0.8 $\mu\text{F}/\text{cm}^2$) represent a reasonable compromise between the competing needs of reducing the capacitance versus ease of channel incorporation and manipulation. A very good method for making these small bilayers is the shaved-aperture method, which is described in detail below (Assembling a Bilayer Setup for High-Resolution Recording: Making a Small Aperture).

Use an Amplifier with Low Internal Noise Voltage. Noise voltages are present in the FET input of the headstage and in the circuitry with which voltage command inputs are buffered and applied to the bilayer. Reduction of the noise voltage in these internal sources is difficult for the investigator to control without being involved in the design and construction of the amplifier. However, when selecting an amplifier, the magnitude of the internal noise voltage sources can be quickly but qualitatively determined by comparing the noise in the current output before and after connection of the amplifier input through a bilayer-sized capacitor to ground. This test should be done without the addition of any resistance in series with the test capacitor to avoid confusing an internal noise voltage source with voltage noise in the access resistance. It should be noted that amplifiers which exhibit low noise when used for patch recording (where the input capacitance is small and the background noise is dominated by thermal noise currents in the feedback resistor and seal resistance) can per-

form poorly when the input capacitance is increased from patch to bilayer values, because of high internal voltage noise.

Use Low-Noise Voltage Command Sources. Although many commercially available amplifiers are equipped with internal voltage command generators, voltage-step protocols will usually require the generation of the voltage command from an external source, usually a computer-driven digital-to-analog (D/A) converter. This can present a problem if the D/A source has a significant noise voltage. This is very likely if the board containing the D/A is mounted internally in a computer, using the computer's power supply. The best configuration is an outboard D/A unit, with optically isolated digital connections and its own, isolated power supply. Once again, a D/A source that provides perfectly suitable voltage commands for patch clamping can fail miserably when used to provide voltage commands for bilayer recordings, because of the much greater sensitivity to voltage noise in the voltage command source. One should also be careful about using digital function generators for producing command voltages such as voltage ramps, as they can introduce considerably more noise than analog function generators.

Minimize the Access Resistance. Even with perfect, noise-free electronics, considerable background current noise can be generated when the thermal voltage noise in the access resistance is voltage clamped across the bilayer capacitance. This source can account for as much as one half the noise under many bilayer recording conditions (Wonderlin et al., 1990). The access resistance responsible for generating the voltage noise is composed primarily of the resistance of the solution within the aperture in which the bilayer is formed and the convergence resistances between each end of the aperture and the bulk solutions (see Wonderlin et al., 1990). Because the resistance of these solutions is inversely related to the salt concentration, it may be possible to reduce the intra-aperture and convergence resistances by increasing the salt concentration, within the limits of the experimental design. Furthermore, the shaved-aperture method can be used to minimize the length of the aperture and, therefore, its resistance. The resistance of the bulk solution should not contribute appreciably to the access resistance when an open chamber design is used; but it can be an important factor if large bilayers are made on the tips of glass pipettes (Wonderlin et al., 1990). Finally, if salt bridges are used to connect the Ag/AgCl pellets to each bath, they should be designed with a low resistance in mind, such as by using relatively large diameter (e.g., 2 mm) glass capillaries filled with a high-salt solution such as 3 M KCl.

Choice of Chamber Construction Materials. When selecting a type of plastic from which to fabricate a recording chamber, one should consider, in addition to factors such as machinability, durability and solvent resistance, the fact that some plastics generate excess current noise when a hole in the plastic is filled with a salt solution and connected to the input of a patch amplifier. For example, when an Axopatch-1B amplifier was connected via an Ag/AgCl electrode to a 0.5 mL well filled with 3 M KCl, the following relative rms noise levels (30 Hz–5 kHz) were measured: high-

density polyethylene (1.0), polystyrene (1.0), polycarbonate (1.0), Teflon (1.0), acrylic (1.4) and nylon (1.5) (Wonderlin et al., 1990). Although the absolute amount of this excess noise is small relative to other sources listed above, this source of noise can be eliminated easily by selecting an appropriate plastic.

Type of Solvent in a Painted Bilayer. We have found that the type of solvent present in a painted bilayer can affect the background current noise. If a bilayer is painted from phospholipids dissolved in decane, the background noise can often be reduced by rewiping the bilayer with hexadecane alone. The reason for the improvement is not known and appears somewhat paradoxical, since it is usually associated with a slightly larger bilayer capacitance.

Maximizing the Bandwidth

Minimization of the background noise currents by one or more of the methods described above may help increase the usable bandwidth by decreasing the amount of low-pass filtering required to clearly discern single channel gating. If the low-pass filter cutoff (-3 dB) frequency is increased to several kilohertz or more, a second, less obvious source of bandwidth limitation may come into play. This limitation is the decreased efficiency of the high-frequency boost circuit used in resistive-headstage amplifiers due to loading the headstage input with large bilayer capacitance. The boost circuit is designed to restore the bandwidth that is lost because of low-pass filtering (< 100 Hz) by the parallel combination of the feedback resistor and its stray capacitance. The high-frequency boost circuit adds a scaled derivative of the headstage current to the raw headstage current, thereby increasing the headstage bandwidth. For patch recording, a boost circuit can work well because of the dominant role of fixed electrical elements, such as the feedback resistance and stray feedback capacitance, whose properties can be optimally compensated in the selection of circuit components. When a resistive headstage amplifier is used for bilayer recordings, however, the loss of bandwidth due to the variable, and frequently large, bilayer capacitance must also be restored. This is much more difficult because the optimal amount of high-frequency boost that is required will change in parallel with any change in bilayer capacitance. Therefore, it is difficult to select components in the design of the amplifier that enable optimal boosting across a large range of bilayer capacitance values. Furthermore, because the bilayer capacitance will often vary by 50% within a day's experiments, it may be very difficult to maintain optimal boost adjustment.

Strategies for Maximizing the Bandwidth

Use a Capacitive-Headstage Patch Amplifier. An integrating-headstage patch-clamp amplifier (e.g., the Axopatch 200B) measures the patch current as the integral of the current flow across a feedback capacitor, rather than as the voltage drop across a feedback resistor. A boost circuit is not required for an integrating-headstage amplifier because the feedback capacitor does not produce any significant low-pass filtering of the patch current. Integrating headstage amplifiers therefore provide a broader recording bandwidth that is also independent of the size of the bilayer capacitance.

Resolving Voltage Steps Across Bilayers

A change of voltage across a bilayer of capacitance C_b by an amount V_{step} requires the movement across the bilayer of electrical charge Q_b where:

$$Q_b = V_{\text{step}} C_b \quad (10)$$

For a resistive-headstage amplifier, the amount of time required to move Q_b is:

$$\text{Charging time} = \frac{Q_b R_f}{V_{\text{max}}} \quad (11)$$

where V_{max} is the maximum voltage that can be applied across the feedback resistor R_f . For example, a headstage with a 50 G Ω feedback resistor and a V_{max} of 10 V can inject charge at a maximum rate of 200 pA, requiring 25 ms to change the voltage across a 100 pF bilayer by 50 mV. During this 25 ms period, the output of the amplifier will be saturated (at V_{max}) and the bilayer will not be voltage clamped. This example illustrates that the primary difficulty associated with applying voltage steps to a bilayer is the requirement for rapid movement of a large amount of charge across the bilayer. For traditional resistive-headstage patch amplifiers this is a nearly insurmountable problem because of the very slow rate at which charge can be delivered to the bilayer capacitance through the large feedback resistance.

A secondary problem is that planar bilayers do not behave as ideal capacitors. The application of a voltage step to a planar bilayer compresses the bilayer (*i.e.*, causes electrostriction). This electrostrictive force can change the relative areas of the bilayer and surrounding annulus, producing a concomitant change in the capacitance of the bilayer. During the period of time that the bilayer capacitance is changing, a capacitive current will flow across the bilayer. Electrostrictive changes in bilayer capacitance are relatively slow (milliseconds to seconds) and rarely large enough to produce capacitive currents that obscure single-channel gating. However, the electrostrictive capacitive current tends to be variable in magnitude and kinetics and it can change significantly as a bilayer “ages” during the course of an experiment. This variability can make it difficult to subtract the electrostrictive component of the capacitive current from the current record.

Strategies for Resolving Voltage Steps Across Bilayers

Reduce the Size of the Bilayer and Annulus. An essential first step is to make small bilayers, because reducing the bilayer capacitance proportionally decreases the charging time. Unfortunately, reducing the bilayer diameter into the 40–60 μm range (10–25 pF) may still result in an excessive saturation time (several milliseconds). Because the magnitude of the electrostrictive change in capacitance depends on the area of the annulus, decreasing the bilayer diameter also reduces this component. The width of the annulus (*i.e.*, in the plane of the bilayer) is also roughly proportional to

the thickness of the margin of the aperture. A substantial, further reduction in the electrostrictive component can be achieved by using the shaved-aperture method, because it produces a margin of the aperture that is very thin (a few micrometers). Other techniques, such as drilling or punching apertures, produce a margin that is much thicker. Finally, any manipulation of the bilayer that produces a “bulkier” annulus, such as addition of excess solvent or repeated wiping, can greatly increase the electrostrictive component and should be avoided.

Use Capacitance Compensation. The capacitance compensation circuits in most commercially available patch clamps are only slightly effective in reducing the duration of saturation because they are designed to compensate the relatively small capacitance of a patch pipette rather than the much larger capacitance of a planar bilayer. Special circuits capable of compensating the larger bilayer capacitance can be added to the headstage, but they require the injection of compensating current into the amplifier input through a large capacitor, which increases the total input capacitance and degrades the noise performance. Sometimes, the electrostrictive capacitive current can be partially subtracted by adjustment of a capacitance compensation circuit with a slow time constant. The BL type of CV-7 headstages (such as the CV-7B/BL) in use with MultiClamp 700 amplifiers has an increased fast pipette capacitance compensation range that allows compensation of up to 300 pF of pipette capacitance.

Decrease the Feedback Resistance. The charging time can be reduced by decreasing the value of R_f thereby increasing the rate at which charge can be delivered to the bilayer. However, the price for this improvement is a proportional increase in the background thermal noise currents in R_f and, therefore, a concomitant decrease in usable bandwidth. Although this may work for large conductance channels, it is hardly a general solution. A better solution is to include both a large (50 G Ω) and a small (50 M Ω) feedback resistor in the headstage with logic-controlled circuitry that can switch between the two. This approach was taken in the CV-4B headstage for the Axopatch 1 series of Axon Cellular Neuroscience amplifiers. During a voltage step, the bilayer capacitance is rapidly charged through the small R_f . Immediately after the bilayer capacitance is charged, the feedback pathway is switched to the large R_f , enabling high resolution recording of single-channel activity. This approach was used successfully to study voltage-dependent activation of K^+ channels from squid (Wonderlin et al., 1990; Wonderlin et al., 1991).

Use a Capacitive-Headstage Patch Amplifier. Capacitive-headstage patch clamps can very rapidly charge the bilayer capacitance with a maximum instantaneously injected charge of:

$$\text{Maximum charge} = V_{\max} C_f$$

where C_f is the feedback capacitance. With a V_{\max} of 10 V and C_f equal to 1 pF, 10 pC of charge can be delivered nearly instantly. This charge is sufficient to change

the voltage across a 100 pF bilayer by 100 mV without saturation of the headstage output. Because integration of a constant patch current will eventually saturate C_f , an integrating headstage requires a reset circuit that periodically discharges the feedback capacitor; this is usually a logic-controlled switch that shunts the feedback capacitor. In some designs, this same reset switch can be activated during a voltage step. Such a “forced reset” allows rapid charging of the bilayer capacitance.

5.10.2. ASSEMBLING A BILAYER SETUP FOR HIGH-RESOLUTION RECORDINGS

Choosing an Amplifier

Traditionally, resistive headstage patch amplifiers have been used in bilayer recording systems. These amplifiers are widely commercially available or they can be built rather inexpensively because of the simple design of the circuitry. Integrating-headstage amplifiers are commercially available.

How should one choose among these amplifiers? The ideal amplifier for high-resolution bilayer recordings should have:

- 1 Low intrinsic current and voltage noise,
- 2 A wide bandwidth, and
- 3 The ability to rapidly charge the bilayer capacitance.

Although integrating headstages have less intrinsic current noise than resistive headstages, there may be little difference in noise performance during actual bilayer recordings due to the dominance in bilayer recordings of current noise produced by the interaction of the bilayer capacitance with various noise voltage sources. With regard to bandwidth, the integrating headstage is a clear favorite because it does not require a high-frequency boost circuit. Adjustment of the high-frequency boost of a resistive headstage with a large, variable bilayer capacitance at the input can be very frustrating. On the other hand, within the 5–10 kHz bandwidth that one might hope to achieve with bilayer recordings, the bandwidth of an integrating headstage should not be affected by the bilayer capacitance. Finally, the integrating headstage is the better choice for rapid charging of the bilayer capacitance during voltage steps, although a switching-feedback resistive headstage (such as the CV-4B headstage for the old Axopatch 1 series of amplifiers) can perform nearly as well (Wonderlin et al., 1990; Wonderlin et al., 1991), since it also provides a low-impedance pathway for charging the bilayer capacitance. It should be emphasized that the rapid charging by either an integrating headstage amplifier or a switching-resistive headstage amplifier does not decrease the slow, electrostrictive component of the capacitive current, whose time course is determined only by the dynamic properties of the bilayer/annulus structure.

When all of the requirements for an amplifier are considered, it is clear that anyone attempting high-resolution recording from bilayers with voltage steps should seriously consider using a capacitive-headstage amplifier.

Choosing a Recording Configuration

There are two primary recording configurations for planar bilayers:

- 1 A bilayer formed over an aperture in a partition separating two open bath chambers (open-chamber configuration); and
- 2 A bilayer formed on the tip of a polished glass pipette (pipette/bilayer configuration), either by “punching” a preformed planar bilayer or by dipping the tip through a lipid monolayer.

The relative merits of these configurations have been discussed in (Wonderlin et al., 1990). Briefly, for bilayer capacitance values larger than a few picofarads, the open-chamber configuration with a shaved aperture will generate less background current noise than the bilayer/pipette configuration, due to the much higher access resistance of the interior of the pipette compared to the open chamber. Therefore, if bilayers must be made large enough to permit incorporation of channels by fusion of vesicles with the bilayer, the open chamber configuration should be used. If channels can be incorporated during the formation of the bilayer (*e.g.*, “tip-dip”) so that bilayers with a very small area (less than a few picofarads capacitance) can be used, then the pipette/bilayer configuration can be used. Finally, the open chamber configuration offers greater flexibility with regard to manipulation of the bilayer and bath solutions.

Making Small Apertures

It is fundamentally important to be able to work with small bilayers, usually with diameters in the range of about 40–60 μm . This size range represents a trade-off between the need to reduce the area (and capacitance) while maintaining a large enough area to ensure adequate incorporation by fusion of vesicles. Among the many techniques available for making apertures in plastic partitions, the shaved-aperture method is especially well suited for making small apertures. This method has been previously described in detail for making small apertures in plastic cups (Wonderlin et al., 1990).

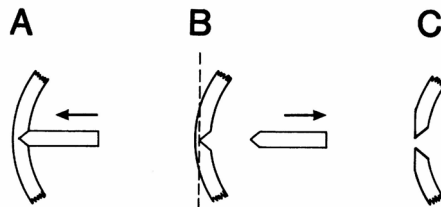


Figure 5.7: Aperture formation in a plastic cup (not drawn to scale).

- A. A metal stylus is warmed and pressed against the inner surface of the cup, producing a cone-shaped depression.
- B. After cooling, the stylus is retracted and the plastic shaved from the outer surface, leaving a thin-edged aperture where the cut intersects the depression in the wall of the cup, as in C. See text for additional details. Reproduced with permission from Wonderlin et al., 1990.

Briefly, a conical metal stylus is warmed and pressed against the inner surface of a plastic cup, forming a cone-shaped depression extending part way across the cup (Figure 5.7). The stylus is then removed and the plastic shaved away from the outer surface, using a disposable microtome blade, until the depression is intersected. The size of the aperture is controlled by varying the depth of shaving. Apertures made using this method have a thin margin beyond which the plastic rapidly increases in thickness, thereby decreasing the stray capacitance across the partition and providing good mechanical strength. The thin margin of the shaved aperture is very important in reducing the size of the annulus and, therefore, the electrostrictive change in capacitance following voltage steps. Following are the essential steps in implementing the method:

- 1** *Making the stylus.* The key to successfully using the shaved-aperture method is the manufacture of a high-quality stylus. Using a lathe and dissecting microscope, stainless steel darning needles can be ground to a very fine tip ($< 5 \mu\text{m}$ diameter) and polished to a very smooth finish using ultra-fine abrasive paper (Thomas Scientific, Swedesboro, NJ). Softer metals can be substituted, but it is more difficult to produce the highly polished tip. The stylus should be examined under high magnification (400x) to ensure that the tip is very smooth.
- 2** *Selecting the plastic.* The original description of the shaved-aperture technique (Wonderlin et al., 1990) recommended polystyrene as a good plastic for recording cups. Since that time, repeated difficulties have been encountered with crazing of the margin of apertures made in polystyrene cups, which sometimes appears to make the cups electrically leaky. More recently, shaved apertures in cups were made from Ultra-Clear centrifuge tubes (Beckman, Colombia, MD). Also, if a flat partition rather than a cup is preferred, shaved apertures have been formed in plastic coverslips (Fisher Scientific, Pittsburgh, PA). The margin of these apertures does not craze and bilayers formed on apertures shaved in these plastics are very stable, lasting several hours. Other plastics can probably be substituted, with the basic requirement being that they cut cleanly so that the margin of the aperture is very smooth.
- 3** *Melting the plastic.* There are many choices of mechanical apparatus for manipulating and heating the stylus. A rather simple method is to mount the stylus in a hole in the tip of a variable temperature soldering iron, and then to mount the soldering iron on a manipulator so that the tip can be carefully pushed into the plastic. Control of the heat is important to ensure replicability and to avoid overheating, which may damage the plastic and, perhaps, the stylus.
- 4** *Shaving the aperture.* It is easiest to shave the apertures while observing with a dissecting microscope. The shaved apertures should be examined under high magnification (400x) before use to ensure they are free from deformations that might interfere with bilayer stability.

Viewing with a Microscope

It is not practical to attempt to work with small bilayers without observing them with a microscope. Bilayers are usually observed under reflected light because the disappearance of reflected light provides a good monitor of bilayer thinning. Quite often, the bilayer is viewed through one eyepiece of a dissecting microscope, while the bilayer is illuminated by light focused from a fiber bundle through the second eyepiece. This method is not useful for small bilayers because of the lack of detail visible with reflected light and the relatively low magnification (40–80x) of most dissecting microscopes. Using a horizontally mounted compound microscope (Nikon Inc., Garden City, NY) with a long working-distance objective (Nikon, E-Plan 10x) and a bilayer recording chamber designed for transillumination provides very good resolution of detail in the bilayer and annulus at a magnification of 100x.

Testing the System

The performance of the recording system should be tested using a dummy bilayer, especially if voltage steps are to be used. The dummy bilayer should use a capacitor with a value close to that expected for the bilayer capacitance. It may also be useful to add a resistor in series with the capacitor to mimic the access resistance. In choosing a capacitor, polystyrene capacitors are preferred. Some other types of capacitors, such as ceramic capacitors, can exhibit very non-ideal properties, with odd relaxations similar to the electrostrictive relaxation of planar bilayers. By simulating a bilayer recording using the dummy bilayer, it is possible to determine the dependence of the background noise and voltage-step response on electrical components with ideal electrical properties, as opposed to the non-ideal electrical properties of components used during experiments, such as the bilayer composition and salt solutions. It also permits optimization of the timing of voltage steps relative to logic-controlled switching between different feedback resistors in a resistive headstage amplifier or the timing of a forced reset in a capacitive headstage amplifier.

Making the Recordings

An example of the voltage-step activation of a delayed rectifier K^+ channel from squid is shown in Figure 5.8. The ultimate success of high-resolution recording in planar bilayers depends not only on the various details described above, but also on the ease of fusion of certain populations of membrane vesicles. Rates of incorporation are likely to be lower for small bilayers than are typical for larger bilayers, but the difference may be reduced by methods such as pressure application of vesicles from a pipette onto the bilayer. Although the high-resolution recording method may increase the difficulty beyond that of traditional bilayer recording techniques, it opens exciting opportunities for new experimental designs and the investigation of a broader range of ion channels.

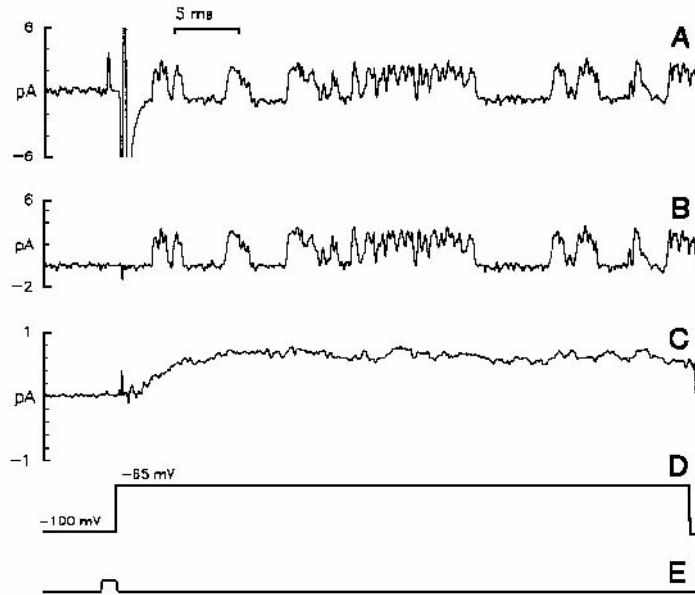


Figure 5.8: Voltage-step activation of a K-channel from squid giant axon axoplasm.

- A. A single, unsubtracted current record showing the response to a voltage step. In A–C, the current is actually inward, but is shown inverted to be consistent with the usual orientation of K-current records. The gain was switched to low 1 ms before the voltage step, producing a small current transient (logic pulse is shown in trace E). The gain was switched back to high 25 μ s after the voltage step.
- B. Current record from which the capacitive current and switching artifact have been digitally subtracted. Blank traces (7 traces in which the channel was not active) were averaged and subtracted from the active trace. Subtraction is very effective in removing the step artifact, and high-resolution recording is established within 1ms after the voltage step.
- C. An average current record simulating a macroscopic response. 240 current traces were averaged, from which the average of the blank records was subtracted, as in B.
- D. Voltage command trace.
- E. Logic pulse used to switch the headstage gain. The headstage was switched to low gain during the rectangular pulse. Reproduced with permission from Wunderlin et al., 1990.

5.11. FURTHER READING

Wonderlin, W.F., Finkel, A., French, R.J., Optimizing planar lipid bilayer single-channel recordings for high resolution with rapid voltage steps. *Biophys. J.*, 58: 289–297, 1990.

Wonderlin, W.F., French, R.J., Ion channels in transit: voltage-gated Na and K channels in axoplasmic organelles of the squid *Loligo pealei*. *Proc. Natl. Acad. Sci. USA*, 88: 4391–4395, 1991.

Hamill, O.P., Marty, A., Neher, E., Sakmann, B., Sigworth, F.J. Improved patch-clamp techniques for high-resolution current recording from cells and cell-free membrane patches. *Pflügers Arch. Eur. J. Physiol.* 391:85–100, 1981.

Sigworth, F.J., Electronic design of the patch clamp. in *Single-Channel Recording*, 2nd Edition, pp. 95–126, Sakmann, B., Neher, E. Eds. Plenum Press, New York, 1995.

6. Signal Conditioning and Signal conditioners

It is rare for biological, physiological, chemical, electrical or physical signals to be measured in the appropriate format for recording and interpretation. Usually, a signal must be “massaged” to optimize it for both of these functions. For example, storage of recorded data is more accurate if the data are amplified before digitization so that they occupy the whole dynamic range of the A/D converter, and interpretation is enhanced if extraneous noise and signals above the bandwidth of interest are eliminated by a low-pass filter.

6.1. WHY SHOULD SIGNALS BE FILTERED?

A filter is a circuit that removes selected frequencies from the signal. Filtering is most often performed to remove unwanted signals and noise from the data. The most common form of filtering is low-pass filtering, which limits the bandwidth of the data by eliminating signals and noise above the corner frequency of the filter (Figure 6.1). The importance of low-pass filtering is apparent when measuring currents from single-ion channels. For example, channel openings that are obscured by noise in a 10 kHz bandwidth may become easily distinguishable if the bandwidth is limited to 1 kHz.

High-pass filtering is required when the main source of noise is below the frequency range of the signals of interest. This is most commonly encountered when making intracellular recordings from nerve cells in the central nervous system. There are low-frequency fluctuations in the membrane potential due to a variety of mechanisms, including the summation of synaptic inputs. The small, excitatory synaptic potentials that the user might be interested in are often smaller than the low-frequency fluctuations. Since excitatory synaptic potentials are often quite brief, the low-frequency fluctuations can be safely eliminated by using a high-pass filter. High-pass filtering is also referred to as AC coupling.

Another type of filter that is often used in biological recording is the notch filter. This is a special filter designed to eliminate one fundamental frequency and very little else. Notch filters are most commonly used at 50 or 60 Hz to eliminate line-frequency pickup.

6.2. FUNDAMENTALS OF FILTERING

Filters are distinguished by a number of important features. These are:

6.2.1. -3 DB FREQUENCY

The -3 dB frequency (f_{-3}) is the frequency at which the signal voltage at the output of the filter falls to $\sqrt{1/2}$, *i.e.*, 0.7071, of the amplitude of the input signal. Equivalently, f_{-3} is the frequency at which the signal power at the output of the filter falls to half of the power of the input signal. (See Section 6.3.9., “*Decibels (dB)*”).

6.2.2. TYPE: HIGH-PASS, LOW-PASS, BAND-PASS OR BAND-REJECT (NOTCH)

A low-pass filter rejects signals in high frequencies and passes signals in frequencies below the -3 dB frequency. A high-pass filter rejects signals in low frequencies and passes signals in frequencies above the -3 dB frequency. A band-pass filter rejects signals outside a certain frequency range (bandwidth) and passes signals inside the bandwidth defined by the high and the low -3 dB frequencies. A band-pass filter can simply be thought of as a series cascade of high-pass and low-pass filters. A band-reject filter, often referred to as a notch filter, rejects signals inside a certain range and passes signals outside the bandwidth defined by the high and the low -3 dB frequencies. A band-reject filter can simply be thought of as a parallel combination of a high-pass and a low-pass filter.

6.2.3. ORDER

A simple filter made from one resistor and one capacitor is known as a first-order filter. Electrical engineers call it a single-pole filter. Each capacitor in an active filter is usually associated with one pole. The higher the order of a filter, the more completely out-of-band signals are rejected. In a first-order filter, the attenuation of signals above f_{-3} increases at 6 dB/octave, which is equal to 20 dB/decade. In linear terminology, this attenuation rate can be re-stated as a voltage attenuation increasing by 2 for each doubling of frequency, or by 10 for each ten-fold increase in frequency.

6.2.4. IMPLEMENTATION: ACTIVE, PASSIVE OR DIGITAL

Active filters are usually made from resistors, capacitors and operational amplifiers. Passive filters use resistors, capacitors and inductors. Passive filters are more difficult to make and design because inductors are relatively expensive, bulky and available in fewer varieties and values than capacitors. Active filters have the further virtue of not presenting a significant load to the source. Digital filters are implemented in software. They consist of a series of mathematical calculations that process digitized data.

6.2.5. FILTER FUNCTION

There are many possible transfer functions that can be implemented by active filters. The most common filters are: Elliptic, Cauer, Chebyshev, Bessel and Butterworth. The frequency responses of the latter two are illustrated in Figure 6.1. Any of these filter transfer functions can be adapted to implement a high-pass, low-pass, band-pass or band-reject filter. All of these filter transfer functions and more can be implemented by digital filter algorithms. Digital filters can even do the seemingly impossible: since all of the data may

be present when the filtering begins, some digital filters use data that arrive after the current data. This is clearly impossible in an analog filter because the future cannot be predicted. Typical digital filters are the box-car smoothing filter and the Gaussian filter.

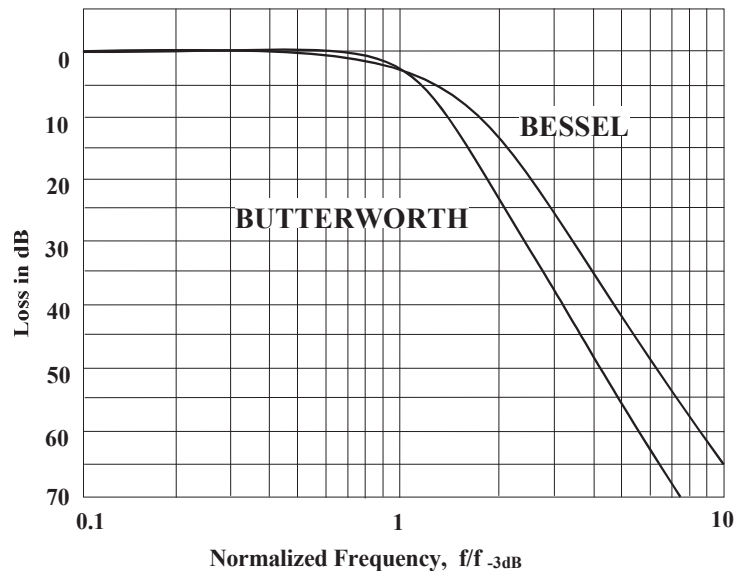


Figure 6.1: Frequency response of 4th-order Bessel and Butterworth filters.

The spectra have been normalized so that the signal magnitude in the pass band is 0 dB. The -3 dB frequency has been normalized to unity.

6.3. FILTER TERMINOLOGY

The terminology in this section is defined and illustrated in terms of a low-pass filter. The definitions can easily be modified to describe high-pass and band-pass filters. Many of these terms are illustrated in Figure 6.2.

6.3.1. - 3 DB FREQUENCY

f_{-3} , defined previously, is sometimes called the cutoff frequency or the corner frequency. While most engineers and physiologists specify a filter's bandwidth in terms of the -3 dB frequency, for obscure reasons some manufacturers label the filter frequency on the front panel of their instruments based on a frequency calculated from the intersection frequency of the pass-band and the stop-band asymptotes. This is very confusing. To make sure that the filter is calibrated in terms of the -3 dB frequency, a sine wave generator can be used to find the -3 dB frequency.

6.3.2. ATTENUATION

Attenuation is the reciprocal of gain. For example, if the gain is 0.1 the attenuation is 10. The term attenuation is often preferred to gain when describing the amplitude response of filters since many filters have a maximum gain of unity. (For accurate measurements, note that even filters with a stated gain of unity can differ from 1.00 by a few percent.)

6.3.3. PASS BAND

Pass band is the frequency region below f_3 . In the ideal low-pass filter there would be no attenuation in the pass band. In practice, the gain of the filter gradually reduces from unity to 0.7071 (*i.e.*, -3 dB) as the signal frequencies increase from DC to f_3 .

6.3.4. STOP BAND

Stop band is the frequency region above f_3 . In the ideal low-pass filter, the attenuation of signals in the stop band would be infinite. In practice, the gain of the filter gradually reduces from 0.7071 to a filter-function and implementation-dependent minimum as the signal frequencies increase from f_3 to the maximum frequencies in the system.

6.3.5. PHASE SHIFT

The phase of sinusoidal components of the input signal is shifted by the filter. If the phase shift in the pass band is linearly dependent on the frequency of the sinusoidal components, the distortion of the signal waveform is minimal.

6.3.6. OVERSHOOT

When the phase shift in the pass band is not linearly dependent on the frequency of the sinusoidal component, the filtered signal generally exhibits overshoot. That is, the response to a step transiently exceeds the final value.

6.3.7. OCTAVE

An octave is a range of frequencies where the largest frequency is double the lowest frequency.

6.3.8. DECADE

A decade is a range of frequencies where the largest frequency is ten times the lowest frequency.

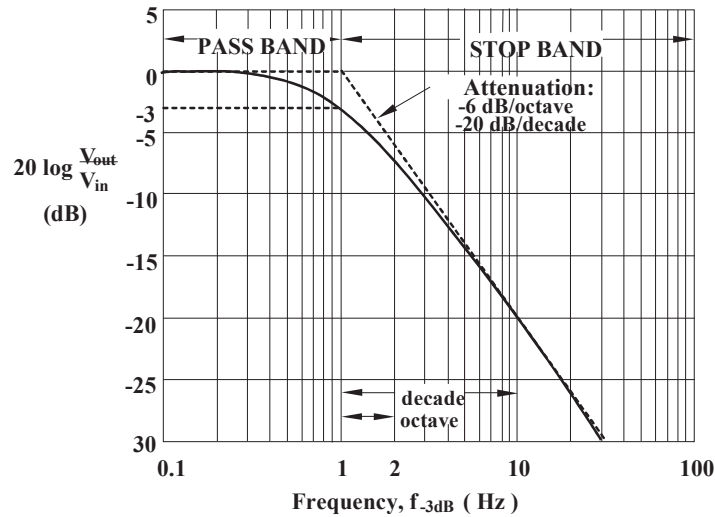


Figure 6.2: Illustration of filter terminology.

A number of the terms used to describe a filter are illustrated in the context of a single-pole, low-pass filter.

6.3.9. DECIBELS (DB)

Since filters span many orders of magnitude of frequency and amplitude, it is common to describe filter characteristics using logarithmic terminology. Decibels provide the means of stating ratios of two voltages or two powers.

Voltage:

$$dB = 20 \log \frac{V_{out}}{V_{in}} \quad (1)$$

Thus, 20 dB corresponds to a tenfold increase in the voltage.

-3 dB corresponds to a $\sqrt{2}$ decrease in the voltage.

Power:

$$dB = 10 \log \frac{P_{out}}{P_{in}} \quad (2)$$

Thus, 10 dB corresponds to a tenfold increase of the power.

-3 dB corresponds to a halving of the power.

Some useful values to remember:

Decibels	Voltage Ratio	Power Ratio
3 dB	1.414:1	2:1
6 dB	2:1	4:1
20 dB	10:1	100:1
40 dB	100:1	10,000:1
60 dB	1,000:1	1,000,000:1
66 dB	2,000:1	4,000,000:1
72 dB	4,000:1	16,000,000:1
80 dB	10,000:1	10 ⁸ :1
100 dB	100,000:1	10 ¹⁰ :1
120 dB	1,000,000:1	10 ¹² :1

6.3.10. ORDER

As mentioned above, the order of a filter describes the number of poles. The order is often described as the slope of the attenuation in the stop band, well above f_{c3} , so that the slope of the attenuation has approached its asymptotic value (see Figure 6.2). Each row in the following table contains different descriptions of the same order filter.

Pole	Order	Slopes	
1 pole	1st order	6 dB/octave	20 dB/decade
2 poles	2nd order	12 dB/octave	40 dB/decade
4 poles	4th order	24 dB/octave	80 dB/decade
8 poles	8th order	48 dB/octave	160 dB/decade

Typically, the higher the order of the filter, the less the attenuation in the pass band. That is, the slope of the filter in the pass band is flatter for higher order filters (Figure 6.3).

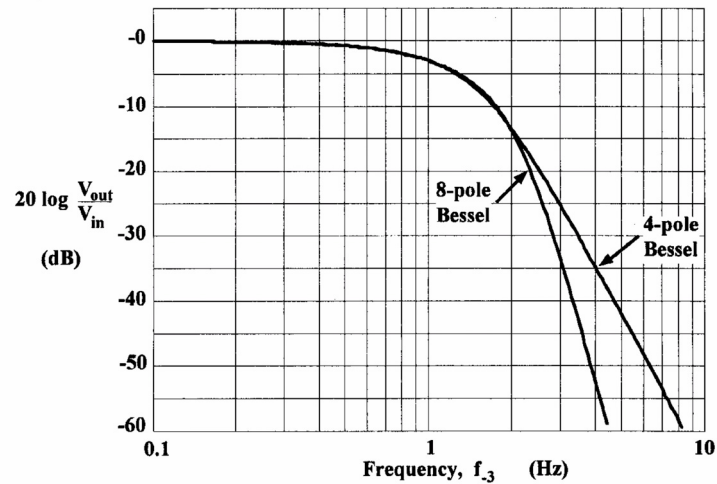


Figure 6.3: Difference between a 4th- and 8th-order transfer function.

6.3.11. 10-90% RISE TIME

The 10-90% rise time (t_{10-90}) is the time it takes for a signal to rise from 10% of its final value to 90% of its final value. For a signal passing through a low-pass filter, t_{10-90} increases as the -3 dB frequency of the filter is lowered. Generally, when a signal containing a step change passes through a high-order filter, the rise time of the emerging signal is given by:

$$t_{10-90} \approx 0.3/f_{-3} \quad (3)$$

For example, if f_{-3} is 1 kHz, t_{10-90} is approximately 300 μ s.

As a general rule, when a signal with $t_{10-90} = t_s$ is passed through a filter with $t_{10-90} = t_f$, the rise time of the filtered signal is approximately:

$$t_r = \sqrt{t_s^2 + t_f^2} \quad (4)$$

6.3.12. FILTERING FOR TIME-DOMAIN ANALYSIS

Time-domain analysis refers to the analysis of signals that are represented the same way they would appear on a conventional oscilloscope. That is, steps appear as steps and sine waves appear as sine waves. For this type of analysis, it is important that the filter contributes minimal distortion to the time course of the signal. It would not be very helpful to

have a filter that was very effective at eliminating high-frequency noise if it caused 15% overshoot in the pulses. Yet this is what many kinds of filters do.

In general, the best filters to use for time-domain analysis are Bessel filters because they add less than 1% overshoot to pulses. The Bessel filter is sometimes called a “linear-phase” or “constant delay” filter. All filters alter the phase of sinusoidal components of the signal. In a Bessel filter, the change of phase with respect to frequency is linear. Put differently, the amount of signal delay is constant in the pass band. This means that pulses are minimally distorted. Butterworth filters add considerable overshoot: 10.8% for a fourth-order filter; 16.3% for an eighth-order filter. The step response of the Bessel and Butterworth filters is compared in Figure 6.4.

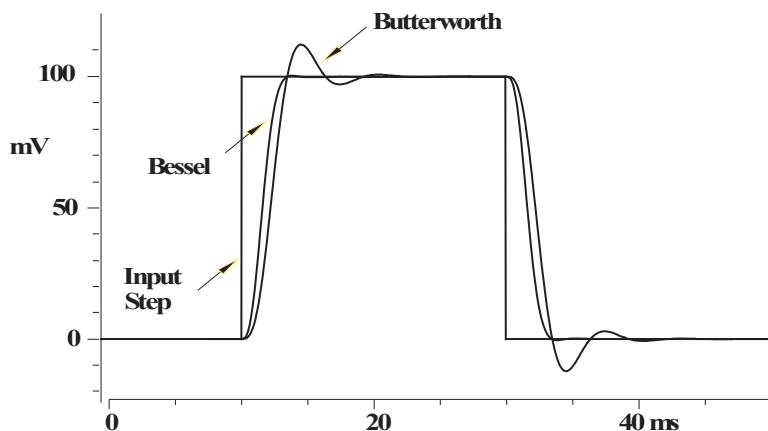


Figure 6.4: Step response comparison between Bessel and Butterworth filters.

The overshoots of fourth-order Bessel and Butterworth filters are compared.

In many experiments in biology and physiology (*e.g.*, voltage- and patch-clamp experiments), the signal noise increases rapidly with bandwidth. Therefore, a single-pole filter is inadequate. A four-pole Bessel filter is usually sufficient, but eight-pole filters are not uncommon. In experiments where the noise power spectral density is constant with bandwidth (*e.g.*, recording from a strain gauge), a single-pole filter is sometimes considered to be adequate.

In the time domain, a notch filter must be used with caution. If the recording bandwidth encompasses the notch filter frequency, signals that include a sinusoidal component at the notch frequency will be grossly distorted, as shown in Figure 6.5. On the other hand, if the notch filter is in series with a low-pass or high-pass filter that excludes the notch frequency, distortions will be prevented. For example, notch filters are often used in electromyogram (EMG) recording in which the line-frequency pickup is sometimes much larger than the signal. The 50 or 60 Hz notch filter is typically followed by a 300 Hz high-

pass filter. The notch filter is required because the high-pass filter does not adequately reject the 50 or 60 Hz hum (see Figure 6.5).

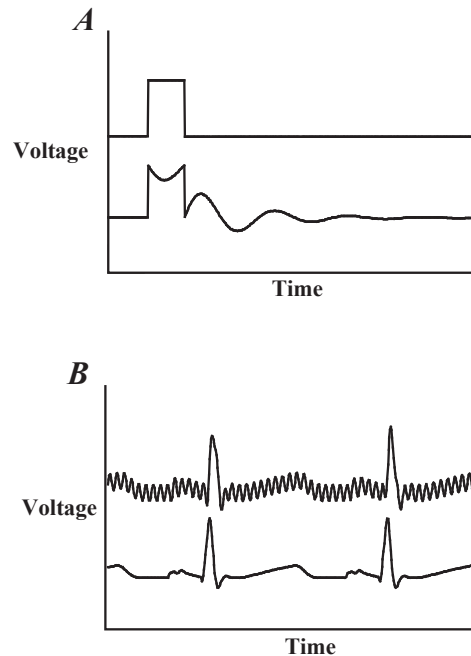


Figure 6.5: Use of a notch filter: inappropriately and appropriately.

A. Shows an inappropriate use of the notch filter. The notch filter is tuned for 50 Hz. The input to the notch filter is a 10 ms wide pulse. This pulse has a strong component at 50 Hz that is almost eliminated by the notch filter. Thus, the output is grossly distorted.

B. Shows an appropriate use of the notch filter. An EKG signal is corrupted by a large 60 Hz component that is completely eliminated by the notch filter.

6.3.13. FILTERING FOR FREQUENCY-DOMAIN ANALYSIS

Frequency-domain analysis refers to the analysis of signals that are viewed to make a power spectrum after they are transformed into the frequency domain. This is typically achieved using a fast Fourier transform (FFT). After transformation, sine waves appear as thin peaks in the spectrum and square waves consist of their component sine waves. For this type of analysis it does not matter if the filter distorts the time-domain signal. The most important requirement is to have a sharp filter cutoff so that noise above the -3 dB frequency does not get folded back into the frequency of interest by the aliasing phenomenon (see Chapter 11).

The simplest and most commonly used filter for frequency-domain analysis in biological applications is the Butterworth filter. This filter type has “maximally flat amplitude” characteristics in the pass band. All low-pass filters progressively attenuate sinusoidal compo-

nents of the signal as the -3 dB frequency is approached from DC. In a Butterworth filter, the attenuation in the pass band is as flat as possible without having pass-band ripple. This means that the frequency spectrum is minimally distorted.

Usually, notch filters can be safely used in conjunction with frequency-domain analysis since they simply remove a narrow section of the power spectrum. Nevertheless, they are not universally used this way because many experimenters prefer to record the data “as is” and then remove the offending frequency component from the power spectrum digitally.

6.3.14. SAMPLING RATE

If one intends to keep the data in the time domain, sufficient samples must be taken so that transients and pulses are adequately sampled. The Nyquist Sampling Theorem states that a bare minimum sampling rate is twice the signal bandwidth; that is, the -3 dB frequency of the low-pass filter must be set at one half the sampling rate or lower. Therefore, if the filter -3 dB frequency is 1 kHz, the sampling theorem requires a minimum sampling rate of 2 kHz. In practice, a significantly higher sampling rate is often used because it is not practical to implement the reconstruction filters that would be required to reconstruct time-domain data acquired at the minimum sampling rate. A sampling rate of five or more times the -3 dB frequency of the filter is common.

If you wish to make peak-to-peak measurements of your data for high-frequency signals, you must consider the sampling rate closely. The largest errors occur when samples are equally spaced around the true peak in the record. This gives the worst estimate of the peak value. To illustrate the magnitude of this problem, assume that the signal is a sine wave and that the following number of samples are taken per cycle of the sine wave. The maximum errors that one could get are then as follows:

5 samples/cycle	19.0% error
10 samples/cycle	4.9% error
20 samples/cycle	1.2% error

The sampling of the peak values varies between no error and the maximum as stated above.

If one intends to transform the data into the frequency domain, Butterworth or Elliptic filters are more suitable than the Bessel filter. These filters have a sharper cutoff near the -3 dB frequency than the Bessel filter, and thus better prevent the phenomenon known as aliasing. With a fourth-order or higher Butterworth filter, it is usual to set f_{-3} to about 40% of the sampling rate. Frequently, researchers do not have a Butterworth filter handy. If a Bessel filter is available, it can be used instead, but f_{-3} would normally be set to about 25–30% of the sampling rate. This is because the Bessel filter attenuation is not as sharp near the -3 dB frequency as that of a Butterworth filter.

6.3.15. FILTERING PATCH-CLAMP DATA

The analog filters that are typically used with a patch clamp are the Bessel and Butterworth types, in either 4-pole or 8-pole versions. If simply regarded from the noise point of view, the Butterworth filter is the best. Empirical measurements carried out MDS Analytical Technologies reveal that the rms noise passed by the filters (relative to a 4-pole Bessel filter) when used with an Axopatch™ 200 amplifier in single-channel patch mode is as follows:

Noise	4-Pole Bessel	8-Pole Bessel	4-Pole Butterworth	8-Pole Butterworth
1 kHz	1.0	0.97	0.95	0.93
5 kHz	1.0	0.97	0.85	0.82
10 kHz	1.0	0.94	0.83	0.80

The table shows that the main reduction in noise is gained by using a Butterworth filter instead of a Bessel filter. The improvement achieved by going from a 4-pole filter to an 8-pole filter of the same kind is small.

However, for the reasons previously discussed above, the Butterworth filter cannot be used for time-domain analysis. Since this is the most common kind of analysis performed on patch-clamp data, Bessel filters are almost invariably used.

6.3.16. DIGITAL FILTERS

Some researchers prefer to record data at wide bandwidths to prevent the loss of potentially important information. An analog filter is used to provide anti-alias filtering, followed by a digital filter implemented at various lower -3 dB frequencies during the analysis. There are many types of digital filters. Two types are described here:

Nonrecursive Filter

The output of a nonrecursive filter depends only on the input data. There is no dependence on the history of previous outputs. An example is the smoothing-by-3's filter:

$$y_n = \frac{x_{n-1} + x_n + x_{n+1}}{3} \quad (5)$$

where y_n and x_n are the output and input samples at sample interval n .

Nonrecursive filters are also known as “finite impulse response” filters (FIR) because their response to a single impulse endures only as long as the newest sample included in the formula (*i.e.*, x_{n+1} in the smoothing-by-3's filter).

Another example of a nonrecursive digital filter is the Gaussian filter. It has a similar form to the smoothing-by-3's filter described above, except that typically there are more terms and the magnitudes of the coefficients lie on the bell-shaped Gaussian curve.

These types of filters have the advantage of not altering the phase of the signal. That is, the mid-point for the rise time of a step occurs at the same time both before and after filtering. In contrast, analog filters always introduce a delay into the filtered signal.

A problem with digital filters is that values near the beginning and end of the data cannot be properly computed. For example, in the formula above, if the sample is the first point in the data, x_{n-1} does not exist. This may not be a problem for a long sequence of data points; however, the end effects can be serious for a short sequence. There is no good solution other than to use short filters (*i.e.*, few terms). Adding values outside the sequence of data is arbitrary and can lead to misleading results.

Recursive Filter

The output of a recursive filter depends not only on the inputs, but on the previous outputs as well. That is, the filter has some time-dependent “memory.” Recursive filters are also known as “infinite impulse response” filters (IIR) because their response to a single impulse extends indefinitely into the future (subject to computer processing limitations).

Digital-filter implementations of analog filters such as the Bessel, Butterworth and RC filters are recursive.

Correcting for Filter Delay

The delay introduced by analog filters necessarily makes recorded events appear to occur later than they actually occurred. If it is not accounted for, this added delay can introduce an error in subsequent data analysis. The effect of the delay can be illustrated by considering two common questions: How long after a stimulus did an event occur (latency measurement)? And, what was the initial value of an exponentially decaying process (extrapolation back to the zero time of a fitted curve)? If the computer program was instructed to record 50 points of baseline and then apply a stimulus, it would be natural, but incorrect, to assume in the subsequent analysis that zero time begins somewhere between points 50 and 51 of the recorded data, since zero time may actually be at point 52 or later.

The delay can be seen in Figure 6.4. The times to the 50% rise or fall point of a step signal (delay) are approximately $0.33/f_3$ for a fourth-order low-pass Bessel filter, and $0.51/f_3$ for an eighth-order Bessel filter. In practice, when using a fourth-order Bessel filter with $f_3 = 1$ kHz and sampling the trace at 6 kHz, the filter delay is 330 μ s. So, the whole record will have to be shifted by 2.0 points with respect to the stimulus events that were programmed.

6.4. PREPARING SIGNALS FOR A/D CONVERSION

Analog-to-Digital (A/D) converters have a fixed resolution and measure signals in a grainy manner. This means that all signals lying between certain levels are converted as if they are the same value. To minimize the impact of this undesirable “quantization” effect, it is important to amplify the signal prior to presenting it to the A/D converter. Ideally, the gain should be chosen so that the biggest signals of interest occupy the full range of the A/D converter but do not exceed it. In most laboratory systems, the full range of the A/D converter is ± 10 V, but other ranges such as ± 5 V and ± 1.25 V are often used in industrial applications.

6.4.1. WHERE TO AMPLIFY

Amplification is possible at a number of different points along the signal pathway. Since the amplification, filtering and offset circuits can themselves introduce noise, the location of the amplification circuitry must be carefully considered. There are several options:

Inside the Recording Instrument

The ideal place to amplify the signal is inside the instrument that records the signal. For example, the Axopatch 200B, MultiClamp 700B, and Axoclamp™ 900A amplifiers from MDS Analytical Technologies contain a variable gain control in the output section that can be used to provide low-noise amplification of the pipette current or membrane potential. The advantage of placing the amplification inside the recording instrument is that the amount of circuitry between the low-level signal and the amplifying circuitry can be minimized, thereby reducing extraneous noise contributions.

Between the Recording Instrument and the A/D Converter

A good place to amplify the signal is after it emerges from the recording instrument, before it is sent to the A/D converter. The CyberAmp® 380 amplifier from MDS Analytical Technologies can be used for this purpose. For the best noise performance, a small amount of initial amplification should be provided in the recording instrument if the signal levels are low. The main advantage of using a multi-channel amplifier such as the CyberAmp is that the gain of each recording pathway can be independently set by the computer. An instrument such as the CyberAmp amplifier has more gain choices than are usually available in a recording instrument.

In either of the examples discussed so far, anti-aliasing filtering is conveniently provided on a per-channel basis after the gain amplification.

After the Channel Multiplexor on the A/D Converter Board

A common place to provide amplification is in a programmable gain amplifier (PGA) located after the channel multiplexor on the A/D converter board. Briefly, in the A/D converter board, many channels are typically digitized by a single A/D converter. The signals are sequentially presented to the A/D converter by a multiplexor circuit. A PGA located after the multiplexor is very economical, since only one PGA is required regardless of the number of channels.

The main advantage of locating a PGA after the multiplexor on the A/D board is that it is inexpensive. However, there are significant disadvantages:

- 1** The PGA has to have extremely wide bandwidth since it must be able to settle within the resolution of the A/D converter at the multiplexing rate. Depending on the number of channels being sampled, this could mean that the bandwidth of the PGA has to be ten to several hundred times greater than the bandwidth of the analog signals. Such fast amplifiers are difficult to design, but in many cases the required speed can be achieved. The less obvious problem is that every amplifier introduces intrinsic noise, and the amount of noise observed on the amplifier output increases with bandwidth. Since the PGA may have several hundred times more bandwidth than the analog signal, it is likely to contribute more noise to the recording than is inherent in the signal. This problem cannot be eliminated or even reduced by filtering because filtering would lengthen the settling time of the PGA. This serious problem limits the usefulness of a shared PGA. This problem does not exist in the previously discussed systems in which there is an amplifier for each channel.
- 2** If the PGA is located on the A/D board, the low-level signals must be brought by cables to the A/D board. Typically, these cables are a couple of meters or more in length and provide ample opportunity for pick up of hum, radio-frequency interference and cross-talk between signals. With careful attention to shielding and grounding, these undesirable effects can be minimized. In the alternative approaches, in which the signals are amplified before they are sent to the A/D converter, the relative impact of these undesirable interferences are reduced in proportion to the amount of early amplification.

Systems that include a PGA on the A/D board are useful when the signals require only a small amount of amplification (ten fold or less) or when the user cannot afford or has not invested in external amplifiers.

6.4.2. PRE-FILTER VS. POST-FILTER GAIN

When low-level signals are recorded, it is essential that the first-stage amplification be sufficient to make the noise contributed by succeeding stages irrelevant. For example, in a microphone amplifier the tiny output from the microphone is first coupled into an extremely low-noise pre-amplifier. After this first-stage amplification, circuits with more modest noise characteristics are used for further amplification and to introduce treble and bass filtering.

If the only rule was to maximize the early gain, all of the gain would be implemented before any low-pass filter, notch filter or offset stages. However, with some signals, too much gain in front of the low-pass filter can introduce a different problem. This occurs when the signal is much smaller than the out-of-band noise.

This problem is illustrated by the signal in Figure 6.6. Panel A shows an input signal consisting of a pair of 1 pA current pulses significantly corrupted by instrumentation noise. When the noisy signal is first amplified by x100 and then low-pass filtered, the amplified

noisy signal saturates the electronics and the noise is clipped. (Note that for clarity, these traces are not drawn to scale.) After low-pass filtering, the signal looks clean, but its amplitude is less than $\times 100$ the original signal because the low-pass filter extracts a signal that is the average of the non-symmetrical, clipped noise. When the noisy signal is first amplified by $\times 10$, then low-pass filtered before a further amplification by $\times 10$, saturation is avoided and the amplitude of the filtered signal is $\times 100$ the original input. Panel B shows the two outputs superimposed to illustrate the loss of magnitude in the signal that was amplified too much before it was low-pass filtered.

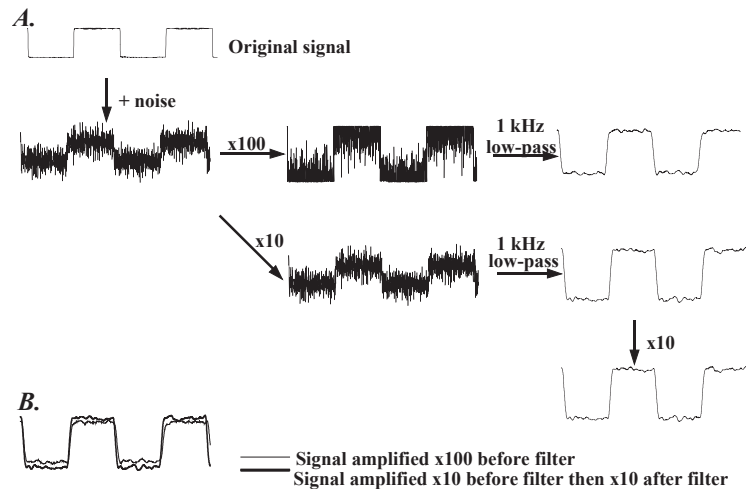


Figure 6.6: Distortion of signal caused by high amplification prior to filtering.

6.4.3. OFFSET CONTROL

In some cases, it is necessary to add an offset to the signal before it is amplified. This is necessary if the gain required to amplify the signal of interest would amplify the DC offset of the signal to the point that it would cause the gain amplifier to saturate.

An example is provided by an electronic thermometer. A typical sensitivity of an electronic thermometer is $10 \text{ mV}/^\circ\text{C}$, with zero volts corresponding to 0°C . A 12-bit A/D converter can measure with an approximate resolution of 5 mV , corresponding to 0.5°C in this example. If the data are to be analyzed at 0.01°C resolution, amplification by a factor of at least $\times 50$, and probably $\times 100$, would be necessary. If the temperatures of interest are between 30°C and 40°C and are amplified by $\times 100$, these temperatures will correspond to voltages between 30 V and 40 V values well beyond the range of the A/D converter. The solution is to introduce an offset of -350 mV before any amplification, so that zero volts will correspond to 35°C . Now when the signal is amplified by $\times 100$, the $30\text{--}40^\circ\text{C}$ temperature range will correspond to voltages between -5 V and $+5 \text{ V}$.

6.4.4. AC COUPLING AND AUTOZEROING

AC coupling is used to continuously remove DC offsets from the input signal. Signals below the -3 dB frequency of the AC coupling circuit are rejected. Signals above this frequency are passed. For this reason, AC-coupling circuits are more formally known as high-pass filters. In most instruments with AC coupling, the AC-coupling circuit is a first-order filter. That is, the attenuation below the -3 dB frequency increases at 20 dB/decade.

When a signal is AC-coupled, the DC component of the signal is eliminated and the low-frequency content is filtered out. This causes significant distortion of the signal, as shown in Figure 6.7.

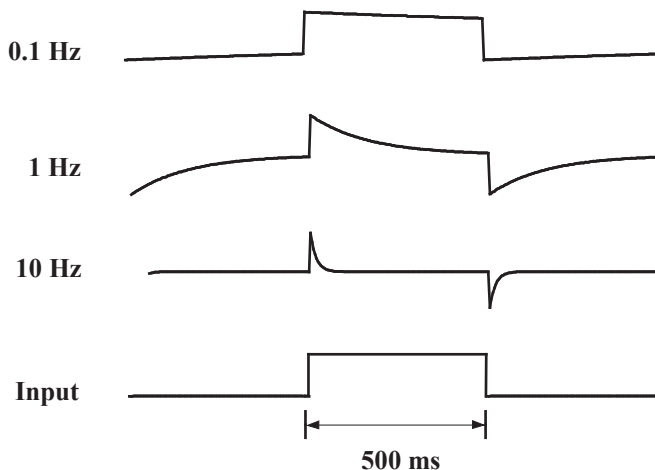


Figure 6.7: Distortion of signal caused by AC-coupling at high frequencies.

A 1 Hz square wave is AC-coupled at three different frequencies. The distortion is progressively reduced as the AC-coupling frequency is reduced from 10 Hz to 0.1 Hz. In all cases, the DC content of the signal is removed. The problem when using the lowest AC-coupling frequencies is that slow shifts in the baseline may not be rejected and transient shifts in the baseline might take a long time to recover.

Since there is less distortion when the AC-coupling frequency is lower, it is tempting to suggest that the AC coupling should always be set to very low frequencies, such as 0.1 Hz. However, this is often unacceptable because some shifts in the baseline are relatively rapid and need to be eliminated quickly.

A significant difference between using an AC-coupling circuit and setting a fixed DC offset is the way the two circuits handle ongoing drift in the signal. With fixed DC offset removal, the ongoing drift in the signal is recorded. With AC coupling, the drift is removed continuously. Whether this is an advantage or a disadvantage depends on whether the drift has meaning.

For very slow signals, even the lowest AC-coupling frequency causes significant distortion of the signal. For these signals, an alternative technique known as autozeroing can be used. This technique is available in some signal conditioners, such as the CyberAmp 380 amplifier, as well as in some amplifiers, such as the Axopatch-1 amplifier. In this technique, the signal is DC-coupled and a sample of the signal is taken during a baseline period. This DC sample value is stored and continuously subtracted by the instrument from the signal until the next sample is taken. In early instruments, the sample was taken using an analog sample-and-hold circuit. These circuits exhibit the problem known as “droop.” That is, the sampled value drifts with time. Later systems, such as the ones used in the CyberAmp 380 amplifier, use droop-free, digital sample-and-hold circuits.

The efficacy of the technique is illustrated in Figure 6.8.

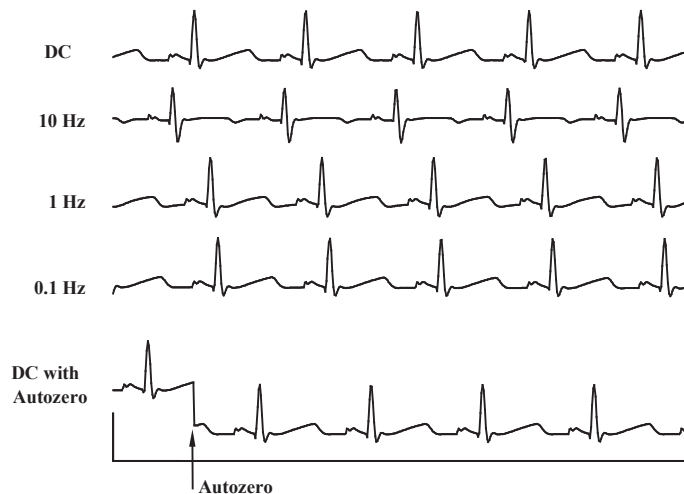


Figure 6.8: Comparison of autozeroing to AC-coupling.

The top trace shows an EKG signal that is sitting on a 5 mV offset resulting from electrode junction potentials. At AC-coupling frequencies of 10 Hz and 1 Hz, the signal is distorted. In the bottom trace, an Autozero command is issued to the signal conditioner (the CyberAmp 380 amplifier) at the time indicated by the arrow. The DC component is immediately removed, but the transients are unaffected.

Autozeroing should be restricted to cases where the time of occurrence of signals is known, so that the Autozero command can be issued during the baseline recording period preceding the signal.

6.4.5. TIME CONSTANT

The AC-coupling frequency is related to the time constant of decay, τ (see Figure 6.7):

$$\tau = \frac{1}{2\pi f_{-3}} \quad (6)$$

The time constants for some common AC-coupling frequencies are:

f_{-3} (Hz)	τ (ms)
100.0	1.6
30.0	5.3
10.0	16.0
3.0	53.0
1.0	160.0
0.1	1,600.0

In one time constant, the signal decays to approximately 37% of its initial value. It takes approximately 2.3 time constants for the signal to decay to 10% of the initial value.

6.4.6. SATURATION

The AC-coupling circuit is the first circuit in most signal conditioning pathways. If a large step is applied to the AC-coupled inputs, the AC coupling rejects the step voltage with a time constant determined by the AC-coupling frequency. If the amplifiers are set for high gain, the output might be saturated for a considerable time. For example, if the gain is $\times 100$, the AC coupling is 1 Hz and the step amplitude is 1 V, the output will be saturated until the voltage at the output of the AC-coupling circuit falls to 100 mV from its initial peak of 1 V. This will take about 2.3 time constants. Since the time constant is 160 ms, the output will be saturated for at least 370 ms. For the next several time constants, the output will settle towards zero.

6.4.7. OVERLOAD DETECTION

An amplified signal may exceed the ± 10 V acceptable operating range inside the instrument in two places: at the input of the various filters and at the output of the final amplifier stage. An example of an overload condition at the input of an internal low-pass filter is shown in Figure 6.6.

It is common practice to place overload-detection circuitry inside the instrument at these points. The overload-detection circuitry is activated whenever the signal exceeds an upper or lower threshold such as ± 11 V. The limit of ± 11 V exceeds the usual ± 10 V recommended operating range in order to provide some headroom. There is no difficulty in

providing this headroom since the internal amplifiers in most instruments operate linearly for signal levels up to about ± 12 V.

Normally, the overload circuitry simply indicates the overload condition by flashing a light on the front panel. In more sophisticated instruments such as the CyberAmp amplifier, the host computer can interrogate the CyberAmp amplifier to determine if an overload has occurred.

6.5. AVERAGING

Averaging is a way to increase the signal-to-noise ratio in those cases where the frequency spectrum of the noise and the signal overlap. In these cases, conventional filtering does not help because if the -3 dB frequency of the filter is set to reject the noise, it also rejects the signal.

Averaging is applicable only to repetitive signals, when many sweeps of data are collected along with precise timing information to keep track of the exact moment that the signal commences or crosses a threshold. All of these sweeps are summed, then divided by the total number of sweeps (N) to form the average. Before the final division, the amplitude of the signal in the accumulated total will have increased by N . Because the noise in each sweep is uncorrelated with the noise in any of the other sweeps, the amplitude of the noise in the accumulated signal will only have increased by \sqrt{N} . After the division, the signal will have a magnitude of unity, whereas the noise will have a magnitude of $1/\sqrt{N}$. Thus, the signal-to-noise ratio increases by \sqrt{N} .

6.6. LINE-FREQUENCY PICK-UP (HUM)

An important consideration when measuring small biological signals is to minimize the amount of line-frequency pickup, often referred to as hum. Procedures to achieve this goal by minimizing the hum at its source are discussed in Chapter 2.

Hum can be further minimized by using a notch filter, as discussed above, or by differential amplification. To implement the latter technique, the input amplifier of the data acquisition system is configured as a differential amplifier. The signal from the measurement instrument is connected to the positive input of the differential amplifier, while the ground from the measurement instrument is connected to the negative input. If, as is often the case, the hum signal has corrupted the ground and the signal equally, the hum signal will be eliminated by the differential measurement.

6.7. PEAK-TO-PEAK AND RMS NOISE MEASUREMENTS

Noise is a crucially important parameter in instruments designed for measuring low-level signals.

Invariably, engineers quote noise specifications as root-mean-square (rms) values, whereas users measure noise as peak-to-peak (p-p) values. Users' preference for peak-to-peak values

arises from the fact that this corresponds directly to what they see on the oscilloscope screen or data acquisition monitor.

Engineers prefer to quote rms values because these can be measured consistently. The rms is a parameter that can be evaluated easily. In statistical terms, it is the standard deviation of the noise. True rms meters and measurement software are commonly available and the values measured are completely consistent.

On the other hand, peak-to-peak measurements are poorly defined and no instruments or measurement software are available for their determination. Depending on the interpreter, estimates of the peak-to-peak value of Gaussian noise range from four to eight times the rms value. This is because some observers focus on the “extremes” of the noise excursions (hence, the x8 factor), while others focus on the “reasonable” excursions (x6 factor) or the “bulk” of the noise (x4 factor).

MDS Analytical Technologies has developed the pCLAMP[®] software to measure the rms and the peak-to-peak noise simultaneously. The peak-to-peak noise is calculated as the threshold level that would encompass a certain percentage of all of the acquired data. For white noise, the corresponding values are:

Percentage of Data Encompassed	Peak-To-Peak Thresholds
95.0%	3.5–4 times rms value
99.0%	5–6 times rms value
99.9%	7–8 times rms value

These empirical measurements can be confirmed by analysis of the Gaussian probability distribution function.

In this Guide and various Axon Cellular Neuroscience product specifications, noise measurements are usually quoted in both rms and peak-to-peak values. Since there is no commonly accepted definition of peak-to-peak values, MDS Analytical Technologies usually uses a factor of about 6 to calculate the peak-to-peak values from the measured rms values.

In an article from Bell Telephone Laboratories (1970), the authors define the peak factor as “the ratio of the value exceeded by the noise a certain percentage of the time to the rms noise value. This percentage of time is commonly chosen to be 0.01 per cent.” This ratio, from tables listing the area under the Gaussian distribution, turns out to be 7.78 times the rms value. Thus, according to this article, the appropriate factor to calculate the peak-to-peak values from the measured rms values is closer to x8.

6.8. BLANKING

In certain experiments, relatively huge transients are superimposed on the signal and corrupt the recording. This problem commonly occurs during extracellular recording of nerve impulses evoked by a high-voltage stimulator. If the isolation of the stimulator is not perfect (it never is), there is some coupling of the stimulus into the micropipette input. This relatively large artifact can sometimes cause the coupling capacitors in subsequent AC amplifiers to saturate. There might be some time lost while these capacitors recover from saturation, and thus valuable data might be wasted.

If it is not possible to prevent the stimulus coupling, the next best thing to do is to suppress the artifact before it feeds into the AC-coupled amplifiers. This is made possible in the Axoclamp 900A amplifier by providing sample-and-hold amplifiers early in the signal pathway. The user provides a logic-level pulse that encompasses the period of the transient. This logic-level pulse forces the sample-and-hold amplifiers into the “hold” mode. In this mode, signals at the input of the sample-and-hold amplifier are ignored. Instead, the output of the sample-and-hold amplifier is kept equal to the signal that existed at the moment the logic-level pulse was applied.

6.9. AUDIO MONITOR—FRIEND OR FOE?

When monitoring data, experimenters need not be limited to their sense of sight. The data may also be monitored with great sensitivity using the sense of hearing. In such cases, the data are input to an audio monitor and fed to a loudspeaker or a set of headphones.

Two types of audio monitor are used. The first is a power amplifier that applies the signal directly to the speaker, thereby allowing signals in the audio bandwidth to be heard. This type of audio monitor is frequently used in EMG monitoring or in central nervous system recording. Each spike is heard as an audible click, and the rate and volume of clicking is a good indicator of the muscle or nerve activity. This type of audio monitor is either called an AM (amplitude modulated) audio monitor, or it is said to be operating in “click” mode.

The second type of audio monitor is a tone generator whose frequency depends on the amplitude of the input signal. Usually, the oscillator frequency increases with increasingly positive signals. This type of audio monitor is often used for intracellular recording. It provides an extremely sensitive measure of the DC level in the cell. This type of audio monitor is either called an FM (frequency modulated) audio monitor, or it is said to be operating in “tone” mode.

Most researchers have a very strong opinion about audio monitors; they either love them or hate them. Those who love audio monitors appreciate the supplementary “view” of the data. Those who hate audio monitors have probably suffered the annoyance of having to listen for interminable lengths of time to the audio output from another rig in the same room. A constant tone can be irritating to listen to, especially if it is high pitched, unless it has an important message for you, such as “my cell is maintaining its potential admirably.”

Audio monitors are standard features in Axon Cellular Neuroscience computer controlled amplifiers. To minimize the potential for aggravation, we include a headphone jack so that users can listen to the audio output without testing the patience of their colleagues.

6.10. ELECTRODE TEST

It is useful to be able to measure the electrode resistance for two reasons. The first reason is to establish the basic continuity of the electrode circuit. Sometimes, electrode leads can break, leaving an open-circuit input and, consequently, no incoming data. The second reason is to verify that the electrode is acceptably attached. For example, it may be that to achieve the low-noise recording levels needed in an EMG recording, the electrode resistance must be less than 5 k Ω .

Some transducer amplifiers allow the electrode impedance to be easily measured. For example, the CyberAmp amplifiers have an Electrode Test facility. When this is activated, an approximate 1 $\mu\text{A}_{\text{p-p}}$, 10 Hz square wave is connected to every input via individual 1 M Ω resistors. The electrode resistance can be directly determined from the amplitude of the voltage response.

6.11. COMMON-MODE REJECTION RATIO

In general, the information that the researcher wants to record is the difference between two signals connected to the positive and the negative amplifier inputs. Often, these signals contain an additional component that is common to both, but that does not contain relevant information. For example, both outputs of a strain gauge might include a DC potential of 2.5 V that arises from the excitation voltage. However, the strain on the gauge generates a microvolt-size difference between the two outputs, but does not affect the 2.5 V “common-mode” voltage. Another example is often seen when recording EMG signals from an animal. Both the positive and the negative electrodes pick up line-frequency hum that has coupled into the animal. The hum picked up by the electrodes may be as large as 10 mV, but it is identical on both electrodes. The EMG signal of interest is the small difference between the potentials on the two electrodes; it may be as small as a few tens of microvolts.

To prevent the common-mode signal from swamping the much smaller differential signal, the positive and negative gains of the amplifier must be nearly identical. In the above EMG example, if the amplifier inputs are exactly unity, the 10 mV of hum that appears equally on both electrodes does not show up at all on the amplifier output. The only signal to appear on the output is the small signal proportional to the EMG potential generated between the two electrodes.

In practice, the positive and negative inputs of the amplifier are never exactly equal. The quality of their matching is measured by the common-mode rejection ratio (CMRR). This is normally quoted in dB, where 20 dB corresponds to a factor of ten. Returning to the EMG example, if the amplifier operates at unity gain with a CMRR of 60 dB (*i.e.*, one part in a thousand), the 10 mV of common-mode hum results in 10 μV of hum

appearing on the amplifier output. This is small, but still significant compared with the smallest EMG signals, so an amplifier with higher CMRR, *e.g.*, 80 dB, may be desirable.

The CMRR of an amplifier varies with frequency. It is best at very low frequencies, while above a certain frequency it diminishes steadily as the frequency of the common-mode signal increases. It is therefore important to verify the CMRR of the amplifier at a frequency that exceeds the expected frequency of the common-mode signal.

The CMRR of the recording system is adversely affected by imbalances in the source resistances of the recording electrodes. This is because the source resistance of each electrode forms a voltage divider with the input resistance of the amplifier. If the source resistances of the two electrodes are not identical, the voltage dividers at the positive and negative inputs of the amplifier are not equal. Returning to the EMG example, if the resistance of one electrode is 9 k Ω , the resistance of the other is 10 k Ω , and the amplifier input resistances total 1 M Ω , then the gain for one electrode is 0.9901 instead of unity, while the gain for the other electrode is 0.9911. The difference is 0.001. Thus, even though the amplifier may have a CMRR of 80 dB or more, the system CMRR is only 60 dB. In some cases, 60 dB is acceptable, but in others it is not. The solution to this problem is to use an amplifier that has very high input resistances of 100 M Ω or more.

If there is a large common-mode signal and a source imbalance of more than a few kilohms, a high input resistance amplifier probe should be used. Several AI 400 series probes are available from MDS Analytical Technologies that have input resistances of 10 gigohms (10¹⁰ Ω) or more. These probes are distinguished on the basis of noise, cost and size.

6.12. REFERENCES

Bell Telephone Laboratories. *Transmission Systems for Communications*. By the members of the technical staff at Bell Telephone Laboratories. Western Electric Company, Inc., Technical Publications. Winston-Salem, North Carolina, 1970.

6.13. FURTHER READING

Hamming, R. W., *Digital Filters*. Prentice-Hall, Inc., Englewood Cliffs, New Jersey, 1977.

Tietze, U., Schenk, Ch., *Advanced Electronic Circuits*. Springer-Verlag, Berlin, 1978.

7. Transducers

Transducers are devices that convert a signal of one form to another. In physiological applications this usually means converting variations of a physical signal, such as temperature or pressure, into variations in voltage that can then be recorded or manipulated as necessary.

There are many different types of transducers available for physiological recording and they range in their requirements for excitation voltages, amplification and recording techniques as well as mechanical connections. In the past this has required a different amplifier for each transducer type. The introduction of the CyberAmp[®] 380 amplifier (MDS Analytical Technologies), a computer-controlled signal-conditioning amplifier, heralded a new approach to interfacing transducers. A small 15-pin socket on each channel of the CyberAmp 380 amplifier provides the excitation voltage, the differential inputs, the offset correction and the filtering required by a wide variety of transducers. This eliminates the need for a dedicated amplifier to suit the transducer type. The AI 400 series probes and adapters can plug into any socket on the CyberAmp 380 amplifier. Within the 15-pin probe connector is a small memory device called an EEPROM (electrically erasable programmable read only memory) that stores such information as the transducer type, its scale factor and the offset. When the transducer is plugged into the CyberAmp 380 amplifier, this information may be automatically loaded by the acquisition software, thereby making the transducer ready for immediate use.

7.1. TEMPERATURE TRANSDUCERS FOR PHYSIOLOGICAL TEMPERATURE MEASUREMENT

Three types of transducers are suitable for physiological temperature measurement: thermistors, integrated circuit (IC) temperature transducers that produce an output current proportional to absolute temperature, and IC temperature transducers that produce an output voltage proportional to absolute temperature.

7.1.1. THERMISTORS

Thermistors are resistors whose resistance drops significantly as temperature increases. They are composed of a compressed and sintered mixture of metallic oxides of manganese, nickel, cobalt, copper, magnesium, titanium and other metals. Thermistors exhibit temperature coefficients many times greater than those of pure metals. For most of them, the resistance falls by 4–6% per °C with increasing temperature.

The response is exponential with temperature, but can be considered to be linear over a range of a few tens of degrees Celsius. By combining multiple thermistors and some resistors, the useful linear range can be extended to span more than 100 °C. The Omega Engineering, Inc. (Stamford, CT) thermistor composites 44018 and 44019 each contain a matched pair of thermistors. When connected by precision resistors to an accurate DC excitation voltage, these probes are interchangeable within ± 0.15 °C over the recommended range of -30 to +100 °C. These probes come in a wide range of shapes and sizes for different applications such as esophageal, rectal and surface body temperature measurements, or for immersion in hostile chemical environments.

Omega Engineering Inc. produces many other thermistor types as do other manufacturers. These other types can also be interfaced to the CyberAmp 380 amplifier via the AI 490 Connector and AI 491 Cable Kits. Several different interface circuits are suggested in the CyberAmp 380 manual.

7.1.2. IC TEMPERATURE TRANSDUCERS THAT PRODUCE AN OUTPUT CURRENT PROPORTIONAL TO ABSOLUTE TEMPERATURE

The most notable of these temperature-dependent current sources are the Analog Devices, Inc. (Norwood, MA) AD590 with a temperature range of -55 to +150 °C and the lower-cost AD592 with a temperature range of -25 to +105 °C. These are not available in the wide range of probe configurations provided by thermistor manufacturers. Most often they are supplied in 0.23" (5.8 mm) diameter metal cans or in 0.25" x 0.093" (6.4 mm x 2.4 mm) ceramic flat packs. These need to be connected to wires and must be insulated for special purposes. The only temperature probe available from Analog Devices is the AC2626, which includes an AD590 enclosed in a 4" (102 mm) or 6" (153 mm) long stainless steel sheath with a 3/16" (4.8 mm) outside diameter.

When connected to a DC voltage source (*e.g.*, the +5 V excitation voltage in the CyberAmp 380 amplifier) these transducers force the current that flows in the circuit to be equal to $1 \mu\text{A}/^\circ\text{K}$. The external circuitry required to use the AD590 is very simple and it is easy to configure for minimum and average temperature measurements by placing transducers in series or in parallel, respectively. The absolute accuracy and interchangeability of these probes is inferior to the Omega Engineering probes described above. In their best and most expensive grade, the interchangeability is ± 0.5 °C at 25 °C. The main advantages of the AD590 temperature probes are that the external support circuitry is very simple and that they are suitable for remote sensing applications. Because the output is insensitive to voltage drops, the devices can be used with twisted-pair cabling hundreds of feet in length.

The Analog Devices semiconductor temperature probes can be interfaced to the CyberAmp 380 amplifier via the AI 490 Connector and AI 491 Cable Kits, with the user providing the interface design based on the range of application circuits provided by Analog Devices and in the manual for the CyberAmp 380 amplifier.

7.1.3. IC TEMPERATURE TRANSDUCERS THAT PRODUCE AN OUTPUT VOLTAGE PROPORTIONAL TO ABSOLUTE TEMPERATURE

Two of the most suitable temperature-dependent voltage sources are the LM35A and the LM135A sensors from National Semiconductor Corporation (Santa Clara, CA). These have absolute accuracies (interchangeability) of ± 0.5 °C and ± 1.0 °C, respectively, at 25 °C. The LM35A has a zero voltage output at 0 °C and a sensitivity of 10 mV/°C. The LM135A behaves as a zener diode with a zero voltage output at 0 °C and a sensitivity of 10 mV/°C. These devices are generally cheaper than the AD590 transducers. They are supplied in approximately 0.2" (5 mm) metal cans or plastic packages, but they are not available in ready-to-use probes.

The National Semiconductor temperature probes can be interfaced to the CyberAmp 380 amplifier via the AI 490 Connector and AI 491 Cable Kits with the user providing the interface design using the range of application circuits provided by National Semiconductor and in the manual for the CyberAmp 380 amplifier.

7.2. TEMPERATURE TRANSDUCERS FOR EXTENDED TEMPERATURE RANGES

Two types of transducers are commonly used for temperature measurements beyond the physiological range: thermocouples and resistance temperature detectors.

7.2.1. THERMOCOUPLES

Thermocouples are economical and rugged transducers, having the advantage of small size with a very fast response time and a wide temperature range. Thermocouples consist of two dissimilar metals in contact. The offset potential between the metals is proportional to temperature (see Table 7.1). The low sensitivity and broad operating range generally make thermocouples more suitable for industrial applications than for physiological ones. Because of their greater sensitivity, thermistors are more popular than thermocouples for most physiological applications. On the other hand, thermocouples can be fabricated in remarkably small sizes, creating the opportunity for some unusual biological applications. For example, micron-dimension thermocouples that can be inserted into single living cells have been described (Cain & Welch, 1974). Commercially available thermocouples can be obtained with diameters as low as 25 μm and thermal time constants as short as 2 ms (Omega Engineering, Inc., Stamford, CT).

Table 7.1: Common Thermocouple Materials.

ANSI Type	Min Value °C	Max Value °C	Sensitivity at 20 °C $\mu\text{V}/^\circ\text{C}$	Material
E	-200	900	60.48	chromel/constantan
J	-200	750	51.45	iron/constantan
K	-200	1250	40.28	chromel/alumel
R	0	1450	5.80	platinum/Pt-13% rhodium
S	0	1450	5.88	platinum/Pt-10% rhodium
T	-200	350	40.28	copper-constantan

Thermocouples require a reference temperature that traditionally was an ice bath but is more commonly provided by a compensation circuit. Complete signal-conditioning modules, such as the Analog Devices AD594 and 3B47 signal conditioners, exist. They contain the differential amplifiers and the temperature compensation circuitry. Alternatively, voltage-output temperature transducers, such as the LM35A, can be used to derive a compensation voltage to apply to the negative input of a CyberAmp 380 amplifier. To interface thermocouples to the CyberAmp 380 amplifier, the user must provide an interface circuit using a temperature transducer for compensation or using the Analog Devices or equivalent conditioning modules. Circuit examples are given in the CyberAmp manuals.

7.2.2. RESISTANCE TEMPERATURE DETECTORS

Resistance thermometers can be made of metals or ceramic-like mixtures. By convention, resistance thermometers made of metals are called Resistance Temperature Detectors (RTD), while the ceramic-like resistance thermometers are called thermistors.

The resistance of most metals increases with increasing temperature. The sensitivity is small, less than 0.4% per °C. The most commonly used metal is platinum because of its wide linear resistance-to-temperature relationship.

Platinum RTD's offer better stability and linearity than thermocouples, but are limited to temperatures below 850 °C. Most platinum RTD's have a resistance of 100 Ω at 0 °C and a positive temperature coefficient of 0.385% per °C at 0 °C.

The simplest way to configure a platinum RTD is to excite it with a small, accurate DC current. Currents of 1 mA or less are used so as to minimize self-heating. A differential amplifier is used to measure the voltage across the RTD. If the excitation current is 1 mA, the sensitivity is 385 μV per °C. To interface RTD's to the CyberAmp 380 amplifier, the user must provide an interface circuit. Circuit examples are given in the CyberAmp manuals.

7.3. ELECTRODE RESISTANCE AND CABLING AFFECT NOISE AND BANDWIDTH

The electrode impedance (resistance), the capacitance of the cable to the electrode, and the amplifier input impedance combine to produce resistive dividers and filters (Figure 7.1) that can substantially degrade the quality of a recorded signal. The easiest solution to these potential problems is to use high-impedance probes (*e.g.*, AI 401, AI 402) and place them as close as possible to the electrodes.

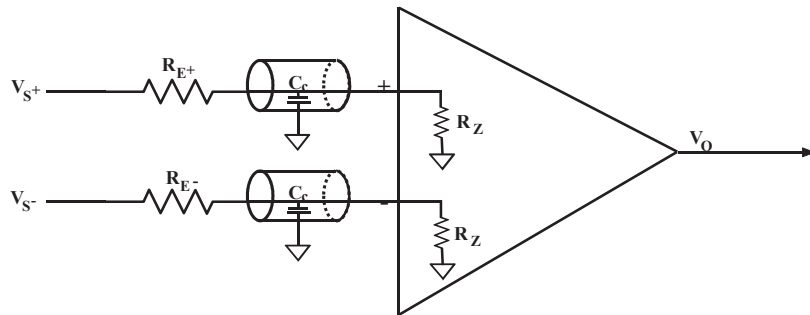


Figure 7.1: Electrode resistance and cabling can degrade a signal.

The electrode impedances (resistances) R_E combine with the amplifier input impedances R_Z to produce resistive dividers. R_Z also combines with the capacitance of the cable to the electrodes C_C to produce low-pass filters. V_S and V_O are the source and output voltages.

7.4. HIGH ELECTRODE IMPEDANCE CAN PRODUCE SIGNAL ATTENUATION

The electrode resistance in series with the amplifier input impedance acts as a voltage divider (Figure 7.2). The CyberAmp 380 amplifier has input impedances of $1\text{ M}\Omega$ and if the electrode resistance is $1\text{ k}\Omega$ this reduces the signal by only 0.1%, since:

$$V_I = \frac{1\text{M}\Omega}{1\text{k}\Omega + 1\text{M}\Omega} V_s \quad (1)$$

However, if the electrode resistance is $100\text{ k}\Omega$, the signal would be reduced by about 9.1%, since:

$$V_I = \frac{1\text{M}\Omega}{100\text{k}\Omega + 1\text{M}\Omega} V_s = 0.909V_s \quad (2)$$

The solution to high electrode resistance is to use a high-input impedance amplifier. If using a CyberAmp 380 amplifier, then you should use a high-impedance probe between it and the electrodes. The AI 401 x10 Low-Noise Differential amplifier probe and the AI 402 X50 Ultra Low-Noise Differential amplifier probe both have input impedances measured in the teraohms ($10^{12} \Omega$).

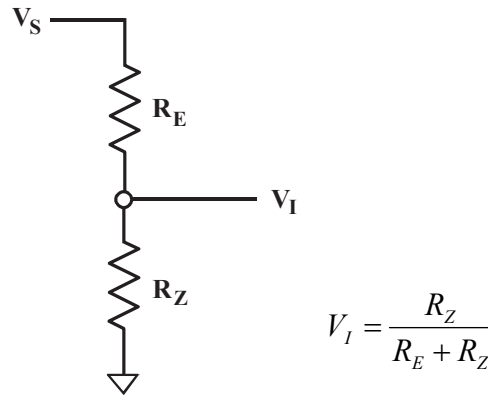


Figure 7.2: High electrode resistance can attenuate a signal and increase crosstalk.

The resistance of each electrode in series with the amplifier input impedance acts as a pair of voltage dividers. This can reduce the recorded amplitude of the signal. If the electrode impedances are not matched, it will reduce the CMRR leading to amplification of common background signals. R_E and R_Z are the electrode and amplifier impedances. V_S and V_I are the source voltage and input voltage to the amplifier.

7.5. UNMATCHED ELECTRODE IMPEDANCES INCREASE BACKGROUND NOISE AND CROSSTALK

When making differential measurements such as EMG, EKG and EEG it is important that both electrodes have similar properties. As we have seen above, high electrode impedance can produce signal attenuation. If we apply Figure 7.2 to both inputs of Figure 7.1, we see that we could easily get greater attenuation of the signal at one electrode than at the other. This can substantially degrade the common mode rejection ratio (CMRR) and result in amplification of common background signals that would otherwise be rejected.

For a differential amplifier, the CMRR is the ratio of the response for a signal at just one input to the response for a common mode signal (applied to both inputs) of the same amplitude. The CMRR of the CyberAmp 380 amplifier is 100 dB (at high gain). That is, the output voltage with a signal applied to just one input is 100,000 times greater than the output voltage with the same signal applied to both inputs. (The ratio of amplitudes is measured in decibels where $\text{dB} = 20 \log_{10}(V_{\text{out}}/V_{\text{in}})$. A ten-fold increase in the ratio equals a 20 dB increase (see Chapter 6).

If the electrode impedance of one electrode connected to a CyberAmp 380 amplifier is 1 k Ω and that of the other electrode 10 k Ω then the CMRR of the system as a whole is reduced 1,000 fold to 41 dB.

Applied to a single channel of the CyberAmp 380 amplifier:

$$V_I = \frac{1M\Omega}{1k\Omega + 1M\Omega} V_s = 0.999V_s$$

$$V_I = \frac{1M\Omega}{10k\Omega + 1M\Omega} V_s = 0.990V_s$$

The difference equals 0.009:

$$CMRR = 20 \log_{10} (0.999 / 0.990) = 41dB$$

As for the problem of the signal attenuation, the solution to a mismatch of electrode resistances is to use an amplifier probe with very high input resistance such as the AI 401 and the AI 402 probes. With each of these probes, the electrode impedances used in the example are too small to have any influence on the CMRR of the probes.

If high-input impedance probes are not available, the CyberAmp 380 amplifier has a built-in capacity to measure electrode impedances and this should be carried out prior to each recording session to ensure a match. This is a good idea anyway as it can reveal the development of faults such as breaks in the electrodes.

Crosstalk from other body signals can occur for additional reasons, although infrequently. For example, if invasive EMG leads are routed subcutaneously near the heart, the EKG can capacitively couple into the EMG leads. This problem is eliminated by recording differentially using lead pairs that are twisted together, or by not routing the EMG leads near the heart.

7.6. HIGH ELECTRODE IMPEDANCE CONTRIBUTES TO THE THERMAL NOISE OF THE SYSTEM

With an active amplifier the only noise sources encountered are the thermal noise of the electrode, the noise provided by the amplifier itself, and crosstalk from other body signals.

Thermal noise, also called Johnson noise, is a voltage produced across the terminals of all resistive elements (including electrodes) due to the random motion of charge carriers within the element. Thermal noise is proportional to the resistance (R) and absolute temperature (T) of the resistive element (see Chapter 11). To minimize the thermal noise con-

tribution, the electrode resistance must be minimized. This is usually accomplished by maximizing the surface area of the electrode and ensuring good electrical contact.

The noise contribution to the signal from the amplifiers is negligible if the amplifier noise is less than the thermal noise of the electrodes. All Axon Cellular Neuroscience amplifiers have very low noise levels. The lowest noise amplifier, the AI 402 x50 differential amplifier probe, has extremely low noise of just $1.1 \mu\text{V}_{\text{p-p}}$ in the DC-10 kHz bandwidth ($0.18 \mu\text{V rms}$). This is approximately equivalent to the thermal noise of a 250Ω resistor. This means that for electrodes whose resistance exceeds 250Ω , the thermal noise of the electrode exceeds the noise of the amplifier.

7.7. CABLE CAPACITANCE FILTERS OUT THE HIGH-FREQUENCY COMPONENT OF THE SIGNAL

The source resistance, together with the capacitance of the cable to the amplifier, act as a simple RC low-pass filter (Figure 7.1). Electrical cables can provide 30–100 pF capacitance per foot (100–300 pF per meter). If a cable has a 1,000 pF capacitance and the electrode resistance is $10 \text{ k}\Omega$, then the cut-off frequency is about 16 kHz. A $100 \text{ k}\Omega$ electrode resistance with the same cable would filter the signal at 1,600 Hz. The appropriate solution is to use an active probe as close to the signal source as possible.

7.8. EMG, EEG, EKG AND NEURAL RECORDING

7.8.1. EMG

Electromyograms (EMG) can be recorded in many ways, each with its own special requirements. Surface EMG electrodes have the advantage of being non-invasive but suffer from artifacts or even total loss of signal during movements. They are also not as selective as implanted electrodes.

Implanted electrodes must be capable of remaining in the same location and must be of an appropriate size and separation. Bipolar electrodes should be placed in parallel with the muscle fibers to record the maximum signal with an electrode spacing of 2–10 mm appropriate for most mammalian muscles. This close spacing of electrodes reduces crosstalk from other muscle sites and is therefore appropriate for selective recording from local areas. Low-frequency components of electrical signals propagate for larger distances in body tissues than do high-frequency components. The bipolar electrode configuration acts as a high-pass filter whose cut-off frequency is determined by electrode spacing. Close spacing results in a high cut-off frequency, thus filtering out some of the remaining low-frequency components from distant muscle activity. However, close electrode spacing also reduces the amplitude of the signal in a non-linear fashion. Larger electrodes reduce the impedance (see *“Noise Arising From Distributed Pipette Resistance and Capacitance”* on page 227) but are less selective regarding the site of muscle activity.

The frequency range of the EMG is 10–2,000 Hz, although the electrode configuration and separation will have considerable influence on what frequencies are recorded. The sig-

nal size ranges from 5 μV –20 mV for surface recording and from 50–1,000 μV for invasive recording.

Several probes are available for recording EMG with the CyberAmp 380 amplifier. These include the AI 401, 402, and 405 active amplifier probes, the AI 417 passive adapter and direct user connection.

7.8.2. EKG

There are probably more books available on electrocardiogram (EKG) recording and analysis than any other electrophysiological topic. The signals are usually of large amplitudes and readily recorded without the need for any amplifier probes. As electrode spacing is reduced, there is an increasing possibility of recording unwanted EMG signals from neighboring muscles. Consequently, the traditional electrode sites are worth considering. The AI 417 passive 2 mm adapter provides a single differential EKG channel and plugs directly into the CyberAmp 380 amplifier.

The normal frequency range of the mammalian EKG is 0.2–100 Hz; its amplitude size is up to 2–3 mV.

7.8.3. EEG

The electroencephalogram (EEG) ranges from 10–300 μV in amplitude and has a frequency range from 0.2–50 Hz. A single differential EEG channel is best recorded with the assistance of one of the low-noise AI 400 series active probes.

7.8.4. NERVE CUFFS

Nerve-cuff recordings have a frequency response to 10 kHz and an amplitude in the low microvolt range. The AI 402, x50 Ultra Low-Noise Differential amplifier probe is designed for this application, with 10 kHz noise of less than 0.18 μV_{rms} (1.1 $\mu\text{V}_{\text{p-p}}$) in the 0.1–10 kHz bandwidth.

The nerve cuffs themselves are very simple to make by running bare stainless steel fine wires through a small length of silicone tubing split longitudinally. Any bared wires that are in contact with the outer surface of the cuff can be insulated with silicone adhesive.

7.9. METAL MICROELECTRODES

The impedance of metal microelectrodes may be several hundred kilohms or more. All of the low-noise AI 400 series active probes are suitable for recording from high-resistance microelectrodes. Since the input capacitance of the AI 401 differential amplifier probe is approximately 5 pF, the largest electrode resistance consistent with maintaining a 10 kHz bandwidth is about 3 M Ω .

7.10. BRIDGE DESIGN FOR PRESSURE AND FORCE MEASUREMENTS

Pressure and force transducers are often constructed using strain gauges connected in a Wheatstone bridge circuit. The basic circuit is shown in Figure 7.3.

The Wheatstone bridge should be considered as two pairs of resistive dividers with the output voltage equaling the difference between the voltages at (A) and (B). The bridge circuit is good for detecting small changes in resistance, and the output is linear in the region of balance, *i.e.*, when the voltage difference is small.

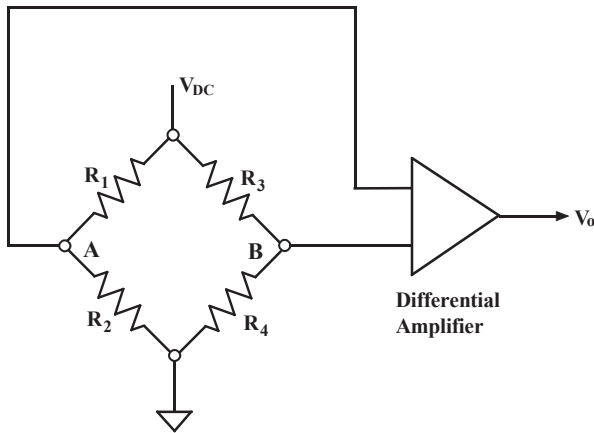


Figure 7.3: Wheatstone Bridge circuit with amplifier.

The largest output comes from having strain gauges for all four resistive elements, although physical constraints may require the user to have only two or even one “active” element. For applications where only two gauges can be used, they should be placed in positions R1 and R2 and the gauges should be located such that one increases in resistance and the other decreases in resistance during the applied pressure or force. This is usually achieved by placing the elements on opposite sides of the beam under strain. When choosing strain gauges, keep in mind that semiconductor types have outputs ten times higher than metal-film types.

The sensitivity of a bridge circuit decreases with increasing temperature and some applications may therefore require the addition of a temperature compensation circuit that should be placed as close as possible to the bridge in order to experience the same temperature changes.

7.11. PRESSURE MEASUREMENTS

In the past, high-quality pressure transducers were very expensive and suffered from significant temperature sensitivity. The introduction of semiconductor pressure transducers

has greatly reduced the cost, decreased the temperature sensitivity and enhanced the range of transducer devices available.

An important point when measuring very low pressures is to set the height of the pressure transducer to that of the sense location in order to avoid hydrostatic errors introduced by fluid-filled catheters. Pressure transducers should also be kept out of the range of heat sources such as heat lamps to avoid temperature-induced increases in the signal output.

Major producers of semiconductor pressure sensors include Honeywell, Inc. (Minneapolis, MN). Blood pressure transducers from Cobe Laboratories, Inc. (Lakewood, CO) have a usable range of -50 to + 300 mmHg. All pressure transducers can be interfaced to the Axon CyberAmp 380 amplifier via the AI 490 Connector and AI 491 Cable Kits.

7.12. FORCE MEASUREMENTS

The requirements for force measurements are so diverse that many people need to make their own force transducer, although some are commercially available (*e.g.*, Grass Instruments Company, Quincy, MA). Force transducers have some compliance and you must consider this when choosing transducers. For example, with the Grass Instruments FT10, a force of 100 N will stretch the device by 1 mm.

For user-designed force transducers, the two main choices are between resistive or semiconductor strain gauges. Resistive gauges are cheaper and generally more rugged while semiconductor strain gauges are smaller and about 10 times more sensitive. Strain gauges are available from Measurement Specialties, Inc. (Hampton, VA).

User-designed force transducers can be interfaced to the CyberAmp 380 amplifier via the AI 490 Connector and AI 491 Cable Kits.

7.13. ACCELERATION MEASUREMENTS

Accelerometers can consist of piezoelectric pressure sensors attached to a test mass, small enough for physiological experiments. Piezoelectric accelerometers can have a wide frequency range (1 Hz to 25 kHz) and a wide dynamic range (0.01–2,500 g). Accelerometers can also consist of strain gauges attached to a mass. Alternative systems use feedback to prevent the test mass from being displaced; the amount of the applied feedback force represents the output signal.

7.14. LENGTH MEASUREMENTS

7.14.1. IMPLANTABLE LENGTH GAUGES

Length can be measured inside an animal using mercury-filled or saline-filled silicone tubing length gauges (Lemon and Prochazka, 1984). As the tubing is stretched, the impedance of the transducer increases. To avoid the generation of bubbles in the tubing, a high-frequency AC signal is used with an AC bridge circuit. In practice, these gauges have

many difficulties and may not be much better than cinematography techniques using markers on the limb joints for measuring muscle lengths.

7.14.2. LINEAR POTENTIOMETERS

Linear potentiometers are inexpensive and very simple to use but must be perfectly aligned to avoid internal damage. Linear potentiometers can be interfaced to the Cyber-Amp 380 amplifier via the AI 490 Connector and AI 491 Cable Kits.

7.14.3. LINEAR VARIABLE DIFFERENTIAL TRANSFORMERS (LVDT)

Linear variable differential transformers are used for accurate and stable measurement of linear position and displacement. Rotary variable differential transformers (RVDT) are similarly used to measure rotation. These devices are very rugged and since there is no contact between the core and the body of the LVDT (or RVDT), there is no friction or wear, providing essentially infinite life. Linearity of $\pm 0.25\%$ over the full range is typical (ADS Transicoil, Inc., Collegeville, PA).

7.15. SELF-HEATING MEASUREMENTS

As a result of applying an excitation current or voltage to the temperature measurement sensor, power is dissipated in the sensor. This power dissipation causes the temperature of the sensor to rise above the ambient temperature that is being measured. This phenomenon is referred to as “self heating.” For most of the temperature sensors used in physiology, it is necessary to keep the power dissipation to a few milliwatts or less. If this condition is met, temperature changes of less than $0.01\text{ }^{\circ}\text{C}$ can be measured.

Other transducers, such as strain gauges, are temperature-sensitive; therefore it is important not to allow self heating in these transducers to cause a temperature rise sufficient to affect the measurement.

7.16. ISOLATION MEASUREMENTS

In industrial environments, it is common for signal leads from transducers to be run over long distances past machinery that can induce large voltages in the leads. To protect the measurement instrument, isolation amplifiers should be used for each transducer. Induced voltages are not commonly a problem in animal physiology applications and, therefore, isolation is not required. Note that if measurements are to be made from human subjects, isolated probes that are approved for human use must be used.

7.17. INSULATION TECHNIQUES

Electrodes that are implanted for long-term recording eventually fail either due to the rupture of a solder joint, breakage of wires at points of repeated flexion, or moisture penetration through the insulation. Although teflon-insulated wire is commonly used, when it is connected to the leads of the transducer it is difficult to join the teflon insulation to the insulation on the transducer leads. A solution is to etch the teflon so that it will adhere to

the adhesive used to join the two insulations. In practice it is often faster and better to use PVC-insulated wires because it is much easier to make a strong adhesion, even though PVC is more permeable to water over the long term. Also, Araldite AV138M (CIBA-GEIGY) and Epoxylite #6001 (Epoxylite Corporation, Anaheim, CA) both provide excellent water-resistant insulation for rigid applications.

Special attention should be paid to providing strain relief where wires, and particularly connections, are repeatedly flexed. Sliding a length of silicon tubing over the stress region often reduces this problem.

7.18. FURTHER READING

Cain, C., Welch, A. J., Thin-film temperature sensors for biological measurement. *IEEE Trans. Biomed. Eng.* BME-21(5), 421–423, 1974.

Cooke, I.R., Brodecky, V., Becker, P.J., Easily implantable electrodes for chronic recording of electromyogram activity in small fetuses. *J. Neurosci. Meth.* 33, 51–54, 1990.

Geddes, L. A., Baker, L. E., *Principles of Applied Biomedical Instrumentation*. John Wiley & Sons, New York, 1989.

Horowitz, P., Hill, W., *Measurements and signal processing. The Art of Electronics*, 14. Cambridge University Press, Cambridge, 1986.

Lemon, R., Prochazka, A. Eds. *Methods for neuronal recording in conscious animals. IBRO Handbook Series: Methods in the Neurosciences, Vol. 4*. John Wiley & Sons, Chichester, 1984.

Loeb, G. E., Gans, C., *Electromyography for Experimentalists*. University of Chicago Press, Chicago, 1986.

8. Laboratory Computer Issues and Considerations

Chapter 8 provides an overview of personal computers. The earlier sections give more detailed information on computer options and the issue of price vs. performance. The last section provides a glossary of computer terms that you may come across when researching computers.

8.1. SELECT THE SOFTWARE FIRST

The first consideration when setting up a personal computer is to determine which software packages will be used, and what kind of computer that software will run on. For specialized applications, such as scientific analysis packages, it is not safe to assume that comparable packages are available for both Macintosh and Windows computers. If one needs a software package for the acquisition and analysis of microelectrode voltage-clamp and current-clamp data, the Axon pCLAMP[®] software suite is available for Windows.

8.2. HOW MUCH COMPUTER DO YOU NEED?

8.2.1. THE MACHINE SPECTRUM: CAPABILITY VS. PRICE

Once you have determined the type of computer you are going to buy, you need to decide how much you are willing to spend for performance and convenience. The main components of the computer that you need to consider are discussed in the following sections. Although very powerful computers have become relatively cheap in recent years, it is still worth considering the motivations for upgrading the various system components.

8.2.2. MEMORY

RAM (Random Access Memory) is the physical device used to store programs and data while the computer is running. When the computer power is off, RAM cannot hold any information, so it is referred to as “volatile” memory. It is used because instructions and data can be read from, and written to, RAM much faster than any other type of memory device. How much RAM you need and can use depends on the type of computer you buy as well as the capabilities of the programs you use.

The usefulness of extra memory depends on the type of applications that you will be running. Acquiring and analyzing very large datasets in general requires more memory than acquiring and analyzing smaller amounts of data.

8.2.3. HARD DRIVE

At the time of writing, 500 GB hard drives are not uncommon, and hard drives with capacity of a terabyte or more are now widely available to consumers.

For traditional electrophysiology experiments, these hard drives provide more than enough storage. For applications that include live cell video at high frame rates, a terabyte of storage is not enough for long-term archiving of data. The good news is that hard drives using USB, Firewire or SATA can be stacked externally, and are cheap enough to be able to keep up with the increasing amounts of data.

For data acquisition, hard disk drive performance may be important. To record long segments of unbroken data, direct acquisition to disk (rather than memory) is necessary, and the speed of acquisition is limited by the drive performance. High hard drive speeds of 5,400 RPM are standard, and for a small price premium 7,200 RPM drives are readily available.

8.2.4. GRAPHICS CARD

Recent versions of the Windows and Macintosh operating systems have numerous extraneous “eye candy” features that can consume a large proportion of a system’s resources without any tangible benefit. To free up the main system processor, dedicated high-powered graphics processors are now included in most modern computer systems.

Computations required to render high-speed or 3D graphics are performed on the graphics card, freeing up the system processor for other tasks. The purchase of a high-end graphics card can therefore increase overall system performance.

8.3. PERIPHERALS AND OPTIONS

One of the design principles of personal computers has been the modularity of design to accommodate user-specific functionality. The descriptions below discuss the peripherals most pertinent to laboratory setups.

8.3.1. DATA BACKUP

As common and everyday as personal computers have become, hard disks are complex mechanical devices requiring precise tolerances in their operation, and are subject to mechanical failure. The lifetime of hard disks is usually several years, but manufacturing defects, physical shocks, or too many power-on cycles can make your hard disk ready to fail at any moment. It is essential that a disk full of programs and data be backed up regularly.

There are two common methods of backing up data: you can backup to another hard drive, or back up to an optical medium such as CD or DVD. With the advent of rewritable optical disk drives, it is possible to store 680 MB of data on a CD, and 4.4 GB on a single-layer DVD.

Although outstripped by hard drives for storage capacity, optical storage has the advantage of being compact for small amounts of data and electrically stable. Another clear advantage of optical storage is that once a CD/DVD has been closed, there is a very low chance of overwriting data. With a hard drive, there is a much higher chance of losing data through accidental overwrite unless special precautions are taken.

On the other hand, hard drives allow data to be recovered and reorganized relatively easily. Optical disks can be almost impossible to recover once they become scratched, and reorganizing data requires data transfer and re-burning.

8.4. RECOMMENDED COMPUTER CONFIGURATIONS

Because computer state-of-the-art changes so quickly, please consult the MDS Analytical Technologies web site for the latest recommended computer specifications.

8.5. GLOSSARY

A/D converter

An Analog-to-Digital converter (ADC) maps analog measurements to digital numbers that the computer can store and use in calculations. See analog and digital.

Analog

Real signals in the physical world are described as analog, meaning that the values change in a continuous manner. A mercury thermometer is an analog measurement device; the mercury rises smoothly in response to changing temperature. However, the computer requires discrete digital numbers to describe measurements of the data. See A/D converter and digital.

ASCII

American Standard Code for Information Interchange. A standardized 7-bit code for exchanging information between computer systems. The 128-character set consists of the alpha-numeric and punctuation characters, as well as control codes such as Escape and Carriage Return. Files on a computer are often stored in a simple ASCII format, so that they can be easily transferred and read by different systems and programs.

Bit

Information is stored in computer memory as a series of bits, which are binary switches (numbers) that can either be on (1) or off (0). A group of eight bits is called a byte, which is a common unit for addressing and storing information.

Boot

To boot a computer refers to the sequence of events that occurs when a computer is switched on. When the computer is turned on, its built-in software instructs the computer to load the operating system from disk into memory, and turns over control of the computer to the operating system.

Byte

A byte is a series of eight bits of data. Since a bit can have two values (zero and one), a byte can have 2^8 (256) values. A character on an IBM text screen is stored in a byte of memory, so there are 256 distinct characters available. A byte is a typical unit for storing data and computer instructions. See word.

Cache

A cache is a place to store often-accessed data or computer instructions, and is designed to provide quicker access for increased performance. A memory cache is faster-than-usual RAM for storing data that the microprocessor requires often from the normal RAM storage area. A disk cache is a RAM storage area for data that is stored on disk but is being read frequently.

CPU

Central Processing Unit. See Microprocessor.

D/A converter

A Digital-to-Analog converter (DAC) transforms digital information from the computer into analog voltages to drive real world devices. See Analog and Digital.

Data acquisition

In the context of computers, data acquisition refers to the analog-to-digital conversion of measurements for storage and analysis by the computer.

Device driver

Software that acts as an extension to the operating system, usually for supporting a hardware device. Mouse pointing devices and network cards are common devices that require a device driver to be loaded when booting the system up. On PC computers, device drivers are files that traditionally have a .SYS filename extension.

Digital

Data represented in discrete, discontinuous form is digital, as opposed to the smooth representation of data as measured by an analog device, such as a pen chart recorder. Computers require discrete digital numbers for storage and processing. See A/D and analog.

DPI

Dots Per Inch is a measure of resolution on a printed page or computer screen. The more dots per inch, the sharper that text or a graphic image will appear. A laser printer typically has a resolution of 300 DPI.

EEPROM

Electrically Erasable Programmable Read-Only Memory. Allows ROM memory chips to be reprogrammed with new information by users in the field. See ROM.

I/O Interfaces

An I/O interface defines the physical interface and communication method for devices attached to the computer, such as the display, printer, mouse and disk storage device. For devices attached internally, such as the display adapter, the physical I/O interface is the computer's internal bus. For external devices, e.g., the mouse or printer, there are several interfaces implemented on Windows and Macintosh computers.

PARALLEL PORT

The parallel port interface, which exists primarily in the Windows world, allows eight bits of data to be transferred at a time (“in parallel”). It offers high speed, but its design allows mostly one-way communication; the external device is very limited in the signals it can send back to the computer. As a result the only devices designed to use the parallel port are those that mostly receive data, the most common example being the printer. While most consumer computers implement this port as a 25-pin connector, commercial printers often use a 36-pin Centronics connector.

Parallel ports are becoming uncommon with the advent of USB printers.

SERIAL PORT

The RS-232 serial port is a general communication interface that allows full, two-way communication, thereby making it much more versatile than the parallel port. It exists on many types of computer systems. Common devices which attach to a serial port include the mouse and the keyboard, but which used dedicated 6-pin PS/2 connectors vs. the general-use 9-pin DB connector.

Serial ports have already been phased out for consumer devices, but because communication using the serial interface is relatively straightforward, serial ports remain useful for low-level device communication. For device development, therefore, one or two serial ports is essential.

When buying a new PC computer for use in a laboratory, you should ensure that it has a serial port.

USB PORT

In just a few years, USB has lived up to its name and become the Universal Serial Bus. Devices such as cameras, phones, printers, scanners, external hard drives, flash drives, keyboards, mice and other consumer products now come with USB as the standard interface. USB is much faster than older protocols such as serial, and so it is suitable for applications that require large amounts of data to be transferred at high speed. Modern scientific instruments such as the MultiClamp™ 700B and Axoclamp™ 900A amplifiers are now being made with USB interfaces, and this trend is likely to continue.

The original implementation of USB 1 has been supplanted by a high-speed version known as USB 2. USB 2 allows high-speed devices, such as the Digidata 1440A digitizer, to be easily connected to either desktop or laptop computers.

KB

A kilobyte is approximately 1,000 bytes. As a computer's natural system of numbers is in base two, a kilobyte actually refers to 2^{10} (1,024) bytes. It is abbreviated with a capital K to distinguish it from the abbreviation for 1,000, as in kHz.

MB

A megabyte is 1,024 kilobytes, or 1,048,576 bytes. See KB.

Memory

See RAM and ROM.

Microprocessor

A microprocessor is a single integrated circuit chip that combines functions for doing logical and mathematical operations, managing memory and communicating with external devices. It is the main control center of a microcomputer.

Operating system

An operating system manages the hardware in a computer and provides a set of services for an application program, such as writing data to a disk drive.

Parallel port

A type of communication interface that transfers data across several parallel lines. Communication is mostly one-way, and the length of the connecting cable is limited. In the PC, the parallel port is used mainly for connecting printers.

PC

Originally referred to the IBM PC, but now refers to any computer compatible with the IBM PC designs based upon Intel CPUs.

RAM

Random Access Memory is composed of specialized integrated circuits designed for storing programs and data. RAM can be quickly read from and written to, so programs execute quickly.

However, when the computer power is off, RAM cannot hold any information.

Resolution

The "sharpness" of images and characters on the computer screen or on printer output. Most accurately described in units of dots per inch.

ROM

Read Only Memory resides on integrated circuits that hold information which is not lost when power is turned off. The contents of the ROM are usually loaded by the manufacturer and are not alterable by the user.

RS-232

A common, standard protocol for communicating over serial ports. It is a general two-way communication interface that transmits data on a single line and receives data on a single line.

SCSI

Small Computer System Interface. This is a type of parallel interface that provides for higher speeds than were possible in the older serial or parallel interfaces, while allowing multiple devices to be connected to a single port.

Serial port

A legacy standard connection, which provides a general two-way communication interface that transmits data on a single line and receives data on a single line. The serial interface no longer exists in most types of computers. Also known as a RS-232 serial port.

Throughput

A measure of performance describing how much data per unit of time can be transferred from device to device in a computer system.

Video display card

A specialize circuit card to handle the complexity of graphics display. High-end graphics cards can be added to computers to upgrade their standard display speeds, resolution and number of colors.

9. Acquisition Hardware

Scientists are always seeking better methods to record and store the growing amounts of data generated in experiments. In electrophysiological experiments, the data are most often in the form of voltage waveforms whose magnitudes vary with time. Data in this form are appropriate for displaying on an oscilloscope or chart recorder, but entirely inappropriate for storing on a computer disk. Since computers can only store discrete numbers, a process of “analog-to-digital” conversion must be undertaken to convert the analog data into a compatible format for the computer.

9.1. FUNDAMENTALS OF DATA CONVERSION

The analog-to-digital (A/D) conversion process can be illustrated by recording temperature during the course of a day, using pencil and paper. One way to do this is to look at the mercury level in a glass thermometer every 30 minutes and write the temperature in a column on a piece of paper. The result is a sequence of numbers, recorded at uniform time intervals, which describes the variations in the temperature during the day. This process illustrates the execution of an analog-to-digital conversion and the creation of an array of data that could be typed into the computer and stored on disk.

Table 9.1: Example Temperature Data.

Time	Digitized Temperature °C
6:00 AM	10
6:30 AM	11
7:00 AM	11
7:30 AM	12
8:00 AM	13
8:30 AM	13
9:00 AM	14
9:30 AM	14
10:00 AM	14
10:30 AM	15
11:00 AM	15
11:30 AM	15
12:00 PM	17
12:30 PM	18
1:00 PM	19
1:30 PM	19

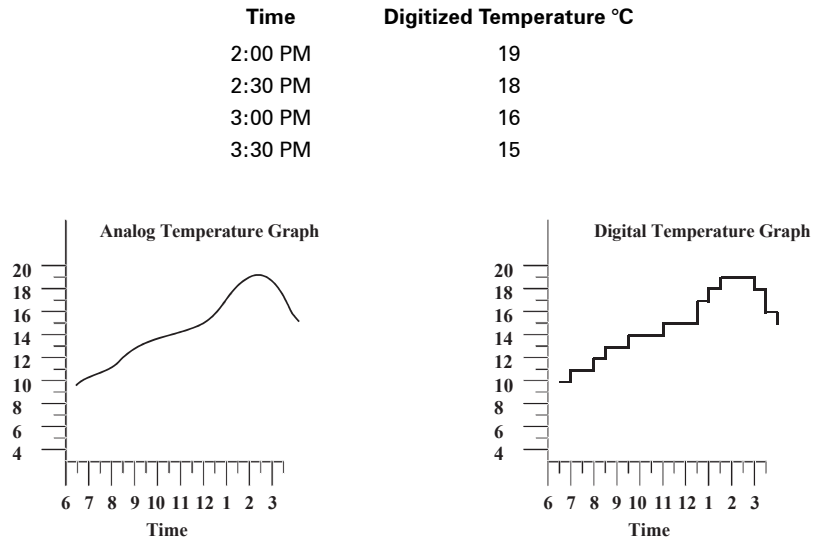


Figure 9.1: Analog-to-digital conversion.

This figure illustrates the analog and the digital representations of the temperature data presented in Table 9.1.

A much easier way to accomplish the same task would be to use a data acquisition board in the computer to directly record the temperature every 30 minutes. In this case the thermometer must report the temperature in a form that the analog-to-digital converter (ADC) can read. Nearly all ADCs require that the data be presented as a voltage. To do so, one uses a different type of thermometer, such as a temperature-dependent resistor in an appropriate circuit, that generates an analog voltage proportional to the analog temperature. The computer is instructed to initiate an analog-to-digital conversion every 30 minutes and store the results on disk.

Sometimes the computer is required to generate an analog waveform that will be proportional to a list of numbers that are held in memory or on disk. In this case, a digital-to-analog (D/A) converter (DAC) is used. The principles of operation of a DAC are similar to those of an ADC, but the operation is the reverse.

9.2. QUANTIZATION ERROR

The ADC converter generates binary numbers that have finite resolution. That is, a small range of analog values will all produce the same binary number after conversion. Returning to the temperature-measurement example above, the hypothetical ADC rounded off all of the temperature values to the nearest degree Celsius reading. That is, only numbers between 0 and 99 °C in steps of 1 °C were allowed. Clearly, the temperature changes continuously between each 30-minute reading, not in 1 °C jumps. The range of analog values that are recorded as the same digital number is the quantization error.

In an ADC, the total measurement range (*e.g.*, 0–100 °C) is divided into a fixed number of possible values. The number of values is a power of two, often referred to as the number of “bits.” Commonly, these values are:

$$\begin{aligned} 8 \text{ bit} &= 2^8 = 256 \text{ values} \\ 12 \text{ bit} &= 2^{12} = 4,096 \text{ values} \\ 16 \text{ bit} &= 2^{16} = 65,536 \text{ values} \end{aligned}$$

To illustrate the impact on the resolution of using an 8-bit, 12-bit or 16-bit ADC, consider the temperature-measurement example where the electronic thermometer circuit generates an analog output from -10 V to +10 V for temperatures in the range -100 °C to +100 °C. In this case, the resolutions are:

$$\begin{aligned} 8 \text{ bit} &= 78.4 \text{ mV} = 0.784 \text{ °C} \\ 12 \text{ bit} &= 4.88 \text{ mV} = 0.0488 \text{ °C} \\ 16 \text{ bit} &= 0.305 \text{ mV} = 0.00305 \text{ °C} \end{aligned}$$

If the ADC is preceded by a programmable-gain amplifier, signals that occupy only a small range, *e.g.*, ± 1 V, can be amplified before conversion so that the full resolution of the ADC can be utilized.

The resolution of a 12-bit ADC with an input range of ± 10 V is 4.88 mV. Although this resolution does not represent a difficult number for a computer-based system to use, some researchers preferred a round number such as 5.00 mV. This could easily be achieved by setting the span of the ADC to ± 10.24 V instead of ± 10 V. Now, many ADC systems are now designed with the ± 10.24 V span (*e.g.*, the Axon Digidata[®] 1440A data acquisition system).

9.3. CHOOSING THE SAMPLING RATE

There is a well-known theorem known as the sampling theorem or the Nyquist theorem stating that data should be sampled at a frequency equal to twice the bandwidth of the signal or faster in order to prevent an artifactual increase in the noise, due to a phenomenon known as aliasing (see Chapter 11), and guarantee that the analog signal can be reconstructed unambiguously from the digital samples.

In practice, it is common to sample at a rate significantly faster than the minimum rate specified by the sampling theorem. This is known as oversampling. Exactly how much oversampling should be used depends upon the type of experiment.

For experiments where the data are analyzed in the frequency domain (*e.g.*, noise analysis, impedance analysis), it is common to oversample only modestly. The main concern is to prevent aliasing. An anti-aliasing filter is introduced between the signal source and the analog-to-digital converter to control the bandwidth of the data.

The factor of twice the analog bandwidth required by the sampling theorem is only applicable if the anti-aliasing filter is ideal, *i.e.*, the gain is unity in the pass band and it abruptly changes to zero in the stop band. Ideal filters cannot be realized, although they can be closely approximated. For frequency-domain analysis it is common to use sharp cutoff filters such as Butterworth or Chebyshev realizations. Sampling is typically performed at 2.5 times the filter bandwidth. For example, if the data are filtered at 10 kHz they should be sampled at about 25 kHz. Slower sampling rates are unacceptable. Faster sampling rates are acceptable, but offer little advantage and increase the storage and analysis requirements.

For experiments where the data are analyzed in the time domain (*e.g.*, pulse analysis, I-V curves), greater oversampling is required because reconstructing the analog signal requires not only an ideal anti-aliasing filter but also an ideal reconstruction filter. The simplest and most common reconstruction filter is to join each sample by a straight line. Other techniques, such as cubic-spline interpolation, can be used, but due to their much more demanding computational requirements they are used infrequently.

The reconstruction problem is discussed in the Sampling Rate section in Chapter 11. There is no commonly accepted rule regarding the sampling rate of data for time-domain analysis. In general, five times the data bandwidth is a common sampling rate, and ten times is considered good. Sampling at 20 times is excessive and is rarely used.

9.4. CONVERTER BUZZWORDS

The terms in this section are defined for a D/A converter. With simple reorganization, these definitions can be re-cast for an A/D converter. Only the more esoteric terms have been defined in this section. It is assumed that the reader already understands conventional terms such as “voltage offset.”

9.4.1. GAIN ACCURACY

Gain accuracy is the closeness with which the output of the D/A converter corresponds to the specified full-scale value when the digital input to the D/A converter is the maximum value.

9.4.2. LINEARITY ERROR

Linearity error is the maximum deviation of the D/A output from a straight line drawn between the minimum and the maximum output.

9.4.3. DIFFERENTIAL NONLINEARITY

When the digital control word changes by a minimal step, *i.e.*, one least-significant bit (LSB), the output value should change by 2^{-n} of the full-scale value, where n is the number of bits in the converter. Any deviation from this ideal change is called the differential nonlinearity error. It is expressed in multiples of LSBs.

9.4.4. LEAST SIGNIFICANT BIT (LSB)

LSB is the value of the smallest possible digital increment.

9.4.5. MONOTONICITY

Monotonic behavior means that for every increase in the digital input to the D/A converter there will be an increase in the analog output. This requires that the differential nonlinearity error be less than 1 LSB.

9.5. DEGLITCHED DAC OUTPUTS

When the input to a digital-to-analog converter changes value, the analog output ideally moves rapidly and monotonically towards its new value. While usually this is the case, for certain changes in value a transient is superimposed on the changing output. This transient is known as a “glitch.”

Glitches occur when several bits in the control word change. Each bit is connected to a set of internal digital logic and analog switches. There is variability in the response time of each part of the circuit, and therefore the response to the new control word does not happen at the same instant for each bit. In addition, charge is injected from the digital logic circuitry into the analog switches. Glitches are worst when a large number of the bits of the digital input to the D/A are changed. For example, when the analog output is required to go from negative to positive, the digital input bits can change from 1111 1111 1111 to 0000 0000 0000. That is, every single bit changes. This change generates the worst glitch.

Glitches can be prevented by including a sample-and-hold circuit at the output of the D/A converter. The sample-and-hold is normally in the “sample” mode so that the output of the D/A converter feeds straight through. However, for one or two microseconds, perhaps less, after the digital input to the D/A converter is updated, “hold” mode is selected so that the glitch, if present, is blocked.

In modern integrated-circuit D/A converters, efforts are made in the design of the chip to match the propagation and activation delays of each bit in the circuit and to minimize the charge injection so that glitches are small in the first place. It is thus becoming increasingly less common for a deglitching circuit to be included. On the other hand, the high-level of integration in modern D/A converters sometimes introduces another problem, called feedthrough noise. This problem occurs when the digital latches that contain the word for the D/A converter are integrated into the same chip. It may happen that because of the proximity of the digital circuits to the D/A converter, digital noise couples into the D/A converter circuit. The coupled signal manifests itself as a pulse on the output of the D/A converter circuit each time the digital word is updated. Strangely, this feedthrough noise often appears even if the D/A value is being held constant. This is because, for simplicity, most software that simultaneously performs A/D and D/A conversions updates the D/A word once per A/D sample, even if the D/A value is not changing. The best solution is to eliminate the feedthrough noise at its source by using separate integrated circuits for the D/A converter latches. This is the approach used in the Digidata 1440A digitizer.

9.6. TIMERS

Most ADC systems have several timers available for a multitude of tasks. The most essential is the provision of a regular clock signal to initiate each A/D conversion. In most systems, one D/A conversion is performed for each A/D conversion, but this is not required and some systems provide for running the D/A converter at a different clock rate to the A/D converter.

Additional timers are used to implement “gear shifting.” This is a technique wherein the acquisition rate is rapidly changed (gear shifted) during acquisition from a low to a high rate or vice versa, without stopping the acquisition.

Uncommitted timers are generally provided for use in frequency measurement, event counting or interval timing. For example, the frequency of nerve spikes can be counted if they are first detected by an event detector that puts out a digital pulse for every spike. An example of event counting is the measurement of the number of photons collected by a photomultiplier tube in a fixed interval. An example of interval timing is measurement of the period of a spinning optical filter wheel so that the optical data collected can be normalized against fluctuations in the rotational speed of the wheel.

9.7. DIGITAL I/O

Digital outputs are used during experiments to control external equipment. For example, an oscilloscope can be triggered before the acquisition commences, or a flash lamp or an isolated stimulator could be activated during the acquisition. In other experiments, several solenoids can be sequentially activated before, during and after the acquisition.

Digital inputs are used routinely in industrial control applications for monitoring the state of solenoids and other apparatuses, but they are rarely used in electrophysiological experiments. The main application for digital inputs in electrophysiology is for triggering acquisitions and for indicating that a tag should be attached to the data.

9.8. OPTICAL ISOLATION

Computers provide quite hostile environments for plug-in data acquisition boards. The rapid switching activity of the digital logic circuits causes electronic noise to radiate directly into plug-in boards installed by the user and to be introduced into the ground reference used by the plug-in boards.

Nevertheless, it is usually possible to design data acquisition systems that do not suffer from extraneous noise pickup. This is achieved by careful layout and good grounding. Grounding and shielding, if applied with great skill and diligence, can sometimes be made to work acceptably for the A/D converter, especially when combined with differential recording. However, it is very difficult to achieve acceptable noise levels on the DAC outputs. The following approach is often invoked for 16-bit systems.

First, move the A/D converter off the plug-in board in the computer to a separate board housed in an external box. This eliminates the problems due to direct pickup of noise generated inside the computer housing. However, it does not eliminate the noise introduced through the system ground. The noise in the system ground can be eliminated by using optical isolation. In this technique, the digital signals to and from the computer are not connected directly. Instead, an optical coupler is interposed in each digital line. A separate power supply is provided for the A/D and D/A side of the optical couplers. This technique allows a low-noise ground to be maintained for the A/D and D/A converters and for the experimental setup.

9.9. OPERATING UNDER MULTI-TASKING OPERATING SYSTEMS

Data acquisition systems are not naturally compatible with multi-tasking operating systems. As a general rule, data acquisition systems are designed to use all of the resources of the computer (*e.g.*, display and disk) and they use these resources on demand, rather than when the computer makes them available.

Interrupt handling represents an acute problem for data acquisition in multi-tasking operating systems. Usually, when an interrupt occurs an immediate response is required. If the multi-tasking operating system is busy updating a screen for a word processor, an immediate response will clearly not be forthcoming. Therefore, high performance clearly requires that the data acquisition task runs as the foreground application. Another problem is that modern computers generally have long interrupt latencies of several hundred microseconds or more. One way to minimize the problem of excessive interrupt latency is to ensure that the data acquisition routine has the highest priority and, in many cases, exclusive control over the computer. Another way to minimize excessive interrupt latency is to provide hardware support in the acquisition system. For example, a memory-buffered data acquisition system can be configured by the acquisition software and left in a “primed” state. When it “sees” an external trigger it can generate an interrupt, then commence the acquisition before it even receives a response from the host.

9.10. SOFTWARE SUPPORT

Nowadays fewer researchers are writing their own data acquisition and analysis software using low-level languages and device drivers. Most researchers are using one of two types of commercially available software. The first type is a rich development environment such as MATLAB or LabVIEW. This environment allows researchers to design their own software without having to become experts in the low-level control of the data-acquisition hardware. The second type of software is a turn-key package, such as pCLAMP[®] software. These packages provide sophisticated acquisition and analysis, but only limited ability to customize them. Nevertheless, they are extremely popular because they perform well and are easy to learn.

9. Acquisition Hardware

When choosing hardware and software for a data acquisition system, we recommend that you choose the software first and then purchase the hardware recommended by the software applications that you have selected.

10. Data Analysis

Chapter 10 provides guidelines to selecting certain key data acquisition parameters, and discusses current methods used in analysis of biological data, including fitting models to data and analyzing single ion-channel recordings. The scope of this discussion is limited to brief, practical introductions with references to more detailed discussion in this Guide and in the literature. The manuals for the various software programs can be used for more specific step-by-step instructions, and the text by Dempster (1993) is a useful collection of standard techniques in this field.

10.1. CHOOSING APPROPRIATE ACQUISITION PARAMETERS

Successful analysis of a data set requires that the signals be recorded using appropriate data acquisition parameters. Following are guidelines to selecting several critical recording parameters.

10.1.1. GAIN AND OFFSET

Sufficient gain and offset should be maintained on all transducers and amplifiers during data acquisition, because data review and analysis software can usually provide only limited amounts of additional (“software”) offset and gain. More than 10x of software gain usually results in excessively jagged traces; this is because the digitized signal does not vary smoothly but is quantized (see Chapter 9), and too much amplification allows the difference between one quantization level and the next to become visible. Software offset is limited to the full range of the analog-to-digital converter (ADC) input, which is usually equivalent to about ± 10 V referred to the input of the ADC. Signal resolution is best preserved when the signal fills this voltage range without exceeding it.

10.1.2. SAMPLING RATE

The sampling rate used should be selected considering the particular experiment. Use of excessively high sampling rates wastes disk space and will increase the time required for analysis. Furthermore, a higher sampling rate is usually associated with a higher filtering frequency, which in turn allows a larger amount of noise to contaminate the signal. Subsequent analysis of the data may therefore require noise reduction using analysis-time filtering, which can be time-consuming. Guidelines to choosing the correct sampling rate are discussed in the following paragraphs (Colquhoun and Sigworth, 1983, and Ogden, 1987).

Biological signals are most commonly analyzed in the time domain. This means that the time dependence of the signals is examined, *e.g.*, to characterize the membrane response to

a voltage-clamp pulse. The usual rule for time-domain signals is that each channel should be sampled at a frequency between 5 and 10 times its data bandwidth. Knowing the value of the data bandwidth is required in order to set the filter cut-off frequency during acquisition and analysis.

For a sinusoidal waveform, the data bandwidth is the frequency of the sine itself. For most biological signals, the data bandwidth is the highest frequency of biological information of interest present in the recorded signal. This can be determined directly by examining a power spectrum of rapidly sampled unfiltered data, though this is rarely done. Alternatively, one can estimate the number of points per time interval required to give a data record whose points can be easily “connected” by eye and calculate the sampling rate directly. The data bandwidth and filter frequency can then be calculated from the sampling rate. For example, if a fast action potential (1 ms to peak) is to be recorded, 25 samples on the rising phase would yield a reasonably good 40 μ s resolution, requiring a sampling rate of 25 kHz and an approximate data bandwidth of 5 kHz.

The rules are more straightforward in some special cases. Single-channel recording is discussed below. For signals with exponential relaxation phases, the sampling rate needed to estimate a time constant depends on the amount of noise present; for moderately noise-free data, at least 15 points should be taken per time constant over a period of 4 to 5 time constants. Many fitting routines will fail if sampling is performed over only 3 time constants, since the waveform does not relax sufficiently far towards the baseline. For a sum of multiple exponentials, the sampling rate is determined in this way from the fastest phase; sampling must extend to 4 time constants of the slowest phase. If this would result in too many samples, a split clock (as in the Clampex program of the Axon pCLAMP[®] suite) or other methods of slowing the acquisition rate during the acquisition, could be employed as long as at least 15 points are taken over each time constant.

When a set of several channels is recorded (*e.g.*, channels 0 through 3), most data acquisition systems sample the channels sequentially rather than simultaneously. This is because the system usually has only one analog-to-digital converter circuit that must be shared among the channels in the set. For example, if four channels are sampled at 10 kHz per channel, one might expect that they would be sampled simultaneously at 0 μ s, 100 μ s, 200 μ s, *etc.* Instead, channel 0 is sampled at 0 μ s, channel 1 at 25 μ s, channel 2 at 50 μ s, channel 3 at 75 μ s, channel 0 again at 100 μ s, channel 1 again at 125 μ s, *etc.* There is therefore a small time skew between the channels; if this causes difficulties in analysis or interpretation, a higher sampling rate can be used to minimize the time skew (but this may cause problems associated with high sampling rates, as mentioned above).

An additional consideration arises from the fact that on many data acquisition systems, including the Digidata[®] 1440A digitizer from MDS Analytical Technologies, the digital-to-analog converter (DAC) is updated whenever the ADC is read, even if there is no change in the DAC output. This means that the DAC is updated only at the sample rate over all channels. For example, if a stimulus is a 0 to 150 mV ramp and 50 samples are acquired from one channel at a sampling interval of 25 μ s, the DAC output will appear as a series of steps each 25 μ s long followed by an upward jump of $150 \text{ mV}/50 = 3 \text{ mV}$,

which may be too large for some electrophysiological applications. Therefore, if a rapidly changing continuous waveform is applied while acquiring slowly, the output waveform should be checked with an oscilloscope and, if necessary, the sampling interval should be increased. The computer preview of a waveform cannot be relied upon for this purpose because it does not account for the effect of sampling. Note, however, that since most users acquire significantly more samples per sweep than 50, this problem will not occur except in very unusual situations.

10.1.3. FILTERING

The signal should be filtered using an analog filter device before it arrives at the ADC. As discussed in Chapter 6 and in Colquhoun and Sigworth, 1983 and Ogden, 1987, this is done to prevent aliasing (folding) of high-frequency signal and noise components to the lower frequencies of biological relevance.

Acquisition-time filtering of time-domain signals is usually performed using a Bessel filter with the cut-off frequency (-3 dB point; see Chapter 6) set to the desired value of the data bandwidth. A 4-pole filter is usually sufficient unless excessive higher frequency noise requires the 6- or 8-pole version. The Bessel filter minimizes both the overshoot (ringing) and the dependence of response lag on frequency. The latter two effects are properties of the Chebyshev and Butterworth filters (see Chapter 6 and Chapter 11, or Ogden, 1987), which are less appropriate for time-domain analysis.

10.2. FILTERING AT ANALYSIS TIME

It is sometimes reasonable to sample data at higher rates than seems necessary, *e.g.*, when a greater bandwidth might be required during analysis. If excessive sample rates are used, the filter frequency must be set to a higher value. Since there is more noise at higher frequency, more noise is likely to contaminate the signal. Therefore, the data must be filtered further during analysis in order to reduce the noise and avoid aliasing of high-frequency signal content.

This analysis-time filtering is performed using filters implemented in software. The Gaussian filter is most commonly used for this purpose because of its execution speed, though the Bessel filter is employed as well. If one wants to write a computer program for a filter, the Gaussian is easier to implement than the Bessel filter (see program example in Colquhoun and Sigworth, 1983). Note that all filters alter the waveform; for example, a Gaussian-filtered step function deviates from the baseline before the time of transition of the unfiltered signal. The user can examine data records filtered at different frequencies to make sure that there is no significant distortion of the quantities of interest, such as time of transition or time to peak.

Another common software filter is smoothing, the replacement of a data point by a simply weighted average of neighboring points, used to improve the smoothness of the data in a record or graph. In contrast to the smoothing filter, the Bessel and Gaussian types have well-known filtering (transfer) functions, so that (i) it is easy to specify an effective cut-off

frequency, and (ii) the effect of the filter may be compensated for by a mathematical procedure analogous to a high-frequency boost circuit in a voltage-clamp amplifier (Sachs, 1983). These advantages are important if the frequency properties must be known throughout the analysis. If not, the smoothing filter is much faster to execute, especially on long data records, and easier to implement if one writes one's own software.

10.3. INTEGRALS AND DERIVATIVES

The integral function is used to calculate the area under a digitized data trace. Applications include measuring the total charge transfer from records of membrane current, and measuring the area under a miniature endplate potential. The integral is generally calculated by direct summation of $y(x_i)\Delta x_i$ between two cursors placed along the x axis. For a data record, $y(x_i)$ is the amplitude at time point x_i , and Δx_i is the sampling interval at that time. For a histogram, $y(x_i)$ is the amplitude of the bin at location x_i , and Δx_i is the bin width of bin i (this allows for nonuniform bin width). The y values must be corrected for any superfluous baseline before integration using a fixed or slanting baseline, as appropriate. If the sample rate were low compared to the rate of change of the signal, so that y values show large changes from one x_i to the next, the integral is considerably less accurate than if significantly more samples were taken. Large inaccuracies can also occur if the signal does not return to baseline by the end of the data set or if part of the data is corrupted by an extraneous signal. In some cases, errors in the integral can be reduced by first fitting a smooth curve to the available data and then using the formula and parameters of the best fit to calculate the integral.

The derivative function is used to determine the rates of change of a digitized signal. This can be used to help in peak location (where the derivative will be near zero), transition detection (large positive or negative derivative), sudden departure from baseline, *etc.* The derivative will, however, amplify noise, making it difficult to determine trends. The signal should therefore be filtered beforehand or fit to a function which can then be used to obtain a noise-free form of the derivative. However, the worse the fit, the greater the error in the derivative.

10.4. SINGLE-CHANNEL ANALYSIS

10.4.1. GOALS AND METHODS

The goal of single-channel current analysis is to reconstruct the idealized current waveforms from which information about the mechanisms of channel function is derived. Specific information can be deduced with respect to channel state diagrams, kinetics of channel opening, closing and gating, channel barrier models, and the effects of channel blocking agents and membrane constituent on channel function.

Articles that present approaches and methods used in single-channel current analysis include Colquhoun and Hawkes, 1983; Colquhoun and Sigworth, 1983; McManus, Blatz and Magleby, 1987; Sigworth and Sine, 1987; and French et al., 1990.

The current from a single ion channel is idealized as a rectangular waveform, with a baseline current of zero (closed-channel), an open-channel current dependent on the conductance and membrane potential, and rapid transitions between these current levels. In practice, this idealized current is distorted by the limited bandwidth of the apparatus and contaminated by noise. Shifts in the baseline may occur during the recordings, and capacitive current spikes are present in sweeps in which voltage changes are applied across the membrane. The current signal is further altered by filtering and by periodic sampling. These effects can impede making confident inferences from data regarding channel behavior.

10.4.2. SAMPLING AT ACQUISITION TIME

In order to adequately reconstruct the transitions, the sampling rate should be no less than 5 times higher than the cut-off frequency of the filter (Colquhoun and Sigworth, 1983; French et al., 1990).

10.4.3. FILTERING AT ACQUISITION TIME

As discussed above, the input signal should be filtered with a Bessel filter during acquisition. The cut-off frequency must usually be set sufficiently low to prevent unacceptably frequent occurrences of noise, which cause false closings and false brief open-close events during the construction of idealized channel currents. French et al., (1990) discuss how to decide on the cut-off frequency for a particular situation: open events of longer duration are more likely to be falsely closed by noise, so it is convenient to specify the longest duration d_{\max} that can be recorded with less than 1% occurrence of these false closings. Once d_{\max} has been specified, the required cut-off frequency f_c can be calculated using the following combination of equations (18) and (19) in French et al., (1990):

$$f_c = \frac{100f_c^*}{d_{\max}FTC^*} \quad (1)$$

Here FTC^* is the observed rate of false threshold crossings measured using recordings made with an arbitrary cut-off frequency f_c^* . FTC^* can be measured from idealized single-channel records generated using a threshold set on the side of the baseline opposite to where transitions are observed. This analysis can be achieved using pCLAMP software.

10.4.4. ANALYSIS-TIME FILTERING

The digital Gaussian filter can be used for additional analysis-time filtering of single-channel records. This introduces symmetrical time delays at both opening and closing and can therefore be used for the unbiased estimation of latencies using the 50% criterion (Section 10.4.6., “*Setting the Threshold for a Transition*”).

10.4.5. GENERATING THE EVENTS LIST

The first step during analysis of single-channel current records is to idealize the current records to a series of noise-free open and closed states having infinitely short (or at least shorter than the sample interval) transition times. This analysis, which can be performed by pCLAMP software, results in a list of durations and amplitudes, called the events list. Several effects that tend to complicate this reconstruction are briefly discussed below; more thorough discussions are presented in the cited literature.

10.4.6. SETTING THE THRESHOLD FOR A TRANSITION

A transition between states of a channel occurs when the current amplitude passes through a threshold between two levels. The most commonly used threshold is 50% of the difference between the levels. The advantage of this threshold setting is that the event durations are not biased because the values of the threshold are the same for both opening and closing transitions.

10.4.7. BASELINE DEFINITION

The accuracy of the threshold method for transition detection depends on the stability of the baseline (*i.e.*, closed-channel) current or, if the baseline is unstable, on the ability of an automated procedure to correctly identify the baseline as it changes. A number of ways have been devised to track a moving baseline, including 1) averaging the baseline current level to get the new baseline; 2) defining the new baseline as that level which maximizes the number of times that the current signal crosses it during the closed state (“zero crossings” method; Sachs, 1983); and 3) defining the new baseline at the peak of the histogram of the baseline current amplitude (*e.g.*, G. Yellen, quoted in Sachs, 1983). pCLAMP software uses a hybrid approach in which the average of the most recent closed channel current level is averaged with the old baseline level, weighted by a selectable factor. Regardless of the method used, the user must carefully monitor the baseline to ensure that any automatic procedure does not lose track of the baseline value.

10.4.8. MISSED EVENTS

Events will be missed if their true durations are shorter than the dead time of the system, which is determined by the filter cut-off frequencies used during acquisition and analysis. Events will also be missed if their superthreshold portions happen to miss the times when the signal is sampled even if their durations are longer than this dead time. The resulting error is minimal if the fastest time constant in the system is much longer than the sampling interval because few events will be shorter than the sampling interval. If this is not the case, the sampling rate must be increased with respect to the filter cut-off frequency (see Section 10.4.2., “*Sampling at Acquisition Time*”).

10.4.9. FALSE EVENTS

The probability of detecting false events depends on the amount and spectrum of noise in the system, the filter characteristics and the rate of sampling (French et al., 1990).

10.4.10. MULTIPLE CHANNELS

The presence of multiple channels complicates the determination of the kinetic behavior of a channel. If a record shows a transition from two open channels to one open, it cannot be determined if the transition was due to the closing of the first or the second channel. A number of methods have been proposed to deal with this ambiguity (French et al., 1990). As a precaution, the amplitude histogram of the raw data can be inspected to determine if multiple channels are present.

10.4.11. ANALYZING THE EVENTS LIST

The second step in the analysis procedure is the extraction of model-specific information from the events list. Because the number of events is usually large, it is often convenient to sort the event data into bins. The binned data may then be fit to a mathematical function whose parameters are related to a state diagram of the channel.

The most common histograms include 1) the dwell time histogram, in which the duration of events is binned and which can be related to state models; 2) the first latency histogram, in which the period of time from stimulus onset to first opening is binned and which is used to extract kinetic information; and 3) the amplitude histogram, in which the amplitudes of the levels or of all points in the records are binned and yield information about the conductance, the system noise and the incidence of multiple channels.

10.4.12. HISTOGRAMS

The simplest histogram is one in which a series of bins are defined, each of which has an associated upper and lower limit for the quantity of interest, *e.g.*, dwell time. Each dwell time will then fall into one of the bins, and the count in the appropriate bin is incremented by one. In the cumulative histogram, a bin contains the number of observations whose values are less than or equal to the upper limit for the bin.

10.4.13. HISTOGRAM ABSCISSA SCALING

Histograms may be scaled and displayed in a number of ways. The most common histogram has constant bin width, a linearly scaled abscissa (x axis), and counts displayed on the ordinate (y axis). A number of alternatives have been developed to improve the treatment of exponential distributions, in which low-time bins have many counts and high-time bins have few, yielding histograms that are difficult to visualize (*e.g.*, McManus et al., 1987; Sigworth and Sine, 1987). One solution is to increase the bin width logarithmically, so that for a single exponential, a constant number of events is expected per bin. This has the disadvantage that the presence of multiple time constants is not evident from the plot if the ordinate is not rescaled. These issues are discussed in the next section.

10.4.14. HISTOGRAM ORDINATE SCALING

If a constant bin width histogram is used, linear scaling of the ordinate is the most common (Figure 10.1 A). If a logarithmic bin width is used, several methods are common.

In one of the methods, the number of counts in each bin is divided by the bin width and plotted on a logarithmic axis, in which case multiple time constants are evident

(Figure 10.1 B). The main difficulty with this scaling is that the bins do not have the same weight during the fit process (Section 10.4.17., “*Fitting to Histograms*”), because the variance of the bin depends on the number of counts it contains. This can be compensated for using the transformation of Sigworth and Sine (1987). In this transformation the bin width is constant and the square root of the number of counts per bin is plotted on the ordinate, with time plotted logarithmically on the abscissa (Figure 10.1 C).

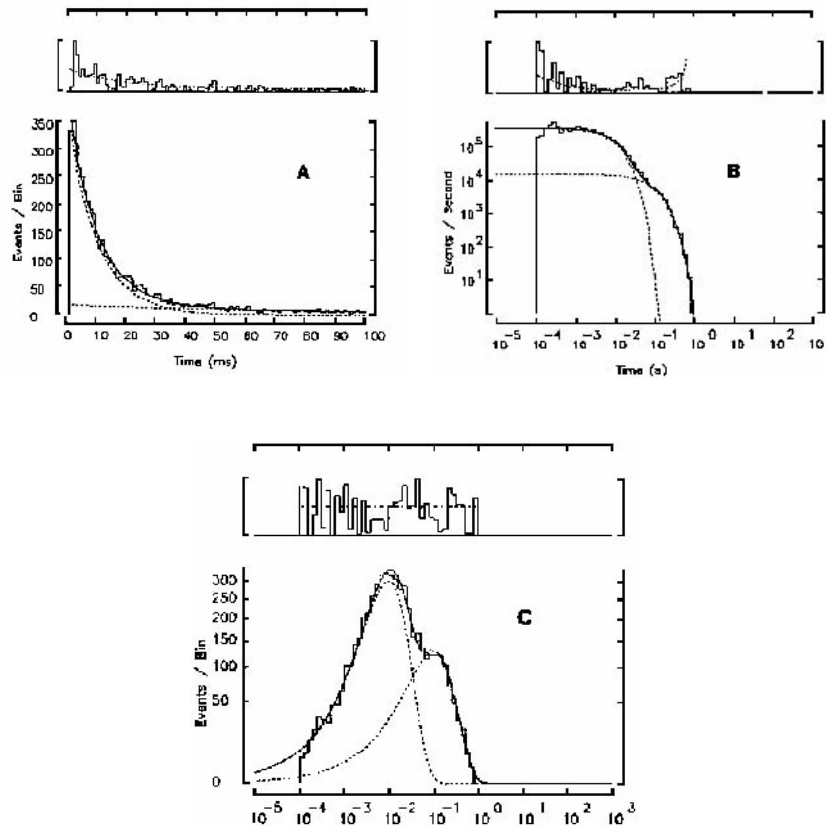


Figure 10.1: Histogram scaling.

Three representations of a dwell-time distribution with two exponential components. 5,120 random numbers were generated according to a distribution with time constants of 10 ms (70% of the events) and 100 ms (30%) and binned for display as histograms in the lower panel of each part of the figure. Superimposed are the theoretical probability density functions for each component (dashed curves) and their sum (continuous curve). In each part of the figure the upper panel plots the absolute value of the deviation of the height of each bin from the theoretical curve, with dashed curves showing the expectation value of the standard deviation for each bin. The upper panels were plotted with vertical expansion factors of 2.1, 5.4, and 3.1 respectively.

A. Linear histogram. Events are collected into bins of 1 ms width and plotted on a linear scale. The 100-ms component has a very small amplitude in this plot.

- B. Log-log display with variable-width (logarithmic) binning. The number of entries in each bin is divided by the bin width to obtain a probability density in events/s which is plotted on the ordinate.
- C. Square-root ordinate display of a logarithmic histogram. Note that the scatter about the theoretical curve is constant throughout the display (reproduced with permission from Sigworth and Sine, 1987).

10.4.15. ERRORS RESULTING FROM HISTOGRAMMING EVENTS DATA

Problems may appear as a result of the histogram process. The first problem may occur in either amplitude or time histograms if the bin size is not an integral multiple of the resolution of the signal. For a dwell time, the resolution is the interval between successive samplings of the ADC channel; for an amplitude, the resolution is determined by the gain and the ADC. The symptom is that occasional or periodic peaks or valleys appear artifactually in the histogram. This problem is less severe if the bin width corresponds to many resolution intervals (*e.g.*, 10). If bin widths are variable, the smallest bin width must likewise include many resolution intervals.

A second problem is called sampling promotion error. Sampling promotion error (Sine and Steinbach, 1986) occurs because data are sampled periodically. Suppose data were acquired with 1 ms sampling rate and dwell times binned into a histogram with bin width equal to the sampling rate (1 ms) and centered around 3 ms, 4 ms, 5 ms, *etc.* The 4 ms bin would therefore contain events whose true dwell times lie between 3 and 5 ms (Figure 10.2). If the dwell times fall exponentially with increasing times, the 4 ms bin would contain more events from 3 to 4 ms than from 4 to 5 ms. The subsequent fit would treat all these events as if they had occurred at 4 ms (the midpoint), thereby resulting in an error. In a single exponential fit, this affects only the intercept and not the time constant; but there may be more subtle effects in a multi-exponential fit. The error is small when the bin width is much smaller (perhaps by a factor of 5) than the fastest time constant present.

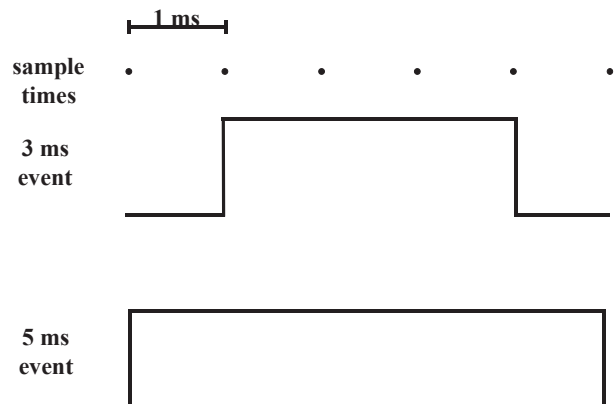


Figure 10.2: Sampling error.

Figure 10.2 illustrates how a 1 ms sampling rate can result in an apparent 4 ms open time for events of between 3 and 5 ms. The dots in the top part of the figure represent times when the signal is sampled. The lower part of the figure shows two events whose waveforms are high at 4 sample times.

A third problem is termed binning promotion error. In an exponentially falling dwell time distribution, a bin is likely to contain more events whose true dwell times are at the left side of the bin than are at the right side. The average dwell time of the events in that bin is therefore less than the midpoint time t . The error occurs when a fit procedure assumes that all the bin events are concentrated at a single point located at the midpoint t , instead of at the average, which is less than t . Binning promotion error can occur in addition to sampling promotion error because binning takes place in a different step. Both of these errors are due to the asymmetric distribution of true dwell times about the bin midpoint. A correction procedure has been proposed by McManus et al., (1987).

The degree of these bin-width-related errors may be reduced independently of the corrective procedures mentioned above, if the fit procedure explicitly uses the fact that a bin actually represents an area instead of an amplitude. Some errors may be eliminated if the individual data points are used without ever using a histogram, as in the maximum likelihood fitting method.

Lastly, as discussed in the section on missed events, short events may not be detected by the 50% threshold criterion. This can give rise to a number of errors in the extracted fit parameters, which relate specifically to state models. For further details, consult the references cited in French et al., 1990.

10.4.16. AMPLITUDE HISTOGRAM

Amplitude histograms can be used to define the conductances of states of single channels. Two kinds of amplitude histograms are common: point histograms and level histograms. The former use all the acquired data points; they are useful mainly for examining how “well-behaved” is a data set. Abnormally wide distributions may result from high noise if the signal were over-filtered, or if baseline drift had been significant. Similarly, the number of peaks will indicate the presence of multiple channels or subconductance states. The all-points histogram will probably not be useful for determining the conductances unless baseline drift is small. Level histograms use only the mean baseline-corrected amplitudes associated with each event in the events list. Such histograms can be fitted to the sum of one or more Gaussian functions in order to estimate conductances.

10.4.17. FITTING TO HISTOGRAMS

Amplitude and dwell time histograms can be fitted by appropriate functions, usually sums of several Gaussian functions for the former and sums of exponentials for the latter (see “*The Chi-Square Function (Least-Squares Method)*” on page 209). The time constants and amplitudes can be related to the parameters of several single-channel models, but this will not be described here.

Histogram bins containing zero counts should usually be excluded from a fit because the chi-square function (see below) is not defined when a bin i contains $N_i = 0$ counts and therefore has $\sigma_i = 0$. Alternatively, adjacent bins can be combined to yield a nonzero content.

10.5. FITTING

10.5.1. REASONS FOR FITTING

Fitting a function to a set of data points, such as a histogram or a time series, may be done for any of the following reasons:

- 1 A function could be fitted to a data set in order to describe its shape or behavior, without ascribing any “biophysical” meaning to the function or its parameters. This is done when a smooth curve is useful to guide the eye through the data or if a function is required to find the behavior of some data in the presence of noise.
- 2 A theoretical function may be known to describe the data, such as a probability density function consisting of an exponential, and the fit is made only to extract the parameters, (*e.g.*, a time constant). Estimates of the confidence limits on the derived time constant may be needed in order to compare data sets.
- 3 One or more hypothetical functions might be tested with respect to the data, *e.g.*, to decide how well the data were followed by the best fit function.

The fitting procedure begins by choosing a suitable function to describe the data. This function has a number of free parameters whose values are chosen in order to optimize the fit between the function and the data points. The set of parameters that gives the best fit is said to describe the data, as long as the final fit function adequately describes the behavior of the data. Fitting is best performed by software programs; the software follows an iterative procedure to successively refine the parameter estimates until no further improvement is found and the procedure is terminated. Feedback about the quality of the fit allows the model or initial parameter estimates to be adjusted manually before restarting the iterative procedure. Fitting by pure manual adjustment of the parameters (the so-called “chi by eye”) may be effective in simple cases but is usually difficult and untrustworthy in more complex situations.

The two following topics will be briefly discussed below: statistics, *i.e.*, how good is the fit and how confident is the knowledge of the parameters, and optimization, *i.e.*, how to find the best fit parameters. The statistical aspects are well discussed in Eadie et al., (1971); Colquhoun and Sigworth (1983) provide examples relevant to the electrophysiologist. A number of aspects of optimization are presented in Press et al., (1988).

10.5.2. STATISTICAL ASPECTS OF FITTING

Statistics deals with the probability of occurrence of events. Probability is difficult to define; there are two ways in which the word is used:

- 1 Direct probability: If we observe that N_1 of N single-channel events have open channel durations between 10 and 20 ms, we say that the probability p_1 of this occurring is N_1/N , as long as N is very large. The probability density function (pdf) is an algebraic expression that when summed or integrated between 10 and 20 ms gives the value of p_1 .
- 2 Inverse probability: If you are told by your physician that you have one of three possible diseases D_1 , D_2 or D_3 , and you ask what the probability is that you have D_2 , the physician might say, "It's either 0 or 1," meaning that either you already have D_2 or you do not have it, but the physician cannot yet determine which of these two situations exists. To be helpful, your physician might give an inverse probability of 0.6, meaning that if you had D_2 , the probability that your particular set of symptoms would have been observed is 0.6.

The Likelihood Function

Inverse probability is more appropriate for the scientist who may have N measurements of open channel durations and wants to know which time constant best describes their exponential distribution. For a particular time constant, τ_j , one can calculate the direct probability of getting those N observed durations by first calculating the probability of observing each duration and then multiplying these individual probabilities together. The resulting number is called the likelihood of the time constant τ_j . One could calculate the likelihoods for many such values of τ and plot the logarithm of these likelihoods versus their respective τ values (Figure 10.3). If N is sufficiently large, this curve will usually be Gaussian. The value τ^* at the peak of the function is called the maximum likelihood value of τ . The root-mean-square spread of the function about τ is known as the standard deviation of τ^* , though this is not the same as a standard deviation of a set of numbers in the direct probability case.

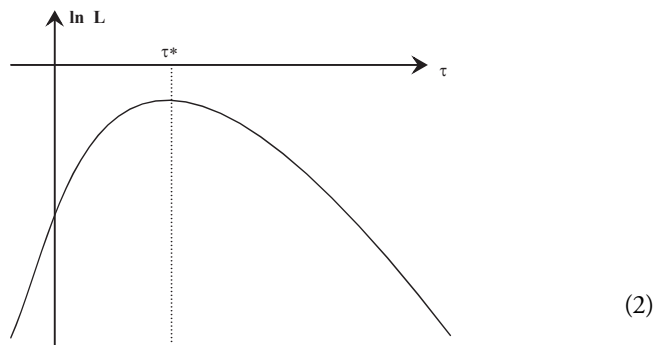


Figure 10.3: The likelihood function.

The logarithm of the likelihood presented as a function of variable τ ; the maximum likelihood of the function occurs at τ^* . For large numbers of samples, the shape of this curve approaches a Gaussian.

It turns out that τ^* reliably converges to the true time constant if the number of events N is sufficiently large. For this reason it is important to either collect a large enough number of data points or repeat the experiment several times so as to reduce the variation of the parameters obtained over the data sets to an acceptable level. If the noise is large or there are sources of significant variability in the signal, the data may be useless except in a qualitative way because of large variations of the best fit parameters between the runs. If one long run is taken instead of several smaller ones, the run can be broken up into segments and the analysis results of the segments compared with each other to assure that convergence is near.

Although the maximum likelihood method is the most reliable, the time requested for the calculations may be prohibitively long. The chi-square method, described below, is an alternative that requires less time.

The Chi-Square Function (Least-Squares Method)

Suppose that a set of p measurements are made at the times x_1, x_2, \dots, x_p , and that the values measured are y_1, \dots, y_p . If each y_i is measured with a measurement error distributed as a Gaussian with standard deviation $\sigma_1, \dots, \sigma_p$, the maximum likelihood method is equivalent to minimizing the chi-square function:

$$\chi^2 = \sum_{i=1}^p \frac{(y_i - y_i^*)^2}{\sigma_i^2}$$

where y_i^* is the fit value corresponding to y_i . Minimizing chi-square is also called the least-squares method. If the fit is made to a data sweep, each y_i is the value measured at the time x_i , and each σ_i is the standard deviation or uncertainty of that value. In the typical case when all the σ_i 's are equal (*i.e.*, the uncertainty in the data does not depend on the time), the σ_i 's can be ignored while performing the search for the best fit parameters, but must be specified if the goodness of fit is to be calculated. If the fit is made to a histogram, each y_i is the numbers of events N_i in bin i , and each σ_i is $\sqrt{N_i}$.

It is much easier to maximize the chi-square function than to minimize the likelihood function, whether for data or for many mathematical functions used as models.

Since the use of the chi-square function is equivalent to the use of the likelihood function only if the uncertainties in the data (*e.g.*, noise) are distributed as Gaussians, the correctness of a least-squares fit can depend on the characteristics of this uncertainty.

The Goodness of Fit

After a best fit has been obtained, the user might wish to know if the fit was good. If the fit to p data points employed M free parameters, the probability of obtaining a chi-square value greater than that of the best fit, given $p-M$ degrees of freedom, can be read from a table of probabilities of chi-square and compared to a chosen significance level.

Often several models are fitted to a single set of data so as to define the best-fit model. Horn (1987) discussed choosing between certain types of models using their respective chi-square values (with the F test) or the logarithm of the ratio of the likelihoods, which follows the chi-square distribution. These tests can help decide whether the model contains irrelevant parameters, *e.g.*, if a three-exponential function was fitted to a set of data containing only two exponentials.

Confidence Limits for the Parameters

An estimate of the confidence limits for each of the parameters is often useful. For a model with one parameter a , some fit programs will derive the standard deviation σ from the dependence of the likelihood or chi-square on the parameter. One then says that the 68.3% confidence limits are within a distance σ_a from a^* , the chosen value for a . This does not mean that 68.3% of the time the true value of a will fall between $a^* + \sigma_a$ and $a^* - \sigma_a$. It does mean that we will be right 68.3% of the time if we assert that these limits include the true a . In the limit of a large number of data sets, a^* will tend to converge to the true value of a .

Suppose there are two parameters a and b to be fit. One can make a two-dimensional contour plot of the likelihood or chi-square function, with each axis corresponding to one of the parameters, showing the probability of the limits including the true parameter values (Figure 10.4). The resultant ellipse is usually inclined at an angle to the parameter axes due to the correlation of the two parameters. These correlations tend to increase the confidence limits, which are indicated by the dotted lines which project to the respective axes. The probability that the confidence limits for the best fit a includes the true a is 0.683, but this does not specify anything about b , as indicated by the shaded region. If, in addition, limits $\pm\sigma_b$ are specified for the best fit b , the joint probability that both sets of confidence limits include the true a and b has an upper limit of $(0.683)^2$ or 0.393, *i.e.*, the probability content of the area inside the ellipse. If one has a five exponential fit with an offset, the analogous cumulative joint probability will be $(0.683)^{11}$, or 0.015, which is quite small.

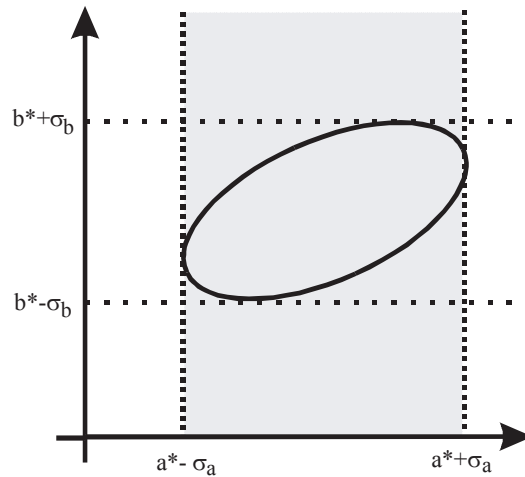


Figure 10.4: Confidence limits.

Two-dimensional contour plot of a likelihood or chi-square function vs. two parameters a and b around the function minimum, with the two sets of dashed lines indicating the respective confidence limits.

Statistical Tests of Significance for Parameters

If one wishes to compare, for example, two time constants from two data sets obtained under different conditions, one must first obtain the standard deviation of the time constant, usually derived from the fitting procedure. Conventional statistical tests, such as the chi-square table, the F test or Student's t test, can then be applied to determine significance.

10.5.3. METHODS OF OPTIMIZATION

Optimization methods are concerned with finding the minimum of a function (*e.g.*, the chi-square) by adjusting the parameters. A global minimum, *i.e.*, the absolute minimum, is clearly preferred. Since it is difficult to know whether one has the absolute minimum, most methods settle for a local minimum, *i.e.*, the minimum within a neighborhood of parameter values. A number of algorithms have been developed to find such a minimum. For example, to find time constants and coefficients in an exponential fit, pCLAMP software allows the user to choose between the following:

- Minimizing the chi-square using the Levenberg-Marquardt method.
- Minimizing the chi-square using the Simplex method.
- Maximizing the likelihood using the variable metric or Simplex method.

Of the three methods, the Simplex method is relatively insensitive to shallow local minima. Though it will reliably find the region of the global minimum or maximum, it may not find the precise location of the minimum or maximum if the function is rather flat in

that vicinity. The Levenberg-Marquardt method is more easily trapped in local minima of the function, but it can provide better fits than the Simplex because it uses the mathematical characteristics of the function being minimized to find the precise location of the minimum or maximum, within the numerical resolution of the computer. This method also provides statistical information sufficient to find the confidence limits.

These methods are iterative, *i.e.*, they continue refining parameter values until the function stops changing within a certain convergence criterion. They also require reasonable starting estimates for the parameters, so that the function to be minimized or maximized is not too far away from its optimum value; a poor starting set can lead some fit programs to a dead end in a shallow local minimum.

For Boltzmann and exponential fits, the Axon Cellular Neuroscience analysis program (Clampfit in the pCLAMP software suite) provides a non-iterative method, in which the data points and function to be fit are transformed using a set of orthogonal Chebyshev polynomials, and the fit function coefficients are quickly calculated using these transformed numbers in a linear regression. This method is very fast and requires no initial guesses, though the parameters may be slightly different than those found by the methods listed above because the underlying algorithm minimizes a quantity other than the sum of squared differences between fit and data.

10.6. REFERENCES

- Colquhoun, D. and Sigworth, F.J. Fitting and Statistical Analysis of Single-Channel Records. in *Single-Channel Recording*. Sakmann, B. and Neher, E., Eds. Plenum Press, New York, 1983.
- Colquhoun, D. and Hawkes, A.G. The Principles of the Stochastic Interpretation of Ion-Channel Mechanisms. in *Single-Channel Recording*. Sakmann, B. and Neher, E., Eds. Plenum Press, New York, 1983.
- Dempster, J. *Computer Analysis of Electrophysiological Signals*. Academic Press, London, 1993.
- Eadie, W.T., Drijard, D., James, F.E., Roos, M., Sadoulet, B. *Statistical Methods in Experimental Physics*. North-Holland Publishing Co., Amsterdam, 1971.
- Horn, R. Statistical methods for model discrimination. *Biophysical Journal*. 51:255–263, 1987.
- McManus, O.B., Blatz, A.L. and Magleby, K.L. Sampling, log binning, fitting, and plotting distributions of open and shut intervals from single channels and the effects of noise. *Pflügers Arch*, 410:530–553, 1987.
- Ogden, D.C. Microelectrode electronics. in *Microelectrode Techniques*. The Plymouth Workshop Handbook. Standen, N.B., Gray, P.T.A. and Whitaker, M.J., eds. The Company of Biologists Ltd., Cambridge, 1987.

Press, W.H., Flannery, B.P., Teukolsky, S.A. and Vetterling, W.T. Numerical Recipes in C. Cambridge University Press, Cambridge, 1988.

Sachs, F. Automated Analysis of Single-Channel Records. in Single-Channel Recording. Sakmann, B. and Neher, E., Eds. Plenum Press, New York, 1983.

Sigworth, F.J. and Sine, S.M. Data transformations for improved display and fitting of single-channel dwell time histograms. *Biophysical Journal*, 52:1047–1054, 1987.

Sine, S.M. and Steinbach, J.H. Activation of acetylcholine receptors on clonal mammalian BC3H-1 cells by low concentrations of agonist. *Journal of Physiology (London)*, 373:129–162, 1986.

Wonderlin, W.F., French, R.J. and Arispe, N.J. Recording and analysis of currents from single ion channels. in *Neurophysiological Techniques. Basic Methods and Concepts*. Boulton, A.A., Baker, G.B. and Vanderwolf, C.H., Eds. Humana Press, Clifton, N.J., 1990.

11. Noise in Electrophysiological Measurements

In the most general sense, noise can be defined as any disturbance that interferes with the measurement of the desired signal. In electrophysiological measurements, such disturbances can arise from the preparation itself, the electrodes that couple the preparation to the measurement instrument, the electronic instrumentation (*e.g.*, voltage-clamp amplifier, patch-clamp amplifier), interference from external sources (*e.g.*, electrostatic and electromagnetic coupling between the circuitry and 50 or 60 Hz power lines, fluorescent lights, video monitors, acoustic noise, and noise associated with mechanical vibrations), and, if the data is digitized (as is usually the case), from the digitization process itself (*e.g.*, quantizing noise, aliasing).

We will begin by discussing the basic noise mechanisms that arise from the physics of the materials and devices that comprise the electrical system. Interference from external sources and noise associated with digitization will be considered later.

The main fundamental types of noise are: thermal noise, shot noise, dielectric noise, and “excess” noise (*e.g.*, $1/f$ noise). These types of noise form the basis for a discussion of amplifier noise and electrode noise.

All the fundamental types of noise are completely random in nature. Their average properties can be measured, but their actual values at any particular instant in time cannot be predicted. The most convenient measure of the amplitude of noise is its root-mean-square (rms) value. Many noise processes have a Gaussian distribution of instantaneous amplitudes versus time. The area under the Gaussian distribution represents the probability that a noise event of a particular amplitude will occur (the total area is unity). The probability that a noise peak will exceed plus or minus one times its rms value is 0.32; the probability of a particular noise peak exceeding plus or minus three times its rms value is 0.003. It is common engineering practice to define peak-to-peak noise as 6 times the rms value; if the noise process has Gaussian distribution, the noise will remain within this bound 99.7% of the time. However, peak-to-peak noise is not as clearly defined as is rms noise, and it is not uncommon to find peak-to-peak noise operationally defined as anything from 5 times to 8 times rms.

When considering noise in the time domain, it is important to know the bandwidth over which the noise process is observed. Noise is made up of many frequency components,

frequently extending from DC to many megahertz or gigahertz. Some noise processes are naturally restricted in bandwidth, but most require the appropriate use of filtering to restrict the bandwidth of the noise while allowing adequate resolution of the signal. When a noise amplitude (rms or peak-to-peak) is discussed, it is appropriate to also note the bandwidth over which the noise is observed and the type of filter that has been used to restrict the bandwidth.

Due to the random nature of noise, uncorrelated noise sources will add in an rms fashion. Thus if E_1 , E_2 , and E_3 are the rms values of three uncorrelated noise sources, the total rms noise, E_T , of these sources together is given by:

$$E_T = \sqrt{E_1^2 + E_2^2 + E_3^2} \quad (1)$$

Because of this relationship, the largest individual source of noise will tend to dominate the total noise. For example, if two noise sources with rms values of $100 \mu\text{V}$ and $20 \mu\text{V}$ are added together, the resulting noise will have an amplitude of $\{(100 \mu\text{V})^2 + (20 \mu\text{V})^2\}^{1/2} = 102 \mu\text{V rms}$.

11.1. THERMAL NOISE

Thermal noise results from random motion of thermally excited charge carriers in a conductor. It is often referred to as Johnson noise or Nyquist noise. For a resistor, thermal noise can be represented as a series voltage noise source or a parallel current noise source as illustrated in Figure 11.1. These two representations are equivalent.

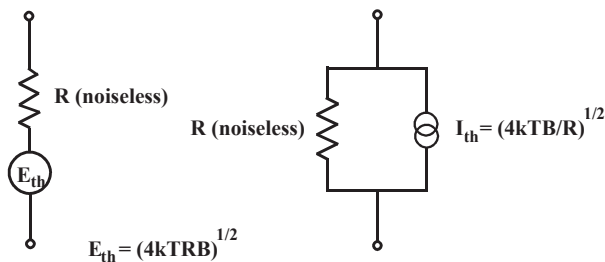


Figure 11.1: Noise equivalent circuits of a resistor.

The power spectral density (PSD) of thermal noise is white, *i.e.*, it does not vary with frequency. Its value, S_{thV}^2 , is given as a voltage noise by:

$$S_{thV}^2 = 4kTR(\text{units: Volt}^2/\text{Hz}) \quad (2)$$

or, equivalently, as a current noise PSD, S_{thI}^2 , by:

$$S_{thI}^2 = \frac{4kT}{R} \quad (\text{units: Amp}^2/\text{Hz}) \quad (3)$$

where k is Boltzmann's Constant (1.38×10^{-23} J/°K), T is the absolute temperature in degrees Kelvin ($^{\circ}\text{K} = ^{\circ}\text{C} + 273$), and R is the resistance in ohms. It should be noted that spectral densities are also often expressed in units of Volt/ $\sqrt{\text{Hz}}$ and Amp/ $\sqrt{\text{Hz}}$.

The variance (also called the noise power) over a bandwidth B (units: Hz) is then:

$$E_{th}^2 = 4kTRB \quad (\text{units: Volt}^2) \quad (4)$$

or

$$I_{th}^2 = \frac{4kTB}{R} \quad (\text{units: Amp}^2) \quad (5)$$

The rms noise over a bandwidth B is given by:

$$E_{th} = \sqrt{4kTRB} \quad (\text{units Volt rms}) \quad (6)$$

or:

$$I_{th} = \sqrt{\frac{4kTB}{R}} \quad (\text{units: Amp rms}) \quad (7)$$

Spectral densities, rms current and voltage noise for bandwidths of 1 and 10 kHz are listed in Table 11.1 for resistances of 100 Ω to 100 G Ω . Note that while thermal voltage noise increases with increasing resistance, thermal current noise decreases as the resistor's value increases.

Table 11.1: Thermal Noise of Resistors.

Resistance Value	1 kHz V noise ($\mu\text{V rms}$)	10 kHz V noise ($\mu\text{V rms}$)	1 kHz I noise (pA rms)	10 kHz I noise (pA rms)	Voltage Density (nV/ $\sqrt{\text{Hz}}$)	Current Density (pA/ $\sqrt{\text{Hz}}$)
100 Ω	0.040	0.126	400	1260	1.26	12.6
1 k Ω	0.126	0.40	126	400	4.0	4.0
10 k Ω	0.4	1.26	40	126	12.6	1.26
100 k Ω	1.26	4.0	12.6	40	40	0.4
1 M Ω	4.0	12.6	4.0	12.6	126	0.126
10 M Ω	12.6	40	1.26	4.0	400	0.040
100 M Ω	40	126	0.40	1.26	1260	0.0126
1 G Ω	126	400	0.126	0.40	4000	0.004
10 G Ω	400	1260	0.040	0.126	12600	0.0013
100 G Ω	1260	4000	0.013	0.040	40000	0.0004

11.2. SHOT NOISE

Shot noise arises when current flows across a potential barrier, *e.g.*, a *p-n* junction in a semiconductor device. Since potential barriers are not present in simple resistive elements, resistors do not display shot noise. Over a bandwidth B, the rms value of the shot noise current is given by:

$$I_{sh} = \sqrt{2qIB} \quad (\text{units Amprms}) \quad (8)$$

where q is the charge of the elementary charge carrier (for electrons $q = 1.6 \times 10^{-19}$ coulomb) and I is the DC current in Amps.

An important example of shot noise is the equivalent input current noise of an operational amplifier that arises from its input bias current I_b (also referred to as gate current for FET¹ input devices). For bipolar transistor input devices, I_b is typically in the range of 1 nA to 1 μA ; for FET input operational amplifiers, I_b (at room temperature) is typically in the range of 1 to 10 pA, and can be less than 0.5 pA for special devices. The rms value of shot noise for operational amplifiers with I_b ranging from 0.1 pA to 1 μA in a 1 and 10 kHz bandwidth are listed in Table 11.2. In capacitive-feedback patch voltage-clamp amplifiers (*e.g.*, the AxopatchTM 200 series amplifiers), shot noise current from the headstage amplifier sets the noise floor at low-to-moderate frequencies. By design these devices display very low levels of shot noise; selected units can have gate currents as low as 0.2 pA, resulting in low-frequency current noise less than that of a 250 G Ω resistor.

1. FET is Field Effect Transistor.

Table 11.2: Shot Noise.

Op Amp Bias Current	1 kHz Shot Noise (pA rms)	10 kHz Shot Noise (pA rms)
1 μ A	18	57
100 nA	5.7	18
10 nA	1.8	5.7
1 nA	0.57	1.8
100 pA	0.18	0.57
10 pA	0.057	0.18
1 pA	0.018	0.057
0.1 pA	0.0057	0.018

11.3. DIELECTRIC NOISE

An ideal lossless capacitor does not produce thermal noise. However, all real dielectric materials display some loss that results in the generation of thermal noise. For dielectrics with relatively low losses, the spectral density of this noise S_D^2 can be described in terms of the dissipation factor D and the capacitance CD of the dielectric:

$$S_D^2 = 4kTDC_D(2\pi f) \quad (\text{units: Amp}^2/\text{Hz}) \quad (9)$$

Where f is the frequency in Hz. The PSD of dielectric noise characteristically rises linearly with increasing frequency. The dissipation factor is often listed as $\tan \delta_e$ where δ_e is the loss angle (note that for small δ_e , $\tan \delta_e \approx \delta_e$); the “quality factor” Q is the inverse of D ($Q = 1/D$). For a bandwidth extending from DC to an uppermost cut-off frequency B, the rms noise current I_D , resulting from a lossy dielectric, is given by:

$$I_D = \sqrt{4kTDC_D\pi B^2} \quad (\text{units: Amp rms}) \quad (10)$$

For the best solid dielectrics (*e.g.*, quartz, sapphire and some ceramics), D is on the order of 10^{-5} to 10^{-4} . For poorer (lossier) dielectrics D can be much higher; *e.g.*, some thermo-setting plastics have D in the range of 0.01 to 0.1. For some glasses used to fabricate patch pipettes, D is at least 0.01. The dissipation factor has some frequency dependence, although in the important range from about 1 kHz to 100 kHz it is usually reasonable to approximate it as a constant. D also shows some temperature dependence (typically decreasing with lower temperatures), although again in the usual range of temperatures it may be considered constant.

Dielectric noise is one consideration in the selection of feedback and compensation capacitors in capacitive-feedback headstages for patch clamping. It must also be considered in the packaging materials, electrode holders, *etc.* for any high-sensitivity current or charge

amplification device. By using high-quality capacitors ($D \leq 0.0001$) the dielectric noise of the feedback and compensation capacitor can be made a relatively insignificant component of the total noise of present day capacitive-feedback headstages. For example, using equation (10) it can be estimated that for $D = 0.0001$ and $C_D = 2$ pF (1 pF feedback capacitor and 1 pF compensation capacitor), the dielectric noise of these components in a 10 kHz bandwidth is only about 0.032 pA rms. Dielectric noise associated with packaging (*i.e.*, with the input gate lead of the patch-clamp headstage) can be somewhat higher. The most important source of dielectric noise in common electrophysiological measurements is the dielectric noise of the glass used to fabricate pipettes for patch voltage clamping. This subject will be considered in greater detail below (see Section 11.6., “*Electrode Noise*”). It is worth noting that a dielectric does not actually have to be in contact with the input of a sensitive current amplifier, such as a patch-clamp headstage, in order to produce noise. For example, a 1 pF capacitor formed by a high-loss dielectric with $D = 0.1$ that is coupled through air to the input by a capacitance of 1 pF can result in approximately 0.35 pA rms in a 10 kHz bandwidth. Thus it is a good idea both in the design of headstage electronics and of an experimental patch clamp set-up not to have exposed, high-loss dielectrics in the immediate vicinity of the input.

11.4. EXCESS NOISE

Excess noise can broadly be defined as any noise that is present in a circuit element in addition to the fundamental noise mechanisms already described. For example, in the presence of direct current all resistors exhibit low-frequency noise whose power spectral density varies inversely with frequency. This noise is present in addition to the thermal noise of the resistor and is usually referred to as “ $1/f$ noise.” Different resistor types display different amounts of $1/f$ noise, with metal film and wirewound types showing the least excess low-frequency noise and carbon composition resistors showing the most. The PSD (in V^2/Hz) of this excess noise rises with decreasing frequency essentially as $1/f$. Its magnitude is directly proportional to the DC current flowing through the resistor. Semiconductor devices also exhibit $1/f$ noise.

High-value (gigohm range) resistors, such as those used as the feedback element in resistive-feedback patch-clamp headstages, also display a form of excess noise that rises with increasing frequency. Generally, such resistors only achieve their thermal noise level (which is the minimum possible) in the frequency range from about 10 Hz to 1 kHz. At low frequencies, $1/f$ noise is observed, and at high frequencies the noise PSD typically rises as f^α , where α is usually in the range of 1 to 2. This noise can result in rms noise from a resistor having several times the predicted thermal noise value in a 10 kHz bandwidth. The elimination of this noise source is one of the motivations behind using capacitive-feedback in patch clamps such as the Axopatch 200 series amplifiers.

11.5. AMPLIFIER NOISE

The intrinsic noise of an operational amplifier can be described by an equivalent input voltage noise E_n in series with the negative (-) input and an equivalent input current noise I_n between the positive (+) and negative (-) inputs (see Figure 11.2). These noise sources have been referred to the input for convenience of analysis. It should be noted, however, that they are measured at the output. For example, in an open-loop situation (such as shown in (Figure 11.2), if the inputs are grounded, the voltage at the negative (-) input will be zero (ground). E_n must be inferred by measuring the output noise voltage and dividing it by the open-loop gain (both are frequency dependent) of the amplifier. On the other hand, in a closed-loop situation (which is always the case when using operational amplifiers, as illustrated in Figure 11.3), E_n will actually appear at the negative (-) input due to the action of the feedback loop.

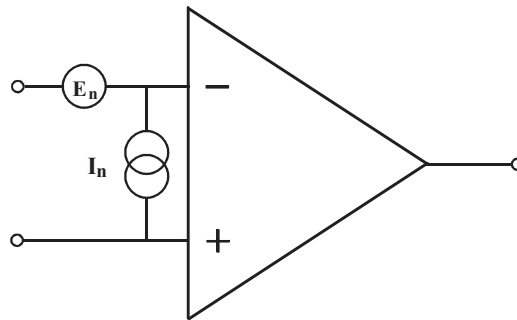


Figure 11.2: Operational amplifier noise model.

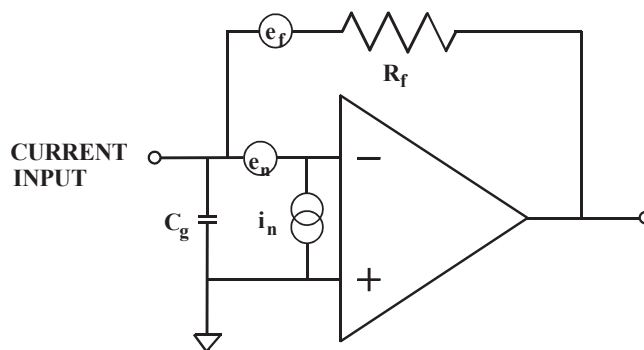


Figure 11.3: Noise model of a simplifier current-to-voltage converter.

When analyzing the noise of an operational circuit it is convenient to consider the noise sources in terms of their power spectral densities. In this case the noise sources will be denoted by lower case symbols, *e.g.*, $e_n(f)$ (units: $V/\sqrt{\text{Hz}}$) or $e_n^2(f)$ (units: V^2/Hz). As a useful example of noise analysis in an operational circuit, consider the simplified current-to-voltage converter illustrated in Figure 11.3. In this circuit e_n and i_n are the input voltage and current noise PSDs, respectively, and e_f is the PSD of the noise (thermal and excess) of the feedback resistor R_f . The current to be measured is introduced at the terminal labeled “input.” For simplicity, the positive (+) input is shown to be grounded. C_g is any capacitance between the negative (-) input and ground; this includes the input capacitance of the amplifier plus strays and is usually about 15 pF. The noise PSD at the output of the IV converter, $S_{out}^2(f)$, can be shown to be:

$$S_{out}^2(f) = i_n^2 R_f^2 + e_f^2 + e_n^2 (1 + 4\pi^2 f^2 R_f^2 C_g^2) \quad (\text{units: } V^2/\text{Hz}) \quad (11)$$

It is useful to present this result in terms of current so it can be compared directly with the current signal being measured. This is accomplished by dividing the above expression by R_f^2 , thus referring the noise to the input. The input referred PSD, $S_{in}^2(f)$, is then given by:

$$S_{in}^2(f) = i_n^2 + \frac{e_f^2}{R_f^2} + e_n^2 \left(\frac{1}{R_f^2} + 4\pi^2 f^2 C_g^2 \right) \quad (\text{units: } \text{Amp}^2/\text{Hz}) \quad (12)$$

In general, i_n , e_n and e_f are all functions of frequency: i_n is the shot noise of the input gate current of the amplifier but usually displays some $1/f$ behavior at low frequencies; e_f is the thermal and excess noise of R_f and e_n also displays $1/f$ behavior at low-to-moderate frequencies. Nevertheless, it is convenient to assume that each of these terms is independent of frequency so that equation (12) can be easily integrated over a frequency band (for instance, DC to some uppermost bandwidth denoted by B). The square root of this result is then the rms noise for the bandwidth B:

$$I_{in} = \sqrt{i_n^2 B + \frac{e_f^2}{R_f^2} B + e_n^2 \frac{B}{R_f^2} + \frac{4}{3} \pi^2 C_g^2 B^3} \quad (13)$$

It should be noted that if it is assumed that e_f is only the thermal noise of the feedback resistor, then the term e_f^2/R_f^2 is simply $4kT/R_f$ (see equation (3) above).

It is instructive to consider the relative magnitudes of the various terms in equation (12) or (13). In the case of a patch voltage clamp, the value of R_f is selected to be very high,

both to provide adequate gain to resolve tiny (pA) currents and to minimize the noise contribution of this resistor; 50 G Ω is common for single-channel recording. The PSD of the thermal noise of an ideal 50 G Ω resistor is 3.2×10^{-31} Amp²/Hz and the rms noise associated with such a component over a bandwidth of 10 kHz is 0.057 pA rms (although as already noted, excess high-frequency noise can increase this value several fold). The shot noise, which accounts for i_n , associated with an input gate current of 0.2 pA would, by itself, produce noise of about 0.025 pA rms in a 10 kHz bandwidth. For a typical high-quality patch-clamp headstage, e_n is about 2–3 nV/ $\sqrt{\text{Hz}}$ at frequencies above about 1 kHz; C_g is usually about 15–20 pF. With these values, the term $(\frac{4}{3}\pi^2 e_n^2 C_g^2 B^3)^{1/2}$ amounts to roughly 0.15 pA rms in a 10 kHz bandwidth. These three terms should be uncorrelated; therefore, they sum in an rms fashion so that the total predicted noise is $(0.057^2 + 0.025^2 + 0.15^2)^{1/2} = 0.162$ pA rms. For a resistive-feedback headstage, actual noise in a 10 kHz bandwidth is normally substantially higher (about 0.25–0.30 pA rms) both because of excess noise from the feedback resistor and because of the characteristics of the low-pass filters that do not abruptly cut off noise at the -3dB bandwidth (Section 11.12., “Filtering”). Nevertheless, it is important to note that for bandwidths above a few kilohertz, the term arising from e_n and C_g dominates total noise. To intuitively understand the origin of this term, it is only required to remember that the current through a capacitor is directly proportional to the rate of change of voltage across the capacitor ($I = C(dV/dt)$). Therefore, the voltage noise at the negative (-) input of the amplifier produces current noise through the capacitor C_g . This noise increases with increasing frequency simply because higher frequency components of the voltage noise involve more rapidly changing voltages. The noise current through the capacitor is supplied by the feedback resistor and therefore appears as noise at the amplifier output.

11.6. ELECTRODE NOISE

Noise associated with recording electrodes is significant and often dominant in most electrophysiological measurements. In microelectrode voltage clamps and the whole-cell variant of the patch voltage-clamp technique, the thermal voltage noise of the electrode is of greatest importance since this noise will exist across the cell membrane and produce large levels of current noise in conjunction with the membrane capacitance. In patch single-channel measurements using the patch clamp, the voltage noise of the electrode is also important; but here the situation is further complicated by such factors as the dielectric noise of the pipette that produces a major source to overall noise. We will consider noise associated with the electrode in single-channel recording and whole-cell patch recording separately, beginning with the single-channel recording.

11.6.1. ELECTRODE NOISE IN SINGLE-CHANNEL PATCH VOLTAGE CLAMPING

There are a variety of mechanisms by which the patch pipette contributes noise to the measured current in the patch voltage-clamp technique. The first mechanism we will consider here is the fact that the holder plus pipette add a significant amount of capacitance to the headstage input. This capacitance reacts with the input voltage noise, e_n , of the

headstage amplifier to produce current noise with a PSD that rises with frequency in essentially the same fashion as the PSD of the open-circuit headstage. In fact, this noise is perfectly correlated with the noise resulting from the intrinsic capacitance, C_{in} , associated with the headstage input. Note that C_{in} consists of the input capacitance of the JFET ($C_{iss} = C_{gs} + C_{gd}$, where C_{gs} is the gate-source capacitance and C_{gd} is the gate-drain capacitance), plus any compensation capacitors connected to the input, plus, for a capacitive-feedback headstage, the feedback capacitor (1 pF for the Axopatch 200 amplifier) and capacitance associated with the reset switch, plus about 1–2 pF of stray capacitance: in total, C_{in} is usually about 15 pF. Denoting the holder plus electrode capacitance as C_{he} , the PSD of the current noise arising from e_n is given by $4\pi^2 e_n^2 (C_{in} + C_{he}) f^2$. The capacitance of the holder can vary from about 1–5 pF; larger capacitances are associated with holders with metallic shielding. The pipette capacitance depends on the depth of immersion of the pipette, the type of glass used, the thickness of the pipette wall, and the use of Sylgard coating. The total capacitance of the pipette will generally be in the range of 1–5 pF. Thus, C_{he} can range from 2–10 pF. With $C_{he} = 2$ pF, the increment in wideband noise from this mechanism above that of the open-circuited headstage should not be much more than 10%. However, with $C_{he} = 10$ pF the noise increment could be more than 50% from this mechanism alone. Obviously, from the point of view of noise, it is important to minimize the capacitance of the holder and pipette.

Dielectric Noise

The basic characteristics of dielectric noise have already been described above (see equations (9) and (10)). Dielectric noise of the pipette can be a major contributor to total noise in patch voltage clamping; in some situations it can be the dominant noise source. The dielectric noise arising from the pipette depends on the dissipation factor D of the glass used to fabricate the pipette, on the pipette capacitance (C_D in equations (9) and (10)), and on the presence of Sylgard coating. The dissipation factor D of glasses other than quartz that have been successfully used for patch pipettes generally falls in the ranges of 0.001–0.01. The dissipation factor for quartz is variously reported to be 10^{-5} to as much as 4×10^{-4} . For Amersil T-08 quartz, which has been used in all of the preliminary tests of quartz pipettes described below, the reported dissipation factor is 10^{-4} . For uncoated pipettes the value of C_D is determined by the dielectric constant ϵ of the glass, the ratio of the outer diameter (OD) to the inner diameter (ID) of the pipette, the depth of immersion of the pipette into the bath, and to some extent by the pulling characteristics of the glass and the geometry near its tip. The dielectric constant ranges from as little as 3.8 for quartz to more than 9 for some high-lead glasses. Typical glass capillaries used in the fabrication of patch pipettes have an OD of 1.65 mm and an ID of 1.15 mm; thus $OD/ID \approx 1.43$. If it is assumed that these proportions ($OD/ID = 1.43$) are maintained as the glass is drawn out in pulling, then for uncoated pipettes the value of C_D will be approximately 0.15ϵ pF per mm of immersion into the bath. For thick-walled glass with $OD/ID = 2$, this value would fall to 0.08 pF per mm of immersion; while for thin-walled glass with $OD/ID = 1.2$ the capacitance would increase to about 0.30ϵ pF per mm.

Actual measurements with uncoated or lightly Sylgard-coated pipettes fabricated from glasses with known ϵ and immersed to a depth of 2–3 mm indicate that these values often

underestimate pipette capacitance; therefore, the dielectric noise is also underestimated. This is probably due to non-uniform thinning near the tip and to some uncertainty as to the true depth of immersion (due to a meniscus of solution around the pipette). For example, using the popular Corning 7052 glass, which has $\epsilon = 4.9$ and with $OD/ID \approx 1.43$, it is not uncommon to measure a pipette capacitance as high as ≈ 3 pF, *i.e.*, about twice the predicted value, when an uncoated pipette or a pipette very lightly coated with Sylgard is immersed at a depth of 2 mm.

Despite this precautionary note, it is clear that, all else being equal, the value of C_D varies linearly with the dielectric constant ϵ of the glass. Equation (10) indicates that if the depth of immersion and the OD/ID ratio are constant, the rms noise for a given bandwidth arising from the lossy dielectric characteristics of pipettes fabricated from various glasses will be proportional to $(D\epsilon)^{1/2}$. Thus the lowest noise glasses are expected to be those that minimize the product of the dissipation factor and the dielectric constant. This relationship has been born out experimentally in tests of some 20 different types of glass used to fabricate patch pipettes (Rae and Levis, Personal Communication).

To illustrate the range of results expected for different glass types, we will consider three pipettes with identical geometry fabricated from three different glasses. It will be assumed that $OD/ID \approx 1.4$, $C_D = 0.2 \epsilon$ pF per mm of immersion, the immersion depth is 2 mm, the pipettes are uncoated or are coated very lightly with Sylgard (so that the coating does not reduce the dielectric noise significantly), and the rms noise is measured at a 10 kHz bandwidth (-3 dB, 8-pole Bessel filter). Corning 7052 glass ($D \approx 0.003$ and $\epsilon \approx 5$) represents reasonably low-loss glasses used to fabricate patch pipettes. Under the above stated conditions, the C_D value of this pipette is 2 pF and the dielectric noise contribution predicted by equation 10 is about 0.17 pA rms, or about 0.2 pA rms if the characteristics of an 8-pole Bessel filter are taken into account. On the other hand, 0080 soda lime glass ($D \approx 0.01$, $\epsilon \approx 7$) represents high-loss glasses, which were commonly used in the early days of patch clamping. Its $C_D = 2.8$ pF and dielectric noise of about 0.44 pA rms is predicted. Finally, Corning 7760 is a very low-loss glass with $D \approx 0.0017$ and $\epsilon \approx 4.5$. With $C_D = 1.8$ pF, a dielectric noise of slightly less than 0.15 pA rms is predicted. These figures are in reasonable agreement with experimental findings that have attempted to separate the components of total noise arising from the dielectric noise of pipettes fabricated from various glasses.

Since the capacitance C_D increases approximately linearly with increasing depth of immersion, the dielectric noise for any particular type of glass and OD/ID ratio should vary approximately as the square root of the depth immersion. From the point of view of noise reduction, it is clearly useful with excised patches to withdraw the pipette tip as close to the surface of the bath as possible. If the patch cannot be excised, then the bath should be as shallow as possible. For example, for a pipette fabricated from Corning 7760, as in the previous example, dielectric noise is expected to decrease from about 0.15 pA rms in a 10 kHz bandwidth for a 2 mm immersion depth to roughly 0.05 pA rms for a 0.2 mm immersion depth. The effect of immersion depth on pipette noise has, at least qualitatively, been verified experimentally. A method employing Silicone fluid to minimize the

effective pipette immersion depth was introduced by Rae and Levis (1992) and is described below.

The above discussion dealt with expected behavior for uncoated pipettes. However, it is common practice (and highly recommended for low-noise measurements) to apply a coating of Sylgard #184 covering the entire tapered region of the pipettes (*i.e.*, approx. 5–10 mm) and extending to within roughly 100 μm of the tip (see Chapter 4). Coating with a hydrophobic substance such as Sylgard is necessary to prevent the formation of a thin film of solution that will creep up the outer wall of an uncoated pipette. Such a film can produce very large amounts of noise in uncoated pipettes. Sylgard coating not only virtually eliminates this noise source but also thickens the wall of the pipette thereby reducing its capacitance. The dielectric constant of Sylgard #184 is 2.9 and its dissipation factor is ≈ 0.002 , which is lower than that of most glasses that have been used for patch pipette fabrication. Thus, coating with Sylgard will reduce dielectric noise of patch pipettes. It is expected that the improvement in noise associated with Sylgard coating will be greatest for glasses with a high D product (*e.g.*, soda lime glass); this has been confirmed experimentally. Improvement of noise should be less for glasses with very low values of D , but coating with Sylgard will reduce the dielectric noise of all glasses. The effects of Sylgard coating on noise are, however, difficult to quantify theoretically primarily because the thickness of the coating is usually not uniform. In particular, it is difficult to achieve a very thick coating very near the tip.

Experimental tests of the noise properties of patch pipettes fabricated from 19 different kinds of glass (see Chapter 4) have confirmed the general conclusions described above. With few exceptions, the noise attributable to the pipette is inversely correlated with the D product of the glass. In addition, thicker-walled pipettes and shallow depths of immersion reduce noise for any particular glass type. Sylgard coating has its greatest effect on the glasses with the poorest inherent electrical properties, but it is important to remember that such coating is necessary for all types of glass.

It has been obvious for some time that pipettes fabricated from quartz should produce only very small amounts of dielectric noise due to the low dielectric constant of quartz ($\epsilon = 3.8$) and, more importantly, its extremely low dissipation factor ($D \approx 10^{-5} - 10^{-4}$). However, due to the high melting point of quartz (≈ 1600 °C), only with the advent of automated laser pullers has it become practical to pull patch pipettes from quartz tubing. A quartz pipette with $D = 10^{-4}$ that is immersed to a depth of 2 mm (again assuming 0.2 ϵ pF per mm of immersion) would be predicted to produce only about 0.03 pA rms of dielectric noise in a bandwidth of 10 kHz (-3 dB, 8-pole Bessel filter); for $D = 10^{-5}$ this value would fall to 0.01 pA rms. Preliminary measurements using Amersil T-08 quartz suggest that the amount of dielectric noise in this situation is closer to 0.04–0.05 pA rms. A more detailed discussion of preliminary estimates of the noise properties of quartz pipettes is provided below.

Dielectric noise is probably the largest source of noise for pipettes fabricated from all glasses other than quartz. For pipettes fabricated from quartz, due to its very low dissipa-

tion factor, sources of noise other than dielectric noise are expected to dominate total pipette noise (“*Noise Properties of Quartz Patch Pipettes*” on page 230).

To summarize, dielectric noise can be minimized by using thick-walled glasses with low values of D and coating the pipette with Sylgard #184. The effects of Sylgard coating are greatest for glasses with relatively poor electrical properties. For excised patches, dielectric noise can be minimized by withdrawing the tip of the pipette as close as possible to the surface of the bath.

It should be noted that dielectric noise will also contribute to the noise associated with the holder. For an Axopatch 200A amplifier with an open circuit noise of 0.06 pA rms in a 5 kHz bandwidth, total noise should not increase to more than about 0.07 pA rms in this bandwidth when the Axon-supplied polycarbonate holder is attached. Part of this noise increment is due to the fact that the holder adds about 1–1.5 pF of capacitance to the headstage input. The rest of the increment in noise associated with the holder is presumably dielectric noise, which can be estimated to account for roughly 0.03 pA rms in a 5 kHz bandwidth.

Noise Arising From Distributed Pipette Resistance and Capacitance

Most of the resistance of a patch pipette resides at or very near its tip. On the other hand, the capacitance of an uncoated pipette can be expected to vary linearly with its depth of immersion into the bath. Therefore, it has sometimes been assumed that current noise arising from the thermal voltage noise of the pipette resistance in conjunction with the pipette capacitance can be assumed to be negligible in comparison with other noise sources. However, significant resistance resides in regions of the pipette that are further removed from the tip. The thermal voltage noise of this resistance will greatly exceed the input voltage noise of the headstage itself, with which it is in series. The actual situation is complicated because both the pipette resistance and capacitance are distributed. In this section we will consider the pipette capacitance to be lossless, and initially the effects of Sylgard coating will not be considered. In order to estimate the noise arising from the distributed pipette resistance and capacitance, we will consider rather idealized pipette geometry.

The pipette has been modeled as a shank and a conical region approaching the tip; the angle of the cone is 11.4° and the tip opening is 1 μm in diameter. With this cone angle the ID of the pipette increases to 100 μm at a distance of 0.5 mm from the tip, 200 μm at a distance of 1 mm from the tip, 300 μm at a distance 1.5 mm from the tip, *etc.* When filled with a solution with a resistivity of 50 $\Omega\text{ cm}$ the pipette will have a total resistance of about 3.2 M Ω . About 2.1 M Ω of this total resistance resides in the first 10 μm from the tip; slightly more than 3 M Ω occurs in the first 100 μm from the tip. However, about 80 k Ω resides in the region from 100–200 μm from the tip, an additional 27 k Ω resides in the region from 200–300 μm ; and about 37 k Ω occurs in the region from 300 μm to 1 mm from the tip. The region from 1–4 mm from the tip adds another 12 k Ω . It has been assumed that the capacitance is uniformly distributed along the pipette with a value of 1 pF/mm of immersion. An Ag/AgCl wire extends into the pipette coming to within

4 mm of the tip and it is assumed that the resistance of the pipette is negligible beyond the tip of the wire (due to the shunting effect of the wire). A noise equivalent circuit of the pipette can be created by lumping the resistance and capacitance of each small segment (*e.g.*, 20–50 μm) of pipette. The approximate circuit is then a ladder network formed of a series of resistors and their equivalent thermal voltage noise sources with a capacitor to ground at each node representing a portion of the pipette immersed in the bath. Rough calculations with such an equivalent circuit indicate that for a depth of immersion of 2 mm the noise arising from this mechanism will be about 0.13 pA rms in a 10 kHz bandwidth. For a 1 mm depth of immersion this value would fall to about 0.10 pA rms. For an idealized pipette identical to the one described here but with a cone angle of 22.6° (total resistance is about $1.6\text{ M}\Omega$) these values fall to about 0.07 pA rms for a 2 mm depth of immersion and about 0.05 pA rms for a 1 mm depth of immersion, both for a 10 kHz bandwidth. Over the frequency range of interest to patch voltage clamping, the PSD (Amp^2/Hz) of this noise should rise with increasing frequency as f^2 .

These calculated values are highly approximate and the assumed geometry is obviously an over-simplification. A variety of factors could increase the noise arising from this mechanism. For example, the noise should increase if there is an extended region behind the tip where the angle of taper is quite shallow, resulting in increased resistance in this region. Noise will also increase if the wire does not protrude as close to the tip as assumed above. In addition, some glasses tend to thin near the pipette tip, resulting in increased capacitance in this region. It should also be noted that shallow depths of immersion would not decrease this noise quite as much as might be expected since this would decrease the pipette capacitance, but not its resistance.

The noise from this mechanism can be reduced in several ways. From the above estimates it seems that noise arising from the distributed resistance and capacitance of the pipette should be smaller than the dielectric noise of pipettes fabricated from even the best known glasses. Nevertheless, with better (lower loss) glasses, particularly quartz, this mechanism could be the dominant source of noise from the pipette itself, and its reduction may become important. First, it is obvious that the geometry of the first few millimeters of the pipette will be an important determinant of the magnitude of this noise; therefore, when possible, pipettes should be pulled to minimize the resistance distal to the tip. Anything that reduces the pipette capacitance per unit length will also reduce this noise. Thus, thick-walled pipettes and glasses with low dielectric constants should provide the best results in terms of noise. Perhaps of more practical importance, coating the pipette with Sylgard #184 can significantly reduce the pipette capacitance, and consequently reduce noise of the type considered here. However, as already noted, it is more difficult to build up a thick coat of Sylgard in the region within the first few hundred micrometers from the tip than in more distant regions. As was the case with dielectric noise, shallow depths of immersion will also reduce the noise arising from pipette resistance and capacitance. Finally, it should also be possible to reduce this noise regardless of the immersion depth by using a fine wire (Ag/AgCl or platinized Ag/AgCl possibly sharpened at the tip) that protrudes as far as possible toward the tip of the pipette. Such a wire will, in effect, short out (in a frequency-dependent fashion) the resistance of the pipette-filling solution in the

region into which it extends; thus, while the pipette capacitance will be unaltered for any given depth of immersion, its resistance up to the end of the wire would be significantly reduced.

In 1992, Rae and Levis have introduced a technique that has been shown to minimize pipette noise arising from all of the mechanisms discussed above. In this technique, the surface of the bathing solution was covered with a layer of Silicone oil (#200 Fluid from Dow Corning, Midland, MI). With excised patches it was then possible to raise the tip of the electrode to within a few micrometers of the saline-oil interface; a sharp line of demarcation could be observed along the pipette at this interface. The electrical characteristics of this oil are apparently quite good², so that only the tip of the pipette that remains in saline appears to contribute to total noise. If 10 μm of the pipette tip remain in saline, it would be expected that the capacitance associated with this length should be roughly 0.01 pF. Dielectric noise associated with the immersed portion of the pipette should be about one tenth of the values predicted for a 1 mm depth of immersion. It should be reasonable to approximate distributed R-C noise in this situation by a lumped resistance equal to the resistance of the pipette other than that arising from the tip itself in series with approximately 0.01 pF. If this resistance is taken to be 2.5 M Ω , the expected noise is only about 7 fA rms in a 10 kHz bandwidth; even for 10 M Ω it is less than 15 fA rms in this bandwidth. The noise increment associated with the pipette capacitance and the headstage input voltage noise is also minimized in this arrangement since the capacitance remains essentially the same as that with the electrode in air. It should also be noted that even when patches cannot be excised, this approach can still be effective if the bath is designed so that the solution level can be lowered, thereby bringing the layer of silicone fluid very close to the cell surface.

Using quartz pipettes with this technique has resulted in noise levels in actual recording situations as low as 0.08 pA rms in a 5 kHz bandwidth (4-pole Butterworth filter). For these experiments, the Axopatch 200A amplifier was used with an open-circuit headstage noise of 0.057 pA rms in a 5 kHz bandwidth; with the holder and electrode attached, but with the electrode tip in air, noise typically increased to about 0.07 pA rms in this bandwidth. In several experiments it was shown that the total noise closely approximated the rms sum of the noise of the headstage plus holder/electrode (electrode in air) and the thermal current noise of the measured DC seal resistance. This implies that dielectric noise and “distributed R-C noise” of the pipette contributed only a negligible amount to total noise in this situation. Rae and Levis (1993) showed that quartz pipettes can be fabricated with the Sutter Instrument P-200 laser-based puller to yield lower noise than they previously achieved, obviating the need for Silicone oil.

Preliminary tests have also been made using this technique with pipettes fabricated from two other types of glass (Corning 7760, Kimble KG-12). Although the noise reduction

2. Although the dielectric characteristics of the specific Silicone fluid used in these experiments is not available, Table 2.5 of *Electronics Designers' Handbook* (1977, L. Giacoletto ed., McGraw-Hill) lists a dissipation factor (D) of 8.5×10^{-5} at 1 kHz and 2×10^{-5} at 100 kHz for Silicone fluid (methyl- or ethyl-siloxane polymer); the dielectric constant ϵ is 2.68.

was significant, results were never as good as those achieved with quartz. For example, the best results achieved with KG-12 were slightly more than 0.10 pA rms in a 5 kHz bandwidth, even when seal resistances in the range of 50–100 G Ω were obtained. For a total noise of 0.105 pA rms, and assuming that the headstage plus holder/electrode in air produced 0.075 pA rms and that a 50 G Ω seal produces 0.04 pA rms, all in a 5 kHz bandwidth, the pipette would be estimated to contribute about 0.06 pA rms in this bandwidth. On the basis of the above discussion, this is several times the amount of noise expected for a pipette fabricated from this glass with 10 μ m of its tip in saline. One possible explanation of at least part of this discrepancy would be to assume that the glass had thinned excessively near the tip. It is also possible that the noise attributed to the seal in arriving at this estimate is too low. More work will be needed to clarify this issue.

Noise Properties of Quartz Patch Pipettes

Since 1991, it is now possible to routinely fabricate patch pipettes from quartz using the Model P-2000 puller from Sutter Instrument Company (Novato, CA). This puller uses a laser to overcome the extremely high melting temperatures needed to draw pipettes from quartz tubing. Preliminary results were made using Amersil T-08 quartz pipettes although, it was difficult to pull small-tipped blunt pipettes with 1.65 mm OD 1.15 mm ID tubing. Pipettes fabricated from this tubing typically had a rather long and relatively narrow shank. This geometry is not ideal for the lowest possible noise. Even so, these pipettes produced significantly less noise than pipettes fabricated from the best glasses used previously (*e.g.*, 7760, 8161). In actual recording situations with pipettes immersed about 3 mm into the bath and with seal resistances \geq 50 G Ω , rms noise in a 5 kHz bandwidth was typically about 0.12–0.13 pA rms using an Axopatch 200A amplifier. Estimates of the contribution of the pipette to this noise were in the range of 0.075–0.09 pA rms in this bandwidth. With the new technique described above (Rae & Levis, 1992), which allows the pipette tip to be positioned within a few micrometers of a layer of Silicone oil covering the surface of the bath, background noise levels as low as 0.08 pA rms in a 5 kHz bandwidth have been achieved in actual single-channel recording situations with quartz pipettes. In such cases the contribution of the dielectric noise and distributed R-C noise of the pipette appears to be negligible in comparison to other noise sources.

More accurate estimates of the noise attributable to the pipette could be made by sealing quartz pipettes to Sylgard. A typical result for approximately a 3 mm depth of immersion is 0.115 pA rms in a 5 kHz bandwidth for pipettes coated with a thin layer of Sylgard to within about 100–200 μ m of the tip. The power spectral density (PSD) of this noise was also measured. An estimate of the PSD attributable to the dielectric noise and distributed R-C noise of the pipette was obtained by subtracting from the total PSD the PSD of the headstage with the electrode in air with a correction made for the effects of the additional capacitance of the immersed pipette (about 2.6 pF) in conjunction with the headstage input voltage noise. The thermal current noise level associated with the DC seal was also subtracted. The resulting PSD was taken to be the best estimate of the noise attributable to the pipette per se. This PSD (Amp²/Hz) increased with frequency with a slope of approximately $f^{1.85}$ in the frequency range from 2–20 kHz. From the PSD it could be estimated that the pipette accounted for about 0.07 pA rms of noise in a 5 kHz band-

width and about 0.17 pA rms in a 10 kHz bandwidth. If it is assumed that the slope of $f^{1.85}$ was composed of a component with a slope of f attributable to the dielectric noise of the pipette and a component with a slope of f^2 , attributed to distributed resistance-capacitance noise of the pipette, it can be estimated that dielectric noise would account for slightly less than 0.06 pA rms in a 10 kHz bandwidth. Distributed R-C noise would then account for about 0.16 pA rms at this bandwidth. The estimated value of dielectric noise is somewhat higher than would be expected from the value of D listed for Amersil TO-8 quartz (0.0001 at 1 MHz) and the measured value of C_D (2.6 pF); with these values, equation 10 predicts ≈ 0.04 pA rms of dielectric noise in a 10 kHz bandwidth. If the above parsing of the noise components is correct, then it can be estimated that the actual value of D for the quartz used was closer to 0.00025. Even if this value is correct, the $D\epsilon$ product for this quartz is still about an order of magnitude lower than that of any other glass used to date for the fabrication of patch pipettes. At the time of this writing, neither different grades (*i.e.*, higher purity) of quartz from the same supplier nor quartz from other manufacturers have been investigated. It should also be noted that the noise component attributed to distributed R-C noise probably could have been reduced if the pipettes tested had a more favorable geometry.

When the same procedure was used to estimate the pipette noise when the depth of immersion was decreased such that the increment in capacitance was about 0.7 pF above that measured with the pipette tip just above the solution, it was found that the noise attributable to the pipette was roughly a factor of two lower than the figures reported above. In this case the estimated pipette noise PSD increased with increasing frequency approximately as $f^{1.9}$ in the range from 2–20 kHz. This is consistent with the prediction that the relative decrease in dielectric noise will be somewhat greater than that of distributed R-C noise as the depth of immersion decreases.

It should be noted that the results for quartz pipettes are qualitatively as well as quantitatively different from those that have been obtained previously from pipettes fabricated with other types of glass. Estimates of pipette noise based on procedures like those described above have been performed for many types of glass (*i.e.*, Figure 11.4). Even for the lowest $D\epsilon$ product glasses (*e.g.*, 7760, 8161, 7740), the estimated pipette noise PSD rises with increasing frequency as $f^{1.1} - f^{1.3}$ (frequency range 2–20 kHz, immersion depth ≈ 2 mm). This indicates that dielectric noise dominates total pipette noise for these glasses. However, for quartz not only is the pipette noise significantly less for a given depth of immersion, but the estimated pipette noise PSD rises much more steeply with increasing frequency ($f^{1.8} - f^{1.9}$ in the 2–20 kHz frequency range)³. This indicates that dielectric noise is no longer the dominant source of noise for patch pipettes fabricated

3. Note, however, that the PSD for quartz pipettes is lower than that of pipettes made from other glasses at all frequencies measured. At sufficiently high frequencies distributed R-C noise should dominate the total noise for pipettes fabricated from any type of glass. However, for quartz pipettes the PSD of distributed R-C noise should exceed that of dielectric noise by 1 kHz; for pipettes made from 7760, distributed R-C noise should not exceed dielectric noise up to 10–20 kHz, and for soda lime (*e.g.*, 0080) pipettes this frequency might be closer to 100 kHz or more. Distributed R-C noise depends on the pipette geometry and a variety of other factors already described; the only influence of the glass type itself—accept in so far as it effects the geometry which can be pulled—is its dielectric constant.

from quartz. The data described above are consistent with the interpretation that for quartz pipettes “distributed R-C noise” has become the dominant noise mechanism due to the greatly reduced contribution of dielectric noise. As more data from quartz pipettes becomes available these estimates and conclusions will doubtlessly be refined.

Noise Arising From Pipette Resistance and Patch Capacitance

The capacitance, C_p , of the patch is in series with the entire pipette resistance, R_e . The thermal voltage noise of R_e will produce current noise in conjunction with the patch capacitance. The PSD of this noise, $S_p^2(f)$, is given by:

$$S_p^2(f) = 4\pi^2 e_e^2 C_p^2 f^2 \quad (14)$$

where $e_e^2 = 4kTR_e$ is the thermal voltage noise of the pipette. The rms noise arising from this mechanism from DC to a bandwidth B is then $(\frac{4}{3}\pi^2 e_e^2 C_p^2 B^3)^{1/2}$. In general, this noise should be quite small, but it can become significant when the patch area is large; *e.g.*, when a large “bleb” of membrane is sucked into the pipette tip. Sakmann and Neher (1983, in *Single-Channel Recording*, Sakmann, B. and Neher E. eds. pp. 37–51) measured patch capacitance for a large number of pipettes with resistances ranging from about 1–10 MΩ. They found that the value of C_p varied from as little as 0.01 pF to as much as 0.25 pF. Despite a very large amount of scatter, they found that C_p and R_e were correlated, with C_p increasing as R_e decreases. The best fit to their data was $C_p = 0.126 \text{ pF}(1/R + 0.018)$, where R is the pipette resistance in MΩ. Using this average relationship it can be predicted that for a “typical” 10 MΩ pipette ($C_p = 0.015 \text{ pF}$) the noise in a 10 kHz bandwidth (8-pole Bessel filter) arising from this mechanism will be about 0.03 pA rms, while for a 1 MΩ pipette (typical $C_p = 0.128 \text{ pF}$) this value will increase to 0.08 pA rms. Sakmann and Neher’s results indicate that in the most favorable situations in terms of “ R_e - C_p ” noise, the rms noise from this mechanism can be as low as 0.01 pA rms in a 10 kHz bandwidth. However, in the least favorable situation ($R_e \approx 2 \text{ M}\Omega$, $C_p \approx 0.25 \text{ pF}$) the noise from this mechanism can be as large as 0.23 pA rms in a 10 kHz bandwidth (8-pole Bessel filter).

11.7. SEAL NOISE

The membrane-to-glass seal that is essential to the patch voltage-clamp technique is the final source of noise associated with the pipette that will be considered here. Seal noise is perhaps the least understood source of noise in the patch clamp technique. The power spectral, $S_{sh}^2(f)$, of the noise arising from the seal for zero applied voltage is given by:

$$S_{sh}^2(f) = 4kT \text{Re}\{Y_{sh}\} \quad (15)$$

where $\text{Re}\{Y_{\text{sh}}\}$ is the real part of the seal admittance Y_{sh} . The minimum estimate of seal noise results from the assumption that $\text{Re}\{Y_{\text{sh}}\} = 1/R_{\text{sh}}$, where R_{sh} is the DC seal resistance. If this assumption is correct, then for a 10 kHz bandwidth, seal resistances of 1, 10 and 100 G Ω would produce noise of 0.4, 0.13 and 0.04 pA rms, respectively. Since values of R_{sh} in the range of 100–200 G Ω are not uncommon, this would imply that the noise associated with a very tight seal would be small in comparison with other sources of patch-clamp noise. However, it is possible that the PSD of seal noise may rise above the minimum level given by $4kT/R_{\text{sh}}$ as frequency increases (*i.e.*, the real part of the seal admittance may increase with frequency) due to the capacitance of the glass and the membrane which make up the wall of the seal. Unfortunately, we have no good theoretical basis upon which to estimate Y_{sh} since the precise nature of the membrane-glass seal is not known.

It is also very difficult to empirically dissect out the noise associated with the seal from total patch clamp noise. We believe that previous attempts to do this have overestimated this noise. For example, as shown in Figure 1-11 of Sigworth (1983), data from F. Sachs and E. Neher indicate a frequency-dependent seal noise PSD ($R_{\text{sh}} \approx 20$ G Ω) that would amount to at least 0.13 pA rms in a bandwidth from DC to 5 kHz. However, with an integrating headstage (*e.g.*, the CV 203BU of the Axopatch 200B amplifier), total noise levels (*i.e.*, including the noise of the headstage, holder, pipette, seal, *etc.*) lower than this value have often been achieved in the same 5 kHz bandwidth in actual recording situations.

Rae and Levis have reported in 1992 measurements using an Axopatch 200A amplifier with quartz pipettes and a novel technique involving placing a layer of Silicone oil on the surface of the bathing solution containing the cells to be patched. This technique allows excised patches to be brought within a few micrometers of the oil-water interface, thereby minimizing the noise contribution of the pipette. With this approach, total noise levels as low as ≈ 0.08 pA rms in a 5 kHz bandwidth were achieved. In several experiments with excised patches, the DC seal resistance was measured (range 40–60 G Ω) and the noise was measured with the tip just beneath the layer of oil and again with the tip withdrawn into the oil. The rms difference of these two noise measurements should be dominated by the seal noise plus the small amount of noise arising from the pipette resistance in series with the patch capacitance. In all cases, it was found that this rms difference for a bandwidth of 5 kHz was close to the thermal current noise predicted from a measured seal resistance (*i.e.*, $(4kTB/R_{\text{sh}})^{1/2}$). Nevertheless, it is well known to anyone who has struggled to achieve the lowest possible noise in patch-clamp measurements that there is considerable variability in the total noise even among patches with very high seal resistances and with all other conditions seemingly identical. Despite the conclusions drawn above, it seems reasonable to guess that some of this variability arises from the seal. Noise associated with the membrane-glass seal represents one of the fundamental limitations of the patch clamp technique, but it now seems clear that under favorable conditions such noise can be as low as 0.03 pA rms in a 5 kHz bandwidth. Rae and Levis (1993) achieved ultra low-noise recording without silicone oil by improving the fabrication of the quartz pipettes.

11.8. NOISE IN WHOLE-CELL VOLTAGE CLAMPING

The noise associated with the whole-cell variant of the patch voltage-clamp technique at moderate to high frequencies will almost always be dominated by current noise arising from the series (pipette) resistance R_s , in conjunction with the membrane capacitance, C_m , of the cell. It should be noted that the measured value of R_s is often 2 or even 3 times higher than the resistance of the pipette prior to achieving a whole-cell recording. Due to the filtering effect of the access resistance and cell capacitance, series-resistance compensation is required to increase the actual bandwidth of current measurement beyond $1/2\pi R_s C_m$. The level of series-resistance compensation is an important determinant of whole-cell voltage clamp noise as well as of the bandwidth and fidelity of recording (see Section 3.3.7., “Series-Resistance Compensation”). The voltage noise PSD of R_s is approximated by $4kTR_s$ (V^2/Hz). It should be noted, however, that in addition to thermal noise a $1/f$ component is expected, particularly when relatively large currents are passed through the pipette. The PSD, $S_{wc}^2(f)$, of the current noise arising from R_s and C_m is given by:

$$S_{wc}^2(f) = \frac{4\pi^2 f^2 e_s^2 C_m^2}{1 + 4\pi^2 f^2 \tau_{sr}^2} \quad (\text{units: Amp}^2/\text{Hz}) \quad (16)$$

where $e_s^2 = 4kTR_s$ and $\tau_{sr} = R_{sr}C_m$ and R_{sr} is the residual (*i.e.*, uncompensated) series resistance, *e.g.*, if $R_s = 10 \text{ M}\Omega$ then for series-resistance compensation levels of 50%, 70% and 90%, R_{sr} will be 5 $\text{M}\Omega$, 3 $\text{M}\Omega$ and 1 $\text{M}\Omega$, respectively. It should be noted that for 100% series-resistance compensation, equation (16) reduces to $4\pi^2 f^2 e_s^2 C_m^2$. This emphasizes that series-resistance compensation (if it is properly designed) only restores the noise to the level that would have resulted from the thermal voltage noise of R_s in series with C_m in the absence of the filtering effect of R_s mentioned above. The rms noise arising from R_s and C_m over a bandwidth from DC to B Hz can be obtained by integrating equation (16) over f from 0 to B.

Patch clamps commonly use (switch in) a 500 $\text{M}\Omega$ feedback resistor for whole-cell voltage clamping. The noise of this resistor dominates open-circuit headstage noise up to bandwidths of about 10 kHz. However, for typical cells the noise arising from R_s and C_m will be larger than that of the headstage for all bandwidths above a few hundred Hz. Even for relatively ideal situations in terms of noise (*e.g.*, a small cell with $C_m = 5 \text{ pF}$ voltage clamped through $R_s = 5 \text{ M}\Omega$), the noise of a 500 $\text{M}\Omega$ feedback resistor will not dominate total noise for bandwidths above about 1 kHz. Figure 11.4 shows the noise PSD and rms noise for a typical whole-cell voltage clamp situation with $R_s = 10 \text{ M}\Omega$ and $C_m = 33 \text{ pF}$ (these are the values used in the Model Cell provided with the Axopatch-1 and the Axopatch 200 series of patch clamp amplifiers). The top panel shows the noise PSD (as computed from equation 16 plus headstage noise) for series-resistance compensation levels of 0%, 50%, 70% and 90%; the noise PSD of an open-circuit headstage alone is shown for comparison. It is instructive to derive an expression for the high frequency plateau of these PSDs (from equation 16). If the fraction of series-resistance compensation is defined as α and $\beta = 1 - \alpha$ (*e.g.*, for 80% compensation $\beta = 0.2$; also note that $R_{sr} = \beta R_s$),

then as $f \rightarrow \infty$, $S_{wc}^2(f) \rightarrow 4kT/(\beta^2R)$. Even without series-resistance compensation ($\beta = 1$) the high frequency plateau is $4kT/R_s$; *i.e.*, 50 times larger than that of a 500 M Ω resistor. With 90% compensation ($\beta = 0.1$) the plateau level is $4kT/(0.01R_s)$, which, in this case, is equivalent to the thermal current noise of a 100 k Ω resistor.

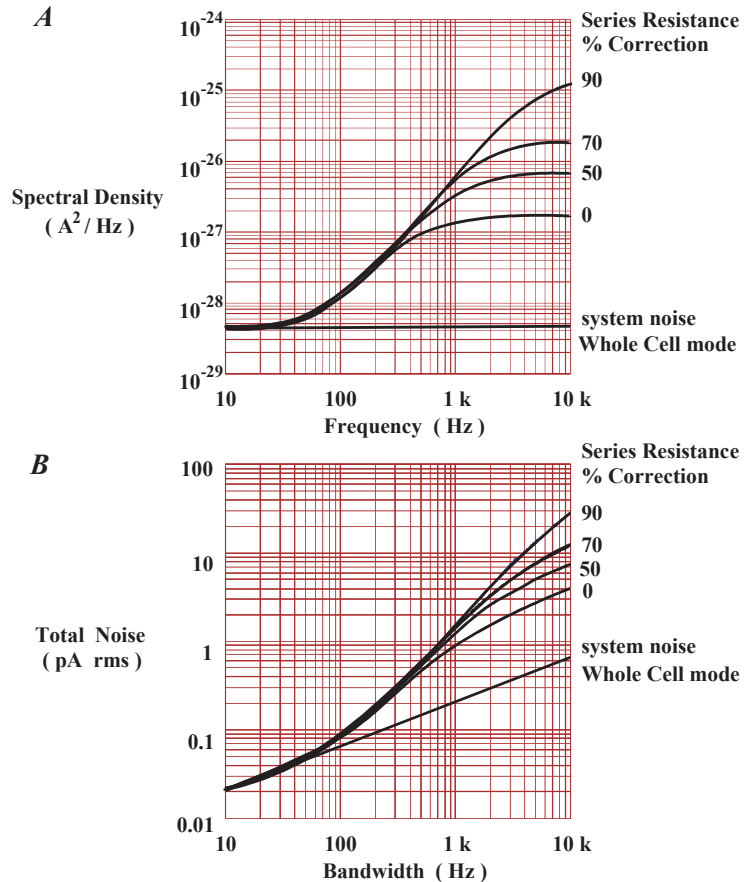


Figure 11.4: Noise in whole-cell voltage clamping.

- A. Power spectral density as a function of frequency for a whole-cell voltage clamp. Cell membrane capacitance is 33 pF and series resistance is 10 M Ω ; cell input resistance has been assumed to be much larger than 500 M Ω . Series-resistance compensation levels of 50%, 70% and 90% are shown. The lower curve (system noise) approximates the open circuit headstage noise in whole-cell mode with a feedback resistor of 500 M Ω .
- B. RMS noise as a function of bandwidth for the same whole-cell voltage clamp situation illustrated in A. Note that the headstage noise dominates total noise in this situation only at bandwidths less than ≈ 100 Hz.

The lower panel of Figure 11.4 shows the total rms noise as a function of bandwidth for the same cell parameters with R_s compensation levels of 0%, 50%, 70% and 90%; the rms noise of the open circuit headstage is also shown. Note that by a bandwidth of only about 200 Hz the total noise is twice that of the headstage alone; therefore, even if a headstage with negligible noise had been used, at this bandwidth total noise would only decline to about 70% of the value shown. As the bandwidth of current measurement increases, the noise of the headstage itself becomes progressively more negligible; with 90% compensation at a bandwidth of 1 kHz, a headstage with no noise would have reduced total noise by less than 1% (recall that the noise of the headstage and the R_s - C_m noise considered here are not correlated and, therefore, add in an rms fashion). It should also be pointed out that the bandwidths in this figure refer to the setting of an external filter (a perfect “brick-wall” filter has been assumed, see Section 11.12., “Filtering”). But it is important to realize that the actual bandwidth of current measurement is limited to $1/2\pi R_{sr}C_m$ (1 pole RC filter). Without series-resistance compensation, in this example the bandwidth is only about 480 Hz and the use of external filter bandwidths much above this will only add noise, not new signal information. The effective bandwidth increases with increasing series-resistance compensation, reaching nearly 5 kHz with 90% compensation.

11.9. EXTERNAL NOISE SOURCES

Interference from external sources can be almost completely eliminated in a well-designed system, but can become the dominant source of noise if proper precautions are not taken. The most familiar form of interference is line-frequency pickup (50 or 60 Hz and harmonics) from power supplies, fluorescent lights, *etc.* Well-designed instruments will not introduce significant amounts of interference from their internal power supplies. However, a typical laboratory environment is full of potential sources of interference from sources external to the electronic instrumentation involved in a particular measurement. In addition to line-frequency pickup, other potential sources of interference include nearby motors, elevators, radio and television stations, and the video monitor of your computer (which produces an annoying timing signal at 16 kHz or higher frequency). High impedance measurements, such as patch clamping or work with intracellular microelectrodes, are particularly sensitive to such external interference.

In most cases such noise sources can be controlled by careful grounding, shielding and filtering. (For a detailed discussion of these techniques see Chapter 2). In some situations, however, shielding can actually increase noise. An example is metal shielding of the pipette holder used in the patch clamp. Such shielding inevitably increases the capacitance at the input of the amplifier (C_g in equations (11) – (13) above) by several picofarads. Even if the mean voltage on the shield is precisely the same as that of the negative input of the amplifier, the noise voltages will differ and lead to increased high frequency noise. For this reason MDS Analytical Technologies does not offer or recommend such shielded holders; it is our experience that grounding of nearby metal objects, such as the microscope, usually provides adequate shielding. Vibration, either transmitted through the floor

or through the air, is another source of external interference and adequate vibration isolation is almost always required for sensitive electrophysiological measurements.

11.10. DIGITIZATION NOISE

Noise arising from digitization is often ignored. Sometimes this is justified since such noise can be negligible with respect to other sources of noise. However, in some situations this potential source of noise can become significant. In order to ensure that this noise remains negligible one needs to understand the types of noise that can arise from digitization and to use analog-to-digital converters, preamplifiers, filters, *etc.* that are appropriate for the measurement of the signal.

Quantization is the approximation of each value of a signal by an integer multiple of an elementary quantity δ , which is the quantizing step. For a 12-bit analog-to-digital converter (ADC) with full-scale range (FSR) of ± 10 V, $\delta = 20 \text{ V}/2^{12} = 4.88 \text{ mV}$; for a 16-bit converter with the same FSR, $\delta = 305 \text{ } \mu\text{V}$. This approximation leads to the addition of a noise signal, called quantizing noise, to the original signal. When the signal being digitized is reasonably large relative to the quantizing step δ , the power of the quantizing noise can usually be approximated by:

$$\frac{\delta^2}{12}$$

and the rms value of the quantizing noise is therefore:

$$\sqrt{\frac{\delta^2}{12}}$$

For a 12-bit ADC with a 20 V FSR this noise value is 1.41 mV rms or about 8.5 mV peak-to-peak.

In the process of analog-to-digital conversion, the signal is sampled as well as quantized. The sampling frequency is denoted by f_s ; *e.g.*, when converting at 1 point every 10 μs , f_s is 100 kHz. In this case all of the quantizing noise power in the ADC output will appear in the frequency band from DC to $f_s/2$. The PSD is usually white (*i.e.*, constant over the frequency band) and has a value of $\delta^2/6f_s$.

It is obvious that the quantizing step δ should be small relative to the signal being measured. This is easily accomplished in most situations by the use of appropriate preamplification to scale the desired signal such that it fills a reasonable portion of the dynamic range of the ADC. Difficulties can arise, however, if you need to measure small changes embedded in large signals. Analog instruments can often have a dynamic range that considerably exceeds that of ADCs. Again, using the capacitive-feedback patch clamp as an

example, noise levels as low as 0.02 pA rms can be achieved at a bandwidth of 1 kHz; moreover, such an instrument can achieve noise this low even with a gain as low as 100 $\mu\text{V}/\text{pA}$. This would amount to an rms noise of only 2 μV . In order to utilize the full dynamic range of such an instrument at this bandwidth, an ADC with 22-bit resolution (and capable of sampling at 2–5 kHz) would be required. To the best of our knowledge, this much dynamic range is not required for electrophysiological measurements and 12- to 16-bit resolution in conjunction with a variable amount of preamplification is quite adequate (see Chapter 9 for further discussion).

11.11. ALIASING

A signal can be determined completely by a set of regularly spaced samples at intervals $T = 1/f_s$ only if it does not contain components with a frequency equal to or greater than $f_s/2$. This is basically a statement of the sampling theorem; f_s is just the sampling frequency mentioned above. The term $f_s/2$ will be denoted by f_n and is often called the Nyquist frequency or folding frequency for reasons that will be described below. Another way of putting this is that for sampled data, frequency is only defined over the range from 0 to f_n ; components with frequencies higher than f_n cannot be described (at least 2 points per cycle are needed to uniquely define a sine wave). Obviously there is nothing (other than good sense) that will stop one from digitizing a signal with frequency components extending many times beyond f_n . However, digitizing frequency components of the signal that lie above f_n will result in “folding back” of these higher frequency components into the frequency range from 0 to f_n , consequently producing aliases.

The term f_n is referred to as the folding frequency because the frequency axis of the power spectral density will fold around f_n in a manner similar to folding a road map or a carpenter’s scale. This folding effect is illustrated in Figure 11.5; frequency components above f_n are shifted to lower frequencies (in the range 0 to f_n). If f_x is the frequency of a signal component (desired or noise) above f_n , then the frequency of its alias, f_a , is given by:

$$f_a = |f_x - kf_s| \quad (17)$$

where the brackets, $| \cdot |$, indicate absolute value, f_s is the sampling frequency, and k is a positive integer taking on whatever value is required so that f_a falls in the range $0 \leq f_a \leq f_n$. For example, with $f_s = 20$ kHz ($f_n = 10$ kHz), a frequency component at 18 kHz will alias to a component at 2 kHz ($f_a = |18 \text{ kHz} - 1 \times 20 \text{ kHz}| = 2 \text{ kHz}$) in the digitized waveform. Similarly, as shown in Figure 11.5, frequency components at 22 kHz, 38 kHz, 58 kHz, 62 kHz, *etc.*, will all alias to 2 kHz in the sampled data.

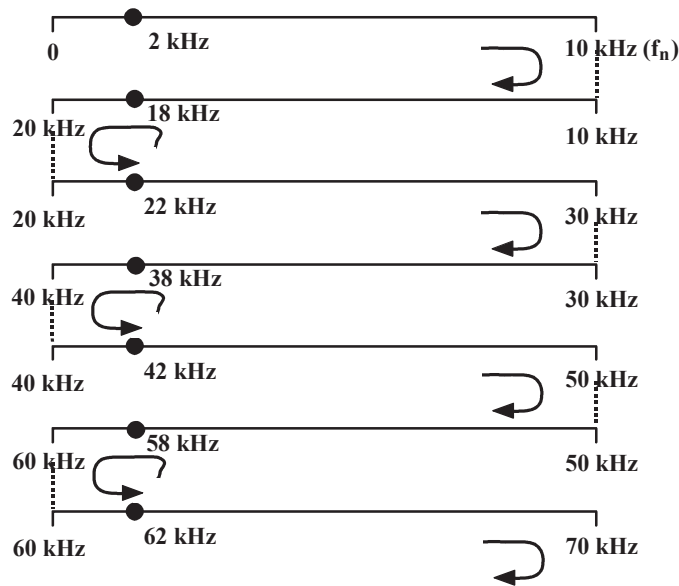


Figure 11.5: Folding of the frequency axis.

In this folding of the frequency axis for $f_s = 20$ kHz ($f_n = 10$ kHz), note that all of the round points shown (18 kHz, 22 kHz, ...) alias to 2 kHz.

As an example of aliasing and the problems it can produce, consider white noise extending from DC to 10 MHz. To be specific we will assume that the PSD of this noise is 10^{-14} V²/Hz (100 nV/Hz); the total noise in the 10 MHz bandwidth is then 316 μ V rms (about 2 mV peak-to-peak). If this noise is sampled at $f_s = 20$ kHz without the use of an anti-aliasing filter, it should be obvious that the rms value of the sampled points will be the same as that of the original data, *i.e.*, 316 μ V. However, the sampled data cannot describe any frequency component greater than f_n , here 10 kHz. If a smooth curve is fitted through the sampled points (*e.g.*, using a cubic spline), you will find that the noise appears to be bandlimited from DC to 10 kHz and that its amplitude is the same as the original data; its power spectral density will be 10^{-11} V²/Hz, *i.e.*, 1,000 times higher than that of the original data because the sampling has folded over the original spectrum 1,000 times. The frequency components above 10 kHz have all been aliased into the frequency band extending from DC to f_n . Clearly, aliasing has not increased the total amount of noise, but it has shifted it from higher to lower frequencies. It is worth considering what will happen if the sampled data is subsequently digitally filtered with a cutoff frequency of 1 kHz. This will result in reducing the noise from 316 μ V rms to 100 μ V rms. However, if the original noise signal had been passed through an analog filter with the same cutoff frequency (1 kHz), the noise amplitude would have been reduced to only 3.16 μ V rms. Once aliasing has occurred it cannot be undone by any digital operation. The solution here is either to sample much faster (> 20 MHz in this example) or, if a 20 kHz sample

rate is required, to use an analog anti-aliasing filter to adequately reduce the amplitude of all frequency components above 10 kHz.

If the PSD of the noise is not white but instead rises as f^2 with increasing frequency—as is the case for high frequency noise from a patch voltage clamp—the consequences of aliasing can be even more severe. As an extreme example, consider a voltage noise of 100 nV/ $\sqrt{\text{Hz}}$ in series with a 10 pF capacitor (see equation (13) and related discussion); in a 10 MHz bandwidth this would produce a current noise of 115 nA rms. Again, assuming a digitization rate of 20 kHz with no anti-aliasing filter, all of this noise would be aliased into the frequency band from DC to 10 kHz, even though the noise in a bandwidth of 10 kHz would have only been about 3.6 pA rms.

Moreover, subsequent digital filtering of the digitized noise with a cut-off frequency of 1 kHz, as in the previous example, would only reduce the noise amplitude to about 35 nA rms, whereas an analog filter set to a 1 kHz bandwidth would have reduced the noise to only 0.115 pA rms—300,000 times less than achieved by digitally filtering the aliased noise. Of course patch clamps do not have a bandwidth of 10 MHz; even with more realistic bandwidths, failure to use proper anti-aliasing filters can greatly increase noise beyond that existing in the bandwidth resolved by the digitization process (*i.e.*, f_n) and can reduce the effectiveness of subsequent digital filtering of the data.

It should be noted that in the above examples it has been assumed that the filter used had an abrupt cut-off at its -3 dB bandwidth. This will normally not be the case when measuring signals in the time domain. Filters with Gaussian or Bessel characteristics (as are used most frequently for electrophysiological measurements) roll off quite gradually beyond their -3 dB bandwidth (f_c) and it is therefore not appropriate when using such filters to eliminate aliasing to set $f_c = f_n$. Recall that the requirement to avoid significant aliasing is that all frequency components above f_n must be adequately attenuated. When using a Bessel filter (typically 4- or 8-pole) for anti-aliasing, the choice of the cut-off frequency relative to f_n depends on the characteristics of the noise and how much aliasing can be tolerated. We advise the use of $f_c \leq 0.4\text{--}0.5f_n$ ($0.2\text{--}0.25f_n$) as a useful and generally reasonable practice.

11.12. FILTERING

The above discussion naturally leads to a brief discussion of filtering. In general, the bandwidth of a filter is selected to reduce noise to acceptable levels so that the desired signal can be adequately observed. As described above, filtering prior to digitization is also necessary to prevent aliasing. If the signal to be measured is large in comparison with the background noise, then the filter bandwidth—and the appropriate digitization rate—can be chosen on the basis of the desired time resolution; wider bandwidths allow more rapid events to be resolved. However, in many electrophysiological measurements very wide bandwidths will result in background noise levels that will obscure the signals of interest. In such situations it is necessary to make compromises between the amount of noise that can be tolerated vs. the time resolution that is achieved after filtering.

There is an interesting—although perhaps unfortunate—relationship between a function and its Fourier transform: as the function gets narrower its transform becomes wider. The impulse response of a filter (time domain; note that the integral of the impulse response is the step response) and its transfer function (frequency domain) are a Fourier transform pair. There are limits on the degree to which signals can be simultaneously “concentrated” in both the time and the frequency domain (in fact, if stated formally, this is the uncertainty principle in the units we are using). In practical terms this means that a filter with a narrow impulse response, and therefore a rapid rise time, will have a rather gradual roll-off in the frequency domain. Conversely, a filter with a sharp cut-off in the frequency domain will have a more spread-out impulse response and slower rise time.

Among commonly used filters, those that provide the best resolution with little or no overshoot and ringing of the step response are the Gaussian and Bessel filters (as the order of a Bessel filter increases it more closely approximates a Gaussian filter). A true Gaussian filter is easy to implement digitally, but is not often produced as an analog filter (although passive filters that are a good approximation of this type can be constructed). Bessel filters are more commonly used in analog applications. The basic characteristics of both filter types are quite similar. A Gaussian filter has an impulse response with the shape of the Gaussian distribution; its step response has no overshoot. The 10–90% rise time of the step response of a Gaussian filter is approximately $0.34/f_c$, where f_c is the -3 dB bandwidth in hertz. However, in the frequency domain the roll-off of this filter is quite gradual. Denoting the transfer function by $H(f)$, $H(f_c) = 0.707$ (-3 dB), $H(2f_c) = 0.25$ (-12 dB), and $H(3f_c) = 0.044$ (-27 dB). An 8th-order Bessel filter closely approximates this response in both the time domain and the frequency domain. Clearly, in terms of noise reduction, a filter whose transfer function rolls off much more quickly after it reaches f_c would appear to be desirable. Analog filters with such characteristics are readily available (*e.g.*, Elliptical and Chebyshev types); in fact, you can buy sharp cut-off filters with $H(f) = 0.01$ (-40 dB) when $f = 1.06f_c$. Digital filters can achieve even sharper cut-offs. Unfortunately, however, sharp cut-off filters are characterized by severe overshoot and prolonged ringing in their step responses. Additionally, for a given value of f_c , their rise times can be nearly twice that of a Gaussian or Bessel filter. Because of this, very sharp cut-off filters are desirable for frequency domain measurements but quite undesirable for measurements in the time domain. In fact, in order to achieve the same time resolution with a sharp cut-off filter that is achieved with a Gaussian or Bessel filter it is necessary to use a higher value of f_c . In this case, the sharp cut-off filter (with its higher f_c) will pass as much or even more noise (depending on the spectral characteristics of the noise) as the more gradual roll-off Gaussian or Bessel filter when the two have been set to provide essentially equivalent time resolution (as judged by step response rise time; see next paragraph). Some “exotic” filter types can produce the same rise time as the Gaussian filter with minimal overshoot and reduce the noise by a small amount; however, unless the noise PSD rises very steeply with increasing frequency, the improvement is only a few percent.

It is instructive to quantitatively compare the performance of a Gaussian or Bessel filter with a very sharp cut-off filter for time-domain measurements. When the underlying signal to be resolved is a square pulse, as is the case with single-channel currents, it is reason-

able to relate the time resolutions of the filter to its 10–90% rise time. For single-channel measurements time resolution is often thought of in terms of the minimum detectable event duration. To some extent, of course, such a minimum duration is dependent on the detection algorithm used. Even so, it is reasonable to approximate the minimum detectable duration in terms of the filter bandwidth as $1/T_r$, where T_r is the 10–90% rise time of the filter. With such an operational definition of time resolution—or minimum detectable duration—it is possible to compare the performances of different filter types. As already noted, for a Gaussian or Bessel filter (8th order) $T_r \approx 0.34/f_c$, where f_c is the -3 dB bandwidth in hertz. A 10th-order Chebyshev filter (0.1 dB pass-band ripple) is a reasonable selection to approximate the “brick wall” characteristic mentioned above; for this filter $H(1.09f_c) = 0.1$ (-20 dB), $H(1.22f_c) = 0.01$ (-40 dB), and $H(2f_c) = -95$ dB. However, for this filter $T_r \approx 0.58/f_c$, *i.e.*, approximately 1.7 times the rise time of a Gaussian or Bessel filter with the same f_c . Moreover the step response is characterized by a peak overshoot of about 20% and sustained ringing which is noticeable up to about $10/f_c$. In order to achieve the same 10–90% rise time with the 10th-order Chebyshev filter that is achieved with a Gaussian or 8th-order Bessel filter, it is necessary to select the -3 dB bandwidth of the Chebyshev filter to be about 1.7 times higher than the -3 dB bandwidth of the Gaussian or Bessel filter. For example, the rise time of a Chebyshev filter with $f_c = 17$ kHz will be approximately the same as that of a Gaussian or Bessel filter with $f_c = 10$ kHz; it should be noted that the step response of the Chebyshev filter will ring severely. Even if the ringing of its step and impulse response is ignored so that it is assumed that the 10th-order Chebyshev filter and the Gaussian or Bessel filter have the same time resolution provided that f_c (Chebyshev) $\approx 1.7f_c$ (Gaussian), it is found that the Gaussian or Bessel filter significantly out-performs the Chebyshev filter in terms of noise in the filtered signal.

For white noise it would be found that the Chebyshev filter would pass approximately 1.3x the noise passed by the Gaussian or Bessel filter, provided, of course, that both filters had the same 10–90% rise time. For noise with a PSD that rises as f^2 , the Chebyshev filter would actually pass about 1.5x the rms noise passed by the Gaussian or Bessel filter, again provided that the filters’ corner frequencies were set to produce the same rise time. Obviously, when time resolution is considered, extremely sharp cut-off filters are not the best selection. Sharp cut-off filters should only be used when frequency domain data (*e.g.*, power spectral density) is being collected.

Finally, as an illustration of the distinction between the -3 dB bandwidth and the uppermost frequency component of noise that can pass through a Gaussian or Bessel filter, consider a noise process ($e^2(f)$) whose PSD (V^2/Hz) rises as f^2 with increasing frequency. On linear scales such noise is shown in Figure 11.6 along with the transfer function of a Gaussian filter (squared, $H^2(f)$) and the noise PSD that will be observed at the filter output (*i.e.*, $H^2(f)e^2(f)$). Note that the square root of the integral of the filtered noise PSD (*i.e.*, the square root of the area under the curve) will be the rms noise. The PSD of the filtered noise does not fall sharply at f_c . In fact, the filtered PSD reaches its peak at about $1.2 f_c$ and does not fall to negligible levels until more than $3 f_c$. This must be remembered when selecting a digitizing rate for any particular -3 dB filter setting if aliasing is to be avoided. In comparison with a filter with a “brick wall” roll-off at the same f_c , the Gaussian filter

will have somewhat more than 40% more noise at its output. But recall that the sharp cut-off filter will have a much poorer time-domain response. In fact, as described above, if the -3 dB bandwidth of the sharp cut-off filter is selected to produce essentially the same time resolution as the Gaussian or Bessel filter, it will pass even more noise in this situation.

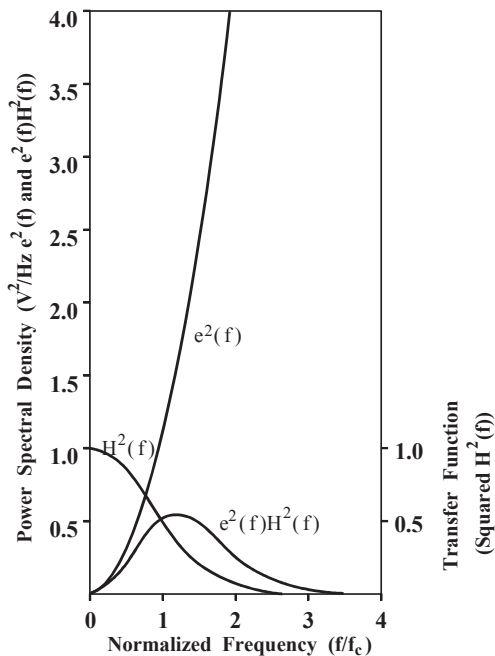


Figure 11.6: Squared transfer function of a Gaussian filter.

Illustrated are squared transfer function of a Gaussian filter ($H^2(f)$), noise process with PSD that arises as f^2 with increasing frequency ($e^2(f)$), and the same noise process PSD after passing through the Gaussian filter ($e^2(f)H^2(f)$). The scales are linear; frequency is normalized to the -3 dB bandwidth (f_c) of the filter; PSD scale is arbitrary. Note that due to the gradual roll-off of the Gaussian filter, the filtered noise still has significant power well beyond f_c .

A useful alternative to adjusting the analog filter bandwidth to attempt to achieve an optimum signal-to-noise ratio is to digitize the data at a rapid rate through a Bessel filter with its -3 dB bandwidth set to prevent aliasing. The wideband digitized data may then be filtered digitally to achieve an acceptable signal to noise level. The digital filter should once again generally be of the Gaussian or Bessel type. In such situations more than one filter are used in series; if these are all of the Gaussian or Bessel type, then the final -3 dB bandwidth, f_{cF} , is approximately given by:

$$f_{cF} = \frac{1}{\sqrt{\frac{1}{f_1^2} + \frac{1}{f_2^2} + \frac{1}{f_3^2} + \dots}}$$

where $f_1, f_2, f_3 \dots$ are the -3 dB bandwidths of the individual filters in series. Of course, the same expression holds for a series combination of analog filters. The disadvantage to this general approach is that initial data storage will be increased due to the high digitization rate; once the data has been digitally filtered it can also be decimated if desired.

11.13. SUMMARY OF PATCH-CLAMP NOISE

11.13.1. HEADSTAGE

At the time of publishing this Guide, the best capacitive-feedback headstage (the CV 203BU of the Axopatch 200B amplifier) has an open-circuit noise of about 0.13 pA rms in a 10 kHz bandwidth (-3 dB, 8-pole Bessel filter). Resistive-feedback headstages have noise of about 0.25–0.30 pA rms in this bandwidth. It is possible that developing capacitive-feedback technology could yield further improvements in noise. In fact, in theory, it should be possible to produce a capacitive-feedback headstage with noise that is only about half of that achieved presently.

11.13.2. HOLDER

The pipette holder contributes noise by increasing the capacitance at the headstage input; some dielectric noise must also be expected. The unshielded polycarbonate holders provided by MDS Analytical Technologies by themselves will only increase the headstage noise by about 10% above its open circuit value even for the lowest noise capacitive-feedback devices. For example, for the Axopatch 200B amplifier with an open-circuit noise of 0.060 pA rms in a 5 kHz bandwidth (as shown on the panel meter), the total noise with the holder attached should not increase beyond 0.070 pA rms (note that larger noise increments probably mean that the holder needs to be cleaned), and will often be as low as 0.065 pA rms. Inserting a saline-filled electrode into the holder will further increase noise even while the electrode tip is in air. With a saline-filled electrode, the noise of the Axopatch 200B with an open-circuit noise of 0.060 pA in a 5 kHz bandwidth will generally increase to about 0.075 pA rms.

11.13.3. ELECTRODE

The noise associated with the patch pipette is determined by the type of glass used, the wall thickness of the glass, the pipette geometry, the use of Sylgard coating, and the depth of immersion into the bath. Dielectric noise is probably the dominant source of noise associated with the electrode for all glasses except quartz. For glasses with lower $D\epsilon$ products—most notably quartz—it can be expected to become a much smaller component of overall noise. Additional noise will arise from the distributed resistance and capacitance of the pipette. For the best glasses presently in common use, this source of noise is probably somewhat less than the dielectric noise of the glass; for very low-loss glasses, such as quartz, it could be the dominant source of pipette noise. A small amount of noise will also result from the thermal noise of the pipette resistance in series with the patch capacitance; only under certain situations (a large patch area) will this “ R_e - C_p ” noise become significant.

Theoretical and experimental results indicate that a pipette fabricated from the lowest-noise glasses (other than quartz) used to date (Corning #7760, #8161) with a moderate coating of Sylgard will produce noise of about 0.2 pA rms in a 10 kHz bandwidth (8-pole Bessel filter) for an immersion depth of about 2 mm. Under favorable circumstances, this value can be cut at least in half when the tip of the pipette is withdrawn to within 100–200 μm of the surface of the bath. For pipettes fabricated from quartz, preliminary results indicate that for a 1 mm depth of immersion, noise of somewhat less than 0.1 pA rms can be expected in a bandwidth of 10 kHz; with the very small immersion depth possible (10 μm or less) with the Silicone-fluid technique described above, it can be estimated that the noise contributed by a quartz pipette falls to less than half of this value. Results obtained for quartz have involved pipettes with relatively long narrow shanks and resistances of roughly 10 $\text{M}\Omega$. Such a geometry is not ideal for achieving the lowest possible noise. As techniques for pulling quartz pipettes improve, and as other grades and suppliers of quartz are investigated, further improvements are likely.

11.13.4. SEAL

The noise associated with the seal is less easily predicted. Certainly a minimum estimate of this noise in a bandwidth B is given by $(4kTB/R_{\text{sh}})^{1/2}$, *i.e.*, the thermal current noise of the DC seal resistance, R_{sh} . For excellent seals in the range of 50–200 $\text{G}\Omega$ this would mean that the minimum noise attributable to the seal is in the range of 0.03–0.06 pA rms in a 10 kHz bandwidth. Recent data suggests that under favorable circumstances seal noise may be as low as these predicted values. However, experience indicates that there is a good deal of variability in the noise of patches even when the seal resistances are very high and all other precautions necessary to minimize noise have been strictly observed. Some of this variability may well arise from the seal.

11.14. LIMITS OF PATCH-CLAMP NOISE PERFORMANCE

A capacitive-feedback headstage, such as the CV 203BU of the Axopatch 200B amplifier, has an open circuit noise of less than 0.13 pA rms in a 10 kHz bandwidth, (bandwidths are the -3 dB frequency of an 8-pole Bessel filter). The total noise is due to contributions from the headstage, holder, pipette and seal. However, peltier cooling has removed the thermal noise from this headstage, reducing total noise from 0.16 to about 0.13–0.14 pA rms in a 10 kHz bandwidth. Of course, the noise associated with the seal is a fundamental limitation of the patch clamp technique. An absolute minimum estimate for seal noise in a 10 kHz bandwidth is about 0.03–0.04 pA rms; this assumes a 100–200 G Ω seal producing only thermal noise. An estimate of the minimum noise associated with an improved holder, quartz pipette and seal in a 10 kHz bandwidth is then about 0.06 pA rms. These figures suggest that as holder and pipette technology continues to improve, it will be worthwhile to continue to seek methods to reduce the noise of the headstage itself. It is reasonable to expect that total noise levels roughly two thirds of the best values achieved to date will become possible. However, to achieve such noise levels, careful attention to every aspect of the patch-clamp technique will be important.

11.15. FURTHER READING

Rae, J.L., Levis, R.A., A method for exceptionally low noise single-channel recording. *Pflügers Arch.* 420, 618–620, 1992.

Rae, J.L., Levis, R.A., Quartz pipettes for single-channel recording. *Biophys.* 64, A201 (P394), 1993.

Sakmann, B. and Neher, E., Eds. *Single-Channel Recording*. New York: Plenum Press, 1983.

A. Appendix: Guide to Interpreting Specifications

A.1. GENERAL

Following are terms commonly used in electrophysiological measurements.

A.1.1. THERMAL NOISE

All resistors generate thermal noise. Thermal noise can be represented by a mean square voltage generator (e_n^2) in series with a noiseless resistor:

$$e_n^2 = 4kTRB$$

where k = Boltzmann's constant (1.138×10^{-23} VC/°K)

T = temperature in °K

R = resistor value in ohms

B = bandwidth in Hertz

The noise specified by this equation has a constant power spectral density within the bandwidth and is zero outside the bandwidth. When noise is measured through a low-pass filter having -3 dB bandwidth f_{-3} , the noise will be greater than the amount predicted because real filters continue to pass signals at frequencies $> f_{-3}$.

The noise of a 10 M Ω resistor measured through various filters is shown in Table A.1.

Table A.1: Noise of a 10 M Ω Resistor in Microvolts rms.

Bandwidth	1-Pole RC	2-Pole Butterworth	4-Pole Butterworth	Infinitely Sharp
DC-100 Hz	5.07	4.27	4.11	4.06
DC-1 kHz	16.0	13.5	13.0	12.8
DC-10 kHz	50.7	42.8	41.1	40.6
DC-100 kHz	160	135	130	128

A.1.2. RMS VERSUS PEAK-TO-PEAK NOISE

It is equally valid to specify noise as rms (root mean square) or peak-to-peak. The ratio of the zero-to-peak value to the rms value is called the crest factor. The value of the crest factor depends on the type of noise. For white noise the crest factor is about 4. Thus the peak-to-peak noise is about 8 times the rms noise.

A.1.3. BANDWIDTH—TIME CONSTANT—RISE TIME

For an exponential response, there are simple relationships between the -3 dB bandwidth (f_{-3} , Hertz), the time constant (τ , seconds) and the 10–90% rise time (t_{10-90} ; seconds):

$$f_{-3} = \frac{1}{2\pi\tau} \approx \frac{1.1}{\pi t_{10-90}}$$
$$t_{10-90} \approx 2.2\tau$$

A.1.4. FILTERS

Low-pass filters are commonly used in electrophysiology to reduce noise. The important parameters of a low-pass filter are the -3 dB frequency, the type and the order.

The -3 dB frequency (f_{-3}) is the frequency where the voltage response falls to $\sqrt{2}$ (0.707). Some manufacturers specify the “cutoff” or “bandwidth” based on the phase response or an asymptotic approximation to the high and low frequency amplitude response. Therefore when using a new filter you should check that the specified settings refer to the -3 dB frequency.

The three types of low-pass filters commonly used in electrophysiology are the Bessel, Butterworth and multiple coincident pole (RC) types. The most important differences are:

- 1 When driven by a step voltage, the RC filter has no overshoot, the Bessel filter has < 1% overshoot and the Butterworth filter has around 10% overshoot.
- 2 When driven by a noisy source, RC filters show the least rejection of the noise at frequencies above f_{-3} , Bessel filters show moderate rejection and Butterworth filters show the most.

The order of a filter refers to the number of poles. Each resistor-capacitor section contributes one pole (inductors are rarely used for bandwidths < 100 kHz). Thus 4th-order, 4-pole and 4 RC sections all refer to the same thing.

The attenuation of high-frequency noise increases with order. At frequencies well above f_{-3} , the attenuation increases at 20 dB/decade (6 dB/octave) for each pole. Thus a 4-pole filter rolls off at 80 dB/decade.

Note: 20 dB attenuation corresponds to a drop in voltage amplitude to one tenth.

A.2. MICROELECTRODE AMPLIFIERS

Noise magnitude is very sensitive to the measurement technique. Specifications should state:

- 1 -3 dB bandwidth and order of the filter used in the measurement circuit. Typically the noise will look 20–30% better if a fourth-order low-pass filter is used instead of a first-order low-pass filter.
- 2 Microelectrode bandwidth. The capacitance neutralization should be adjusted so that the -3 dB bandwidth of the microelectrode is the same as the -3 dB bandwidth of the measurement circuit.

A.2.1. VOLTAGE-CLAMP NOISE

Almost impossible to specify. Depends on cell mode, electrode model, capacitance neutralization setting, electrode interactions, electrode resistances, current measurement techniques, bandwidth of measurement circuit and clamp gain.

A.2.2. 10–90% RISE TIME (t_{10-90})

The time for the response to go from 10% to 90% of the final value.

If a voltage step is applied to a microelectrode headstage via a resistor, the resistor should have a very low stray capacitance. Otherwise the stray capacitance couples the step directly into the headstage input and artificially fast rise times are measured. A better estimate of the rise time can be made by passing a current step out of the headstage into a load resistor.

For consistent comparisons, rise times should be measured with the capacitance neutralization adjusted for zero overshoot.

A.2.3. 1% SETTling TIME (t_1)

When microelectrodes are to be used in a discontinuous (switching) single-electrode voltage clamp, the more relevant specification is t_1 , the time taken for the response to go from 0% to 99% of the final value.

A.2.4. INPUT CAPACITANCE

In a circuit using capacitance neutralization and other compensation techniques, it is meaningless to specify a value for the input capacitance. The efficacy of the neutralization circuit depends on the magnitude of the electrode resistance and the measurement technique.

For an electrode with resistance R and an exponential response to a step input, the effective input capacitance can be estimated from:

$$C_{in} = \frac{0.45t_{10-90}}{R} = \frac{0.22t_1}{R}$$

For example, if $t_{10-90} = 10 \mu\text{s}$ and $R = 10 \text{ M}\Omega$, then $C_{in} = 0.45 \text{ pF}$.

A.2.5. INPUT LEAKAGE CURRENT

Both well designed and badly designed headstages are normally adjustable to zero leakage current. This ability in itself is not an important test of quality. The correct measure of quality is the sensitivity of the input leakage current to temperature changes which occur after the adjustment is made. Changes of $\pm 10 \text{ }^\circ\text{C}$ can be expected in a typical laboratory environment.

A.3. PATCH-CLAMP AMPLIFIERS

A.3.1. BANDWIDTH

The bandwidth of a patch-clamp headstage is usually measured by injecting current into the headstage input through a small capacitor. No holder or electrode is attached to the input.

The bandwidth during an experiment is usually much lower. It is typically limited by the electrode resistance and membrane capacitance, as well as by stray capacitances. For example, if a $5 \text{ M}\Omega$ electrode is used to clamp a whole cell having 20 pF of membrane capacitance, the time constant for measuring membrane currents is $100 \mu\text{s}$ ($5 \text{ M}\Omega \times 20 \text{ pF}$). This corresponds to a -3 dB bandwidth of 1.6 kHz , far below the 100 kHz that may be specified. 80% series-resistance compensation would improve this to 8 kHz . Nevertheless, it is still better to have a headstage with very wide bandwidth because in some cases series-resistance compensation may work better.

A.3.2. NOISE

The ideal RMS current noise in selected bandwidths is shown in Table A.2 for various feedback resistors. These figures assume ideal resistors (which only have thermal noise) and noiseless electronics.

Table A.2: rms Current in Picoamps.

BANDWIDTH	500 M Ω	1 G Ω	5 G Ω	10 G Ω	50 G Ω
DC-1 kHz	0.182	0.128	0.057	0.041	0.018
DC-3 kHz	0.331	0.234	0.099	0.074	0.033
DC-10 kHz	0.574	0.406	0.181	0.128	0.057

No patch-clamp amplifier can meet these ideal specifications. The difference between a value in the table and the actual value is the excess noise. The excess noise is always proportionately worse in the wider bandwidths.

⚠ WARNING: The specified noise in a 10 kHz bandwidth will be misleadingly low if the headstage does not have a 10 kHz bandwidth. If the manufacturer only specifies the 10–90% rise time or the time constant, use the conversion factors given in the General section to verify that the bandwidth is sufficient to make the noise specification meaningful.

Index

Numerics

- 1% settling time 249
- 1/f noise 220
- 10-90% rise time 249

A

- AC coupling 158
 - overload detection 160
 - saturation 160
 - time constant 160
- Acceleration measurements 177
- Accelerometers 177
- Acquisition hardware 189
 - analog-to-digital conversion 189
 - analog-to-digital converter 190
 - differential nonlinearity 192
 - digital I/O 194
 - digital-to-analog converter 190
 - gain accuracy 192
 - glitch 193
 - least significant bit 193
 - linearity error 192
 - monotonicity 193
 - multi-tasking operating systems 195
 - optical isolation 194
 - software support 195
 - timers 194
- Agar bridge 85
- Aliasing 238
 - Bessel filter 240
 - folding frequency 238
 - Gaussian filter 240
 - Nyquist frequency 238
- Amphotericin B 121
 - use in stock solutions 121
- Amplifier noise 221
- Amplifiers
 - amplification 155
 - microelectrode 249
 - 1% settling time 249
 - 10-90% rise time 249
 - input capacitance 249
 - input leakage current 250
 - noise 249
 - patch clamp 13
 - patch-clamp 250
 - bandwidth 250
 - noise 250
 - voltage clamp 13
- Analog-to-digital (A/D) conversion 189
 - optical isolation 194
 - quantization error 190
 - sampling rate 191
- Analog-to-Digital conversion 155
 - preparing signals 155
- Analog-to-digital converter (ADC) 190, 237
- Anti-aliasing 55
- Antibiotic partitioning 122
- Anti-vibration tables 21
- Audio monitor 163
 - amplitude modulated 163
 - frequency modulated 163
- Autozeroing 158
- Averaging 161

B

- Backup 182
- Bandwidth 248
- Bath error potentials 40

- Clamp V_b using a bath clamp 43
- clamp V_b using a virtual ground current monitor 44
- measure and subtract V_b 43
- minimizing R_b 41
- series resistance compensation 42

- Bessel filter 240, 241
 - aliasing 240

- Bilayer experiments 77

- Bilayer techniques 129
 - maximizing the bandwidth 133
 - minimizing noise 130
 - resolving voltage steps 134
 - setup 136

- Bioelectricity 1

- Blanking 163
 - sample-and-hold 163

- Bootstrapping 36

- Brain slices 19
 - blind technique 106
 - cleaning technique 103
 - patch-clamp recording 102
 - thick slice 20
 - thin slice 20

- Bridge balance 30

- Bridge design
 - pressure and force measurements 176

- Buzz 45
 - for cell penetration 45

C

- Cable capacitance
 - filtering capabilities 174

- Cabling
 - affect on noise and bandwidth 171

- Capacitance
 - input 249

- Capacitance compensation 35
 - pipette-capacitance compensation 64
 - whole-cell 66

- Capacitance neutralization 56

- Capacitor feedback headstage 74

- Capacitors
 - currents through 12
 - electrical fields 11

- Cell penetration 45

- Chebyshev filter 242

- Chebyshev polynomial fitting 212

- Chloriding silver wire 87

- Clear 45
 - for cell penetration 45

- Command generation 45

- Common-mode rejection ratio (CMRR) 164

- Computer issues 181
 - software selection 181

- Conductance 3, 7, 9, 15, 16

- Conductors 3

- Continuous single-electrode voltage clamp (cSEVC) 58

- Controlled current source 53

- Crosstalk 172

- Current
 - through capacitors 12

- Current clamp 14, 29

- Current conventions 80

- Current monitor 33

D

- Data acquisition parameters 197

- D/A update rate 198

- data bandwidth 198

- filtering 199, 201

- gain 197

- offset 197

-
- sampling rate 197, 201
 - multiple channels 198
 - multiple exponentials 198
 - single-channel recording 198
 - time skew 198
 - Data backup 182
 - Dielectric noise 219, 224
 - quartz pipettes 224
 - Sylgard 224
 - Differential nonlinearity 192
 - Digital I/O 194
 - Digital-to-analog converter (DAC) 190
 - feedthrough noise 193
 - Digitization noise 237
 - Discontinuous current clamp 57
 - Discontinuous single-electrode voltage clamp
 - comparison with TEVC 57
 - Dissipation factor 224
 - Driven shield 36
 - Duty cycle selecting 56
- E**
- Electrical currents 1
 - Electrical instruments
 - perfect and real 7
 - Electrical interference 21
 - ground-loop noise 22
 - magnetically-induced pickup 22
 - radiative electrical pickup 21
 - Electrical isolation methods 21
 - Electrical potentials 1
 - Electrical properties 89
 - Electrocardiogram (EKG) 172, 175
 - Electrode
 - noise 223
 - Electrode impedance
 - affect on noise and bandwidth 171
 - high 171
 - contributes to thermal noise 173
 - unmatched
 - increases noise and crosstalk 172
 - Electrode noise 223
 - Electrode resistance
 - affect on noise and bandwidth 171
 - see pipette resistance 79
 - Electrode test 164
 - Electrodes 85
 - chloriding silver wire 87
 - glasses 87, 89
 - holders 87
 - junctional potential 86
 - liquid junction potential 86
 - metal microelectrodes 175
 - microelectrode pullers 88
 - microelectrodes 85
 - micropipettes 85
 - noise 89
 - patch micropipettes 86
 - patch pipettes 87
 - silver, silver-chloride 85
 - silver/silver chloride 9, 10
 - Electroencephalogram (EEG) 172, 175
 - Electromyogram (EMG) 172, 174
 - Equipment placement 23
 - Excess noise
 - 1/f noise 220
 - Excess noise (1/f noise) 220
 - Extracellular recording 27
 - multiple-cell 28
 - setup 19
 - single-cell 28
- F**
- Filter
 - anti-aliasing 55

Filter terminology

- 10-90% rise time 149
- 3db frequency 145
- attenuation 146
- decade 146
- decibels 147
- octave 146
- order 148
- overshoot 146
- pass band 146
- phase shift 146
- stop band 146

Filtering 240

- acquisition time 199, 201
- analysis time 199, 201

Filters 248

- 3db frequency 144
- band-pass 144
- band-reject 144
- Bessel 240, 248
- Bessel filter 150
- Butterworth 248
- Butterworth filter 150, 151, 152
- Chebyshev 242
- correcting for filter delay 154
- digital 153
 - finite impulse response 153
 - Gaussian 154
 - nonrecursive 153
 - recursive 154
- frequency domain analysis 151
- function 144
- high-pass 143
- low-pass 143
- noise 247
- notch filter 143, 150
- Nyquist Sampling Theorem 152
- order 144

patch-clamp data 153

pole vs. order vs. slopes 148

RC 248

related terminology 144, 145

sampling rate 152

time domain analysis 149

Fitting 207

Chebyshev polynomials 212

chi-square 209

confidence limits 210

goodness of fit 210

likelihood 208

motivation 207

optimization methods 211

statistical aspects 208

statistical tests 211

Folding frequency 238

Force measurements 176, 177

G

Gain 156

pre-filter vs. post-filter gain 156

Gain accuracy 192

Gaussian filter 240, 241

aliasing 240

Giant excised membrane patch method 117

pipette fabrication 118

seal formation 118

Gigaseal-Macropatch voltage clamp 110

Gigaseals 71

Glass

dissipation factor 224

Glass compositions 91

Glasses 89

electrical properties 89

see electrodes 87

thermal properties 91

- types
 - noise properties 92
- Glitch 193
- Ground-loop noise 22

H

- Headstage
 - bandwidth 75
 - capacitor feedback 74
 - current gain 35
 - Dynamic range 75
 - for ion-sensitive microelectrodes 39
 - Linearity 75
 - noise 75
 - resistor feedback 71
- Headstages
 - for intracellular recording 38
 - for ion-sensitive microelectrodes 39
- High electrode impedance
 - can produce attenuation 171
- Holders 87
 - for micropipettes 79
- Hum 21, 161
 - differential amplification 161
 - notch filter 161

I

- I/O interfaces 185
- Implantable length gauges 177
- Input leakage current 250
- Insulation measurements 178
- Intracellular recording
 - bath error potentials 40
 - bootstrapping 36
 - bridge balance 30
 - capacitance compensation 35
 - command generation 45

- current clamp 29
- current monitor 33
- headstage current gain 35
- junction potentials 32
- leakage current 39
- track 32
- virtual ground 34
- voltage clamp 46
- voltage follower 29
- Wheatstone bridge 30

Ions

- in electrodes 9
- in solutions 9

- Isolation measurements 178

J

- Johnson noise 216
- Junction potentials 32
- Junctional potential 86

L

- Laboratory setup 19
 - list of equipment 24
- Large cells
 - voltage clamp 48
- Leachable components 94
- Leakage current 39
- Least significant bit 193
- Least squares 209
- Length measurements
 - implantable length gauges 177
 - linear potentiometers 178
 - linear variable differential transformers 178
- Linear potentiometers 178
- Linear variable differential transformers 178
- Linearity error 192
- Line-frequency pick-up 161

Liquid junction potential 86
Loose-patch recording 109
Loose-Patch voltage clamp 111

M

Macropatch recording 109
Magnetically-induced pickup 22
Maximum likelihood 208
Mechanical requirements
 extracellular recording 19
Mechanical vibration 45
 for cell penetration 45
Membrane capacitance
 per unit area 68
Membrane capacitance
 measurements 78
Membrane potential 55
 ripple 55
Metal microelectrodes 175
Microelectrode pullers 88
Microelectrodes
 glass
 tight seals 16
Micromanipulators 19, 20
 remote-controlled 20
Micropipette holders 79
Micropipette selection 51
Microscope
 brain slice 20
 extracellular recording 19
 single-channel recording 20
Monotonicity 193
Multiple-cell recording 28
Multi-tasking operating systems 195
Muscle
 measuring
 implantable length gauges 177

N

Negative capacitance
 see capacitance compensation 37
Nerve cuffs 175
Noise 172, 215, 250
 aliased, in voltage clamp 55
 aliasing 238
 amplifier 221
 capacitance 227
 capacitance neutralization 56
 dielectric 215, 219, 224
 digitization 237
 electrode 223, 245
 excess (1/f noise) 215, 220
 external sources 236
 headstage 244
 high-impedance probes 171
 holder 244
 in single-channel patch voltage clamping 223
 in two-electrode voltage clamp recording 51
 Johnson 173
 patch capacitance 232
 patch clamp 246
 peak-to-peak 161, 215, 248
 pipette resistance 227, 232
 quantizing noise 237
 quartz patch pipettes 230
 recording from bilayers 130
 rms 248
 rms noise 161
 root-mean-square (rms) 215
 seal 232, 245
 shot 215, 218
 silicone oil 229
 sources 215
 thermal 173, 215, 216, 247
 power spectral density (PSD) 216

thermal (Johnson, Nyquist) 216
voltage-clamp 249
whole-cell voltage clamping 234
Nyquist frequency 238
Nyquist noise 216
Nyquist theorem
 see Sampling theorem 191
Nystatin 121
 use in stock solutions 121

O

Offset control 157
Offset removal 51
Ohm's law 5
Oocytes
 Xenopus 97
Optical isolation 194
Optical requirements
 extracellular recording 19
 single-channel recording 19
Overload detection 160

P

Patch
 rupturing 68
 zap 68
Patch clamp 15, 153
 amplifier noise 221
 capacitor feedback headstage 74
 data, filtering 153
 resistor feedback headstage 71
 single channel 70
Patch clamp noise 244
 limits 246
 summary 244
 electrode 245
 headstage 244
 holder 244
 seal 245
Patch micropipettes 86
Patch pipettes 87
 coating 88
 concentric, with loose-patch clamp 116
 electrical properties 89
 fabrication 87
 firepolishing 88
 from quartz tubing 230
 glasses 89
 noise 89
 noise properties 92
 pulling 88
 thermal properties 91
Perforated patches
 cellular voltage measurements 125
 other uses 125
 recording from 121
perforated vesicles
 recording from 121
Perforated-patch technique
 advantages 123
 disadvantages 123
 minimizing access resistance 124
Peripherals 182
Pipette fabrication 118
Pipette resistance measurement 79
Pipette solutions 85
Pipette-capacitance compensation 64
Pipettes 85
 glasses 89
 micropipettes 85
 properties
 single-channel vs. whole cell recording 89
Positive feedback (correction) 59
Pressure
 measuring very low 176

Pressure measurements 176

Q

Quantization error 190

Quantizing noise 237

Quartz patch pipettes 230

Quartz pipettes 224

R

Radiative electrical pickup 21

Resistor feedback headstage 71

Resistors 3

 seal 16

 single-channel recording 3

Rise time 248

S

Sample-and-hold 163

Sampling rate

 choosing 191

 oversampling 191

 sampling theorem 191

Sampling theorem 191

Saturation 160

Seal 71, 79

Seal formation 118

Seals

 pretreatment of muscle cells for best 118

Self-heating measurements 178

Series resistance compensation 59

 limitations 64

 positive feedback (correction) 59

 supercharging (prediction) 61

Shielding 21, 22

Shot noise 218

Signal conditioners 143

AC coupling 158

amplification 155

audio monitor 163

autozeroing 158

averaging 161

blanking 163

common-mode rejection ratio 164

differential amplification 161

electrode test 164

gain 156

line frequency pick-up (hum) 161

noise measurements 161

offset control 157

overload detection 160

peak-to-peak 161

programmable gain amplifier (PGA) 155

saturation 160

stimulus coupling 163

time constant 160

Signal conditioning 143

Silicone oil 229

Single-cell recording 28

Single-channel

 patch clamp 70

Single-channel analysis

 baseline estimation 202

 events

 false 202

 missed 202

 multiple channels 203

 events list 202, 203

 false closings 201

 filtering 201

 goals 200

 histograms 203

 errors 205

 sampling rate 201

 threshold 202

Single-channel patch clamp
 seal 71
Single-channel recording
 bilayer techniques 129
 setup 19
Small cells
 voltage clamp 52
Software 181
Software support 195
Space clamp
 considerations 69
Specifications 247
Stimulus coupling 163
Supercharging (prediction) 61
Sylgard 224, 228

T

Temperature transducers 167, 169
 resistance thermometers 170
 thermistors 167
 thermocouples 169
Thermal noise 173, 216
Time constant 160, 248
Time-domain analysis 149
Timers 194
Track 32
Transducers 167
 acceleration measurements 177
 accelerometers 177
 for extended temp. ranges 169
 force measurements 176, 177
 IC temperature, current 168
 IC temperature, voltage 169
 insulation techniques 178
 isolation measurements 178
 length measurements 177
 metal microelectrodes 175

 pressure measurements 176
 resistance temp. detectors 170
 self-heating measurements 178
 temperature transducers 167
 thermistors 167
 thermocouples 169

V

Vibration isolation methods 20
Virtual ground 34
Voltage clamp 14, 46
 anti-aliasing filter 55
 capacitance neutralization 56
 common errors 54
 controlled-current source 53
 current and voltage measurement 56
 error 49
 gigaseal-macropatch 110
 ideal 47
 large cells 48
 loose-patch 111
 membrane conductance changes 50
 micropipette selection 51
 noise 51
 real 47, 48
 signal bandwidth 56
 small cells 52
 stability 50
 step response and bandwidth 49
Voltage conventions 80
Voltage divider 7
Voltage follower 29
Voltage pulses
 applied to loose-patch pipette 115

W

Wheatstone bridge 30, 176

Whole-cell capacitance compensation 66
Whole-Cell clamp
 combining with focal current recording 111
Whole-cell mode
 dSEVC or cSEVC 69
 rupturing the patch 68
Whole-cell voltage clamping 234
 noise 234

X

Xenopus oocytes
 definition 98
 patch clamping of 101
 recording from 97
 two-electrode voltage clamping of 99

Z

Zap 69